Université Paris 7 « Denis Diderot »

Propriétés physiques et Dynamique des objets sans atmosphère du système solaire

Habilitation à diriger des recherches

Présentée par

Mirel BIRLAN

Institut de Mécanique Céleste et de Calculs des Ephémérides
Observatoire de Paris

Jury:

Professeur ***Marcello FULCHIGNONI***	**Président**
Astronome ***Alberto CELLINO***	**Rapporteur**
Professeur ***Guy MOREELS***	**Rapporteur**
Astronome ***Antonella BARUCCI***	**Examinateur**
DR CNRS ***Jean-Eudes ARLOT***	**Examinateur**
Professeur ***Richard BINZEL***	**Examinateur**
Astronome ***William THUILLOT***	**Examinateur**
Astronome ***Jean SOUCHAY***	**Examinateur**

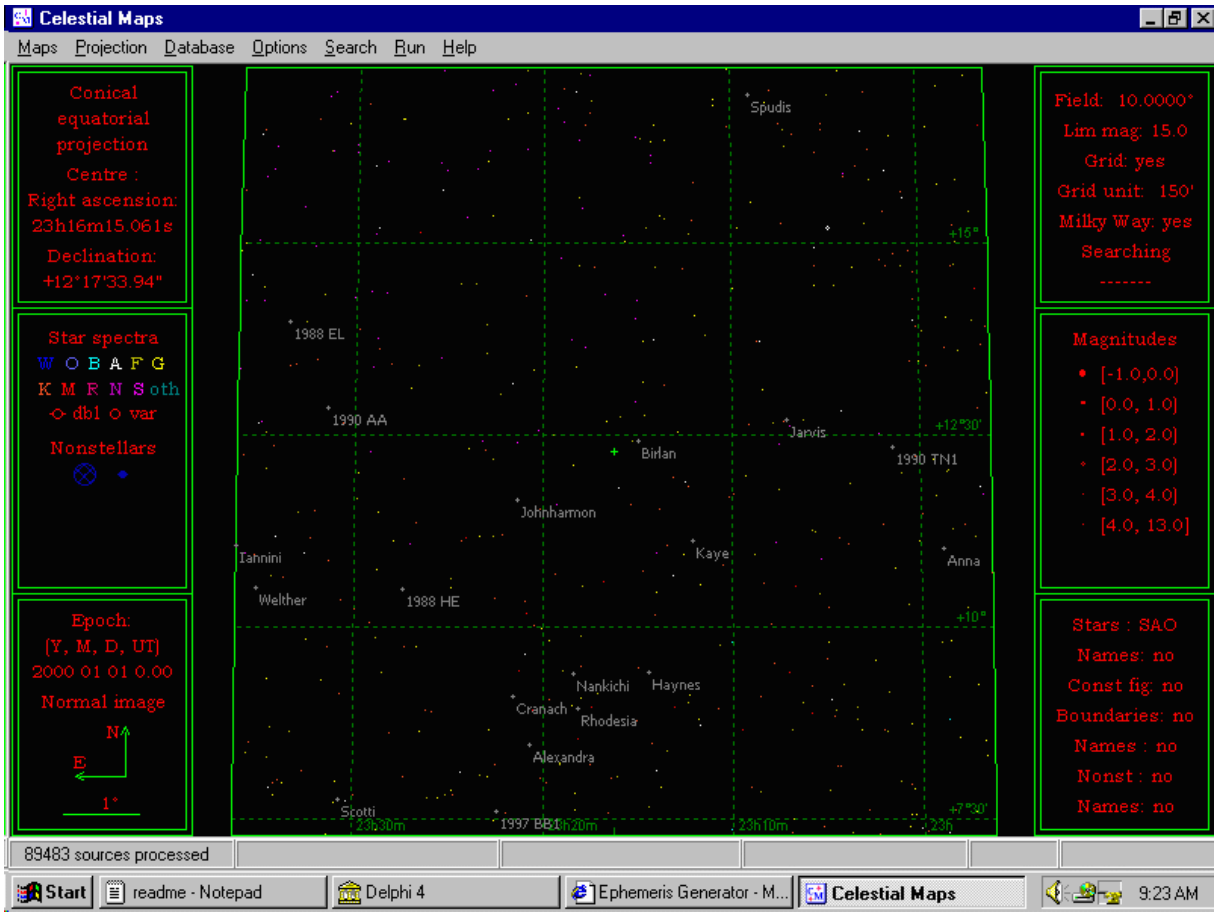
Celestial Maps
Maps Projection Database Options Search Run Help
Conical equatorial projection
Centre :
Right ascension:
23h16m15.061s
Declination:
+12°17'33.94"
Star spectra
W O B A F G
K M R N S oth
db1 o var
Nonstellars
Epoch:
[Y, M, D, UT]
2000 01 01 0.00
Normal image
N
E
1°
Field: 10.0000°
Lim mag: 15.0
Grid: yes
Grid unit: 150'
Milky Way: yes
Searching
Magnitudes
[-1.0,0.0]
[0.0, 1.0]
[1.0, 2.0]
[2.0, 3.0]
[3.0, 4.0]
[4.0, 13.0]
Stars : SAO
Names: no
Const fig: no
Boundaries: no
Names : no
Nonst : no
Names: no
Spudis
1988 EL
1990 AA
Birlan
Jarvis
1990 TN1
Johnhiarmon
Kaye
Anna
Iannini
Welther
1988 HE
Nankichi
Haynes
Cranach
Rhodesia
Alexandra
Scotti
1997 BB1
+15°
+12°30'
+10°
+7°30'
23h30m
23h20m
23h10m
89483 sources processed
Start
readme - Notepad
Delphi 4
Ephemeris Generator - M...
Celestial Maps
9:23 AM

Motto : **Sapere Aude**
Pense par toi-même

A Mariana

et à nos enfants

Diana, Mirela, Daniel et Florian

Peut-être parmi ceux qui écoutent y a-t-il un être jeune; quelqu'un qui se méfie de ses capacités, qui est écrasé par la pensée de sa propre médiocrité, prêt à se donner en aveugle comme beaucoup l'ont fait avant lui. Permettez-moi de lui parler. Je lui dirai: "Mon ami, tu n'es pas un médiocre ou, si tu l'es, cela ne compte pas. Ne pense pas à ce que, choses dignes ou horribles, les autres ont fait avant toi. Pense seulement que, à sa façon, ta vie est une occasion unique. Si au début je t'ai demandé ce que tu penses de toi-même ce n'est pas pour obtenir la réponse : j'en pense du bien ou du mal ! Mais pour que tu te souviennes qu'il faut te battre davantage avec toi-même ; qu'à l'intérieur de toi, quelqu'un d'autre est en train de dormir; une personne plus intéressante que tu n'imagines, un chrétien meilleur que tu ne le montres, peut-être un héros; avant tout un être brave, tout simplement. Prend en soin, ne le laisse pas trop dormir ! "

Constantin NOICA

Qu'est ce qu'est, que peut l'être, l'homme médiocre

Interventions Radiophoniques, Bucarest, 1936

Avant-propos

Par objet sans atmosphère nous considérons tout objet qui gravite autour du Soleil, de dimension inférieure à 2000 km de diamètre, qui ne peut développer ni garder une atmosphère. Du fait de leur nombre, cette définition englobe essentiellement les astéroïdes (ou les petits corps), les objets trans-neptuniens, les comètes, et certains satellites des planètes.

L'intérêt pour les études des petits corps réside principalement dans son apport essentiel à la cosmogonie du Système Solaire. Les deux dernières décennies nous ont permis d'accéder à une connaissance jamais encore atteinte concernant notre système solaire en général et plus particulièrement le domaine des corps de taille réduite (diamètre inférieur à 1000 km). L'image actuelle des petits corps dans le système solaire nous montre une variété de familles et de populations, aussi bien d'objets situés à l'intérieur de l'orbite de la Terre qu' au-delà du système Pluton-Charon. En fonction des orbites des objets sans atmosphère, on parle d'astéroïdes géocroiseurs, de Mars croiseurs, d'astéroïdes de la ceinture principale, d'astéroïdes situés dans des points de stabilité Lagrange, de Centaures, de trans-neptuniens, de comètes à courte ou à longue période.

Plusieurs questions fondamentales ont jalonnées les acquis scientifiques concernant les petits corps. Voici celles que l'on peut citer parmi les plus importantes:

- Pourquoi n'y a-t-il pas une planète massive entre les orbites de Mars et de Jupiter plutôt que des milliers de planétésimaux ?
- Quel est le lien entre les différents catégories de petits corps (astéroïdes, comètes et météors) ?
- Quelle est leur masse volumique ? Que sait-on de leur composition minéralogique ?
- S'agit-il de corps massifs ou de « tas de gravas » maintenus par un faible champ gravitationnel ?
- Peuvent-ils nous fournir la clé permettant de déchiffrer la composition de la nébuleuse planétaire précédant le système planétaire actuel ?
- Comment s'effectue et se répartit le transfert de moment cinétique entre la nébuleuse primordiale, le Soleil et les planètes ?
- Comment leur influence a-t-elle marqué l'histoire du système planétaire en général et celle de la Terre en particulier ? Quels sont les moments les plus importants de notre civilisations marqués par leur présence ?

Chacune de ces questions est génératrice d'un domaine scientifique distinct, en particulier en cosmogonie du système solaire. Plus concrètement, connaître la nature de la surface des astéroïdes et leur minéralogie, étudier les phénomènes de transfert radiatif dans les cas d'objets sans atmosphère, déterminer leur période de rotation propre (synodique), leur forme, le sens de rotation propre ainsi que la position de l'axe ou des axes de rotation, observer les astéroïdes « in situ » dans plusieurs longueurs d'onde grâce aux sondes spatiales, analyser les mécanismes de résonance ainsi que les processus de collisions mutuelles, font partie de ces « détails » qui permettent de mieux connaître la population astéroïdale et finalement de construire des modèles physiques plus fiables.

L'intérêt pour la population de petits corps du système solaire s'est accru aussi grâce à l'important nombre de missions spatiales ayant comme objectif leur étude « in situ ». Le succès des sondes spatiales Galileo, NEAR, a marqué la fin de la dernière décennie du XX^{ème} siècle. Pour la première fois, les images et des paramètres physiques obtenus ont permis l'obtention des formes d'astéroïdes, l'analyse de leur surface et de leur « relief », la présence d'un possible champ magnétique ainsi que leur environnement proche.

De par son grand nombre, la population astéroïdale représente un « champ d'expérimentation » aussi bien pour des mécanismes dynamiques (résonances, mécanismes de transfert et évolution chaotique des orbites) que pour des modèles physiques. L'analyse poussée des observations de haute qualité obtenues aussi bien « in situ » que par les grands télescopes au sol nous montre une population d'objets d'une grande variété, considérés quelques décennies auparavant simplement comme hypothèses de travail « peu probables ». Les scientifiques se sont rendus à l'évidence de la présence de systèmes doubles parmi les astéroïdes, ils ont accepté également l'astéroïde comme agglomération de petits cailloux maintenus ensemble par un faible champ gravitationnel afin d'expliquer leur faible masse volumique. Les astéroïdes survolés par des sondes spatiales nous ont montré des surfaces criblées de cratères, signe que les collisions dans le système solaire est un phénomène qui a eu une grande importance dans l'état actuel du système solaire. La séparation du noyau de la comète SL9 en plus de 20 parts sous l'effet de marée du champ gravitationnel de Jupiter nous a permis pour la première fois l'observation d'une prévision théorique (la limite Roche) et la mise en évidence de l'aspect « fragile » d'un noyau cométaire, confirmant en partie le modèle de « neige(glace) sale » de Fred Whipple.

La recherche scientifique présentée s'inscrit dans l'effort quotidien des scientifiques pour l'exploitation de nouvelles données fournies par des instruments au sol, en utilisant de nouvelles techniques. Cette activité vise également l'obtention de résultats issus de nouveaux

intervalles de longueur d'onde (comme celui de l'infrarouge proche dans le cas d'objets sans atmosphère du système solaire) mais également l'amélioration des techniques d'observations et d'optimisation des processus de réduction des données. Plusieurs des ces travaux ont été faits dans le cadre des recherches au sol liées aux missions spatiales en cours (ROSETTA) et futurs (DAWN et VENUS EXPRESS).

J'ai employé plusieurs techniques d'observation afin de mieux comprendre les propriétés physiques et dynamiques des corps sans atmosphère de notre système solaire : observations photographiques, photoélectriques ainsi qu'imagerie et spectroscopie par l'intermédiaire des cameras CCD. Les images astronomiques m'ont permis l'étude de leur rotation propres ainsi que leur couleurs (chapitre I.2.). La spectroscopie à la longueur d'onde du visible et du proche infrarouge (chapitre I.3.) ont permis l'analyse plus détaillée de la composition de la surface des objets, la connaissance plus précise de la composition minéralogique et la mise en valeur de la diversité des spectres. La dynamique des petit corps a été abordée également sur plusieurs aspects (chapitre I.4.).

L'analyse des spectres des petits corps en proche infrarouge m'a permis d'approfondir davantage les connaissances sur les différents techniques d'observations (chapitre I.1). Ainsi, j'ai pu démarré un projet de création d'un Centre d'Observation à Distance en Astronomie à Meudon, alternative aux campagnes d'observations, sans effectuer la mission au télescope (souvent nécessaires et peu pratiques).

Un autre volet dans mes préoccupations scientifiques a été aussi l'exploitation des résultats issus des observations. L'analyse des couleurs et des albédos m'a permis des études statistiques sur des échantillons significatifs d'astéroïdes de la ceinture principale, mais également sur la population des objets trans-neptuniens(chapitre II.1). J'ai pu affiner les taxonomies modernes ainsi que les méthodes d'analyse statistique. Pour la première fois, notre équipe de recherche a effectué des études statistiques sur des couleurs d'objets trans-neptuniens avec des résultats notables, références pour la caractérisation de cette population mais également pour les scénarios de formation du système solaire.

Observations de petits corps ; Préparation au sol des missions spatiales

I.1. Méthodes et outils liés aux observations ; la télé-observation

I.2. Photométrie des petits corps ;

I.3. Spectroscopie visible et infrarouge proche des objets du système solaire

I.4. Astrométrie et systèmes de références.

De nos jours l'observation des objets du système solaire, dans le domaine spectral du visible et de l'infrarouge proche, est faite par des détecteurs CCD[1]. L'analyse d'un objet sans atmosphère réside essentiellement dans l'interprétation du rayonnement électromagnétique réfléchi par l'objet. L'étape d'observation est donc essentielle pour l'obtention de résultats scientifiquement viables. Plusieurs composants liés à l'observation peuvent être conceptuellement différenciés : la conception des instruments adéquats pour un domaine particulier de l'astronomie, l'établissement d'une technique d'observation, l'établissement

[1] CCD – abbreviation de Charge Coupled Device (Detecteur avec transferts de charge electrique)

d'un protocole optimal d'obtention des observations, la réalisation d'une méthode de réduction des données d'observations,…

Les observations astronomiques suivent les acquis technologiques actuels, la spécialisation au sein même de l'activité d'observation astronomique devient une composante indispensable à la vie d'un astronome. De plus, les observations au sol s'imposent par un volet d'activités (par exemple l'interférométrie de haute résolution) qui actuellement sont difficilement envisageables dans l'espace extra-atmosphérique. Des données obtenues par de nouvelles générations de télescopes (Keck, VLT, Gemini,…) dotés de nouveaux types d'instruments et détecteurs concurrencent les données obtenues par les missions spatiales. Cette compétition fait que les deux volets d'obtention de données (les observations « in situ » délivrées par les missions spatiales et les observations au sol) permettent actuellement une complémentarité de certains aspects scientifiques. Nous assistons également à un transfert des connaissances techniques et technologiques (comme celles de planification automatique des tâches ordinaires d'instruments, de transfert des données, de commande à distance des instruments,…) entre les techniques astronomiques au sol et celles embarquées sur des sondes spatiales.

Ce chapitre traite des observations faites par le biais de mon expérience en matière de télé-observations ainsi que les techniques d'observation et réduction.

I.1 Méthodes et outils liés aux observations ; la télé-observation

Des efforts d'optimisation des observations astronomiques, de flexibilité et d'ergonomie des programmes sont effectués par toutes les équipes d'astronomes autour du globe. Les jalons sont les suivants :

- Une nouvelle génération de grands télescopes dont les plus représentatifs sont les géants VLT et Keck, permet actuellement l'obtention de résultats scientifiques à la mesure de leurs dimensions. Les télescopes avec des ouvertures de 2-4 mètres deviennent ainsi accessibles à des projets fondamentaux pour lesquels les mots-clefs « mission spatiale dans les trois prochaines années » peuvent être remplacés par « intérêt pour des projets spatiaux à long terme ». Ils permettent aussi des projets pilotes d'instrumentations de nouvelle génération.
- Les télescopes à ouverture de 2-4 mètres sont l'objet d'une forte pression sur le temps d'observation. Souvent les temps accordés sont des courtes périodes (1-2 jours). Cela impose un effort important de la part des initiateurs des programmes (les voyages + le temps d'observation + le temps de ré-adaptation = 7-9 jours au total pour une mission de 2 jours), et implique une augmentation inutile des « temps morts ».
- Depuis peu, certains télescopes d'ouvertures de 2-4 m offrent la possibilité de faire des observations à distance (remote observing). Afin d'encourager ce type d'observations, le temps consacré aux observations à distance, peut être, un critère de sélection important s'ajoutant à la pertinence scientifique du projet d'observations.
- L'implication des institutions scientifiques (dans le cas concret l'Observatoire de Paris) dans plusieurs projets instrumentaux et technologiques de pointe entraîne également une stratégie concernant les nouvelles technologies. Par

exemple, les observations à distance (remote observing) sur les instruments propriété du LESIA montés sur des télescopes au sol permettent de faire un usage optimal des moyens techniques et vont à terme réduire les besoins en mission.

Les premiers essais de télé-observations à l'Observatoire de Paris ont démarré au mois de décembre 2001 entre Meudon et Mauna Kea –Hawaii, par le pilotage du télescope IRTF (InfraRed Telescope Facility) de 3 m de diamètre situé au Mauna Kea, Hawaii. Ultérieurement cette activité a été formalisée dans le projet intitulé **Centre d'Observation à Distance en Astronomie à Meudon (CODAM)**.

Le but du projet CODAM est de fédérer les scientifiques de l'Observatoire de Paris afin de répondre à leur besoin d'exécuter des programmes d'observation à distance à partir de Meudon, sans qu'il soit nécessaire d'effectuer la mission sur le site du télescope. Loin d'être un substitut des programmes d'observation classiques, le projet est conçu pour offrir plus de flexibilité dans le programme scientifique des chercheurs, en contournant les problèmes liés à la fatigue du trajet (voyage + décalages horaires), les difficultés physiologiques liées à l'altitude à laquelle les télescopes sont installés. Enfin, ce projet offre la possibilité d'importantes économies financières pour le laboratoire, les sommes d'argent (déboursées au sein du budget de missions d'observations) pouvant ainsi être allouées à d'autres projets.

L'organisation d'un centre de contrôle à distance repose sur le concept d'infrastructure informatique unique afin de répondre aux besoins concrets des différentes manipulations astronomiques (technologies informatiques diverses, flux des données variable, temps de latence différents, architectures informatiques hétérogènes, politiques sécuritaires hétérogènes). L'activité courante consiste non seulement en une infrastructure matérielle, mais également une concentration des compétences techniques et scientifiques. L'expérience acquise dans les quatre dernières années montre qu'une mission de télé-observation est réussie quand plusieurs conditions sont remplies : une bonne connaissance du télescope et du détecteur, une bonne relation de travail entre l'équipe technique au sommet et celle de la salle de contrôle à distance, une bonne liaison Internet, un climat de confiance et de collaboration entre les institutions. Un autre volet des activités au sein du centre de contrôle est la veille technologique nécessaire pour toute mise à jour des instruments et télescopes avec capacités de télé-observations. Enfin, un dernier volet des activités consiste en l'identification des instruments propices à l'implémentation de cette activité.

Une première étape du projet, intitulée CODAM/IRTF, a été faite pour l'utilisation du spectrographe SpeX, qui couvre l'intervalle spectral 0.8-5 microns. L'infrastructure informatique pour cet instrument comporte :

- deux stations de travail sous Linux, permettant la gestion du spectrographe et du télescope à travers des liens sécurisés (tunnels ssh)
- un PC doté d'une webcam et un microphone, permettant une liaison audio-vidéo permanente avec le personnel technique de l'IRTF, au sommet de Mauna Kea, Hawaii ;
- trois connexions Internet ordinaires
- une liaison téléphonique utilisée en cas d'urgence et de panne de la liaison audio-vidéo

Des nos jours, plus de 40 nuits d'observations ont été effectuées avec SpeX-IRTF. Les données scientifiques obtenues ont été le sujet de plusieurs articles, communications et conférences. L'activité d'observation est comparable avec celle effectuée par une mission sur place. De plus, l'observateur ne subit pas les désagréments d'un longue voyage (souvent sur plusieurs fuseaux horaires) et les caprices de la météo lors des observations. Le décalage horaire entre Meudon et Hawaii (11 h) est idéale en ce qui concerne les télé-observations, l'observateur peut ainsi observer pendant son programme normal de recherche.

Le second développement sous l'intitulé CODAM est celui du combinateur interférométrique FLUOR qui travaille actuellement comme instrument invité sur le système CHARA situé au Mont Wilson en Californie. L'instrument FLUOR est la propriété du LESIA de l'Observatoire de Paris qui dispose de 20% de temps d'observation garanti sur le complexe des quatre télescopes (de 1 m de diamètre) qui représentent le système CHARA.

La mise en œuvre des activités de télé-observations nécessite une nouvelle technologie de transmission d'informations par l'informatique (celle des réseaux virtuels privés) ainsi qu'une liaison vidéo pour la surveillance à distance des télescopes et des conditions météo.

Références

M. Birlan, M.A. Barucci, W. Thuillot – *Solar system observations by remote observing technique : useful experience for robotic telescope strategies.* **Astronomische Nachricthen** No. **6-8**, 571-573, 2004.

A. Merand, **M. Birlan,** T. ten Brummelaar, V. Coudé du Foresto, R. Lelu de Brach - *Remote observations with FLUOR and the CHARA Array***, SPIE**, (in press), 2004

M. Birlan, R. Binzel – *Paris Observatory Remote Observing January-May 2002: Sharing the Experience to Educational Astronomy,* Global Hands-On Universe Conference Proceedings, Paris, July, 2002

S. J. Bus, A. J. Denault, J. T. Rayner, R. P. Binzel, **M. Birlan -** *Remote observing at the NASA Infrared Telescope Facility (IRTF)***,- SPIE** Conference**,** Advanced Global Communications Technologies for Astronomy II, Hawaii, August, 2002

Astron. Nachr./AN **325** (2004) 6/7, xxx–xxx

Solar system observations by remote observing technique : useful experience for robotic telescope strategies.

M. BIRLAN[1,2,⋆], A. BARUCCI[3], and W. THUILLOT[1]

[1] IMCEE, Observatoire de Paris, 77 avenue Denfert-Rochereau, 75014 Paris Cedex, France
[2] Astronomical Institute of the Romanian Academy, Cutitul de Argint - 5, 040557 Bucharest, Romania
[3] LESIA, Observatoire de Paris-Meudon, 5 Place Jules Janssen, 92195 Meudon Cedex, France

Received; accepted; published online

Abstract. Remote observations between Paris Observatory and Mauna Kea - Hawaii have been started two years ago. Nowadays ten runs have been already conducted from the remote observing center located in Meudon. The main topics of our investigations were devoted to physical studies of minor planets (Binzel et al. 2004, Birlan et al. 2004) and to spectral investigations of planetary atmospheres. Our experience attained its maturity and the acquired feed-backs allow us to discern between the advantages and difficulties of this observing technique. The main purpose of this paper is to share the remote observing experience and to valorize it in the frame of robotic telescope concept.

Key words: remote observing, spectroscopy, minor planets

1. Introduction

One of the strategies of modern groundbased observational astronomy is to perform the observations in remote mode. In the astronomy vocabulary this denomination was introduced for the groundbased telescopes in the eight decade of the XX-th century. Until then several derived notion were implemented in the vocabulary. We talk about remote observing, passive and active remote observing, distribute remote observing or remote observing center (Zijlstra et al. 1997). All these definitions are in connection to the degree of implementation of the control of instrument and telescope from the distant observer.

Remote operation allows the observer to reside in a location that may be more comfortable than a high altitude summit and may reduce observer fatigue if no travel is required from her/his home institution. Such observations could be an answer to the service mode (or queuing mode) proposed by the staff of some large telescopes. The observer will be entirely responsible for the strategy adopted during the observations and the requirements of his scientific program (exposure time, signal-to-noise ratio, photometric or spectroscopic standards necessary for data reduction, airmass requirements,...) could be better accomplished.

⋆ Mirel.Birlan@imcce.fr

The remote observing must not be seen as the technique which could entirely replace ordinary missions to the telescope. The successful remote observing observations are the result of several factors: qualification of the observers for the science obtained through the program, difficulty of program in the frame of the routine work, degree of knowledge of the instrument and detector by the observer, knowledge and training with new procedures implemented in new versions of software for the telescope and the detector, coordination between the remote observer and the technical staff located near the telescope (array of telescopes).

2. CODAM - The Remote Observing Center at Meudon

The main principle of the remote observing center is to use the same technical infrastructure, for implementing several telescopes and instruments. For this purpose, we conceived the informatics and the logistic to the centre in order to be able of a quick switch between different types of astronomic observations.

First tests of observations starts on January 2002 in Meudon Observatory. The remote observing tests were conducted from Meudon during several runs, and the idea of

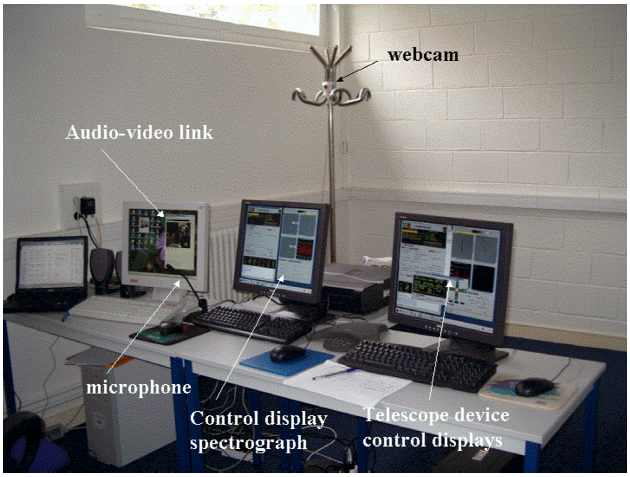

Fig. 1. Remote observing center at Meudon. This image was taken during its inauguration, on November 4, 2003

the Remote observing Center crystallized after six month. Our successful experiment was realized using IRTF 3 m telescope located in Mauna Kea, more than 12,000 km away from Meudon. The concept of remote observing center was imposed by the identification of several telescopes and instruments who are used by the researcher from Paris Observatory. Nowadays, the remote observing technique is perceived like an alternative to the classical observing mission, a service which allow a more flexible schedule for the scientist. The experience acquired with SpeX/IRTF attained its maturity; in parallel the remote observing tests have been started in interferometry, with CHARA system, located on Mount Wilson, in California. Investigations concerning other telescopes and instruments are also foreseen.

2.1. Remote observing with SpeX/IRTF

For the first run of Jannuary 2002, several tests and training sessions were organized beforehand. During these tests compatible computers for guiding and image acquisition were selected, and the strategy of the audio/video link was chosen. For the observers in Meudon, the observing hours occurred during relatively normal working daylight hours. Observation sessions began at 5 a.m. local time and finished at 5 p.m. local time.

The observations are realized through an ordinary network link, without the service quality warranty. Thus, the passband for our link was variable, in function of the traffic between Hawaii and Meudon.

The telescope and the instrument X environment control panels were exported to Meudon via two secure links (ssh tunnels). Two PC's under Linux operating system are devoted to the instrument and telescope control (Fig. 1). In order to have a permanent audio/video link, we use the IP link as it was the most compatible with IRTF operations. Thus, our audio/video link was established with a Polycom professional video-conference system (on Mauna Kea), and webcam / NetMeeting software (at Meudon). In our strategy we can dispose of a telephonic line with an audio-conference system for the unusual case of a completely broken audio/video link.

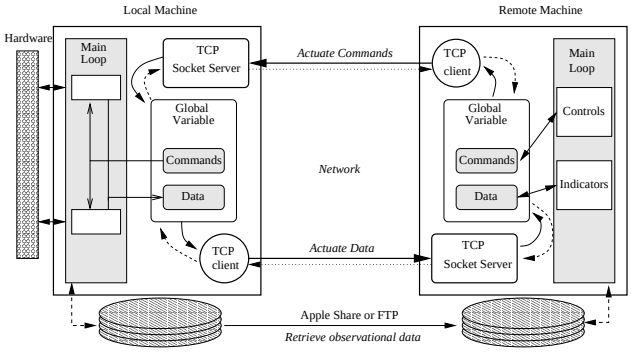

Fig. 2. Design of the client/server architecture for FLUOR/CHARA. The software and queries are written in Labview environment (Merand et al, 2004)

The SpeX instrument (IR spectrograph) was utilized for different scientific purposes.SpeX could be used in several scientific modes (low-resolution or high resolution spectroscopy) in the spectral interval 0.8-5.3 micron.

Nowadays more ten runs summing more than thirty night of observations were done by remote observing. During these runs a wide variety of procedures were commanded remotely: the focus of the telescope, setup of the guiding procedure, manual tracking, setup of the spectrometer and a preliminary analysis of the observations. The mean delay between the image acquisition in Mauna Kea and the refresh on the Meudon displays was 1.5-2 seconds approximately and it was quite stable independently of the internet traffic (our runs were done during the working days as well as during the weekends, as scheduled to IRTF). For all procedures, except for manual guiding on faint objects, such delays did not impede the efficient performance of the observing process. Thus, we estimate the efficiency of our observations very close of these obtained by a classic mission to the telescope.

2.2. Remote observing with FLUOR/CHARA

FLUOR is the acronym of Fiber Linked Unit for Recombination, an interferometric beam combiner developed by researchers and engineers of LESIA, Paris Observatory (Coude du Foresto et al. 2003). FLUOR was installed was installed to the Center for High Angular Resolution Astronomy (CHARA) Array, located at Mount Willson, California, in 2002.

The peculiar status of this instrument inside CHARA as well as the scientific interest for its results, allow of the strategy of remote observing from Meudon. The implementation of remote technique followed several steps such as: tests of physical link from Meudon to CHARA through a VPN technology, design of the client software for FLUOR instrument and the tests of this client in emulation mode, new facilities implementations in the remote observing center - video-projection system for scientific data.

On June 18, 2004, the tests were conducted with real data. From CODAM, we command for the first time the telescopes

and the beam combiner CHARA classic. The fringes of interference for the star HD 138852 were recorded for the first time remotely.

This success of our test was possible only by the close collaborations between the FLUOR and CHARA teams. The next step of our schedule will be the test of client software with real FLUOR data (Fig. 2).

3. Scientific results

During more than ten remote observing runs between CODAM and IRTF/SpeX, several scientific programs of planetology have been scheduled. The main programs were devoted to the solar system objects, mainly as support for the groundbased science in support to futures space missions. In this frame, we can cite the observations of asteroids candidates for Rosetta mission fly-by, and the high resolution spectroscopy of the deeper atmosphere of Venus for preparing the future Venus Express mission of the European Space Agency. Several runs were also devoted of near-infrared spectroscopy of Near-Earth Asteroids (Binzel et al. 2004) and the asteroids from the Main Belt.

The near-IR spectroscopy obtained by remote observations at IRTF was very important for the choice of the asteroids 21 Lutetia and 2867 Steins as targets to the Rosetta fly-bys. The IR observations (Fig. 3) of 21 Lutetia show a flat, featureless spectra, with a small positive slope. The comparaison of several meteorite spectra could conclude to the similarity of the asteroid spectrum with the chondritic materials (Vigarano meteorite from the CV3 carbonaceous chondrite group and Sevrukovo meteorite from the L6 ordinary chondrite group). For the Rosetta mission scientific objectives (finding clues of the formation and the evolution of the Solar System), 21 Lutetia is a very good candidate for 'in-situ' investigations.

4. Conclusion

The remote observing experience acquired during the last four years allow us to conclude the importance this observing mode. Remote observing technique can be considered a powerful interactive tool, with a good efficiency concerning the scientific results. All these assertions are relative to a good informatics infrastructure, for relatively high traffic rates, and the good compatibility of network materials. The quality of remote observations are highly dependent of the knowledge of the instrument and the telescope. Thus, the remote observers must be informed about the changes of the software and the implementation of new routines for the telescope and instrument.In the same time, the team of the telescope must inform the observers (through an e-mail list, web-page updates,...) concerning these modifications. For a efficiency estimated as 90% of that obtained by ordinary missions, we estimate the remote as a good alternative solution of observations, especially during the short runs. The facility of remote observing with instruments ideally located at 11-12 hours of difference offers the possibility to observe during the daylight

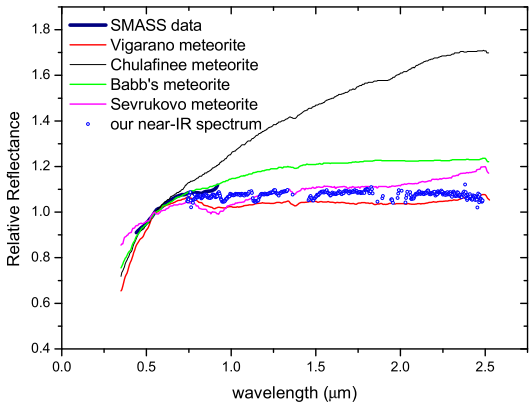

Fig. 3. The composite spectrum of the asteroid 21 Lutetia (the visible data from the SMASS program and the IRTF near-IR spectrum) was compared with several spectra of meteorites representative for some meteoritic groups. The near-IR spectrum of the asteroid is flat and featureless and can be noted the relative resemblance of it with those of chondritic meteorites (e.g. Vigarano and Sevrukovo). The figure contains also the spectra of two meteorites with high content of metallic atoms (Babb's Mill and Chulafinee) in order to mark the discrepancy of spectra. The meteorite spectra were published by Gaffey in 1976.

and increase the performance of observers by eliminating the fatigue of long distance travels.

Another important aspect of the remote observing is the access of the students to time on medium and large aperture telescopes. Students have the potential to be involved in the scientific proposals as a way of learning how to propose their own ideas. Remote observing could allow a strong background in observational techniques as well as experience with the telescope and the instruments.

The flexibility and the interactivity offered by remote observing should be considered in designing of robotic telescope strategies. The wide range of astronomical observations are function of the scientific goals, and it will be difficult to implement all type of observations for same robotic telescope. The choice of observation routines and scientific purposes could deserve also a reflection concerning the implementation of interactive routines which operate remotely.

References

Binzel, R.P.B., Birlan, M., Bus, S.J., et al.: 2004, PSS, 52(4), 291
Birlan, M., Barucci, M.A., Vernazza, P. et al. : 2004, NewAst 9(5), 333
Coude du Foresto, V., Borde, P., Merand, A., et al.: 2003, SPIE 4838, 280
Merand, A., Birlan, M., et al.:2004, SPIE Glasgow(in press)
Zijlstra, A.A., Wallander, A., Kaper, L., Rodriguez, J.A.: 1997, ASP 109, 1256

Remote observations with FLUOR and the CHARA Array

Antoine Mérand[a], Mirel Birlan[a], Rémi Lelu de Brach[a] and Vincent Coudé du Foresto[a]

[a] LESIA, UMR8109 Paris Observatory 5, place Jules Janssen 92295 Meudon CEDEX, (FRANCE)

ABSTRACT

Two years ago, the FLUOR interferometric beam combiner moved from IOTA (Infrared Optical Telescopes Array, Mount Hopkins, AZ) to the Center for High Angular Resolution Astronomy (CHARA) Array (Mount Wilson, CA). Apart from offering the largest baselines in the northern hemisphere, this array can be fully operated remotely to allow observations from a distant place. We present here the automations added to the FLUOR hardware, as well as software modifications made in order to allow us to observe from Paris Observatory. We required the remote service to be as reactive as local observations, implying frequent communications between the instrument and the remote observer. We took particular attention to the available bandwidth and reactivity imposed by the secured connection (Virtual Private Network). The first tests are presented.

1. INTRODUCTION

Remote observation tends to widespread in astronomy. For astronomers living far from the observing site, it may save traveling money and time. Moreover, some programs are not well adapted to few short runs a year: synoptic programs, like the survey of a slowly time-variable object, require a small amount of observing time every month or so.

1.1. The CHARA Array

The CHARA Array is an Optical stellar interferometer consisting in 6 telescopes, six delay lines (to equalize the path differences between telescopes aiming at the same star) and a Light Combination Laboratory (ten Brummelaar et al. 2003[1]). The all instrument is installed atop Mount Wilson, CA. This array can be operated from the remote operations center for Georgia State University's CHARA in the campus in Atlanta GA. The Cleon C. Arrington Remote Operations Center was designed to allow secure connection with the Mount Wilson site without cutting down the end-to-end latency.

1.2. FLUOR

The Fiber Linked Unit for Optical Recombination (FLUOR) is an interferometric combiner using single mode fiber as spatial filters and fiber coupler to combine the light from two telescopes in the infrared K band (mean wavelength, $\lambda = 2.2\,\mu m$). In 2002, FLUOR moved from the Infrared Optical Telescope Array (IOTA, Mount Hopkins, AZ) to the CHARA Array. (for a full description of FLUOR, see Foresto et al. 2003[2]).

2. CONTROL ARCHITECTURE

Existing publications describe the control software implemented to operate the CHARA Array (e.g. Fallon et al. 2003[3]). The FLUOR control software only handles correction to the CHARA optical path difference (OPD) active system (a pair of active delay lines) and specific hardware for FLUOR, thanks to different I/O boards, including:

- A fast scanning mirror that modulates the OPD between the two incoming beams in order to record the interferometric fringes,
- A near infrared detector,
- Step motors used to automatically and finely tune the alignment of the star on the inputs fibers

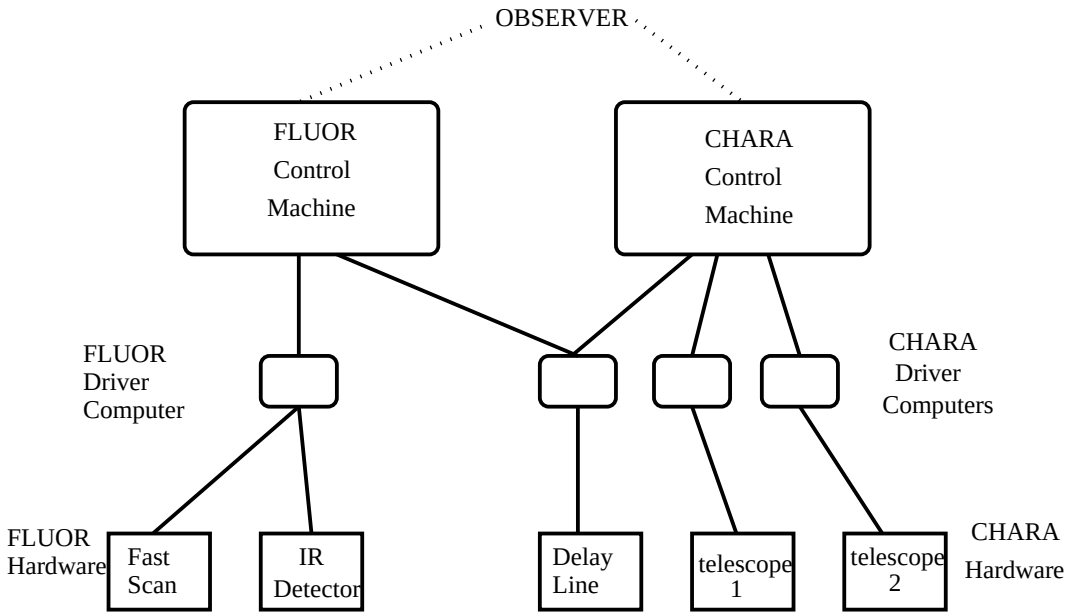

Figure 1. Control of FLUOR/CHARA. on the left, the CHARA control machine runs a single program that controls the whole array via intermediate computers dedicated to a single task and/or hardware device. The FLUOR side follows the same scheme: a Control Machine sequences the observations and access the FLUOR hardware via a dedicated computer.

The FLUOR Software is written in LabVIEW and runs on PowerMac computers under Mac OS X. On IOTA, The software was running on a single machine. On CHARA, a machine, sitting next to the optical table, is dedicated to the hardware low-level control. Another machine, in a comfortable control room, sits next to the CHARA computer that runs the master control software (see Fig.1). The FLUOR control machine runs the FLUOR Master software that sequences the observation and computes the corrections sent to CHARA active delay lines in order to correct from low frequency atmospheric perturbation of the OPD, as well as small drifts in the astrometric model that runs the delay lines. While observing with FLUOR, all CHARA sub-systems (telescopes, delay lines, shutters etc.) are controlled by the CHARA master program.

2.1. Observation cycle

Observing a target (science target or calibration star) with FLUOR/CHARA takes between 15 and 20 minutes. This cycle includes:

1. Aiming the two telescopes at the star (including locking the tip-tilt servo), positioning the delay lines.
2. Once the beams are stabilized (thanks to the tip-tilt system), optimizing the injection to the entrance fibers. This is done by rasterizing the focal plane with step motors moving a flat mirror (Fig. 2) while recording the flux in the photometric outputs. Optimizing consists in going back to the optimum position.
3. Looking for fringes. Usually, the observer has to scan a few millimeters around the delay lines supposed zero OPD position. FLUOR makes a scan (see next item) and then sends a given step to the active delay line if fringes are not found.
4. Recording scans. FLUOR, thanks to its Fast-Scan mirror, modulates the OPD with respect to time (over about 180 microns, 7 times the fringe packet length — 25 microns —). By the same time, the intensity is recorded out of the four output fibers: two photometric channels for further processing and two interferometric channels. Fringes are detected by a simple algorithm, the centroid of the fringe packet is computed and a correction is sent to the delay line.

Send correspondance to A. Mérand, E-mail: antoine.merand@obspm.fr

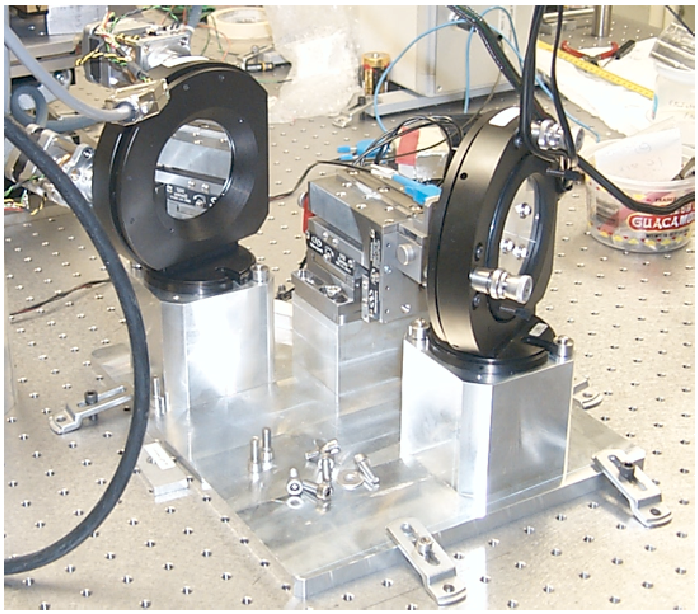

Figure 2. Input stage used to optimize the injection. The plan mirror (left) collects the beam from the telescope and sends it the off-axis parabola (right, behind the mount) in order to focus on the single-mode fiber. The plan mirror mount can be tilted in order to change the star position on the focal plan and thus optimize the injection in the fiber. This process, fully automated, increases the efficiency of the remote mode.

5. All shutter closed, dark frames are recorded. Usually, this time is used to aim at the next target (first item).
6. Checking visually the Data thanks to a synthetic display.

2.2. Latency requirements

Observing remotely usually does not offer the same reactivity because of end-to-end latency. In that section, requirements will be described using the same structure used to describe the observation cycle (previous section):

1. **Aiming the telescopes.** This part is made using CHARA control software and remote control interface (see Fallon et al. 2003[3]), we rely on their implementation.
2. **Optimizing injection.** This process, as described previously, is fairly automatic. Fist, the observer sends a starting signal and then waits for the rasterized focal image. The observer can follow the process but latency is not an issue here.
3. **Looking for fringes.** This process is highly demanding on latency. Recording a single scan (a fringe packet) takes fairly one second. Every second, the remote observer has to receive the fringe packet. Once again, FLUOR control software is mainly automated: an algorithm is used to detect the fringes in the scan. If so, the software stops sending constant steps to the delay lines and starts recording data on the current delay line position. A single false detection thus stops the searching process, the observer can decide to resume it. In that process, it is crucial for the remote observer to get every single scan.
4. **Recording data.** Once fringes are found, the FLUOR software compensates for slow drifts easily: while observing on site, we usually send the fringe signal to a loud-speaker in order to "keep an ear" on the system. If fringes are lost, the searching process (previous item) should resume. This steps requires also quality monitoring: signal to noise ratios, raw visibility estimation etc. have to be send for every scans. This is the most demanding part, in term of latency, of the observing.

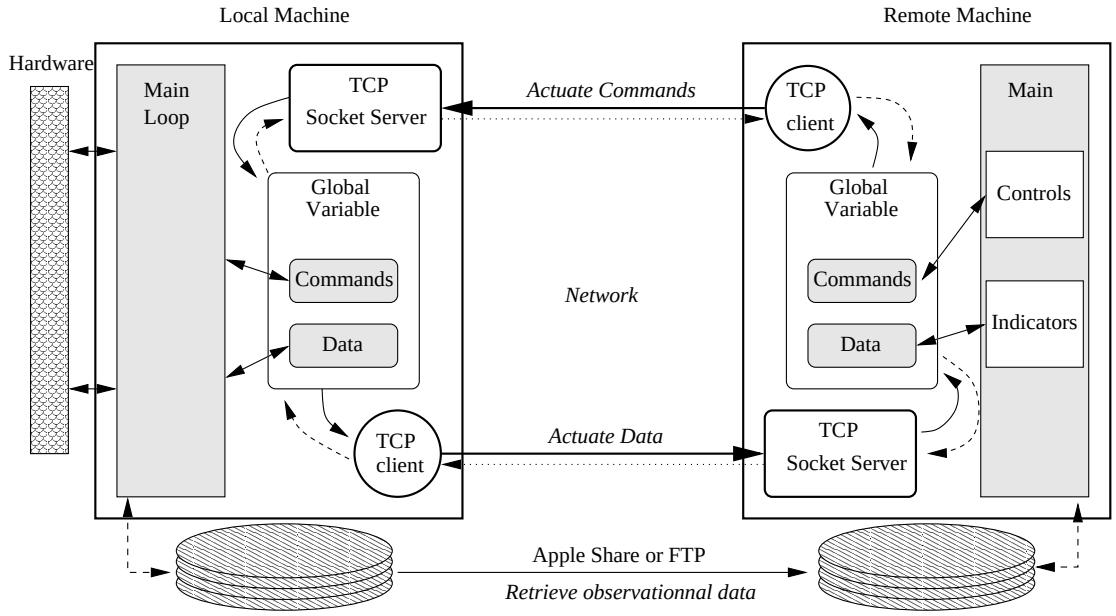

Figure 3. Implementation of the remote computer (right) with respect to the current FLUOR control computer (called local machine, left). The local machine is the same represented in Fig. 1, upper left. This machine is on Mount Wilson site, connected on the local network. Each machine runs a TCP server, allowing to receive text-based messages. The remote machine uses simple text commands while the local machine sends a status report, as well as a very small of data, quick looks essentially (thick lines between clients and servers). Acknowledge messages are sent back when a server receives commands or data (dotted lines).

5. **Dark Frames.** Nothing has to be done here. The observer only wants to have progress status.
6. **Checking Data quality.** This is done based on the actual file. Remote latency is not an issue: data are recorded on site and then downloaded on the remote computer thanks to a FTP (file transfer protocol) server.

It appears that a few tasks only are demanding regarding end-to-end latency, especially items number 3 and 4 (if the FLUOR software fails to keep the fringes in the scanned OPD range, which happens rarely).

2.3. REMOTE CONTROL ARCHITECTURE FOR THE FLUOR SOFTWARE

Considering that the observing cycle is fairly automated and that latency is only an issue for a small number of task, we decided to leave the FLUOR Software running on a computer located on Mount Wilson. Doing so, we protect ourselves against long latency events that can occur during a few seconds or even longer: the FLUOR control remains autonomous and only accepts commands. It sends for each scan a status report (a few tens of ASCII characters) and a quick look signal. We did not modify the software much, we only added a TCP client/server module to the LabVIEW software. Text-based control commands are sent to a dedicated TCP port, while the FLUOR control software can send data (mainly quick-look data) to a server (a listener) running on the remote machine (Fig. 3). The actual data are recorded on site and then retrieved by the remote observer. The two computers are connected to the same local network via a Virtual Private Network (VPN) protocol. This solution is used also to control the CHARA Array other the Internet (see Fallon et al. 2003[3]).

3. FIRST TESTS AND PROSPECTS

Using an emulation mode, we undertook observations using only FLUOR software (CHARA was not involved) from Paris/Meudon Observatory in December 2003. This emulation mode reproduces all steps of the observing

cycle, generates data. Without increasing the duration of a scan (which lasts roughly one second) by waiting for TCP transactions, it has been possible to receive the status string and quick-look data every single scans. Moreover, even operated from the other side of the Atlantic Ocean, the FLUOR control software remained reactive.

In the future, FLUOR/CHARA remote observations will take place in a dedicated room, the "Centre d'Observations à Distance pour l'Astronomie de Meudon" (CODAM) in Paris/Meudon Observatory. Located on the Meudon Campus, this room is also equipped for video conference. Observations were already made from this room using the NASA Infrared Telescope Facility on Mauna Kea with the SpeX instrument (see Birlan et al. 2004[4] for latest results).

4. CONCLUSION

An analysis of the requirements for a remote observing mode was made for the FLUOR interferometric beam combiner, installed on the CHARA Interferometric Array. We presented the actual implementation, consisting in adding a TCP client and server modules to the FLUOR control Software, another computer, running symmetric servers and client is used to send text-based commands and receive quick-look and status informations thru the Internet, the connection being secured by a Virtual Private Network (VPN) protocol. First tests were successfully undertaken, though using an emulation mode, showing promising results.

REFERENCES

1. T. A. ten Brummelaar, H. A. McAlister, S. T. Ridgway, N. H. Turner, L. Sturmann, J. Sturmann, W. G. Bagnuolo, and M. A. Shure, "An Update of the CHARA Array," in *Interferometry for Optical Astronomy II. Edited by Wesley A. Traub. Proceedings of the SPIE, Volume 4838.*, pp. 69–78, Feb. 2003.
2. V. Coude du Foresto, P. J. Borde, A. Merand, C. Baudouin, A. Remond, G. S. Perrin, S. T. Ridgway, T. A. ten Brummelaar, and H. A. McAlister, "FLUOR fibered beam combiner at the CHARA array," in *Interferometry for Optical Astronomy II. Edited by Wesley A. Traub. Proceedings of the SPIE, Volume 4838.*, pp. 280–285, Feb. 2003.
3. T. Fallon, H. A. McAlister, and T. A. ten Brummelaar, "Remote operation of the CHARA array via the Internet," in *Interferometry for Optical Astronomy II. Edited by Wesley A. Traub . Proceedings of the SPIE, Volume 4838.*, pp. 1193–1200, Feb. 2003.
4. M. Birlan, M. A. Barucci, P. Vernazza, M. Fulchignoni, R. P. Binzel, S. J. Bus, I. Belskaya, and S. Fornasier, "Near-IR spectroscopy of asteroids 21 Lutetia, 89 Julia, 140 Siwa, 2181 Fogelin and 5480 (1989YK8), potential targets for the Rosetta mission; remote observations campaign on IRTF," *New Astronomy* **9**, pp. 343–351, June 2004.

Paris Observatory Remote Observing January-May 2002; Sharing the Experience to Educational Astronomy [1]

Mirel BIRLAN[1], Richard BINZEL[1,2]
[1]Observatoire de Paris-Meudon, LESIA, 5 - Place Jules Janssen, 92195 Meudon CEDEX, France,
e-mail : *Mirel.Birlan@obspm.fr*
[2] Department of Earth, Atmospheric, and Planetary Sciences, Massachusetts Institute of Technology, Cambridge, MA 02139 USA
e-mail: *rpb@mit.edu*

Abstract: This paper describes the accomplishments and difficulties of the remote observing campaign between Meudon and the NASA Infrared Telescope Facility on Mauna Kea. The experiment is a three institutions initiative: IRTF team (Dr. S.J. Bus), MIT (Professor R. Binzel), and Paris Observatory (Dr. Mirel Birlan). During 4 observing runs between January and May 2002 we used the SpeX instrument to measure spectra in the range 0.9 - 2.5 microns for a spectroscopic study of near-Earth asteroids and the observation of 4979 Otawara, a flyby-target of the Rosetta mission. All target acquisition and data acquisition procedures were successfully commanded from Meudon with minimal delays in system response. The efficiency of the observing program was virtually the same as if the observers had been on location.

Our successful experiment could be applied for astronomy students. The students will be able to observe and will stimulate theirs initiative in astronomy science. The "live" observations is suggestive for students and will complete the whole teaching sequence, from doing their own observations, through data-reduction techniques, and finally, deducing science results.

One strategy of modern groundbased observational astronomy is to perform observations in a remote mode. Remote operation allows the observer to reside in a location that may be more comfortable than a high altitude summit and may reduce observer fatigue if no travel is required from her/his home institution.

Several weeks of effort were devoted in order to determine the best conditions for the success of the experiment we describe here. Our goals for remote science operation included having control of the instrument and the target acquisition/guider system. Equally important was the good communication between the Principal Investigator and the telescope operator on Mauna Kea. High speed and real time command and response for the instrument, telescope, data, and human communication links were essential to the success. Careful preparation and testing of hardware options showed that all objectives could be achieved during the period of the observing run.

This experiment was completed through an ordinary network link, without the service quality warranty. Thus, the bandwidth for our link was variable, and was a function of the traffic between Hawaii and Meudon.

For this experiment, several tests and training sessions were organized beforehand. During these tests compatible computers for guiding and image acquisition were selected, and the strategy of the audio/video link was chosen. During the pre-observing period, several workstations and terminals were tested. The main conclusion was that the X-windows export through Meudon is highly dependent on the machines we use: the export windows tests were

[1] Presented to *Global Hands-On Universe*, 24-29 July 2002, Paris, France

unsatisfactory for COMPAQ workstations and terminals, as well as for one of the SUN workstations. Finally, two Sparc workstations (with the operating systems 5.7 and 5.8 respectively) were found to be very well suited for the experiment (Figure 1).

The incompatibility of both video conference systems (through a phone line in Meudon, and the IP link in Mauna Kea), constrained us to choose either an IP link or a phone link. Our decision was to use the IP link as it was the most compatible with IRTF operations. Thus, our audio/video link was established with a Polycom professional video-conference system (on Mauna Kea), and webcam / NetMeeting software (at Meudon).

Figure 1 (Left side) Remote control room in Meudon Observatory. In this image the audio/video link is located on the left screen, the SpeX control and the guiding windows on the center and right screen respectively. (Center) SpeX instrument control window. Observing modes and data acquisition are controlled by the window on the left. Spectral images and their preliminary analysis are displayed and controlled on the right. Upper right window of the display shows the spectrum of the asteroid 2002AA in both A and B positions of the slit, after a preliminary treatment. (Right Side) Audio/video link as it was seen from Meudon.

For this collaborative experiment between MIT, IRTF, and Meudon, targets were chosen according to the scientific interests of the investigators at each institution. Priority was given to the science program for which the time was allocated: the compositional investigation of near-Earth asteroids. Supplementary targets included 4979 Otawara, a flyby target for the Rosetta mission planned by the European Space Agency.

The apparent V magnitudes of the measured asteroids were typically in the interval 15-17. The guiding for each object was performed using automatic mode for all but the faintest targets. For the latter, manual tracking was used. For data calibration, the solar analogs Landolt 93-101, Hyades 64, and Landolt 102-1081 were also observed during the course of the night (Binzel et al, submitted 2002).

All software was re-started at the beginning of each night. During the three nights, the audio/video link was very stable and useful for our remote experiment. This link dropped for small intervals during the runs, most likely the result of limits imposed by network security protocols. The telescope/guider control links and SpeX instrument control links remained fully linked and stable throughout all the nights.

All the observations were saved on the Mauna Kea computer system, and subsequently transferred to Meudon after the experiment using ftp.

The spectrum of the asteroid 4979 Otawara (on the top of the figure) illustrates the science. The infrared spectrum of the asteroid 4979 Otawara allows us to classify it as an S-type asteroid (silicate materials, where the 1 micron and 2 microns broad absorption features are characteristics of olivine and pyroxene). The S-type asteroids may be the parent bodies of the ordinary chodrite (OC) meteorites (Fornasier et al submitted 2002)

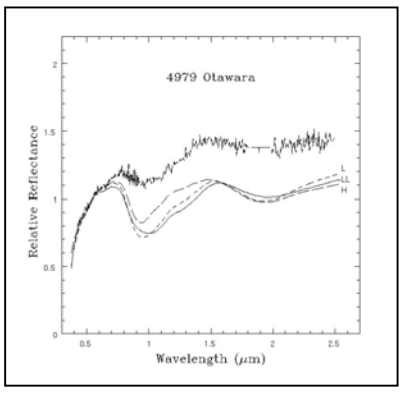

Conclusion:

Our successful experiment demonstrates a new teaching tool for students studying in astronomy. The students will be able to observe and have the observations stimulate their initiative in astronomy science. The "live" observation perception is different from a classical training exercise of astronomy in a class room and is a far more attractive opportunity for students. Within a small budget, a student can be able to complete the whole teaching sequence in practical astronomy, from doing their own observations, learning about the data-reduction technique, and obtaining the final scientific products.

Another important aspect of this experiment is the access of the students to time on medium and large aperture telescopes. Through remote observing participation a student gains a strong background in observational techniques as well as experience with the telescope and instruments. Students also have the potential to be involved in the scientific proposal process as a way of learning how to propose their own ideas.

Since our last run, two remote centre have been decided: one in Meudon Observatory, and the other one in Massachusetts Institute of Technology. Système d'Observations à Distance Astronomique (SODA) is the name of the remote system from Meudon Observatory, and the program was started in July 2002. MIT Remote Command Center became operational in September 2002 while Meudon Remote Command Center will become operational in February 2003.

Reference:

1. Binzel, R.P., Birlan, M., Bus, S.J., Harris, A., Rivkin, A.S., Fornasier, S.– *Spectral Observations for Near-Earth Objects Including Potential Target 4660 Nereus: Results From Meudon Observations at the NASA Infrared Telescope Facility (IRTF)*, **Planetary & Space Science** (submitted August 2002)
2. Fornasier, S., Barucci, M.A., Binzel, R.P., Birlan, M**.**, Fulchignoni, M., Barbieri, C., Bus, S.J., Harris, A.W., Rivkin, A.S., Lazzarin, M., Dotto, E., Erikson, A., Doressoundiram, A., Bertini, I., Peixinho, N., - *A portrait of 4979 Otawara, target of the Rosetta space mission*, **Astronomy & Astrophysics** (submitted April 2002)S.,

Remote observing at the NASA Infrared Telescope Facility

Schelte J. Bus[a], Anthony J. Denault[a], John T. Rayner[b], Richard P. Binzel[c], and Mirel Birlan[d]

[a]Institute for Astronomy, Univ. of Hawaii, Hilo, HI 96720
[b]Institute for Astronomy, Univ. of Hawaii, Honolulu, HI 96822
[c]Massachusetts Institute of Technology, Cambridge, MA 02139
[d]Observatoire de Paris, Meudon Cedex 92195, France

ABSTRACT

The NASA Infrared Telescope Facility (IRTF) on Mauna Kea now offers observers the opportunity to carry out their observations remotely. They can choose to work from the mid-level station at Hale Pohaku, from a dedicated remote observing room at the Institute for Astronomy in Hilo, or from their home institution. As a test of our remote capabilities, observations have been successfully obtained by observers from an office at the Observatoire de Paris in Meudon, France. Their observing program utilized SpeX, the IRTF's low- to medium-resolution near-IR spectrograph and imager, to measure the 0.8-2.5 micron reflectance spectra of fast moving, near-Earth asteroids. All target acquisition, guiding, and instrument control was commanded from Meudon. We describe this observing campaign, and provide details about the techniques we have developed for remote observing.

Keywords: remote observing

1. INTRODUCTION

The NASA Infrared Telescope Facility (IRTF) is a 3.0-m telescope located at an altitude of 4160 m, near the summit of Mauna Kea on the Big Island of Hawaii. The IRTF was established by NASA in 1979 to provide ground-based observations in support of spacecraft missions and basic solar system research. While half of the observing time on the IRTF is reserved for studies of solar system objects, observing proposals are accepted from the entire astronomical community. The IRTF receives observing proposals from astronomers across the US and from many foreign countries.

To best meet the needs of its observers while making the most efficient use of telescope time, the IRTF provides considerable flexibility in its scheduling of observing time. This scheduling puts high priority on approved programs that require time-critical observations. In addition, long-term synoptic or survey programs may be allocated several short slots of time spread over an observing season. To further enhance this flexibility in scheduling and to help relieve observers of some of the burdens (both time and cost) of traveling to Hawaii, members of the IRTF staff have been working to develop the tools and techniques required for remote observing.

When using either SpeX or NSFCAM (two of the facility instruments currently supported at the IRTF), observers now have the opportunity of carrying out their observations remotely. If they should choose to travel to Hawaii, but want to avoid the difficulties of working at the summit, observers have the option of observing from the mid-level station at Hale Pohaku (at an elevation of 2900 m on the slope of Mauna Kea), or from a dedicated remote observing room at the Institute for Astronomy in Hilo. The Hilo remote room is similar in concept to that used by other observatories on Mauna Kea[1]. Observers also have the option of working from their home institution by logging in via the Internet. To make use of this option, observers need access to a minimum level of computing power to provide sufficient connectivity to the IRTF instrument control computers: a workstation (UNIX workstation, PC with Linux, or Windows with X-terminal emulation software are acceptable platforms), dual X-windows monitors supporting 1280 x 1024 resolution in either 8-bit pseudo color or 24/32-bit true color graphics mode, a web camera with video-conferencing software, and fast (Ethernet) connection to the Internet (preferably with an average transfer rate of 100 kb/s or better). For researchers living many time zones from Hawaii, working from their home institution has the added benefit of requiring a smaller shift in sleep schedule in order to carry out nighttime observations in Hawaii.

2. ELEMENTS OF REMOTE OBSERVING

There are a number of different elements that make remote observing successful at the IRTF. The main element is the high-speed bandwidth between both our telescope and base facility, and on the Internet. Having a high-speed (>10MB Ethernet) connection between our telescope and base facility has fueled our desires to implement remote capabilities in the design and construction of instrumentation. As the Internet bandwidth and reliability has increased, it has prompted us to extend our remote observing capabilities further and further.

2.1 Remote capabilities for instrument software

Our previous generation of instrument software (used for the instruments NSFCAM and CSHELL) was developed in the early 1990s. At that time, remote observing was not considered a viable mode of operation for the IRTF. However, client-server separation and network-based communication greatly influenced our design strategy, as seen in Figure 1. The instrumentation software was separated into 3 major applications:

1. The instrument control software (IC). The IC software provides control of all instrument hardware. There are various processes for data acquisition, a command-line interpreter, motor control, temperature control, and control of other miscellaneous hardware.

2. X Windows-based User Interface (commonly referred to as the XUI). The XUI provides an easy to use interface to the IC. Command and status information is transmitted using TCP sockets. The XUI also receives data from the IC to be saved on the local workstation.

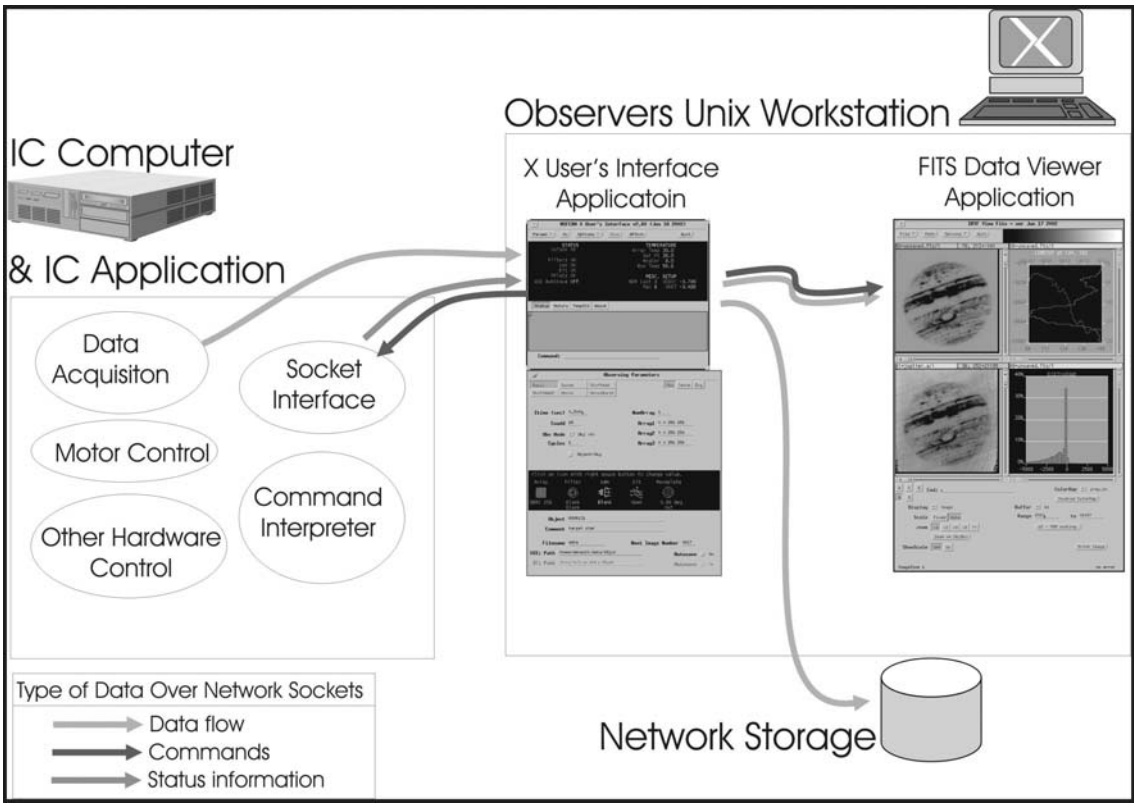

Figure 1. NSFCAM / CSHELL software model

3. A FITS Image Viewer (VF) is a stand-alone FITS data viewer with some image manipulation and graphing functions. It is able to accept commands and FITS data using TCP sockets.

These applications were designed to run on separate computers. The IC software runs in the IC computer located near the instrument, while the XUI and the data viewer run on a Unix workstation located in our observer work area. These applications exchange commands, status, and data using TCP sockets.

Although not initially designed for remote observing, as the Internet bandwidth increased, we began experimenting with running the instruments between Mauna Kea and the IfA campus in Manoa (island of Oahu), and then eventually to the mainland (continental U.S.). Observers at Lowell Observatory in Flagstaff, Arizona were the first to routinely use NSFCAM in this remote mode. By using preset macros to carry out many of the instrument operations, the real-time interaction by the observer was kept to a minimum during these earliest attempts at remote observing.

In 1998, the IRTF started building SpeX. SpeX is a medium-resolution 0.8-5.4 micron spectrograph that utilizes a 1024 x 1024 InSb array. SpeX also contains a 512 x 512 InSb array camera that can be used in imaging mode and as a slit-viewing guider[2]. When it came time to develop the SpeX software, a fundamental consideration was to include remote capabilities that would provide for both remote support and remote observing.

The software design treats SpeX as two separate instruments, a spectrograph and an imager, with each having an independent but almost identical set of software. Our basic software applications are still the Instrument Control (IC), X-User's Interface (XUI), and FITS data viewer (now renamed as DV).

Some slight design changes were implemented to allow for remote observing, depicted in Figure 2.

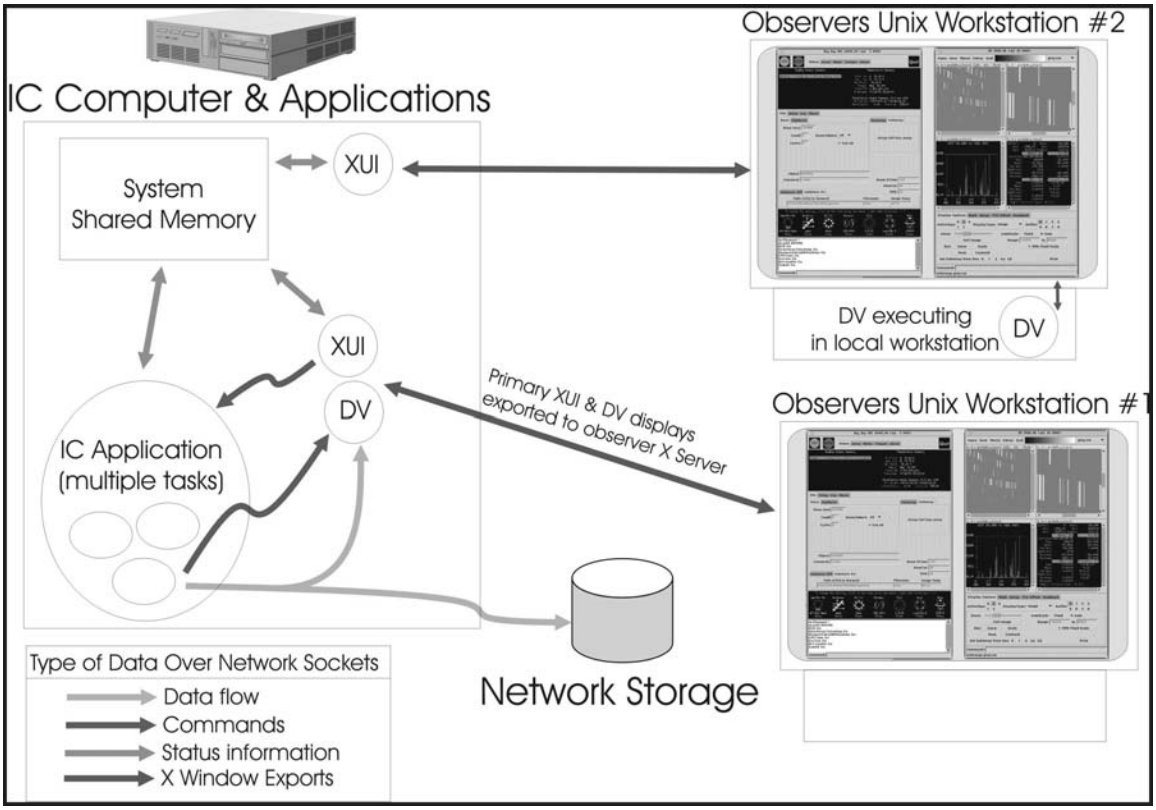

Figure 2. Illustration of the SpeX software design.

The key decisions in the design were:

1. The IC computer should be able to run the IC, XUI, and DV application. For our instrument computer, we selected a VME-based SPARC single-board computer. Our array image acquisition is controlled from VME DSP co-processor boards. Thus, our SPARC host can function as both the IC computer and XUI computer, and all our software applications can run from a single host. The IC application still handles all instrument control. The IC saves its data as FITS files and can write FITS images to sockets. The IC can be configured to send data to up to two DV data ports (TCP sockets). These data ports can be located on the local host or a remote host.

2. The IC and XUI now must run in the same computer. A shared memory area is used to hold all instrumentation parameters. The IC has read and write access, while the XUI has only read access. Commands are generated via the XUI and passed to an IC message queue. The XUI display is normally exported to the observer's workstation. For the purpose of trouble-shooting and observer support, multiple instances of the XUI can now be exported to different hosts.

3. Multiple instances of the data viewer are now possible within the same computer, or DV can be executed on a remote host. This provides the option of exporting the DV X-display from our instrument host or running DV on the observer's workstation.

2.2 Video conferencing

The IRTF is equipped with the following video conferencing system:

1. A Polycom ViewStation FX H.232 unit and 27" TV monitor at the telescope. This monitor and camera can be positioned at different locations within the warm room area occupied by the telescope operator and observer. The field of view and camera angle can be controlled either locally or by an observer working in the dedicated remote room in Hilo.

2. A Polycom ViewStation FX H.232 unit and 27" TV monitor in the Hilo remote observing room, shown in Figure 3. Field of view and camera angle can be remotely controlled from the summit.

Figure 3. Picture of the IRTF Hilo Remote Observing Room. Close up of Polycom unit communicating with telescope operator (left) and observer (right) on the summit.

The remote observers have the option of communicating with the telescope operators or other observing personnel (local observers) via these Polycom units. The remote site must have compatible equipment at their end. However, H.232 is a widely supported audio/video-over-IP protocol that is supported by many video conferencing products. The simplest client can be a PC with a video camera running Microsoft NetMeeting. While the Polycom ViewStation is an example of specialized equipment with higher quality and more advanced options than are available on common web cameras, we have found that remote observers can connect in using NetMeeting, usually with quite good results.

2.3 TCS1 status window

Operation of the IRTF still relies on the original Telescope Control System (TCS) that was built in the 1970s. It is not surprising, therefore, that the TCS is incapable of providing any type of remote services. However, we have developed a simple TCS status window tool that provides some telescope control similar to that of a hardware hand paddle. This window is shown in Figure 4.

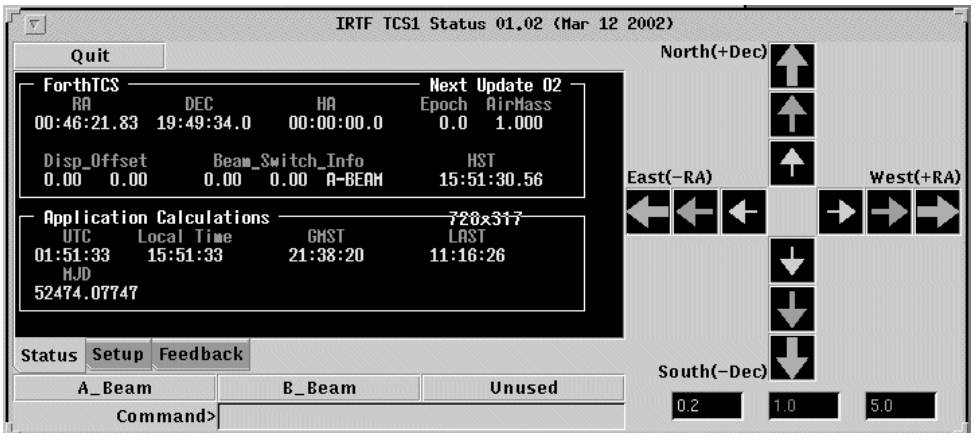

Figure 4. TCS status window.

The TCS1 status window provides a display of the current telescope position, time, and corresponding pointing parameters. Below the status display are buttons that allow the user to execute beam switches and input simple telescope control commands. To the right of the display are multi-colored arrow buttons for offsetting the telescope, a kind of virtual hand paddle. The multiple guide buttons were included to provide different step sizes (in arcseconds) that can be defined by the user.

3. EXPERIMENT IN REMOTE OBSERVING

A significant test of our remote observing capabilities came in January 2002 when observations were successfully obtained by Binzel and Birlan from an office at the Observatoire de Paris in Meudon, France, 11 time zones (about 12,070 km) from Mauna Kea. Their observing program used SpeX in its low-resolution prism mode to measure the 0.8 – 2.5 micron reflectance spectra of faint near-Earth asteroids. All aspects of target acquisition, guiding and instrument control were successfully commanded from Meudon for 2.5 nights. As the support astronomer and scientific collaborator on this project, Bus was present at the telescope throughout this run, but did little to intervene in the observations once all pieces of the remote observing system were up and running. His presence at the telescope was to accompany the telescope operator (thus fulfilling the Mauna Kea mandatory 2-person rule at the summit), and as a precaution in case there was a loss in Internet connectivity. As it turned out, the connection to Meudon was virtually flawless for the entire run.

The observatory at Meudon has a 6 Mb/s Ethernet link into the Internet, and currently experiences average transfer rates of 50-60 kb/s. The equipment used consisted of two SPARC workstations and a PC with a web camera. The workstations were used to display the XUI and DV windows exported by both the spectrograph and imager/guider ICs for SpeX. The TCS1_Status window was also used to monitor the pointing status of the telescope and to allow guiding corrections as necessary. An additional X-term window was used to command focus changes on the telescope. Audio/video conferencing was achieved using Microsoft NetMeeting that was installed on a PC located near the workstations. A measure of the time delay for the echo heard over the Polycom at the telescope revealed that the round-trip audio signal takes about 0.5 seconds, but the video transmission tended to be much slower. The video component would also freeze, often for several seconds before refreshing. This regular loss of video signal had no significant impact on the overall operation of either the telescope (operated from the summit) or the instrument (operated from Meudon), and did not effect the level of scientific output.

Due to their close proximity to Earth, the asteroids that were observed during this run had large non-sidereal motions. While the telescope drive rates were adjusted to compensate for much of this motion, small guiding corrections needed to be regularly applied. For the brighter asteroids, this was accomplished automatically by the auto-guiding software that is part of the SpeX imager. For the faintest targets, however, guide corrections needed to be made by hand using the software guide paddle in the TCS1_Status window. Since the integration times used for the guider images (typically 5 s or longer) were significantly longer than the image transmission time to Meudon (~ 1 s), there was no loss in guiding resolution by making these corrections from Meudon. Binzel and Birlan were able to guide the telescope just as if they were present on the summit.

Images of the spectral data were also transmitted to Meudon in real time via the DV window, while the FITS images (each measuring about 4 Mb) were stored on a local disk at the telescope. This data was archived at the IRTF and transferred to Meudon via ftp for analysis at the end of the observing run.

Three additional IRTF observing runs have been carried out remotely from Meudon by Binzel and Birlan with results comparable to their first attempt. Minor difficulties were encountered, especially in the ability to carry out video conferencing, due to the addition of a secure firewall at the IRTF and modifications to the firewall in Meudon. These changes in security meant that connections needed to be tested and troubleshot prior to each observing run.

The four successful runs carried out from Meudon provided a valuable learning experience and have helped us refine many aspects of our remote observing strategy. We realize that the most significant factor related to our capabilities for remote observing is the bandwidth and reliability of the Internet. The results we have achieved thus far are very encouraging and should only improve over time as the Internet grows. We anticipate that within a couple of years, the majority of observers using the IRTF will be making their observations remotely, in many cases without traveling any farther than to their office.

4. REFERENCES

1. R. I. Kibrick, S. L. Allen, and A. Conrad, “Remote observing with the Keck Telescope from U.S. mainland”, *Proc. SPIE* **4011**, pp. 84-92, 2000.
2. J. T. Rayner, D. W. Toomey, P. M. Onaka, A. J. Denault, W. E. Stahlberger, D. Y. Watanabe, and S.-I. Wang, “SpeX: a medium-resolution IR spectrograph for IRTF”, *Proc. SPIE* **3354**, pp. 468-479, 1998.

I.2. Photométrie des petits corps

Pendant mes recherches, j'ai employé plusieurs type de détecteurs, notamment la camera CCD et le photomètre photoélectrique, pour les problèmes liés à la photométrie.

Dans le cas des objets sans atmosphère, la technique de photométrie d'ouverture, dans le cas d'un photomètre à un seul détecteur, comporte une certaine séquence (observation de l'objet, du fond du ciel à coté de l'objet, suivie par une observation de l'étoile de comparaison), qui introduit des erreurs dues aux variations de l'atmosphère, durant cette courte période. Pour avoir une bonne précision, il faut alterner le plus rapidement possible les observations de l'astéroïde et de l'étoile de comparaison. L'équipement photoélectrique est capable de détecter des variations de luminosité nettement plus petites que celles obtenues avec la photométrie photographique. Cette technique est cependant de moins en moins utilisée dans les observations actuelles en raison d'une manipulation un peu difficile en comparaison de celles nécessitées par les technique nouvelles (photométrie CCD).

Les CCD constituent une famille de récepteurs à semi-conducteurs basés sur l'effet photoélectrique. De nos jours, les CCD ont quasiment remplacés (dans leur intervalle de longueur d'onde) les autres types de détecteurs sur des télescopes de grande, moyenne et petite taille et permettent de faire des observations d'objets sans atmosphère du système solaire, peu lumineux. Un autre avantage notable de l'utilisation des caméras CCD est la possibilité (voir nécessité) d'un post-traitement des images obtenues. Plusieurs techniques de traitement/réduction en chaîne (pipe-lines) se sont développées afin d'obtenir les résultats finaux.

En première instance, les observations photométriques nous permettent d'en déduire la magnitude des objets, ainsi que leur couleurs. La variation temporelle de la magnitude nous mène à la courbe de lumière de l'objet avec, en première approche, l'obtention de la période de rotation propre de l'objet. L'observation de l'une ou de plusieurs courbes de lumières du

même objet, à différentes oppositions et géométries, permet d'en déduire la position du pôle de l'objet et d'obtenir des informations sur la morphologie et la forme de l'objet. D'autre part, les différentes couleurs obtenues pour des objets distincts permettent une conclusion provisoire concernant les propriétés physiques de leur surfaces.

Les observations photométriques effectuées pendant mes recherches se sont inscrites sur trois programmes distincts :

- la photométrie des astéroïdes cibles de la mission spatiale Rosetta ;
- la photométrie des astéroïdes de petite taille (diamètre inférieur à 50 km) de la ceinture principale ;
- la photométrie des astéroïdes de période de rotation propre très longue ;

Au total j'ai observé 55 courbes de lumière, pour 21 astéroïdes dont 19 sont des astéroïdes de petite taille (Birlan et al, PSS, 1996, Florczack et al, 1997). J'ai pu obtenir environ 4% de l'ensemble des périodes de rotation déterminées jusqu'à maintenant, pour les astéroïdes de petite taille. C'est la première fois que l'on estime la période de ces astéroïdes. La plage des périodes de rotation propre obtenues est très large, entre 2.4 heures et 35 heures. Dans le cas des astéroïdes à période de rotation courtes, j'ai employé une nouvelle technique, avec un échantillonnage des images plus rapide. Les courbes de lumière présentent des amplitudes dans l'intervalle 0.2-1.0 magnitudes. Les observations ont permis de résoudre la courbe de lumière des deux astéroïdes censés avoir une longue période.

L'étude statistique des périodes de rotation sur l'ensemble des astéroïdes de petite taille montre que la distribution expérimentale/observée peut être reproduite par une combinaison des trois distributions de type Maxwell.

Parmi les astéroïdes observés, sept astéroïdes ont été des candidats au survol par la mission spatiale ROSETTA (Doressoundiram et al, A&A, 1999). Ces observations font partie du programme de préparation au sol de la mission, afin d'avoir une meilleure connaissance de la physique des candidats. Même si ces candidats ne sont pas retenus, les résultats obtenus sont importants pour la population astéroïdale dans son ensemble, permettant ainsi de mieux préciser les conditions de formation du Système Solaire.

Les couleurs et les spectres obtenus pour 4979 Otawara, astéroïde cible de ROSETTA, et 9969 Braille, astéroïde cible de la mission DEEP SPACE 1 (Lazzarin et al, A&A, 2001) ont permis de les classer dans les classes taxonomiques des astéroïdes avec une évolution thermique importante (types taxonomiques S, V, Q)

L'imagerie CCD de comètes représente un volet particulier des activités d'observations. Ainsi, les observations de la comète Hyakutake ont permis l'obtention de paramètres tels que la configuration de l'environnement au voisinage du noyau et l'orientation de la queue.

Références :

Birlan M., Barucci M.A., Angeli C., Doressoundiram A., DeSanctis M.C. - *Rotational properties of asteroids: CCD observations of nine small asteroids* **Planetary and Space Science** vol. **44**, n. **6**, 555-558, 1996.

Florczak M., Dotto E., Barucci M.A., **Birlan M.**, Erikson A., Fulchignoni M., Nathues A., Perret L., Thebault P. - *Rotational properties of main belt asteroids: Photoelectric and CCD observations of 15 objects* **Planetary and Space Science** vol. **45**, n. **11**, 1423-1435, 1997.

Doressoundiram A., Weissman P.R., Fulchignoni M., Barucci M.A., LeBras A., Colas F., Lecacheux J., **Birlan M.**, Lazzarin M., Fornasier S., Dotto E., Barbieri C., Sykes M.V., Larson S., Hergenrother C. - *4979 Otawara: Flyby target of the Rosetta mission* **Astronomy & Astrophysics** , vol **352**, n. **2**, 697-702, 1999.

Lazzarin M., Fornasier S., Barucci M.A., **Birlan M.** - *Groundbased investigation of asteroid 9969 Braille, target of the spacecraft mission Deep Space 1* **Astronomy and Astrophysics**, n. **375**, 281-284, 2001.

Vaduvescu 0., Stefanescu G., **Birlan M.** - *CCD and photographic observations of the comet C/1996B2 (Hyakutake)* **Romanian Astronomical Journal**, vol. **8**, 43-51, 1998.

Pergamon
Planet. Space Sci., Vol. 44, No. 6, pp. 553–558, 1996

0032–0633/96 $15.00+0.00

PII: S0032–0633(96)00019–0

Rotational properties of asteroids: CCD observations of nine small asteroids

M. Birlan,[1,2] M. A. Barucci,[2] C. A. Angeli,[2] A. Doressoundiram[2] and M. C. De Sanctis[3]

[1]Astronomical Institute of the Romanian Academy, str Cutitul de Argint-5, Bucharest 28, Romania
[2]Observatoire de Paris, 92195 Meudon Principal Cedex, France
[3]Univ. of Rome, Istituto Astronomico, Via Lancisi 29, 00161 Rome, Italy

Received 24 November 1995; revised 30 January 1996; accepted 30 January 1996

Abstract. The observational programme on small asteroids (diameter less than about 50 km) is continued to enlarge the available dataset of small asteroids. The results are presented of CCD observations of nine small asteroids ($D \leq 23$ km), performed in France with the 1.2 m telescope at Haute Provence Observatory and with the 2 m telescope at Pic du Midi Observatory. A total of 27 single night lightcurves for nine asteroids were obtained. All the objects were observed for the first time and rotational periods have been determined for all of the observed asteroids: 1992 Galvarino ($P_{syn} = 7^h.004$), 2419 Moldavia ($P_{syn} = 2^h.412$), 2921 Sophocles ($P_{syn} = 4^h.778$), 3247 Di Martino ($P_{syn} = 5^h.445$), 3623 Chaplin ($P_{syn} = 8^h.361$), 3986 Rozhkovskij ($P_{syn} = 4^h.26$), 4436 1983 EX ($P_{syn} = 6^h.656$), 5046 1981 DQ ($P_{syn} = 6^h.050$) and 1992 YG3 ($P_{syn} = 8^h.91$).

Introduction

The study of asteroid spin rates may provide information on the collisional evolution of main belt asteroids. Fulchignoni *et al.* (1995) have performed a statistical analysis of asteroid rotational periods and reanalysed the rotational rate distribution of a whole "high quality" sample of 516 asteroids. They found that the small object population ($D \leq 50$ km) can be represented by a linear combination of three Maxwellian functions which have been interpreted in terms of collisional evolution of the asteroid population. However, the present sample of asteroid rotations is still poor in the small diameter range and some bias exists. For this reason, we continue our observational campaigns aiming to determine the rotational properties of small asteroids.

In this paper, the results of CCD observations of nine small asteroids ($D \leq 23$ km), carried out in France at Haute Provence Observatory and Pic du Midi Observatory, using respectively the 1.2 and 2 m telescopes, are presented. The aspect data are listed in Table 1, where in the last column we have reported the mean magnitude level V(1,α), which corresponds to the zero level on the composite lightcurve plots. In Table 2 we summarize the values found for the synodic rotational period, the amplitude of the lightcurve, and the diameters (Tholen, 1992). The reported observations are not corrected for the light-time.

Observations and data reduction

Observations have been carried out in the V band, with the 2 m telescope (Pic du Midi Observatory) in January 1993, for the asteroid 1992 YG3, and with the 1.2 m telescope (Haute Provence Observatory) between April and October 1995 for the other objects. The transformation to the V magnitude has been carried out observing groups of standard stars (Landolt, 1983). When the conditions of the sky were not photometric, the data were reduced only taking into account the differential extinction between the asteroid and the comparison star.

For the nine observed asteroids we determined the synodic rotational period, and the corresponding uncertainty, by applying Fourier analysis as described in Harris *et al.* (1989). The composite lightcurves of the observed asteroids are presented in Figs 1–9.

Results

1992 Galvarino, considered by ESA as one of the alternative candidates of the Rosetta mission, was observed

Correspondence to: A. Barucci

Table 1.

Date 0 UT	R.A. 2000.0 h m s	Decl. 2000.0 ° ′	Long 2000.0	Lat. 2000.0	r AU	Δ AU	Phase deg	$V(1,\alpha)$ mag
1992 Galvarino								
1995 09 26	03 28 29.5	+10 37.8	52.4	−8.0	3.058	2.320	14.63	10.35
1995 09 27	03 28 21.4	+10 32.9	52.4	−8.0	3.058	2.310	14.41	10.35
1995 09 28	03 28 12.0	+10 27.8	52.3	−8.1	3.059	2.300	14.18	—
1995 09 29	03 28 01.2	+10 22.7	52.2	−8.2	3.059	2.290	13.94	—
2419 Moldavia								
1995 09 26	01 17 05.9	+03 09.5	18.9	−4.6	2.168	1.190	7.81	11.50
1995 09 27	01 16 22.4	+03 00.4	18.7	−4.6	2.168	1.186	7.30	11.49
1995 10 02	01 12 30.1	+02 14.1	17.5	−5.0	2.163	1.171	4.81	—
2921 Sophocles								
1995 10 01	00 15 52.8	+00 17.2	3.7	−1.3	2.773	1.773	1.40	11.17
1995 10 02	00 15 10.2	+00 12.2	3.5	−1.3	2.774	1.775	1.80	—
3247 Di Martino								
1995 09 28	01 15 04.5	+04 21.8	18.9	−3.3	2.680	1.698	5.50	—
1995 09 29	01 14 10.9	+04 17.2	18.7	−3.3	2.679	1.695	5.07	—
1995 09 30	01 13 16.5	+04 12.6	18.5	−3.2	2.679	1.693	4.64	10.96
3623 Chaplin								
1995 10 01	23 12 23.0	−09 25.5	345.3	−3.9	2.615	1.661	8.37	10.43
1995 10 02	23 11 45.9	−09 29.3	345.2	−3.9	2.615	1.667	8.77	—
3986 Rozhkovskij								
1995 09 26	22 46 25.0	+01 05.7	343.4	+8.2	2.231	1.265	9.13	10.93
1995 09 27	22 45 35.9	+01 00.0	343.2	+8.2	2.230	1.268	9.60	10.93
4436 1983 EX								
1995 04 26	13 58 37.8	+11 44.5	203.1	+22.2	3.292	2.354	7.49	11.93
1995 04 27	13 57 51.7	+11 45.3	202.9	+22.2	3.293	2.357	7.64	11.94
1995 04 28	13 57 05.9	+11 45.9	202.7	+22.1	3.293	2.360	7.79	11.97
5046 1981 DQ								
1995 09 28	22 47 47.9	+10 03.2	347.3	+16.3	2.478	1.527	9.28	—
1995 09 29	22 47 12.7	+09 52.6	347.1	+16.2	2.478	1.530	9.57	—
1995 09 30	22 46 38.6	+09 41.9	346.9	+16.1	2.477	1.533	9.88	11.35
1992 YG3								
1993 01 17	07 57 55.6	+20 19.8	117.4	−0.3	2.701	1.717	0.22	—
1993 01 19	07 56 10.7	+20 26.1	117.0	−0.3	2.699	1.716	0.72	—
1993 01 20	07 55 18.2	+20 29.2	116.8	−0.3	2.699	1.716	1.16	—
1993 01 21	07 54 25.8	+20 32.3	116.6	−0.2	2.698	1.716	1.61	—
1993 01 22	07 53 33.6	+20 35.4	116.4	−0.2	2.698	1.717	2.05	—

Table 2.

Asteroid	Rot. period (h)	Amplitude (mag)	D (km)
1992 Galvarino	7.004±0.003	≥0.59	10.50
2419 Moldavia	2.412±0.003	0.14±0.03	7.28
2921 Sophocles	4.778±0.005	0.16±0.04	8.35
3247 Di Martino	5.445±0.006	0.51±0.05	17.70
3623 Chaplin	8.361±0.005	0.97±0.02	13.80
3986 Rozhkovskij	4.26±0.03	0.26±0.05	10.50
4436 1983 EX	6.656±0.006	0.40±0.05	23.00
5046 1981 DQ	6.050±0.003	0.21±0.03	11.50
1992 YG3	8.91±0.03	0.36±0.05	15.10

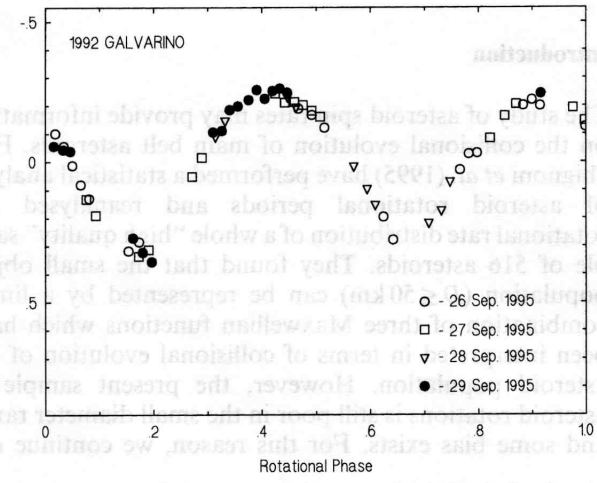

Fig. 1. Composite lightcurve of the asteroid 1992 Galvarino in rotational phase. 0 phase corresponds to UT 1995 Sep. 26, $3^h.012$

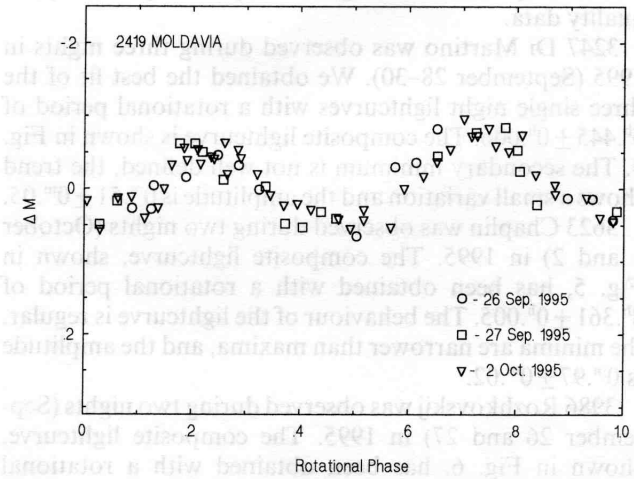

Fig. 2. Composite lightcurve of the asteroid 2419 Moldavia in rotational phase. 0 phase corresponds to UT 1995 Oct. 2, $0^h.205$

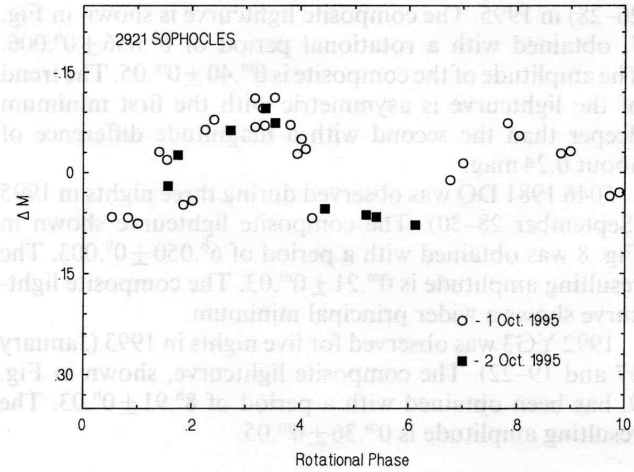

Fig. 3. Composite lightcurve of the asteroid 2921 Sophocles in rotational phase. 0 phase corresponds to UT 1995 Oct. 1, $0^h.279$

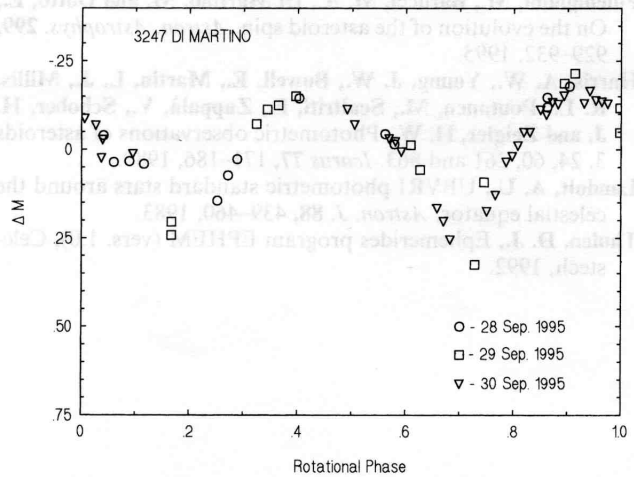

Fig. 4. Composite lightcurve of the asteroid 3247 Di Martino in rotational phase. 0 phase corresponds to UT 1995 Sep. 28, $2^h.239$

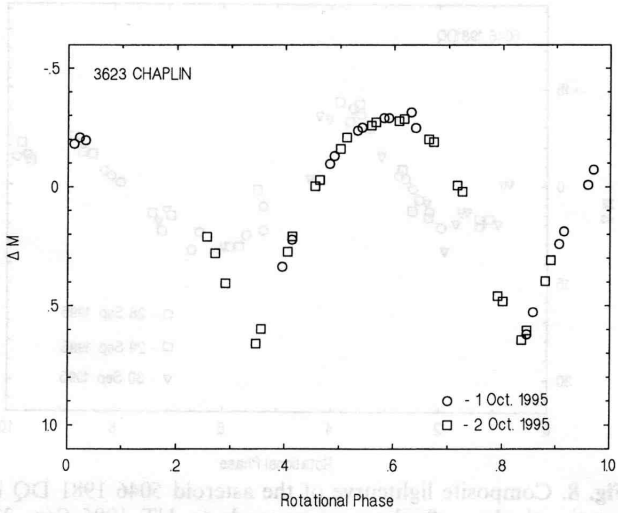

Fig. 5. Composite lightcurve of the asteroid 3623 Chaplin in rotational phase. 0 phase corresponds to UT 1995 Oct. 1, $0^h.185$

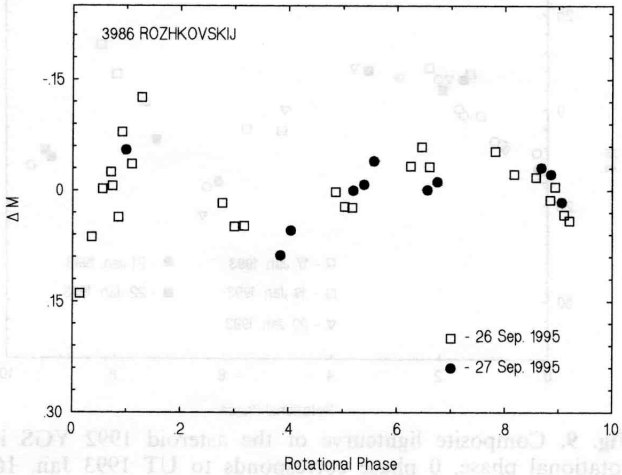

Fig. 6. Composite lightcurve of the asteroid 3986 Rozhkovskij in rotational phase. 0 phase corresponds to UT 1995 Sep. 26, $19^h.743$

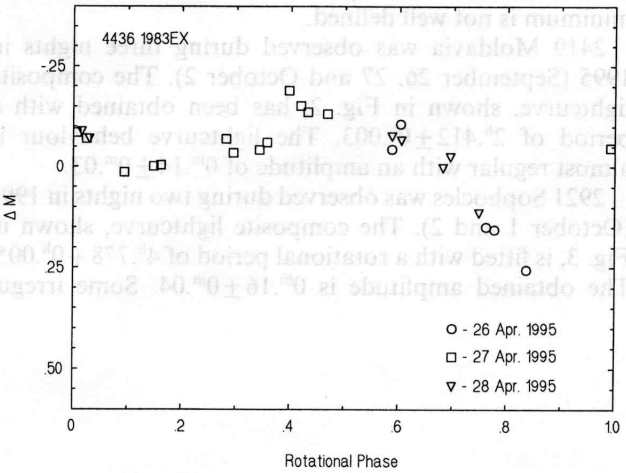

Fig. 7. Composite lightcurve of the asteroid 4436 1983 EX in rotational phase. 0 phase corresponds to UT 1995 Apr. 25, $21^h.366$

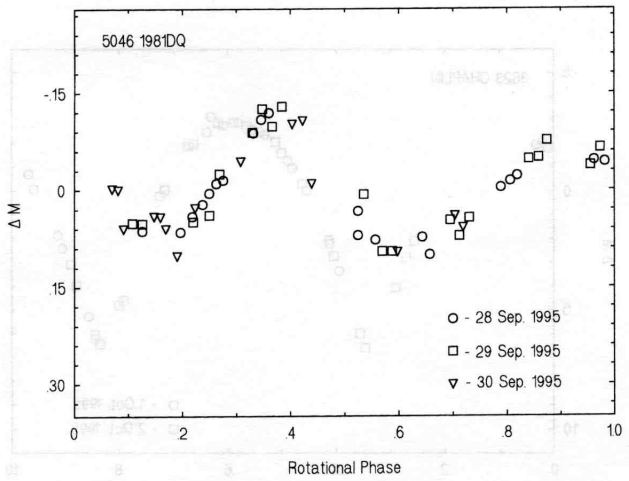

Fig. 8. Composite lightcurve of the asteroid 5046 1981 DQ in rotational phase. 0 phase corresponds to UT 1995 Sep. 27, $23^h.611$

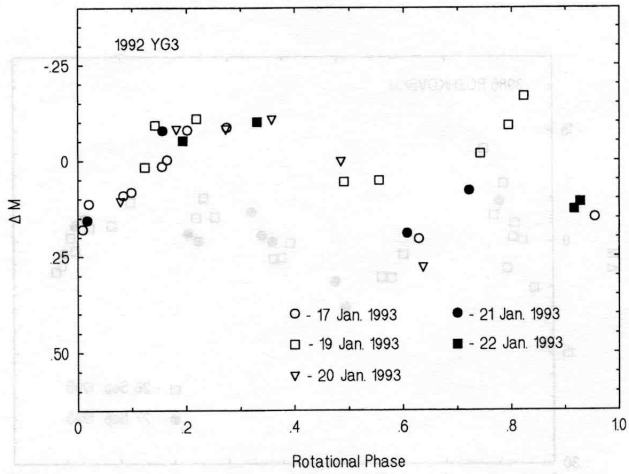

Fig. 9. Composite lightcurve of the asteroid 1992 YGS in rotational phase. 0 phase corresponds to UT 1993 Jan. 16, $17^h.784$

during four nights in 1995 (September 26–29). The composite lightcurve, fitted with a period of $7^h.004 \pm 0^h.003$, is shown in Fig. 1. The lightcurve amplitude can be larger than $0^m.59$ and seems symmetric even if the secondary minimum is not well defined.

2419 Moldavia was observed during three nights in 1995 (September 26, 27 and October 2). The composite lightcurve, shown in Fig. 2, has been obtained with a period of $2^h.412 \pm 0^h.003$. The lightcurve behaviour is almost regular with an amplitude of $0^m.14 \pm 0^m.03$.

2921 Sophocles was observed during two nights in 1995 (October 1 and 2). The composite lightcurve, shown in Fig. 3, is fitted with a rotational period of $4^h.778 + 0^h.005$. The obtained amplitude is $0^m.16 \pm 0^m.04$. Some irregularities are present in the lightcurve, probably due to poor quality data.

3247 Di Martino was observed during three nights in 1995 (September 28–30). We obtained the best fit of the three single night lightcurves with a rotational period of $5^h.445 \pm 0^h.006$. The composite lightcurve is shown in Fig. 4. The secondary minimum is not well defined, the trend shows a small variation and the amplitude is $0^m.51 \pm 0^m.05$.

3623 Chaplin was observed during two nights (October 1 and 2) in 1995. The composite lightcurve, shown in Fig. 5, has been obtained with a rotational period of $8^h.361 \pm 0^h.005$. The behaviour of the lightcurve is regular, the minima are narrower than maxima, and the amplitude is $0^m.97 \pm 0^m.02$.

3986 Rozhkovskij was observed during two nights (September 26 and 27) in 1995. The composite lightcurve, shown in Fig. 6, has been obtained with a rotational period of $4^h.26 \pm 0^h.03$. The computed lightcurve shows an amplitude of $0^m.26 \pm 0^m.05$ and an irregular trend with fluctuations probably due to poor quality data. Other possible periods cannot be excluded.

4436 1983 EX was observed during three nights (April 26–28) in 1995. The composite lightcurve is shown in Fig. 7, obtained with a rotational period of $6^h.656 \pm 0^h.006$. The amplitude of the composite is $0^m.40 \pm 0^m.05$. The trend of the lightcurve is asymmetric with the first minimum deeper than the second with a magnitude difference of about 0.24 mag.

5046 1981 DQ was observed during three nights in 1995 (September 28–30). The composite lightcurve shown in Fig. 8 was obtained with a period of $6^h.050 \pm 0^h.003$. The resulting amplitude is $0^m.21 \pm 0^m.03$. The composite lightcurve shows a wider principal minimum.

1992 YG3 was observed for five nights in 1993 (January 17 and 19–22). The composite lightcurve, shown in Fig. 9, has been obtained with a period of $8^h.91 \pm 0^h.03$. The resulting amplitude is $0^m.36 \pm 0^m.05$.

Acknowledgements. We are grateful to Dr François Colas for his assistance with the image processing ASTROL software.

References

Fulchignoni, M., Barucci, M. A., Di Martino, M. and Dotto, E., On the evolution of the asteroid spin. *Astron. Astrophys.* **299,** 929–932, 1995.

Harris, A. W., Young, J. W., Bowell, E., Martin, L. J., Millis, R. L., Poutanen, M., Scaltriti, F., Zappalà, V., Schober, H. J. and Zeigler, H. W., Photometric observations of asteroids 3, 24, 60, 261 and 863. *Icarus* **77,** 171–186, 1989.

Landolt, A. U., UBVRI photometric standard stars around the celestial equator. *Astron. J.* **88,** 439–460, 1983.

Tholen, D. J., Ephemerides program EPHEM (vers. 1.0), Celestech, 1992.

Pergamon
Planet. Space Sci., Vol. 45, No. 11, pp. 1423–1435, 1997

0032–0633/97 $17.00+0.00

PII: S0032–0633(97)00121–9

Rotational properties of main belt asteroids: photoelectric and CCD observations of 15 objects*

M. Florczak,[1,2,3] E. Dotto,[3,4] M. A. Barucci,[3] M. Birlan,[5] A. Erikson,[6] M. Fulchignoni,[3,7] A. Nathues,[6] L. Perret[3] and P. Thebault[3]

[1]ON/CNPq, Dep. Astrofísica, 20921 Rio de Janeiro, Brazil
[2]CEFET, Dep. Física, 80000 Curitiba, Brazil
[3]Observatoire de Paris, 92195 Meudon Principal Cedex, France
[4]Università di Padova, Dip. di Fisica, V. Marzolo 8, 35131 Padova, Italy
[5]Astronomical Institute of the Romanian Academy, str. Cutitul de Argint 5, Bucharest 28, Romania
[6]DLR, Institute of Planetary Exploration, Rudower Chausse 5, D-12489 Berlin, Germany
[7]Université Paris 7, Paris, France

Received 19 March 1997; accepted 20 May 1997

Abstract. In this paper we present the results of several observational campaigns carried out during 1996 at the 1.2 m telescope of the Haute Provence Observatory (France) and at the 1.5 m Danish, 0.9 m Dutch, 0.6 m Bochum and 0.5 m telescopes of the European Southern Observatory (ESO, La Silla, Chile), in order to enlarge the available sample of know asteroid rotational periods.

A total of 64 single night lightcurves for 15 asteroids were obtained. The rotational periods have been determined for 12 objects, with different quality code: 424 Gratia (P_{syn} = 19.47 h), 440 Theodora (P_{syn} = 4.828 h), 446 Aeternitas (P_{syn} = 15.85 h), 491 Carina (P_{syn} = 14.87 h), 727 Nipponia (P_{syn} = 4.6 h), 732 Tjilaki (P_{syn} = 12.34 h), 783 Nora (P_{syn} = 34.4 h), 888 Parysatis (P_{syn} = 5.49 h), 1626 Sadeya (P_{syn} = 3.438 h), 2209 Tianjin (P_{syn} = 9.47 h), 2446 Lunacharsky (P_{syn} = 3.613 h) and 3776 Vartiovuori (P_{syn} = 7.7 h). For 1246 Chaka, 1507 Vaasa and 1994 Shane the complete rotational phase was not covered and for two of them it was possible to find only an indication of the rotational period.

Introduction

The knowledge of the asteroid spin rate is an important tool to gain information on the collisional evolution state of the asteroid population. Binzel *et al.* (1989) showed that the intermediate size range is important in terms of collisional evolution: the limit between 100 km and 125 km is considered as very representative because it seems to be the transition region between the larger primordial asteroids and the population of the smaller objects which are supposed to be the fragments, results of collisional events. Fulchignoni *et al.* (1995), analysing the rotational rate distribution for a sample of 516 main belt asteroids, found, for small objects ($D \leq 50$ km), the superimposition of three sub-populations: the more populated (similar to the distribution of larger objects) and the slow and the rapid rotator ones. Harris (1996), analyzing the rotational spin of asteroids with mean diameter $D \leq 10$ km, pointed out an absence of very rapid rotators, and an excess of slow rotators: the first characteristic (cut-off for period of less than 2.25 h) seems to imply a "rubble pile" structure, while the excess of slow rotators can be due to a state of non-principal axis rotation, or "tumbling" (Harris, 1994).

In order to enlarge the available data set of asteroid spins, we are carrying out a long-term observing program.

In this paper we present 64 lightcurves of 15 asteroids, obtained during 1996 by CCD observations at the 1.2 m telescope of the Haute Provence Observatory (France) and at 0.9 m Dutch, 1.5 m Danish and 0.6 m Bochum telescopes of the European Southern Observatory (ESO, La Silla, Chile) and by photoelectric observations carried out with the 0.5 m telescope at ESO. For all the objects, with the exception of 783 Nora, lightcurves were measured for the first time. The survey has been carried out on small asteroids: 13 out of the 15 observed objects have a diameter $D < 50$ km, while the remaining objects have a diameter of about 90 km.

Two of the observed asteroids (732 Tjilaki and 2446

*Based on observations carried out at the European Southern Observatory (ESO), La Silla, Chile.

Correspondence to: M. A. Barucci. E-mail: BARUCCI@obspm.fr.

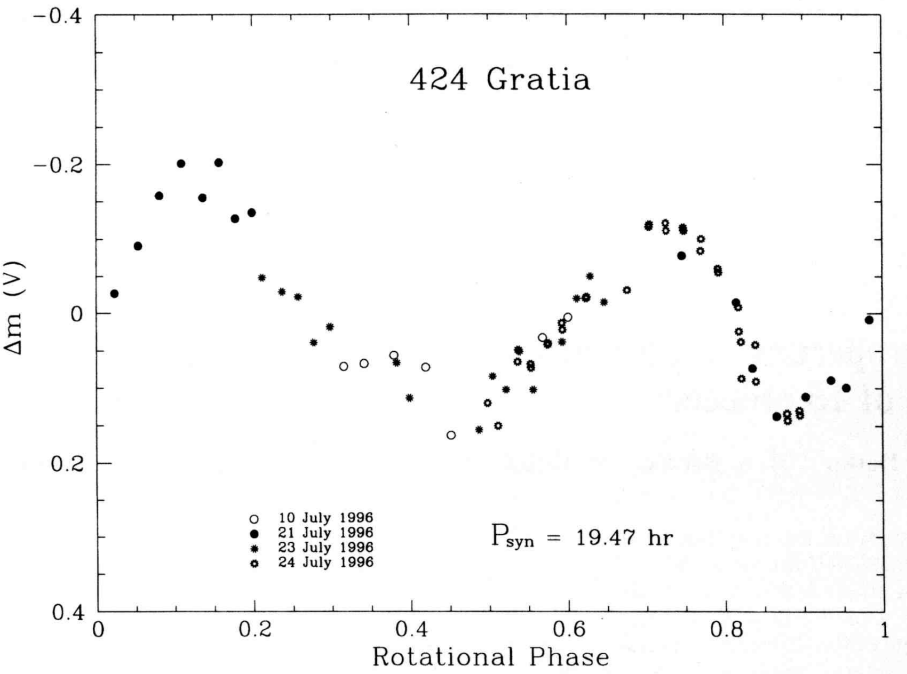

Fig. 1. Composite lightcurve of the asteroid 424 Gratia in rotational phase. Zero phase corresponds to U.T. 1996 July 22.0

Lunacharsky) are possible candidates for the Rosetta mission : 732 Tjilaki is an alternative candidate for the mission to comet P/Wirtanen, while 2446 Lunacharsky is a candidate for other Rosetta comet rendezvous opportunities (ESA, SCI(93)7).

Observations and data reduction

All the observations reported here have been obtained in the V-band. The transformation to the standard system has been carried out observing groups of standard stars, taken from the Harvard E-regions (Graham, 1982), Landolt (1983) and Guide Star Photometric Catalog (Lasker *et al.*, 1988). The data reduction procedure has been carried out using the standard method described by Hardie (1962). The photoelectric observations have been reduced using the ESO photometric reduction package RANBO2. The CCD observations have been reduced with either the software package IRAF or ASTPHOT, a synthetic aperture photometric package developed at DLR. When the conditions of the sky were not photometric, the data have been reduced only taking into account the differential extinction between the asteroid and the comparison star. The aspect data, calculated using the Ephemerides Program Ephem (version 1.1, Tholen, 1996) and the telescope used are listed in Table 1 : the mean magnitude level $V(1,\alpha)$, reported in the ninth column, corresponds to the zero level of the respective composite lightcurve. We determined the synodic rotational period, and the corresponding uncertainty for 12 asteroids, by applying Fourier analysis as described in Harris *et al.* (1989). The composite or single lightcurves of the observed asteroids, corrected for the lightime, are presented in Figs 1–15.

Results

The main results are listed in Table 2: the synodic rotational period (when determined), the corresponding reliability code (according to Harris and Young, 1983), the amplitude of the lightcurve and the diameter of each object. The observations of individual objects are discussed below.

424 *Gratia*

This asteroid was observed at the ESO during four nights (10, 21, 23, 24 July 1996) for a total of more then 30 h. The composite lightcurve, shown in Fig. 1, has been obtained with a period of 19.47 ± 0.01 h. The lightcurve is quite regular with an amplitude of 0.32 ± 0.02 mag.

440 *Theodora*

We observed this asteroid at the 0.9 m Dutch telescope of the ESO during two nights (24 and 25 July 1996) for a total of about 18 h. The composite lightcurve, shown in Fig. 2, is quite symmetric with well defined maxima and minima. The computed rotational period is 4.828 ± 0.004 h and the maximum amplitude of the light variation is 0.43 ± 0.03 mag.

446 *Aeternitas*

This asteroid was observed at the 0.5 m ESO telescope during three nights (8–10 July 1996) for a total of about

Table 1. Aspect data of the observed asteroids

Date (0 UT)	R.A. (2000)	Decl (2000)	Longi-tude (2000)	Lati-tude (2000)	r (AU)	Δ (AU)	Phase	V (mag)	Observed
424 Gratia									
96/07/10	19 34 13	−24 02 37	290.7	−2.3	2.996	1.981	1.39	—	0.5m ESO
96/07/21	19 24 11	−24 48 49	288.3	−2.7	2.988	1.982	3.35	—	0.5m ESO
96/07/23	19 22 24	−24 56 32	287.9	−2.8	2.986	1.985	4.11	—	0.5m ESO
96/07/24	19 21 31	−25 00 17	287.7	−2.8	2.985	1.988	4.49	—	0.9m Dutch ESO
440 Theodora									
96/07/24	20 08 49	−19 44 45	299.4	+0.3	2.444	1.428	0.57	—	0.9m Dutch ESO
96/07/25	20 07 43	−19 47 24	299.1	+0.4	2.444	1.428	1.07	—	0.9m Dutch ESO
446 Aeternitas									
96/07/08	19 13 18	−38 25 31	284.1	−15.9	2.484	1.491	6.47	—	0.5m ESO
96/07/09	19 12 16	−38 29 16	283.9	−15.9	2.483	1.491	6.54	—	0.5m ESO
96/07/10	19 11 13	−38 32 48	283.7	−15.9	2.483	1.491	6.64	—	0.5m ESO
91 Carina									
96/02/09	09 18 51	−00 57 21	141.7	−15.8	3.133	2.174	5.00	—	1.5m Danish ESO
96/02/10	09 18 08	−00 49 38	141.5	−15.7	3.134	2.173	4.93	—	1.5m Danish ESO
96/02/11	09 17 24	−00 41 47	141.3	−15.6	3.135	2.174	4.88	—	1.5m Danish ESO
96/02/22	09 09 50	+00 50 59	138.9	−14.7	3.145	2.195	6.07	9.6	0.6m Bochum ESO
96/02/23	09 09 12	+00 59 50	138.7	−14.7	3.145	2.199	6.29	9.6	0.6m Bochum ESO
96/02/24	09 08 35	+01 08 44	138.5	−14.6	3.146	2.203	6.52	9.6	0.9m Dutch ESO
96/02/25	09 07 58	+01 17 40	138.3	−14.5	3.147	2.208	6.76	9.6	0.9m Dutch ESO
96/02/26	09 07 22	+01 26 37	138.1	−14.4	3.148	2.212	7.00	9.6	0.9m Dutch ESO
96/02/27	09 06 47	+01 35 36	137.9	−14.3	3.149	2.217	7.26	9.6	0.9m Dutch ESO
727 Nipponia									
96/07/23	19 32 20	−14 08 50	291.8	+7.5	2.646	1.641	4.16	—	0.5m ESO
96/07/24	19 31 26	−14 16 47	291.6	+7.4	2.645	1.642	4.48	—	0.9m Dutch ESO
732 Tjilaki									
96/02/09	07 21 16	+08 27 30	109.9	−13.5	2.501	1.607	11.94	—	0.9m Dutch ESO
96/02/11	07 20 02	+08 41 53	109.6	−13.3	2.500	1.619	12.65	—	0.9m Dutch ESO
96/02/13	07 18 54	+08 56 21	109.3	−13.1	2.499	1.631	13.35	—	0.9m Dutch ESO
96/02/17	07 16 57	+09 25 20	108.7	−12.7	2.498	1.658	14.71	11.4	0.6m Bochum ESO
96/02/18	07 16 32	+09 32 34	108.6	−12.6	2.497	1.666	15.04	11.4	0.6m Bochum ESO
96/02/19	07 16 09	+09 39 47	108.5	−12.5	2.497	1.673	15.36	11.4	0.6m Bochum ESO
96/02/20	07 15 48	+09 46 58	108.4	−12.4	2.497	1.681	15.68	11.5	0.6m Bochum ESO
96/02/21	07 15 29	+09 54 07	108.3	−12.3	2.496	1.689	15.99	11.5	0.6m Bochum ESO
96/02/22	07 15 11	+10 01 15	108.2	−12.1	2.496	1.697	16.30	11.5	0.6m Bochum ESO
96/02/23	07 14 55	+10 08 21	108.1	−12.0	2.495	1.706	16.60	11.5	0.6m Bochum ESO
783 Nora									
96/02/09	09 35 16	+13 57 39	140.8	−0.3	2.805	1.819	0.71	—	0.9m Dutch ESO
96/02/10	09 34 17	+14 05 23	140.5	−0.3	2.803	1.817	0.28	—	0.9m Dutch ESO
96/02/11	09 33 19	+14 13 07	140.3	−0.2	2.802	1.816	0.22	—	0.9m Dutch ESO
96/02/17	09 27 27	+14 59 13	138.7	−0.0	2.796	1.814	2.89	11.4	0.6m Bochum ESO
96/02/18	09 26 29	+15 06 47	138.4	+0.0	2.794	1.815	3.34	11.4	0.6m Bochum ESO
96/02/19	09 25 32	+15 14 18	138.2	+0.0	2.793	1.816	3.79	11.5	0.6m Bochum ESO
96/02/20	09 24 34	+15 21 45	137.9	+0.1	2.792	1.817	4.23	11.5	0.6m Bochum ESO
96/02/21	09 23 38	+15 29 08	137.7	+0.1	2.791	1.819	4.67	11.6	0.6m Bochum ESO
96/02/22	09 22 41	+15 36 27	137.4	+0.2	2.790	1.821	5.11	11.6	0.6m Bochum ESO
96/02/23	09 21 46	+15 43 42	137.2	+0.2	2.788	1.823	5.54	11.6	0.6m Bochum ESO
96/02/24	09 20 51	+15 50 51	136.9	+0.3	2.787	1.826	5.98	11.6	0.9m Dutch ESO
96/02/25	09 19 57	+15 57 55	136.7	+0.3	2.786	1.829	6.41	11.6	0.9m Dutch ESO
96/02/26	09 19 03	+16 04 54	136.4	+0.4	2.785	1.832	6.83	11.6	0.9m Dutch ESO
96/02/28	09 17 19	+16 18 34	136.0	+0.5	2.782	1.839	7.67	11.6	0.9m Dutch ESO
888 Parysatis									
96/07/21	19 20 49	−17 42 45	288.5	+4.3	2.977	1.971	3.49	—	0.5m ESO
96/07/24	19 18 10	−18 00 21	287.9	+4.1	2.927	1.975	4 57	—	0.9m Dutch ESO
1246 Chaka									
96/10/03	00 20 14	+37 50 37	20.6	+32.3	1.882	0.968	17.32	—	1.2m OHP
96/10/04	00 19 20	+37 47 30	20.4	+32.3	1.884	0.969	17.16	—	1.2m OHP

Table 1—*Continued.*

Date (0 UT)	R.A. (2000)	Decl (2000)	Longi-tude (2000)	Lati-tude (2000)	r (AU)	Δ (AU)	Phase	V (mag)	Observed
1507 Vaasa									
96/10/05	00 35 19	+25 35 30	17.8	+19.9	1.814	0.845	11.35	—	1.2m OHP
96/10/06	00 34 24	+25 30 58	17.6	+19.9	1.816	0.846	11.18	—	1.2m OHP
1626 Sadeya									
96/02/09	07 07 14	+01 27 53	107.3	−20.9	1.903	1.021	18.29	—	1.5m Danish ESO
96/02/10	07 06 35	+01 20 09	107.1	−21.0	1.905	1.030	18.71	—	1.5m Danish ESO
96/02/11	07 05 59	+01 12 46	107.0	−21.2	1.908	1.039	19.11	—	1.5m Danish ESO
96/02/12	07 05 25	+01 05 42	106.8	−21.3	1.911	1.048	19.51	—	1.5m Danish ESO
96/02/22	07 02 13	+00 10 58	106.1	−22.3	1.939	1.148	22.96	12.5	0.6m Bochum ESO
96/02/23	07 02 08	+00 06 52	106.1	−22.4	1.942	1.159	23.26	12.5	0.6m Bochum ESO
1994 Shane									
96/10/03	00 07 31	+17 42 59	8.2	+15.4	2.198	1.217	6.99	—	1.2m OHP
96/10/04	00 06 48	+17 33 29	8.0	+15.3	2.199	1.219	7.02	—	1.2m OHP
2209 Tianjin									
96/07/25	18 12 45	−20 34 02	272.2	+2.8	2.959	2.033	9.74	—	0.9m Dutch ESO
96/07/26	18 12 08	−20 35 16	271.1	+2.8	2.959	2.039	10.07	—	0.9m Dutch ESO
2446 Lunacharsky									
96/07/12	22 03 02	−18 05 56	325.7	−5.7	2.031	1.124	17.48	—	0.9m Dutch ESO
96/07/13	22 02 42	−18 09 52	325.6	−5.7	2.032	1.117	17.04	—	0.9m Dutch ESO
3776 Vartiovuori									
96/07/12	18 07 18	−57 10 18	270.4	−33.7	3.128	2.265	11.56	—	0.9m Dutch ESO
96/07/13	18 06 05	−57 10 04	270.2	−33.7	3.129	2.269	11.69	—	0.9m Dutch ESO

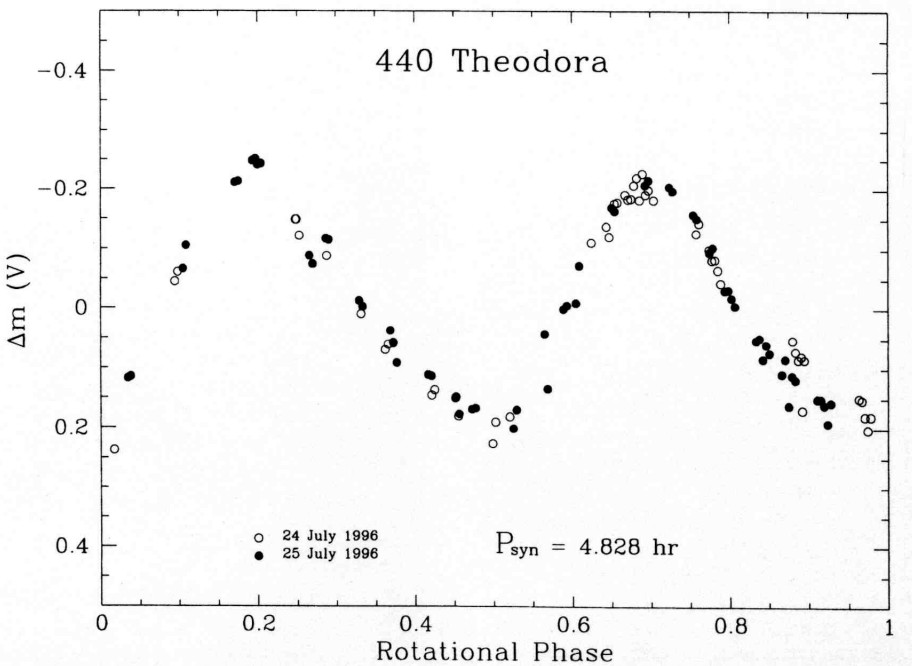

Fig. 2. Composite lightcurve of the asteroid 440 Theodora in rotational phase. Zero phase corresponds to U.T. 1996 July 25.0

Table 2. Physical parameters of the observed asteroids

Asteroid	Rotational Period (hr)	Reliability Code[a]	Amplitude (mag)	D (km)
424 Gratia	19.47±0.01	3	0.32±0.02	87[b]
440 Theodora	4.828±0.004	3	0.43±0.03	19[c]
446 Aeternitas	15.85±0.01	2	>0.33	45[b]
491 Carina	14.87±0.01	3	0.12±0.02	97[b]
727 Nipponia	4.6±0.1	1	0.14±0.02	32[b]
732 Tjilaki	12.34±0.01	3	0.19±0.03	38[b]
783 Nora	34.4±0.5	2	0.08±0.02	40[b]
888 Parysatis	5.49±0.01	3	0.23±0.02	44[b]
1246 Chaka	>20	1	—	18[b]
1507 Vaasa	>14	1	—	10[c]
1626 Sadeya	3.438±0.009	3	0.22±0.02	30[c]
1994 Shane	—	—	—	26[c]
2209 Tianjin	9.47±0.01	3	0.42±0.02	16[b]
2446 Lunacharsky	3.613±0.004	3	0.41±0.02	10[c]
3776 Vartiovuori	7.7±0.1	2	0.12±0.02	24[b]

[a]Meaning of the reliability codes:
1: the result is based on fragmentary lightcurves, may be completely wrong;
2: the result is based on less than full coverage, so that the period may be wrong by 30% or so;
3: sure result with no ambiguity and full lightcurve coverage.
[b]by IRAS (Tedesco *et al.*, 1992)
[c]estimation by Tholen (1996), based on the values of the magnitude and the location on the Solar System.

17 h. Figure 3 shows the composite lightcurve obtained with a rotational period of 15.85±0.01 h with an amplitude larger than 0.33 mag. The rotational phase is not well covered, only two minima and one maximum are defined, and therefore the period is given with a quality code 2.

491 *Carina*

We observed this object at ESO for 9 nights during 1996 for about 35 h. The composite lightcurve shown in Fig. 4 has been obtained fitting the data with a synodical period of 14.87±0.01 h. The lightcurve amplitude is 0.12±0.02 mag.

727 *Nipponia*

This asteroid was observed at the 0.5 m and 0.9 m Dutch telescopes of the ESO during two nights (23–24 July 1996). More than 11 h of observations are available, but because the poor quality of the data, only a tentative solution for the rotational period can be given. Figure 5 shows the composite lightcurve obtained with $P_{syn} = 4.6 \pm 0.1$ h and a quality code 1.

732 *Tjilaki*

This asteroid has been considered as an asteroid target in the Phase A study of the Rosetta mission for an alternative (non baseline) mission to comet P/Wirtanen. We observed this asteroid at ESO for 10 nights during February 1996 for about 35 h and the best fitting rotational period is 12.34±0.01 h. The composite light-curve obtained, shown in Fig. 6, is very asymmetric with a difference between

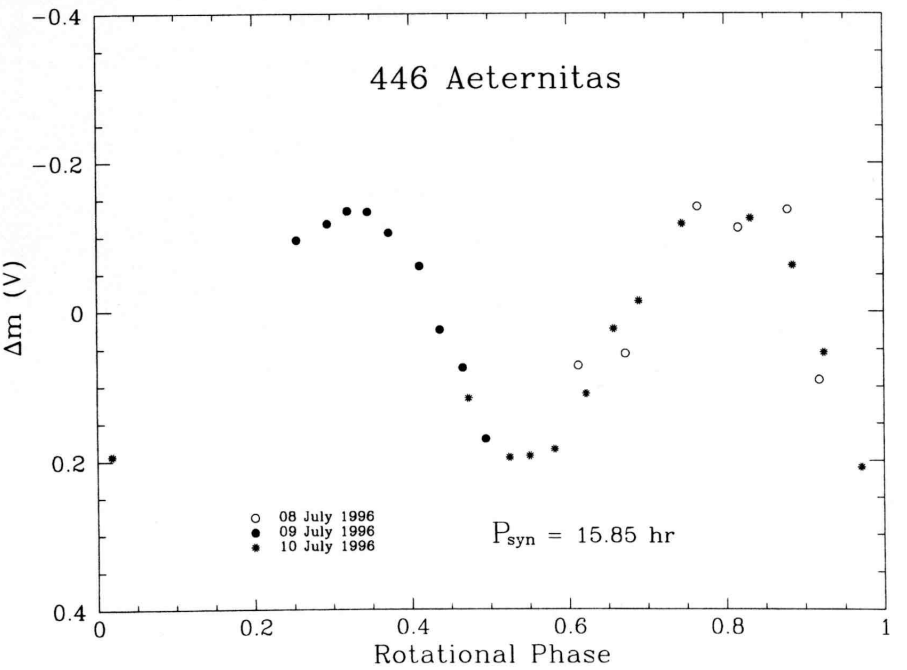

Fig. 3. Composite lightcurve of the asteroid 446 Aeternitas in rotational phase. Zero phase corresponds to U.T. 1996 July 9.0

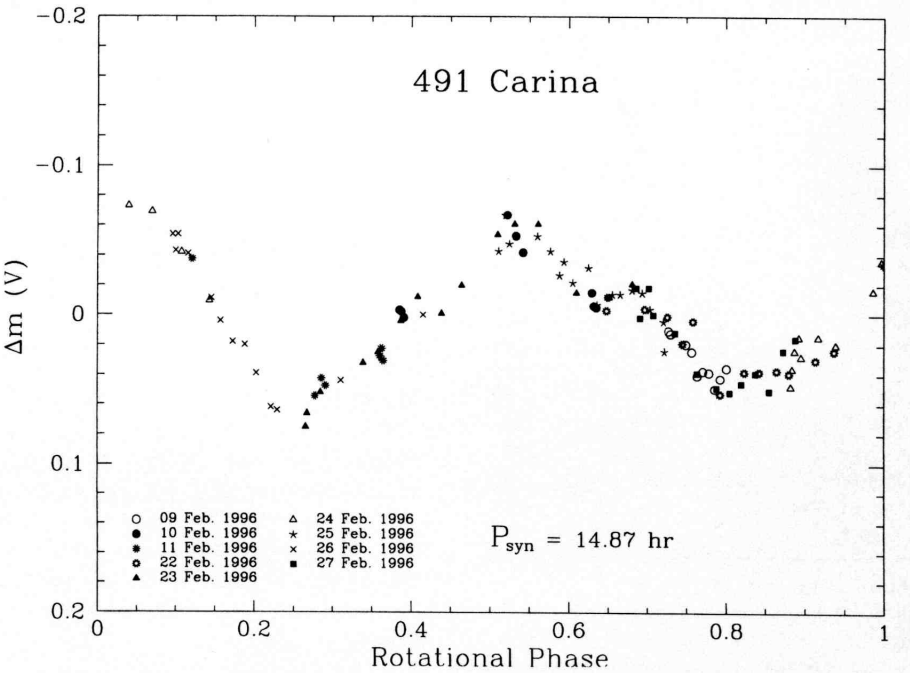

Fig. 4. Composite lightcurve of the asteroid 491 Carina in rotational phase. Zero phase corresponds to U.T. 1996 February 21.0

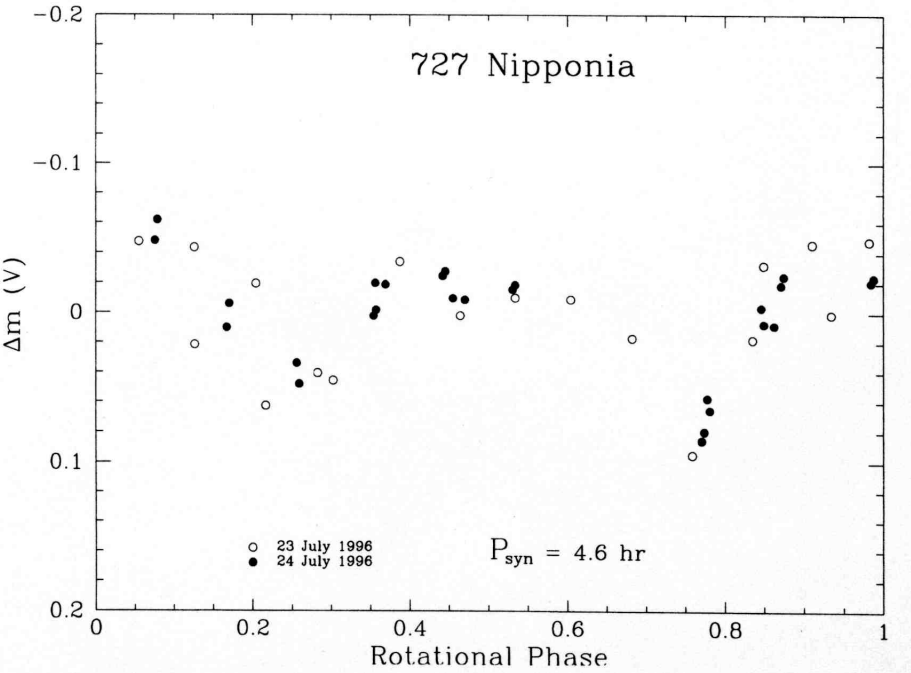

Fig. 5. Composite lightcurve of the asteroid 727 Nipponia in rotational phase. Zero phase corresponds to U.T. 1996 July 24.0

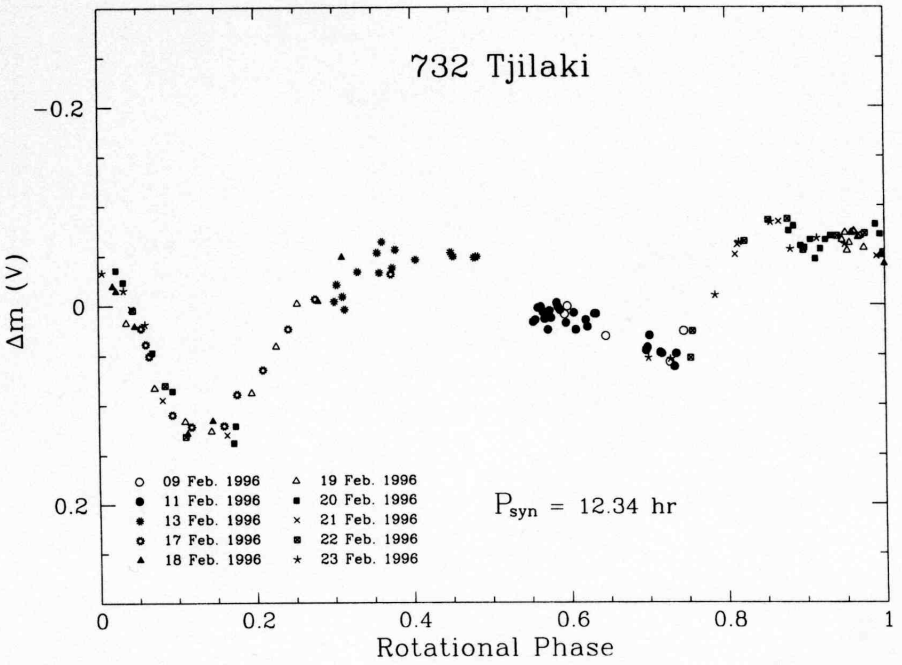

Fig. 6. Composite lightcurve of the asteroid 732 Tjilaki in rotational phase. Zero phase corresponds to U.T. 1996 February 17.0

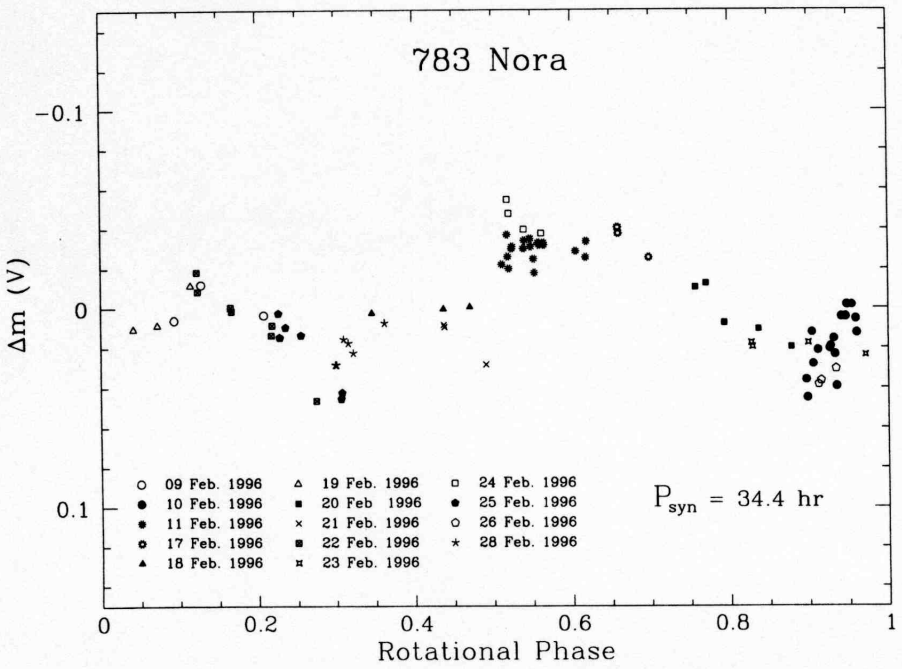

Fig. 7. Composite lightcurve of the asteroid 783 Nora in rotational phase. Zero phase corresponds to U.T. 1996 February 19.0

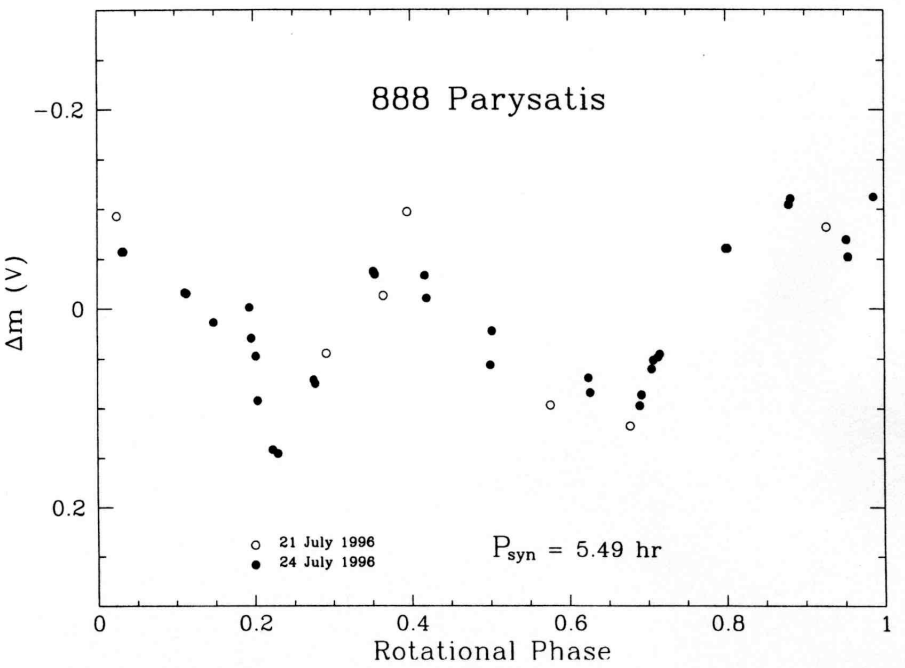

Fig. 8. Composite lightcurve of the asteroid 888 Parysatis in rotational phase. Zero phase corresponds to U.T. 1996 July 24.0

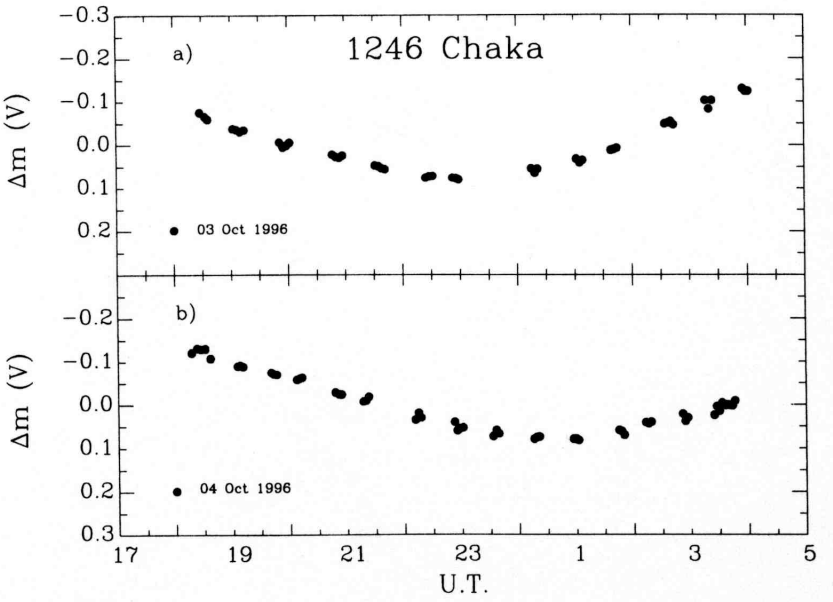

Fig. 9. Single night lightcurves of the asteroid 1246 Chaka for the nights (a) 1996, October 3 and (b) 1996, October 4

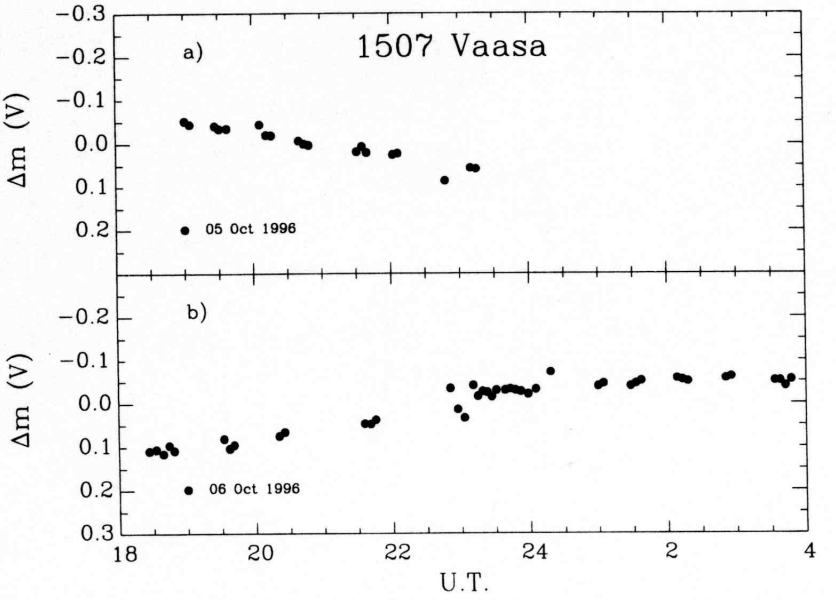

Fig. 10. Single night lightcurves of the asteroid 1507 Vaasa for the nights (a) 1996, October 5 and (b) 1996, October 6

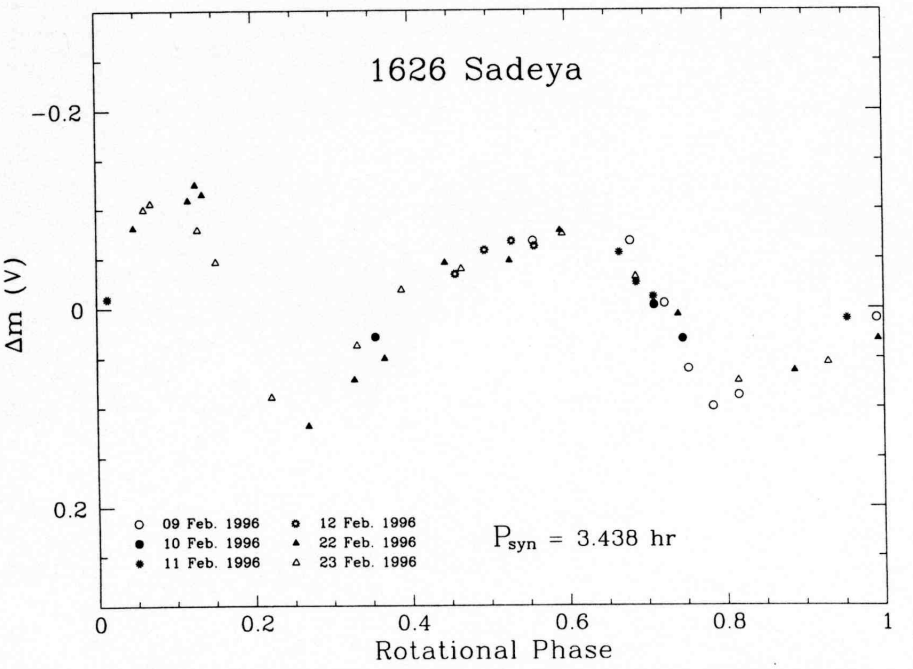

Fig. 11. Composite lightcurve of the asteroid 1626 Sadeya in rotational phase. Zero phase corresponds to U.T. 1996 February 17.0

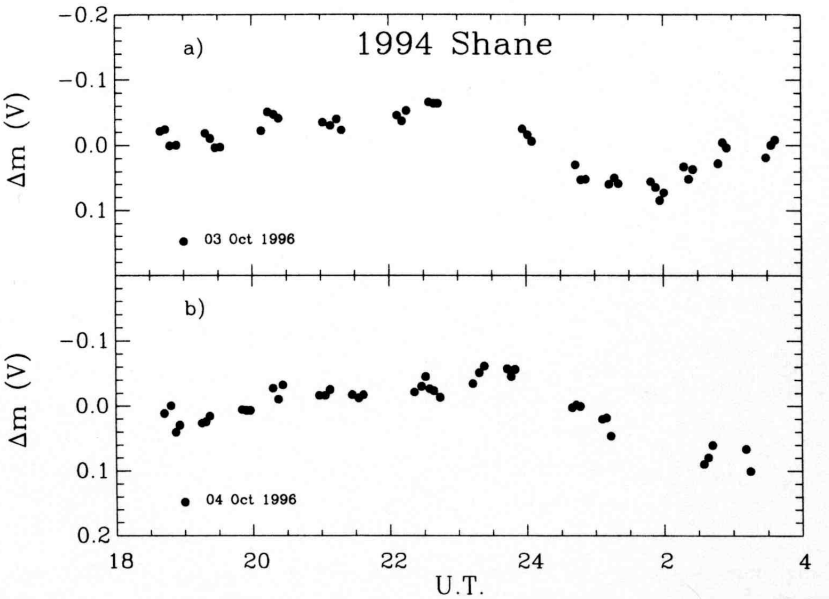

Fig. 12. Single night lightcurves of the asteroid 1994 Shane for the nights (a) 1996, October 3 and (b) 1996, October 4

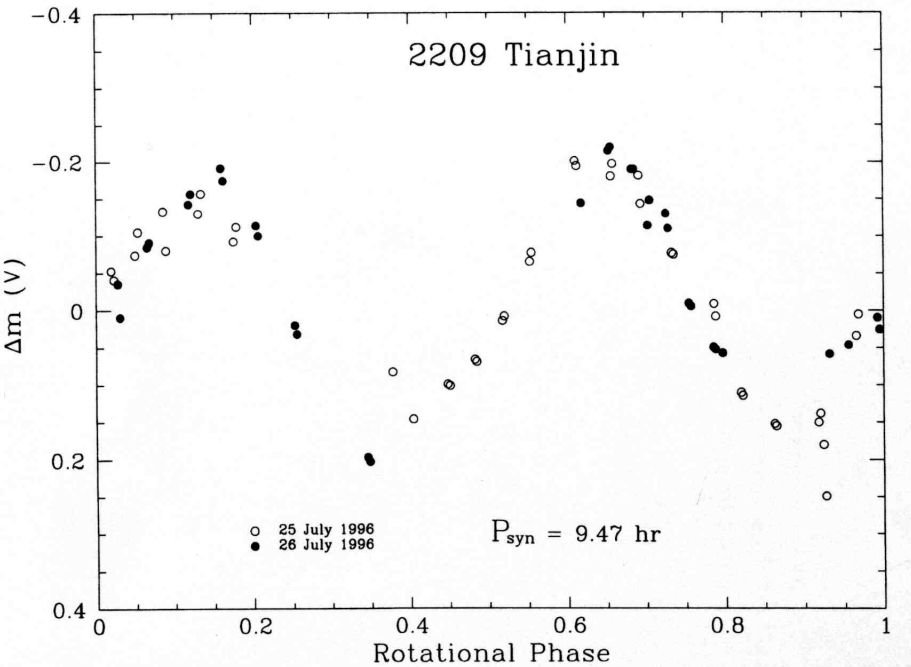

Fig. 13. Composite lightcurve of the asteroid 2209 Tianjin in rotational phase. Zero phase corresponds to U.T. 1996 July 26.0

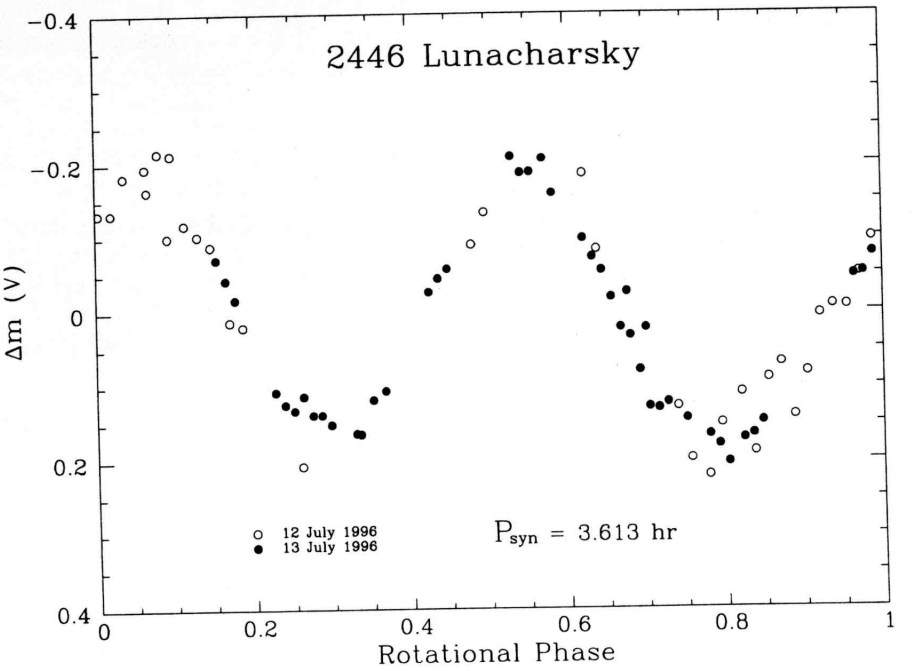

Fig. 14. Composite lightcurve of the asteroid 2446 Lunacharsky in rotational phase. Zero phase corresponds to U.T. 1996 July 13.0

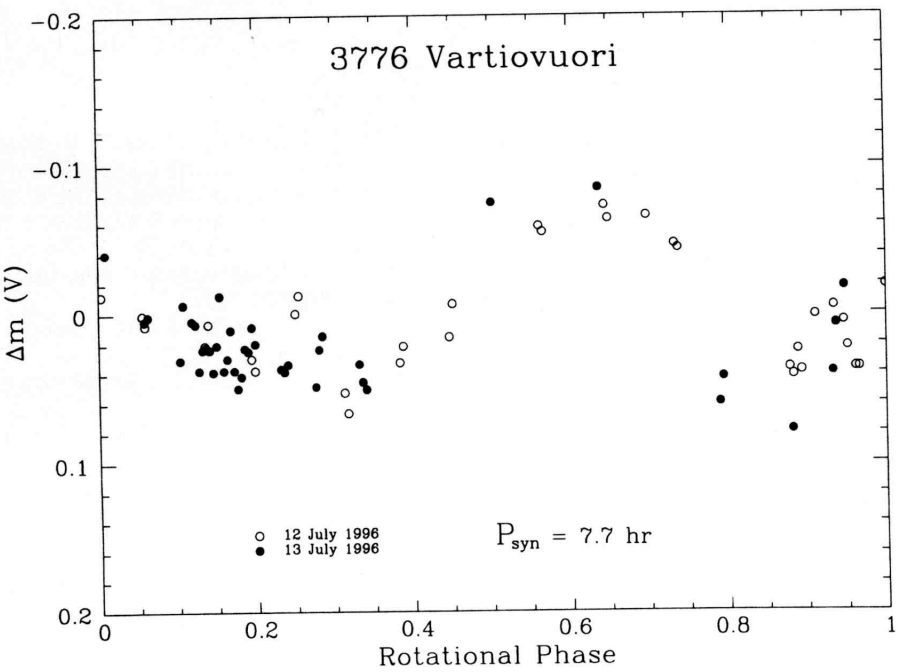

Fig. 15. Composite lightcurve of the asteroid 3776 Vartiovuori in rotational phase. Zero phase corresponds to U.T. 1996 July 13.0

the principal and secondary minima of 0.07 mag. The lightcurve amplitude is 0.19 ± 0.03 mag.

783 *Nora*

This object was observed for one night during the 1990 apparition (Lagerkvist *et al.*, 1992) and the lightcurve obtained suggested a long rotational period. During the 1996 apparition we reobserved 783 Nora during 14 nights. The obtained data are very close to the opposition, phase angles ranging between 0.2 and 8°. Figure 7 shows the composite lightcurve with a rotational period of 34.4 ± 0.5 h. However, owing to the long rotational period, the large dispersion and the small amplitude (0.08 ± 0.02 mag), alternative rotational periods cannot be completely excluded.

888 *Parysatis*

We observed 888 Parysatis at ESO during two nights (21–24 July 1996) for a total of about 15 h. The composite lightcurve, shown in Fig. 8, has been obtained by fitting the single night lightcurves with a rotational period of 5.49 ± 0.01 h. The obtained amplitude is 0.23 ± 0.02 mag.

1246 *Chaka*

1246 Chaka was observed at the 1.2 m telescope of the OHP during 2 nights (3–4 October) for a total of about 20 h. The two single night lightcurves (Fig. 9) display two different wide minima suggesting a period longer than 20 h.

1507 *Vaasa*

We observed 1507 Vaasa during two nights (5 and 6 October) in 1996 at the 1.2 m telescope of the OHP for about 14 h. The available single night lightcurves, shown in Fig. 10, did not allow us to determine an unique rotational period. From the available data it seems longer then 14 h.

1626 *Sadeya*

1626 Sadeya was observed during 1996 for 6 nights 9, 10, 11, 12, 22, 23 February) at ESO for more than 13 h. The composite lightcurve, shown in Fig. 11, is very asymmetric with a principal maximum wider and brighter than the secondary one. The computed rotational period is 3.438 ± 0.009 h and the amplitude obtained is 0.22 ± 0.02 mag.

1994 *Shane*

This object has been observed at the 1.2 m telescope of the OHP during two nights (3 and 4 October 1996). The individual lightcurves are shown in Fig. 12 and seem to cover the same maximum. This constrains the rotational period to be either 12 h or a longer multiple of 6 h (such as 18 or 24 h) but no definitive conclusion can be drawn from the available data.

2209 *Tianjin*

2209 Tianjin was observed with the 0.9 m Dutch telescope at ESO during two nights in 1996 (25–26 July) for a total of about 16 h. The composite lightcurve, obtained with a rotational period of 9.47 ± 0.01 h, is shown in Fig. 13 with a maximum amplitude of 0.42 ± 0.02 mag.

2446 *Lunacharsky*

We observed this object in 1996 at the 0.9 m Dutch telescope at ESO (12–13 July) for more than 9 h. Figure 14 shows the composite lightcurve, obtained fitting the observed data with a rotational period of 3.613 ± 0.004 h. The lightcurve is quite asymmetric with an amplitude of 0.41 ± 0.02 mag.

3776 *Vartiovuori*

3776 Vartiovuori was observed at the 0.9 m Dutch telescope of the ESO for more than 15 h (12–13 July 1996). The composite lightcurve, shown in Fig. 15, has been obtained fitting the single night lightcurves with a rotational period of 7.7 ± 0.1 h. However, a somewhat longer rotational period (11.5 h) cannot be completely excluded with the available data.

Acknowledgements. E. Dotto and M. Florczak thank ESA and CNPq, respectively, for the financial support during the present research.

References

Binzel, R., Farinella, P., Zappalà, V., Cellino V. (1989) Asteroid rotation rates: distributions and statistics. In *Asteroids II*, eds. R. Binzel, T. Gehrels, and M. S. Matthews, pp. 416–441. University of Arizona Press, Tucson, AZ.

Fulchignoni, M., Barucci, M. A., Di Martino, M. and Dotto, E. (1995) On the evolution of the asteroid spin. *Astron. Astrophys.* **299,** 929–932.

Graham, J. A. (1982) UBVRI standard stars in the E-regions. *P.A.S.P.* **94,** 244–265.

Hardie, R. H. (1962) Photoelectric reductions. In *Astronomical techniques*, Vol. II. *Stars and Stellar Systems*, ed. A. W. Hintler, pp. 178–208. The University of Chicago Press, Chicago and London.

Harris, A. W. (1994) Tumbling asteroids. *Icarus* **107,** 209–211.

Harris, A. W. (1996) The rotation rates of very small asteroids: evidence for "rubble-pile" structure. *Lunar Planet. Sci.* **XXVII,** 493–494.

Harris, A. W. and Young, J. W. (1983) Asteroid rotation—IV. 1979 observations. *Icarus* **54,** 59–109.

Harris, A. W., Young, J. W., Bowell, E., Martin, L. J., Millis, R. L., Poutanen, M., Scaltriti, F., Zappalà, V., Schober, H. J. and Zeigler, H. W. (1989) Photometric observations of asteroids 3, 24, 60, 261 and 863. *Icarus* **77,** 171–186.

Lagerkvist, C.-I., Magnusson, R., Debehogne, H., Hoffmann, M., Erikson, A., De Campos, A. and Cutispoto, G. (1992) Physical studies of asteroids—XXV Photoelectric photometry of asteroids obtained at ESO and Hoher List Observatory. *Astron. Astrophys. Supl. Ser.* **95,** 461–470.

Landolt, A. U. (1983) UBVRI photometric standard stars around the celestial equator. *Astron. J.* **88,** 439–460.

Lasker, B. M., Sturch, C. R., Lopez, C., Mallamas, A. D., McLaughlin, S. F., Russell, J. L., Wisniewski, W. Z., Gillespie, B. A., Jenkner, H., Siciliano, E. D., Kenny, D., Baumert, J. H., Goldberg, A. M., Henry, G. W., Kemper, E. and Siegel, M. J. (1988) The guide star photometric catalog. *Astroph. J. Suppl. Ser.* **68,** 1–90.

Tedesco, E. F., Veeder, G. J., Fowler, J.W, and Chillemi, J. R. (1992) The Iras Minor Planet Survey PL-TR-92-2049.

Tholen, D. J. (1996) Ephemerides Program Ephem version 1.1, Celestech.

ASTRONOMY AND ASTROPHYSICS

4979 Otawara: flyby target of the Rosetta mission⋆

A. Doressoundiram[1,2], P. R. Weissman[1], M. Fulchignoni[2,3], M.A. Barucci[2], A. Le Bras[2], F. Colas[4], J. Lecacheux[2], M. Birlan[2], M. Lazzarin[5], S. Fornasier[5], E. Dotto[2,8], C. Barbieri[5], M.V. Sykes[6], S. Larson[7], and C. Hergenrother[7]

[1] Jet Propulsion Laboratory, 4800 Oak Grove Drive, Pasadena, CA 91109, USA
[2] Observatoire de Paris, DESPA, 5, Place Jules Janssens, 92190 Meudon, France
[3] Université de Paris VII, Paris, France
[4] IMCCE, 77 avenue Denfert-Rochereau, 75014 Paris, France
[5] Osservatorio Astronomico di Padova, vicolo dell'Osservatorio, 5, 35122 Padova, Italy
[6] Steward Observatory, University of Arizona, Tucson, AZ 85719, USA
[7] Lunar and Planetary Laboratory, University of Arizona, Tucson, AZ 85719, USA
[8] Osservatorio Astronomico di Torino, 10025 Pino Torinese, Italy

Received 20 September 1999 / Accepted 2 November 1999

Abstract. An international observing campaign was organized to determine the physical and chemical characteristics of asteroid 4979 Otawara, which is the first target of the Rosetta mission (flyby on July 10, 2006). Knowledge of the physical parameters of the flyby targets is required for both refinement of the design of the spacecraft and the instrument payload, and optimization of the mission trajectory and scenarios. We present the results of observations obtained from December, 1998 through March, 1999. The spectral classification of 4979 Otawara could be either a pyroxene and/or olivine-rich S-type asteroid or a V-type asteroid, a member of the Vesta dynamical family. Further observations are needed in order to discriminate between the two spectral types. The synodic rotation period of Otawara is $P_{syn} = 2.707 \pm 0.005$ hr. The lower limit for the axial ratio of the enveloping ellipsoid is $a/b \geq 1.3$. The circular effective radius is 2.0 or 1.3 km in the case of an S-type or a V-type asteroid, respectively. A lower limit on its density is obtained: $\rho_{min} \geq 1.9\,\mathrm{g\,cm^{-3}}$ if we assume that Otawara is an aggregate or rubble pile object. However, if Otawara is a single solid body, no constraint can be set on its density. 4979 Otawara is a small, fast rotating asteroid (FRA) and hence, will be a particularly interesting target to be studied from a spacecraft, since no fast rotator has been visited yet.

Key words: minor planets, asteroids – planets and satellites: individual: 4979 Otawa

1. Introduction

The International Rosetta Mission is the planetary cornerstone mission of the European Space Agency. The mission is devoted to the study of the nature of primitive small bodies in the solar system. The baseline mission includes two asteroid flybys: 4979 Otawara on July 10, 2006 and 140 Siwa on July 23, 2008, and the exploration of comet 46P/Wirtanen. The Rosetta spacecraft will rendezvous with the comet in March 2012 at 4.2 AU from the Sun. The spacecraft will be put into an orbit around the comet nucleus and an instrumented probe will land on the nucleus surface.

Several other spacecraft missions to comets and asteroids are now either on their way, under development, or in the planning stages. These include NEAR, Deep Space 1, Stardust, Contour and Muses C. Knowledge of the physical parameters of the target bodies is required for both refinement of the designs of the spacecraft and their instrument payloads and optimization of the mission trajectories and scenarios.

An international observing campaign was organized to determine the physical and chemical characteristics of the Rosetta asteroid targets. Results for 140 Siwa have been published by Schober & Stanzel (1979), Harris & Young (1980), Lagerkvist et al. (1992) and Barucci et al. (1998). This paper deals with the first results obtained for 4979 Otawara.

2. Observations and data reduction

We observed 4979 Otawara during seven runs from December, 1998 to March, 1999. The purpose of these observations was to obtain lightcurve photometry, color photometry and spectroscopy. The specifics of the observations, including observing conditions and orbital geometry for the asteroid are shown in Table 1.

2.1. Observations

Steward Observatory (SO): Two nights of data were obtained on December, 13–14, 1998 with the 2.3 m telescope of Steward Observatory on Kitt Peak (Arizona). The telescope was equiped with the facility 2k×2k CCD imaging system at the cassegrain

Send offprint requests to: A. Doressoundiram (alain.doressoundiram@obspm.fr)

⋆ partly based on observations carried out at the European Southern Observatory (ESO) of La Silla, Chile, and at Steward Observatory, University of Arizona, Tucson, AZ USA.

Table 1. Observational circumstances

UT date	r (AU)	δ (AU)	α (deg.)	Telescope	Filter or $\delta\lambda$
1998 Dec 13	2.463	1.714	17.9	Steward Obs. 2.3m	R
1998 Dec 14	2.462	1.704	17.6	Steward Obs. 2.3m	R
1998 Dec 16	2.462	1.686	17.1	Pic du Midi Obs. 1.0 m	R
1998 Dec 17	2.461	1.676	16.8	Pic du Midi Obs. 1.0 m	R
1998 Dec 18	2.460	1.666	16.5	Pic du Midi Obs. 1.0 m	R
1999 Jan 08	2.248	1.503	8.1	Haute-Provence Obs. 1.2 m	V
1999 Jan 12	2.245	1.483	6.2	Haute-Provence Obs. 1.2 m	V
1999 Jan 20	2.439	1.457	2.1	Pic du Midi Obs. 1.0 m	R
1999 Jan 23	2.437	1.453	0.6	Pic du Midi Obs. 1.0 m	R
1999 Jan 24	2.436	1.452	0.5	Pic du Midi Obs. 1.0 m	R
1999 Jan 23	2.437	1.453	0.6	Table Mountain Obs. 0.6m	R
1999 Feb 14	2.418	1.497	10.7	European Southern Obs. NTT 3.6m	BVRI
1999 Feb 15	2.417	1.502	11.2	European Southern Obs. NTT 3.6m	BVRI
1999 Feb 16	2.416	1.507	11.6	European Southern Obs. NTT 3.6m	BVRI
1999 Mar 15	2.389	1.722	20.9	European Southern Obs. 1.5m	4500–9000 Å
1999 Mar 16	2.388	1.732	21.2	European Southern Obs. 1.5m	4500–9000 Å

focus. The CCD was binned 2×2 for data taking, giving an image scale of 0.32 arcsec per pixel. The data were taken with the Harris R filter (λ=0.63 microns). Both nights were photometric with seeing of 1.5–3 arcsec. Integration times were 400 to 600 sec. The telescope was guided at the asteroid rate.

Pic du Midi Observatory (PDM): 4979 Otawara was observed with the Pic du Midi Observatory (France), 1 m telescope during two runs: in December, 1998 (16, 17 and 18) and January 1999 (20, 23 and 24). The telescope was equiped with a Thomson CCD imaging system (388×284). A F/D=6 focal reducer was used giving an image scale of 0.75 arcsec per pixel. The data were taken with the Cousins R filter (λ=0.60 microns). The nights were photometric with an average seeing of 1.8–2.2 arsec. Integration times were 180 to 300 sec. guided at sidereal rate.

Haute Provence Observatory (OHP): 4979 Otawara was observed during the nights of January 8 and 12, 1999 with the 1.2 m telescope of Haute-Provence Observatory, France. The CCD was a TK 1024×1024, and the pixel-scale was 0.69 arcsec. The data were obtained with the Cousins V filter (λ=0.53 microns), and the exposure times ranged from 60 to 420 sec. The nights were not photometric, with a seeing of 2.4–3 arcsec. Thus, only relative photometry between the asteroid and the comparison stars was possible for this run.

Table Mountain Observatory (TMO): 4979 Otawara was observed on January 23, 1999 at Table Mountain Observatory (California). A Photometrics CCD (1024×1024) was used at the cassegrain focus of the 0.6 m telescope. The image scale was 0.52 arcsec per pixel. Digital images were recorded through a Bessel R filter with central wavelength of 0.64 microns. The night was photometric and the seeing ranged between 1 and 3 arcsec. The exposure time was 720 sec. The telescope was guided at the asteroid rate.

European Southern Observatory, NTT: Broadband color observations were obtained on February 14–16, 1999 using the SuSI2 CCD camera of the 3.6 m ESO New Technology Telescope (NTT) on La Silla, Chile. The image scale was 0.16 arcsec per pixel. Digital images were recorded through Bessel B, V, R, and I filters with central wavelengths at 0.421, 0.544, 0.642 and 0.795 microns, respectively. The nights were photometric with an average seeing of 1.2–1.8 arsec. The integration times were 60 to 90 sec.

European Southern Observatory, 1.5 m: Spectroscopic observations of 4979 Otawara were obtained in March, 1999 at the European Southern Observatory on La Silla (Chile). The 1.5 m telescope was equipped with a Boller & Chivens spectrograph and a Loral Lesser CCD detector (2048×2048 pixels). The grating used had 225 gr/mm, with a dispersion of 331 Å/mm in the first order. The CCD has 15 μm square pixels, giving a dispersion of about 5 Å/pixel in the wavelength direction. The spectral range is about $0.48 < \lambda < 0.88$ μm with a FWHM of about 10 Å. The spectra were recorded through a slit oriented in the east–west direction. The slit was opened to about 8 arcsec in order to reduce effects due to differential refraction and the possibility of losing signal due to guiding errors of the telescope.

The spectroscopic observations of 4979 Otawara were performed on two different nights: the first on 15 March 1999, at 01 31 27 UT, with a 1 hour exposure, the second on 16 March 1999, at 01 11 58 UT, with 1 hour and 10 minutes of exposure time. During the observations, Otawara had a visual magnitude of about 18.4 and was at an airmass of about 1.6.

2.2. Data reduction

Photometry: The CCD images obtained were reduced and calibrated in a standard manner using aperture photometry (PHOT task in IRAF Digiphot package, MAGNITUDE/CIRCLE in MIDAS, and ASTROL software developped by Francois Colas from IMCCE). First, an average bias frame was subtracted from each science image. Pixel-to-pixel variations in the CCD sensitivity were removed by dividing the frames by a median of several images (flats) of the twilight sky. The instrumental magnitudes were measured using aperture photometry. The radius of

the aperture used was typically about twice the average seeing. This was deemed optimum since it is large enough to include most of the point spread function, yet small enough to minimize background sky noise. Sky subtraction was performed using a 7–12 pixels wide annulus around the asteroid or reference star. Finally, for magnitude calibration purposes, observations of standard stars (Landolt, 1992) were obtained over a wide range of airmasses and stellar types. The zero point, extinction and colour terms obtained from the Landolt fields were then used to convert instrumental magnitudes to apparent magnitudes. The errors quoted take into account both the instrumental error given by photon statistics alone and the calibration error. The latter error came from the scatter in the field star photometry. When the sky conditions were not photometric, as on the nights of 8 and 12 January 1999, the data have been reduced taking into account the differential extinction between the asteroid and the comparison stars.

Spectroscopy: During each night, we also recorded bias, flat–field, calibration lamp, spectrophotometric standard and solar analog stars (Hardorp, 1978) spectra at different intervals throughout the night. The solar analog stars (we observed Hyades64, HD44594, HD89010, HR6060, HD144585, HD76151) are necessary to remove the solar contribution from the spectra of the asteroid and to obtain the asteroidal reflectivity versus wavelengh. The spectral behaviour of the stars was very similar during each night. Moreover, to obtain Otawara's reflectivity, we used the solar analog with the closest airmass to that of the asteroid, that is HD 44594 for the first observation, and Hyades 64 for the second.

The spectra were reduced using standard data reduction procedures with the software packages Midas and IDL. The spectra are normalized to unity at 5500 Å and have been smoothed with a median filter technique.

3. Reflectance Properties

3.1. Colors

BVRI band images were obtained at the NTT (ESO) on February 14 to 16, 1999. The B - V, V - R and V - I colors are presented in Table 2. These colors fall within the S spectral type region (Schevchenko & Lupishko, 1998). However information at longer wavelength is necessary to distinguish between other close spectral types such as the types M or V. The BVRI data will be compared and discussed along with the spectroscopic results presented below.

3.2. Spectrum

The spectra obtained on the two nights in March (Fig. 1) appear very similar. The reflectance slope measured in the spectral range 5000–8000 Å, is $8.2 \pm 0.1\%/10^3$ Å, for the night of 15 March 1999 and $7.1 \pm 0.2\%/10^3$ Å, for the night of 16 March 1999. Small differences are associated with noise and also with the presence of spurious characteristics due to a non-perfect subtraction of sky absorption bands. Both spectra show a strong absorption feature longwards of 8000 Å. This feature is the well known 0.9 μm band associated with silicate minerals (pyroxene and olivine). Its position and depth is related to the presence and abundance of both silicates (Gaffey et al. 1993).

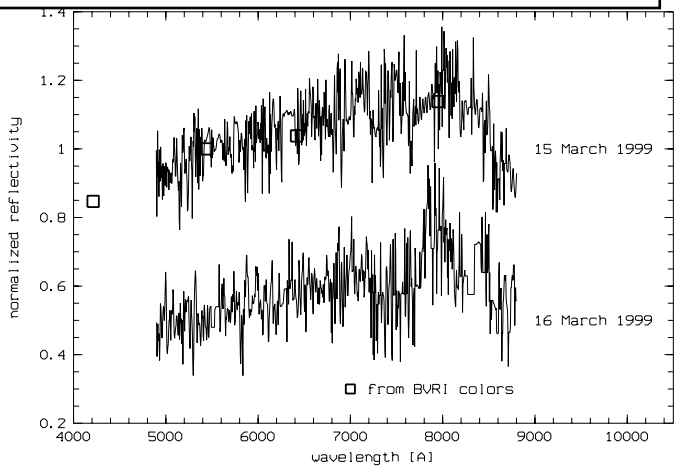

Fig. 1. Reflectance spectra of 4979 Otawara obtained on March 15 (top) and 16 (bottom), 1999. The spectra are normalized to unity at 5500 Å and have been vertically offset for clarity. Broadband color data from the ESO NTT on February 14–16, 1999 are also plotted (squares) on the top spectrum.

Table 2. Colors of 4979 Otawara

UT date	B-V	V-R	V-I
1999 Feb 14	0.87 ± 0.02	0.37 ± 0.01	0.84 ± 0.02
1999 Feb 15	0.86 ± 0.02	0.46 ± 0.02	0.83 ± 0.02
1999 Feb 16	0.82 ± 0.03	0.38 ± 0.02	0.82 ± 0.03
weighted mean	0.86 ± 0.01	0.40 ± 0.01	0.83 ± 0.01

The relative reflectances obtained from the BVRI color photometry are also plotted in Fig. 1. The reflectivity has been computed using solar colors. It can be seen that the broadband colors agree quite well with the spectroscopic measurements.

In order to characterize the spectral type of Otawara, we used the G-mode analysis applied to asteroids by Barucci et al. (1987) and Birlan et al. (1996). We found that the spectral types V and SV are most likely to match the spectrum of Otawara in Fig. 2. Extended spectral coverage (especially beyond 1 μm) and knowledge of the albedo would allow us to discriminate between the two spectral types. The V-type is associated with the asteroid 4 Vesta and HED meteorites (Binzel & Xu 1993).

The SV type is somewhat intermediate between the V and S-types. The appearance of the strong 0.9 μm band is suggestive that Otawara is a pyroxene and/or olivine-rich S-type asteroid

The possible association with the V-type is surprising and exciting. Indeed, all the known V-type asteroids are either members of the Vesta dynamical family (Zappala et al. 1995, Binzel & Xu 1993) or are near-Earth asteroids (Cruikshank et al. 1991). Asteroid 4979 Otawara is a main belt asteroid and does not belong to either of these populations. However, according to Migliorini et al. (1997) the Vesta family is much more extended than previously determined and extends close to the ν_6 and 3:1

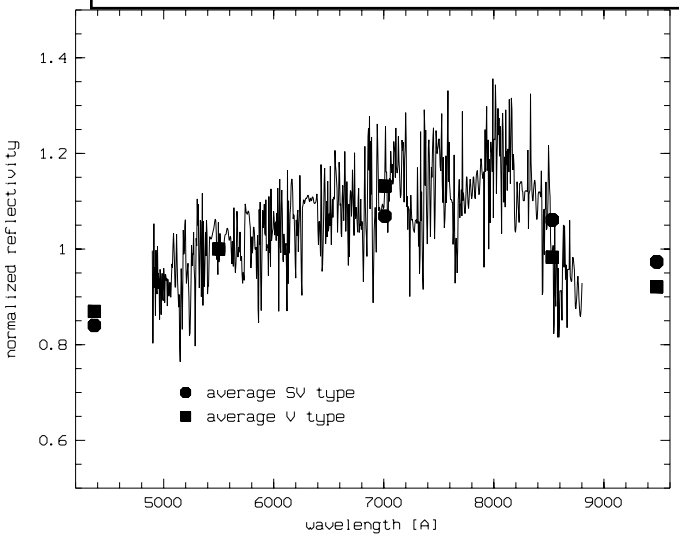

Fig. 2. Spectrum of 4979 Otawara compared with the mean spectrum of SV and V spectral type asteroids (Birlan et al., 1996).

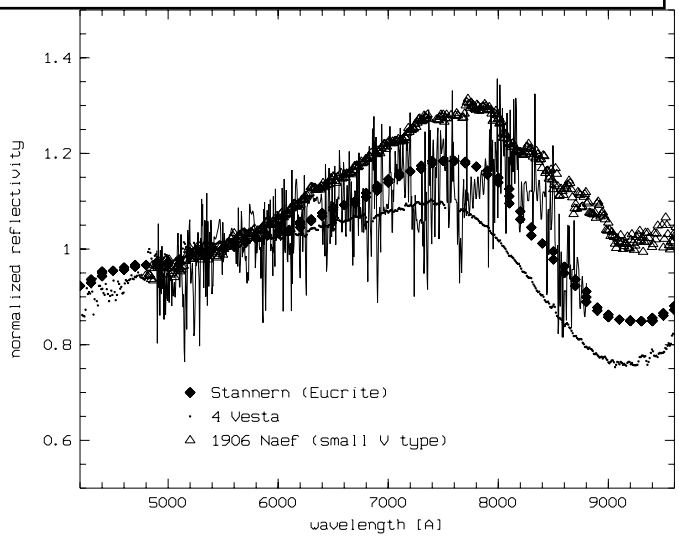

Fig. 3. A good match is obtained between the spectrum of 4979 Otawara and the spectrum of a eucrite (filled diamonds). The spectra of 4 Vesta (dotted line) and 1906 Naef (open triangles) are plotted for comparison. Eucrite spectrum is from Gaffey (1976) and spectra of Vesta and Naef are from SMASS (Xu et al. 1995).

resonances (a $\approx$ 2.15 and a $\approx$ 2.5 respectively). The position of Otawara in proper elements space is a = 2.168AU, e = 0.117 and sin i = 0.0071. Therefore, 4979 Otawara, which lies close to the ν_6 resonance, may in fact be a Vesta family member.

We also found a good match for the spectrum of Otawara with the spectrum of a eucrite meteorite, (Gaffey et al., 1976) suggesting once again a V-type classification (Fig. 3). The spectra of two Vesta family members: 4 Vesta and 1906 Naef are also plotted in Fig. 3. The latter one is a small asteroid (d = 6 km) like 4979 Otawara (see next section). It can be seen that Otawara' spectrum is comparable and certainly lies in the spectral range of the Vesta family.

4. Photometry

4.1. Rotation period

Because different filters were used in the observations and the observations were made over a wide range of phase angles, we analysed the three sets of photometric data independently in order to search for the asteroid's rotation period: 1) the data obtained in December, 1998 with the R filter ($16.5 < \alpha < 17.9$ degrees where α is the phase angle), 2) the data obtained in January 1999 with the R filter when the asteroid was very close to opposition ($0.5 < \alpha < 2.1$ degrees) and 3) the data obtained with the V filter in January 1999 ($6.2 < \alpha < 8.1$ degrees). We determined the synodic rotation period and the corresponding uncertainty by assuming a double-peaked lightcurve and by applying a Fourier analysis as described in Harris et al. (1989). We found rotation period of 2.707 $\pm$ 0.005, 2.707 $\pm$ 0.005 and 2.63 $\pm$ 0.01 hours for the three data sets, respectively. The disagreement in the third data set is likely the results of the fact that these data were taken under non-photometric conditions. Combining all three data sets, we found the best rotation period for Otawara

$$\mathrm{P_{syn}} = 2.707 \pm 0.005\,\mathrm{hr}.$$

The composite lightcurves, shown in Figs. 4, 5 and 6, are consistent and have symmetric double-peaks, typical of a ellipsoidal shape-dominated lightcurve. The peak-to-peak amplitude is 0.25 $\pm$ 0.04 mag for the December R data, 0.29 $\pm$ 0.05 mag for the January R data and 0.27 $\pm$ 0.03 mag for the January observations in the V filter.

4.2. Shape

The highest peak-to-peak amplitude is Δm = 0.29. If we assume that the brightness variation of Otawara is purely shape-induced, with no albedo features, we can model the asteroid as a tri-axial ellipsoid with semi-axes a, b and c where $a > b > c$. We, then can estimate a lower limit for the axial ratio:

$$\frac{a}{b} \geq 10^{0.4\Delta m} \quad (1)$$

The lightcurve amplitude of 4979 Otawara thus implies an axis ratio of $a/b \geq 1.3$. This corresponds to an elongation of at least 30%.

4.3. Size

We attempted to fit the data using the standard H, G magnitude system. Due to insufficient data, poor coverage down to subdegree phase angles and possibly the use of different R filters, we could not obtain reliable absolute magnitude and slope parameters. Thus we choose to compute the absolute magnitude assuming G = 0.24 (S-type) and 0.49 (V-type). These latter values are the mean values of the parameter G for the respective compositional types, calculated from a sample containing 98 objects (Schevchenko & Lupishko, 1998).

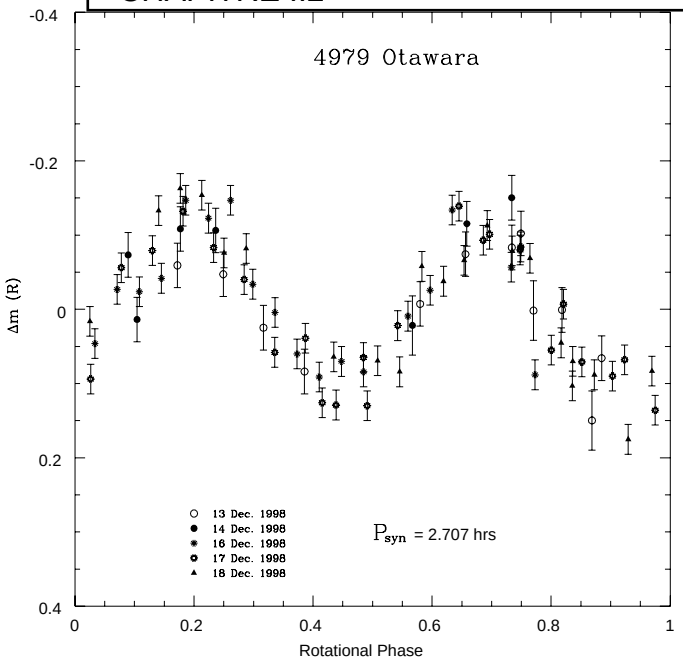

Fig. 4. Composite lightcurve of 4979 Otawara in rotational phase obtained in December 1998 in the R filter.

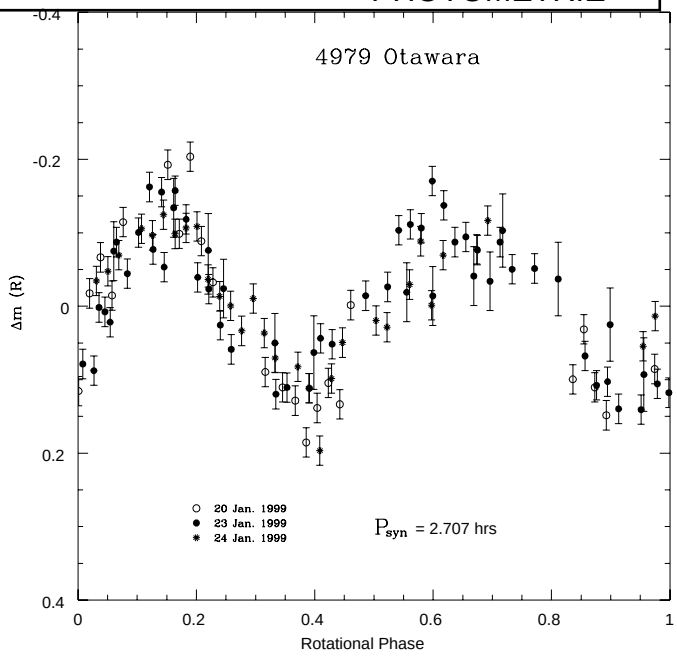

Fig. 5. Composite lightcurve of 4979 Otawara in rotational phase obtained in January 1999 in the R filter.

The absolute magnitude H_R is computed following Bowell et al. (1989). The mean absolute magnitude for all the nights in the R filter is:

$\mathrm{H_R} = 14.08 \pm 0.04$ assuming an S-type,
$\mathrm{H_R} = 14.23 \pm 0.04$ assuming an V-type.

If we assume an albedo of 0.19 or 0.38 as typical respectively for S and V-type asteroids (Tedesco et al. 1989), these correspond to a circular effective radius of 2.0 or 1.3 km, for S and V-types respectively. Knowing its axial ratio, (assuming $b = c$) we can then infer that 4979 Otawara is an elongated body having semi-axes $a = 2.4$ km and $b = 1.9$ km for a typical S-type albedo, and $a = 1.6$ km and $b = 1.2$ km for a V-type albedo.

5. Internal properties

Given its small size and its rotation period, 4979 Otawara belongs to a group of special interest, the small and fast rotating asteroids (FRAs). Typically observed lightcurve amplitudes of FRAs like Otawara are much smaller than those of slower rotators, indicating that the FRAs are less elongated, rather spheroidal bodies. For instance, for NEAs with $P > 4$ hr, the mean amplitude is 0.69 $\pm$ 0.05 mag, whereas for $P < 4$ hr, the mean amplitude is 0.21 $\pm$ 0.03 mag (Pravec, 1999). Observational and theoretical studies of small, fast rotating asteroids show that they have distinct properties that bring important information to our understanding of the collisional evolution of the asteroid population (see Pravec, 1999 for the latest review of this subject). In particular, FRAs, unlike asteroids with longer periods, are near the rotational break-up limit for aggregates

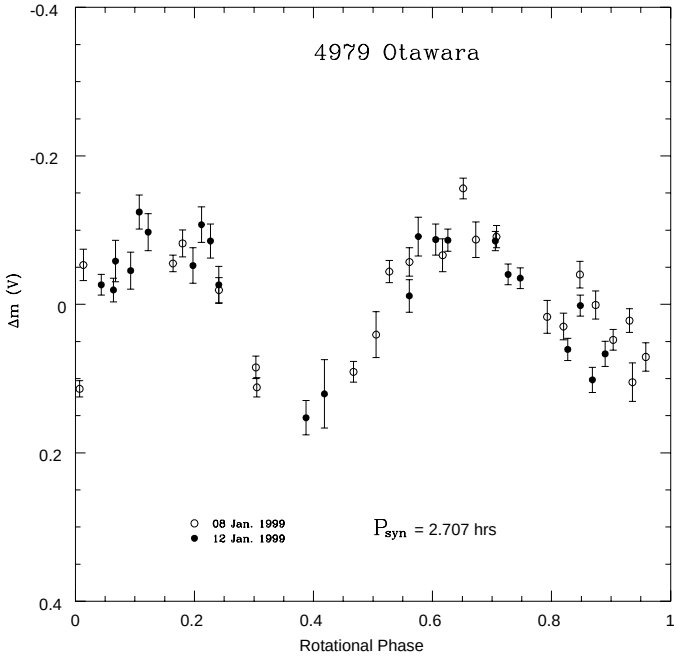

Fig. 6. Composite lightcurve of 4979 Otawara in rotational phase obtained in January 1999 in the V filter.

with no tensile strength, assuming plausible bulk densities for asteroids.

If Otawara is an aggregate or "rubble pile" object we can constrain its density knowing its rotation period and shape. If a body has no tensile strengh, a minimum density is required in order to resist centrifugal disruption. This is obtained by simply equating the centrifugal acceleration with the gravitation acceleration for the elongated body. Thus the minimum density ρ_{min}

for a body with axis ratio a/b and rotation period P is (Harris, 1996)

$$\rho_{min} \approx \left(\frac{3.3^h}{P}\right)^2 \frac{a}{b} \quad (2)$$

Applying this formula to 4979 Otawara, we find:

$\rho_{min} \geq 1.9.$

This density rules out densities as low as that of the C type asteroid 253 Mathilde ($\approx 1.3 \pm 0.4$ g cm^{-3}) found by the NEAR spacecraft team (Veverka et al. 1997) but allows densities comparable to that of 243 Ida (2.6 ± 0.5 g cm^{-3}) found by the Galileo imaging team (Belton et al. 1995). Hovewer, if 4979 Otawara is a single, consolidated body, then the fast rotation period gives us little information about its density.

6. Conclusion and discussion

Asteroid 4979 Otawara was observed on seven occasions from December 1998 through March, 1999. The main results of these observations are the following:

- Otawara exhibits a solar reflected spectrum indicating either a pyroxene and/or olivine-rich S-type asteroid, or a V-type asteroid, a member of the Vesta dynamical family. Further observations, in particular at near-infrared wavelenghs are needed in order to discriminate between the two spectral types.
- The synodic rotation period of Otawara is $P_{\rm syn} = 2.707 \pm 0.005$ hr.
- The lower limit for the axial ratio of the enveloping ellipsoid is $a/b \geq 1.3$.
- The circular effective radius is 2.0 or 1.3 km in the case of an S-type or a V-type asteroid, respectively.
- 4979 Otawara is a small, fast rotating asteroid (FRA). A lower limit on its density is obtained, $\rho_{min} \geq 1.9$, if we assume that Otawara is an aggregate or "rubble pile" object.

Asteroid 4979 Otawara will be a particularly interesting target to be studied from a spacecraft, since no fast rotator asteroid has been visited yet. The fast rotation of Otawara will allow the onboard Rosetta remote sensing instruments to image and measure the asteroid surface characteristics during one complete rotation of the asteroid at the highest possible resolution.

Further CCD photometric observations near opposition, occuring at different celestial latitudes, are necessary in order to determine the rotation pole direction of this asteroid. Also, additional spectroscopic observations are needed, in particular observations in the near infrared. Spectra taken at different rotational phases (Doressoundiram et al., 1997) will give a better estimate of the surface composition and its homogeneity/heterogeneity.

Acknowledgements. The authors thanks P. Pravec and A.W. Harris for helpful discussions. This work was supported in part by the NASA Planetary Astronomy Program. It was performed in part at the Jet Propulsion Laboratory under a contract with the National Aeronautics and Space Administration.

References

Barucci M.A., Capria M.T., Coradini A., Fulchignoni M., 1987, Icarus 72, 304
Barucci M.A., Doressoundiram A., Fulchignoni M., et al., 1998, Planet. Space Sci. 46, 75
Belton M., Chapman C., Thomas P., et al., 1995, Nature 374, 785
Binzel R.P., Xu S., 1993, Science 260, 186
Birlan M., Fulchignoni M., Barucci M.A., 1996, Icarus. 124, 352
Bowell E., Hapke B., Domingue D., et al., 1989, In Asteroids II (R.P. Binzel, T. Gehrels, M.S. Matthews, Eds.), pp. 524 Univ. of Arizona Press, Tucson
Cruikshank D.P., Tholen D.J., Hartmann W.K., Bell J.F., Brown R.H., 1991, Icarus 89, 1
Doressoundiram A., Barucci M.A., Fulchignoni M., 1997, A&A 325, L9-L11
Gaffey M.J., 1976, J. Geophys. Res. 81, 905
Gaffey M.J., Bell J.F., Brown R.H., et al., 1993, Icarus 106, 573
Gradie J.C., Chapman C.R., Tedesco E.F., 1989, In Asteroids II (R.P. Binzel, T. Gehrels, M.S. Matthews, Eds.), pp. 316 Univ. of Arizona Press, Tucson
Hardorp J., 1978, A&A 63, 383
Harris A.W., Young J.W., 1980, Icarus 43, 20
Harris A.W., Young J.W., Bowell E., et al., 1989, Icarus 77, 171
Harris A.W., 1996, Lunar and Planetary Science 27, 493
Harris A.W., Harris A.W., 1997, Icarus 126, 450
Lagerkvist C.-I., Magnusson P., Debehogne H., et al., 1992, A&AS 95, 461
Landolt A.U., 1992, Icarus 72, 304
Migliorini F., Morbidelli A., Zappala V., et al., 1997, Meteor. & Planet. Sci. 32, 903
Pravec P., 1999, Icarus in press
Schober H.J., Stanzel R., 1979 A&AS 38, 265
Shevchenko V. G., Lupishko, D. F., 1998 AJ 97, 580
Tedesco E. F., Williams J. G., Matson D.L., et al., 1989 Solar System Research 32, 220
Veverka J., Thomas P., Harch A., et al., 1997, Science 278, 2109
Xu S., Binzel R.P., Burbine T.H., Bus S.J., 1995, Icarus 115, 1
Zappala V., Bendjoya P., Cellino A., Farinella P., Froeschle C., 1995, Icarus 116, 291

A&A 375, 281–284 (2001)
DOI: 10.1051/0004-6361:20010789

Astronomy & Astrophysics

Research Note

Groundbased investigation of asteroid 9969 Braille, target of the spacecraft mission Deep Space 1⋆

M. Lazzarin[1], S. Fornasier[1], M. A. Barucci[2], and M. Birlan[2]

[1] Dip. di Astronomia, Vic. Osservatorio 5, 35122 Padova, Italy
[2] Obs. de Paris, 92195 Meudon Principal Cedex, France

Received 19 December 2000 / Accepted 24 May 2001

Abstract. Asteroid 9969 Braille (1992 KD) was encountered on July 29, 1999 by the Deep Space 1 mission, the first of NASA's New Millennium Program, launched on October 24 1998. The data obtained by the space mission seem to indicate a composition of the object similar to that of Vesta. To complete the information obtained in the infrared region by the Deep Space 1 mission we have performed a visible spectroscopic and photometric investigation of the asteroid respectively with the 1.5 m telescope and the NTT of ESO, La Silla. The spectrum was obtained in the spectral range 4500–8200 Å and, for the photometry, *BVRI* filters were used. In this paper we report the results of the analysis of the data obtained indicating that, on the basis of our visible data, the composition of the asteroid may range from V-type to Q-type, but we observe also a strong similarity to the H-type ordinary chondrites.

Key words. solar system: general – minor planets – asteroids

1. Introduction

In the last years, the number of space missions devoted to the investigation of comets and asteroids has increased due to the importance of studying these small bodies for the understanding of the origin and evolution of our Solar System. In fact, comets and asteroids are believed to be the most primitive objects in the Solar System and they hold many clues about the physical, thermal and compositional conditions present during the formation of the Solar System. In particular, the investigation of the composition of these bodies can give fundamental information on these subjects. In this context, we have made a spectroscopic and photometric study of the asteroid 9969 Braille (1992 KD), a target of the Deep Space 1 mission.

The Deep Space 1 is the first of a series of technology demonstration probes being developed by NASA's New Millennium Program to test new technologies for future space and Earth-observing missions. The spacecraft made a fly-by with the asteroid 9969 Braille (formerly known as 1992 KD) on 29 July 1999. Just after the encounter with Braille, NASA decided to extend the DS1 mission to fly-by the dormant comet Wilson-Harrington in January 2001 and comet Borrelly in September 2001.

Along with the technology demonstrations, the probe carries the Miniature Integrated Camera-Spectrometer (MICAS), an instrument combining two visible imaging channels with UV and IR spectrometers. MICAS was used to study the chemical composition, geomorphology, size, spin-state, and atmosphere of 9969 Braille (Soderblom et al. 1999). DS1 carries also the Plasma Experiment for Planetary Exploration (PEPE), an ion and electron spectrometer which is able to measure the solar wind during cruise, the interaction of the solar wind with the target bodies during encounters, and the composition of the cometary coma.

Deep Space 1 arrived within 26 km of asteroid 9969 Braille at 04:46 UT on July 29, 1999. The asteroid was not successfully imaged during the close flyby due to an on-board target-tracking problem. Two images were obtained 914 and 932 s after the closest approach from about 14 000 km and a dozen infrared spectra were

Send offprint requests to: M. Lazzarin,
e-mail: lazzarin@pd.astro.it

⋆ Based on observations carried out at the European Southern Observatory (ESO) of La Silla, Chile, programs N.62S-0173 and N.62S-0305A.

obtained about 3 minutes later, revealing what is probably a V-type classification of this NEA (Soderblom et al. 1999). The images show that 9969 Braille has an irregular shape, and is approximately 2.2 km along its longest side and 1 km at its shortest.

The study of Braille is also interesting in itself: it was discovered by E. F. Helin in 1992 (Helin et al. 1992) and very little was known about it before the encounter with the spacecraft. It was discovered as an Amor asteroid and a successive more accurate determination of the orbit classified it as a Mars crosser. The study of these objects is important because they represent one of the most peculiar classes of objects in the Solar System and their origin is not well understood yet. This population is very diverse in nature, many having unusual shapes (very elongated or bifurcated); binary systems have been discovered among the population. Some of these objects have a complex, non–principal axis rotation state while some others display very long rotational periods, which are not easily explained by the current dynamical and collisional models.

Their diversity is also reflected by the different taxonomic types present in the population: S, C, V, M, Q and D types have been identified to date (Binzel et al. 1997).

The origin of these bodies also is not well understood. We know that their present orbits are unstable over time scales much shorter than the age of the Solar System, and that over these time scales NEAs are ejected or collide with the Sun or a planet. Because the cratering record on the Moon suggests a fairly constant NEA population during the past 2 billion years, new NEAs must be continuously supplied by some sources in order to maintain the present steady state. Currently, two sources for NEAs have been identified. The first one is the Main Belt, where gravitational perturbations by the major planets cause dynamical resonances which provide escape routes. The second source is represented by extinct comets. A good number of NEAs represent the final evolutionary state of comets, that is, a devolatilized nucleus. An example is the asteroid Apollo 4015, the next target of the DS1 mission, which was the comet Wilson Harrington in 1949. It is not clear, however, what the efficiency of the delivery mechanism is, and what percentage of the NEAs we observe today comes from the one or other source. One way of addressing this problem is to characterize these objects spectroscopically, in order to derive their mineralogy.

Another interpretation of the origin of Braille, theorized by some astronomers, is that it may have been knocked off of Vesta and in effect the data obtained from the DS1 present on the WEB site of the DS1 at JPL would suggest a V-type composition.

Also Hicks et al. (1999) investigated Braille obtaining *BVRI* photometric data: they find colors closer to those of ordinary chondrite and basaltic achondrite meteorites than those of the vast majority of main-belt asteroids.

Binzel et al. (2001) also made a spectrum of Braille in the visible region suggesting a similarity to Q-type asteroids (A. W. Harris, private communication).

We have spectroscopically and photometrically investigated 9969 Braille in order to obtain information on its surface composition and its possible variations and in particular to complete the data obtained in the infrared region by the DS1 mission. A spectrum between about 4500 and 8200 Å and *BVRI* data have been compared; unfortunately, observations planned in the near infrared have not been successfull owing to bad weather conditions.

2. Observations and data reduction

Spectroscopy: we performed a spectroscopic investigation of 9969 Braille on 17 March 1999 at the European Southern Observatory of La Silla (Chile), with the 1.5 m telescope equipped with a Boller & Chivens spectrograph and a Loral Lesser CCD as detector (2048×2048 pixels). The grating used was a 225 gr/mm, with a dispersion of 331 Å/mm in the first order. The CCD has a 15 μm square pixels, giving a dispersion of about 5 Å/pixel in the wavelength direction. The spectral range is about $0.45 < \lambda < 0.82$ μm with a FWHM of about 10 Å.

The spectrum was recorded through a slit oriented in the East–West direction. The slit was opened to about 8 arcsec in order to reduce effects due to differential refraction and the possibility of losing signal due to guiding errors of the telescopes.

9969 Braille was observed on 17 March 1999, at 01:30:58 UT, with an exposure time of 75 min. During the observation, Braille had a visual magnitude of about 18.3, and an airmass of about 1.1.

We also recorded bias, flat–field, calibration lamp spectra, and solar analog stars' spectra at different intervals throughout the same night.

The solar analog stars observed (Hyades64, HD 44594, HD 89010, HR 6060, HD 144585, HD 76151) (Hardorp 1978), are necessary to remove the solar contribution from the spectrum of the asteroid and to obtain the asteroidal reflectivity. The spectral behaviour of the stars was very similar during the night with differences in the reflectivity gradient around $1\%/10^3$ Å. To obtain the asteroid spectrum reflectivity we then divided the spectrum of the asteroid by the spectrum of the solar analog with airmass closest to that of the asteroid (Hyades64).

The spectrum was reduced using ordinary procedures of data reduction (Luu & Jewitt 1990) with the software packages Midas and IDL.

These procedures include: subtraction of the bias from the raw data, division by flat field, cosmic ray removal, background subtraction, collapsing the two dimensional spectra, wavelength calibration, atmospheric extinction correction. Wavelength calibration was made using a lamp with He, Ar, Fe and Ne emission lines. The residuals of the wavelength calibration were $\leq$2 Å. After these procedures, we normalized all the spectra, both of asteroids and solar analog stars, at 1 around 5500 Å.

The spectrum was then smoothed with a median filter technique. Some spurious, easily recognizable, features

Table 1. Color indices with relative errors of Braille. Two obervations were performed during the 13–14 night: at 1:36 UT and 5.51 UT.

Date	$B-V$	$V-R$	$V-I$
13–14 Feb.	0.791 ± 0.030	0.411 ± 0.013	0.708 ± 0.018
13–14 Feb.	0.813 ± 0.032	0.441 ± 0.010	0.708 ± 0.015
14–15 Feb.	0.817 ± 0.045	0.468 ± 0.011	0.728 ± 0.020

due to an incomplete removal of sky lines (in particular of the water telluric bands around 7200 Å and of the O_2A band around 7600 Å) are present on the asteroid spectrum. The spectrum of Braille is reported in Fig. 1.

Photometry: the broadband color data were obtained at NTT of ESO on two nights (February 14–15, 1999). The SUSI2 CCD camera (55×55) at the f/11 Nasmyth focus of the 3.5 m New Technology Telescope (NTT) was used to obtain direct images. The EEV camera (ESO No. 46) was selected for our observations with the Bessel B, V, R, and I filters (central wavelength at 0.421, 0.544, 0.642 and 0.795 μm respectively). The observations were carried out in 2×2 binning mode, yielding a pixel scale of 0.16 arcsec/pixel. The seeing throughout the run was in the range 0.6–1.5 arcsec. The exposure time was 90 s.

The CCD images were reduced and calibrated with a standard method using aperture photometry (MAGNITUDE/CIRCLE in MIDAS). First, bias and flat-field corrections were performed. The instrumental magnitudes were measured using aperture photometry. The radius of the aperture used was typically about twice the average seeing. This was deemed optimum since it is large enough to include most of the point spread function, yet small enough to minimize background sky noise. Sky subtraction was performed using a 7–12 pixels wide annulus around the asteroid or reference star. Finally, for magnitude calibration, observations of standard stars were obtained over a wide range of airmasses and stellar types (three fields PG0942, SA107, and SA95 were used, Landolt 1992). The zero point, extinction and colour terms obtained from the Landolt fields were then used to convert instrumental magnitudes to apparent magnitudes. The errors quoted take into account both the instrumental errors given by photon statistics alone and the calibration error. The latter error came from the scatter in the field star photometry.

3. Results and discussion

BVRI band images were obtained at NTT on February 14 to 15, 1999. The $B-V$, $V-R$ and $V-I$ colors are reported in Table 1.

Little variation on the photometric data could be attributed to surface composition variations of the object.

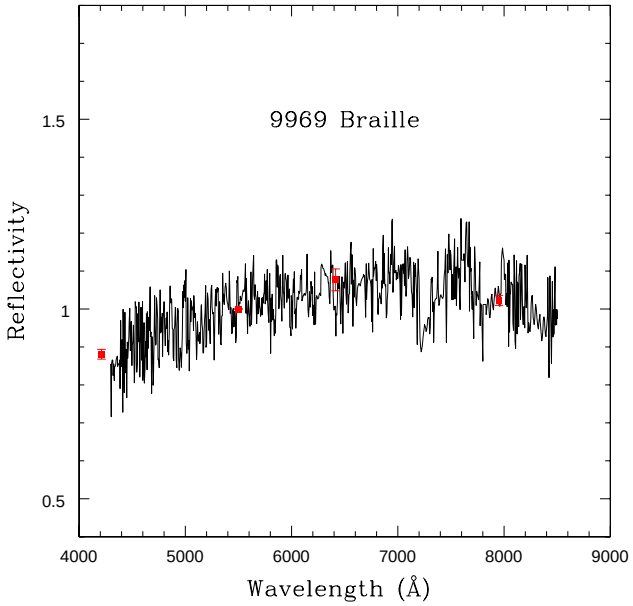

Fig. 1. Reflectance spectrum of 9969 Braille obtained on 17 March 1999 at ESO-La Silla. The spectrum is normalized at 1 around 5500 Å. The average broadband color data with the relative errors are also reported (squares) on the spectrum.

The spectrum of 9969 Braille (Fig. 1) has a reflectance slope of $(7.13 \pm 0.29)\%/10^3$ Å computed in the spectral range of 4300–7200 Å. It also presents some spurious features due to an imperfect subtraction of sky absorption bands (for example the water telluric band around 7200 Å).

The average relative reflectance obtained from the *BVRI* color photometry is also plotted in Fig. 1. The reflectivity from the photometric data was computed using solar colors. We adopted the maximum semi-dispersion as the error bar. The broadband colors agree quite well with the spectroscopic data.

In order to characterize the spectral type of 9969 Braille we used the extension of the G-mode multivariate method (Fulchignoni et al. 2000). The taxonomic classes proposed by Birlan et al. (1996) were taken into account. The results of our analysis reveal that 9969 Braille could be a V or SV asteroid. However, the spectrum of Braille does not cover the whole spectral interval of the defined classification; our analysis underlines the affinity of the asteroid to a given taxonomic class.

In Fig. 2 we compare the spectrum of Braille with that of Vesta and the result is a good match.

However, we also tried a comparison with the spectrum of a Q-type asteroid (1862 Apollo), with the average spectrum of V-type and S-type asteroids (Bus 1999) and with the spectra of several H, L and LL ordinary chondrites. What results is that in effect Braille is similar to Vesta, and compatible, within the errors, with the average of V-type asteroids, but also with the Q-type spectrum (Fig. 2). Moreover, the comparison with ordinary

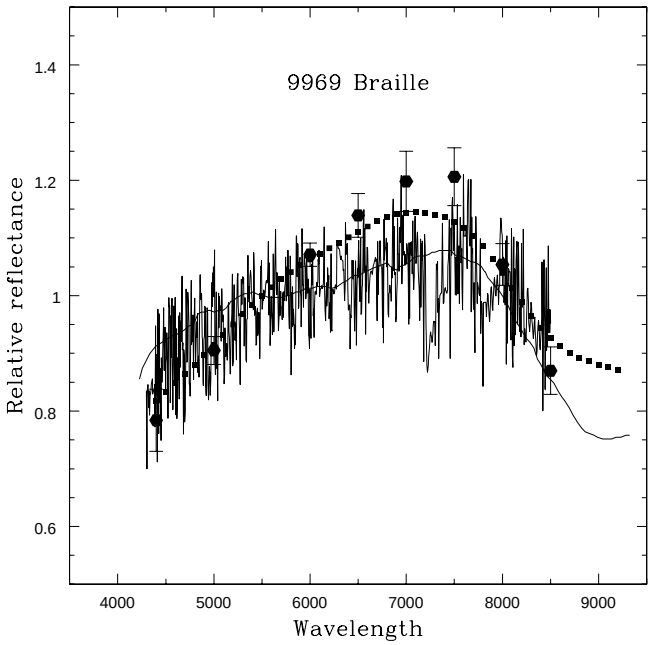

Fig. 2. Spectrum of 9969 Braille superimposed on the spectrum of asteroid Vesta (continuum) (Binzel et al. 1993), the average spectrum of V-type (hexagons) and the spectrum of the Q-type asteroid 1862 Apollo (squares) (Bus 1999).

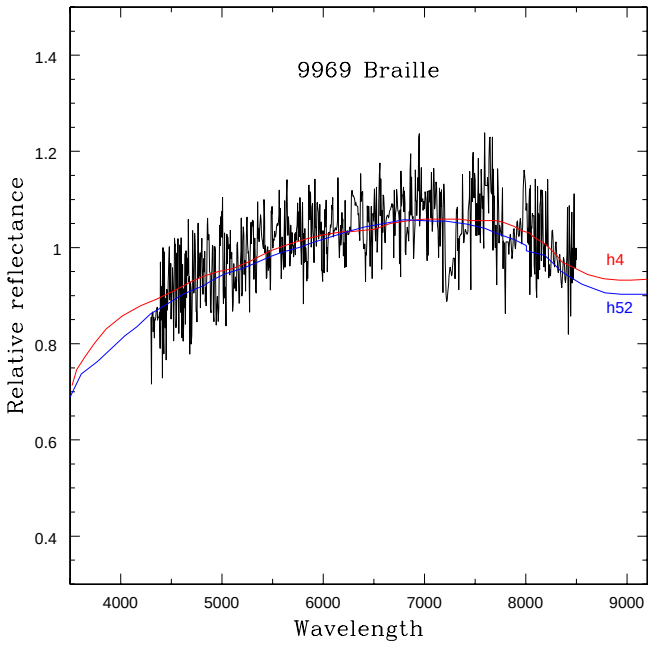

Fig. 3. Spectrum of 9969 Braille superimposed on the spectra of ordinary chodrites H4 and H52.

chondrites has revealed that the spectrum of Braille is pratically indistinguishable from that of H4 and H52 ordinary chondrites (Fig. 3). Instead, our spectrum is incompatible with that of the average spectrum of S-type asteroids (redder than the spectrum of Braille).

So, from our data we might confirm the data obtained in the infrared region by the Camera-Spectrometer MICAS of the Deep Space 1 during its fly-by with Braille on 29 July 1999 and reported by Soderblom et al. (1999). However, on the basis of our visible spectrum of Braille other interpretations of its composition are also possible: in fact it ranges between the Q-type and V-type and it shows a strong similarity with the ordinary chondrites H4 and H52 (Fig. 3).

4. Conclusion

Asteroid 9969 Braille was spectroscopically and photometrically observed during two observational runs at ESO with the 1.5 m telescope and the NTT respectively. From the data obtained here a clear conclusion on the composition of Braille is not easy to draw as the spectrum is compatible with that of Vesta, but also with the Q-types. A strong similarity is in particular evident with the ordinary chondrites. So we think that further observations, in particular in the near infrared, would help to define the surface composition of Braille.

References

Binzel, R. P., Harris, A. W., Bus, S. J., & Burbine, T. H. 2001, Icarus, in press
Binzel, R. P., Bus, S. J., & Burbine, T. H. 1997, Am. Astron. Soc., DPS Meeting, BAAS, 29, 05.01
Binzel, R. P., & Xu, S. 1993, Science, 260, 186
Birlan, M., Fulchignoni, M., & Barucci, M. A. 1996, Icarus, 124, 352
Bus, S. J. 1999, Ph.D. Thesis
Fulchignoni, M., Birlan, M., & Barucci, M. A. 2000, Icarus, 146, 204
Hardorp, J. 1978, A&A, 63, 383
Helin, E. F., Lawrence, K., Rose, P., Alu, J., & Williams, G. V. 1992, IAUC 5531
Hicks, M. D., Buratti, B. J., Rabinowitz, D. L., et al. 1999, 30th Annual Lunar and Planetary Science Conference, Houston, TX, abstract, No. 1719
Landolt, A. U. 1992, Icarus, 72, 304
Luu, J. X., & Jewitt, D. C. 1990, AJ, 99, 1985
Soderblom, L., Boice, D., Britt, D., et al. 1999, Am. Astron. Soc., DPS Meeting, BAAS, 31, 34.03

CCD AND PHOTOGRAPHIC OBSERVATIONS OF THE COMET C/1996 B2 (HYAKUTAKE)

OVIDIU VĂDUVESCU, GABRIEL ŞTEFĂNESCU, MIREL BÎRLAN

Astronomical Institute of the Romanian Academy
Str. Cuţitul de Argint 5, 75212 Bucharest 28, Romania

Abstract: About 200 CCD images of the comet C/1996 B2 - HYAKUTAKE were obtained and reduced, using four approaches by PPM stars and one by a GSC star, in March 20, 24, 25 and April 1-st, 1996, in Bucharest. Also, three photographically plates were reduced using PPM stars. The O-C analysis of the astrometric data allowed testing the accuracy of both the observational technique and the reduction method. The variation of the orientation of the comet's tail was also computed.

Key words: comet, appulse, astrometry, CCD

1. INTRODUCTION

Comets, together with asteroids, play an essential role in the knowledge of the origin and evolution of the Solar System. The spectacular and rare visible naked-eye apparitions of a comet in the inner Solar System become a major event for the astronomical community.

C/1996 B2 (Hyakutake) was announced at the end of January 1996, and became one of the "comets of the century" at the end of this century. The close approach opportunities from the Earth allowed favorable conditions of ground-based observations, even for the modest instruments.

More than 400 comets were observed photographically at Bucharest Observatory (Vass, 1994). The double refractor Prin-Merz of the Astronomical Institute in Bucharest has an F = 6m/D = 38cm and works as an astrograph, both photographically and CCD. The plates have a field by 2°×2° and ensure a limiting magnitude 12 (at maximum 30 min exposure time). The CCD has 768×512 pixels, "sees" a 4'×2.5' field and a limiting magnitude 15 (at 15 seconds time of integration). It is used in binning mode 2, 1pixel = 0.62".

2. ASTROMETRICAL OBSERVATIONS

In two cloudless nights we obtained three photographically positions of Hyakutake (March 20-th and 24-th), which were measured using an

Rom. Astron. J., Vol. 8, No. 1, p. 43–51, Bucharest, 1998

ASCORECORD machine, and were reduced with a classical least-squares method, using five-PPM stars. The results are given in Table 1.

Table 1

Photographic positions of the comet C/1996 B2

Date	Topocentric positions		Geocentric positions	
	α_{2000}	δ_{2000}	α_{2000}	δ_{2000}
$1996^y3^m20^d.930716$	$14^h\ 52^m\ 21^s.956$	4° 40' 13".04	$14^h\ 52^m\ 20^s.330$	4° 40' 47".93
1996 3 20 .950107	14 52 20 .179	4 47 27 .77	14 52 18 .776	4 48 02 .66
1996 3 24 .951746	14 35 33 .646	53 04 50 .37	14 35 30 .493	53 06 30 .85

Since the equipping of the mentioned instrument with the CCD, although various sources have been observed (the Saturnian satellites, asteroid appulses, globular clusters), C/1996 B2 is the first cometary object observed by CCD in Bucharest. His spectacular passing near the Earth in March 1996 offered the opportunity to test this new astrometrical technique on the comet observations.

March 24/25 was the most fruitful night of observation, because of the minimum distance of the comet from the Earth, which produced the greatest proper motion at that time 1'/min (Marsden, 1996), and due to the good meteorological conditions.

The possibility to make astrometrical observations using a CCD was discussed previously (Văduvescu & Vass,1995). Comparing with the photographical observations, the main problem of the CCD consists in the small field of the receptor (10.4016'2), and consequently in the small density of the catalogue stars in the field (0.025 PPM stars/CCD field). Nevertheless, there are two important advantages of the CCD: the very short integration time (and accordingly a lot of exposures), and the procedure of the measurement of the source's position (such as the Gauss distribution of the light intensities). This method gives good results mainly to diffuse sources (as the nucleus of the comets), comparing to the visual method at the measuring machine for astrometric positions.

In order to plot the path of the comet through the stars, graphical software, *Celestial Maps v.4.5* was used (Văduvescu & Bîrlan, 1996). Both the program and the ephemeris certified the accuracy of the predictions. Thus, in March 24/25 the comet approached four-PPM stars (PPM34602 at 22^h0^m, PPM34601 at 22^h34^m, PPM34595 at 0^h36^m, and PPM34582 at 1^h39^m, all in UT). At these moments, 15, 22, 20 and respectively 26 CCD exposures were made using 5-s times of integration (the stars has V_{ph} = 11.1, 10.1, 10.3 and 8.0 respectively).

The method of reduction uses the *one-star* reference systems (Văduvescu & Vass, 1995), and the orientation of the CCD was solved using *two - PPM stars* in the vicinity of the comet. All the 83 positions of the nucleus were reduced and reported to the Central Bureau for Astronomical Telegrams.

The reduced positions of the comet are presented in Figure 1. We can observe the good agreement between the results obtained by the two methods.

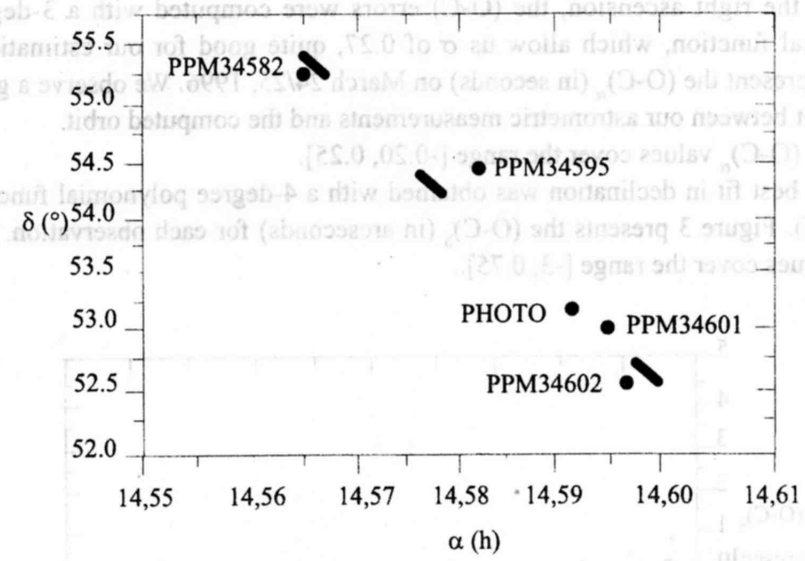

Fig. 1. – Reduced photographic and CCD positions of the comet C/1996 B2

We estimated the possibility to make astrometry using a single reference catalogue star. For this purpose, the (O-C) estimation is a good indicator. We used the comparison of our observations with the computed positions of Smithsonian (B. Marsden, private correspondence). Then, we used a polynomial fit.

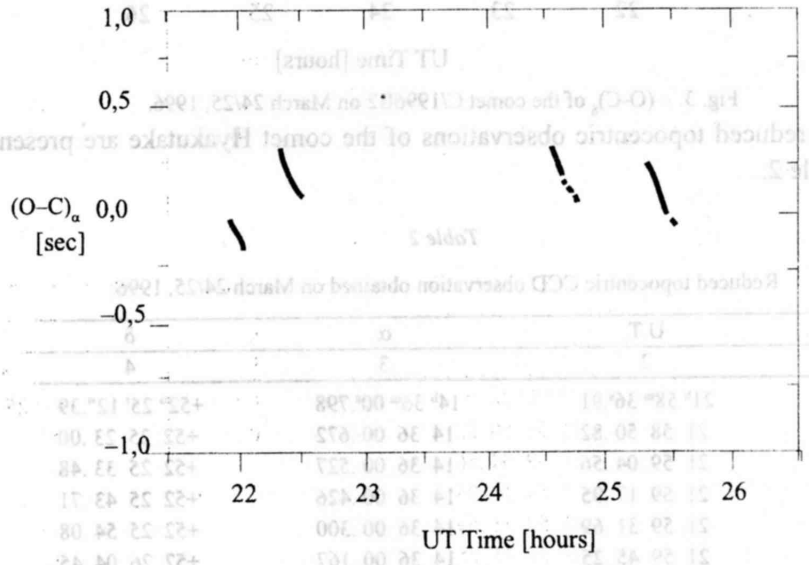

Fig. 2. – $(O-C)_\alpha$ of the comet C/1996B2 on March, 24/25, 1996.

For the right ascension, the (O-C) errors were computed with a 3-degree polynomial function, which allow us σ of 0.27, quite good for our estimations. Figure 2 present the $(O-C)_\alpha$ (in seconds) on March 24/25, 1996. We observe a good agreement between our astrometric measurements and the computed orbit.

The $(O-C)_\alpha$ values cover the range [-0.20, 0.25].

The best fit in declination was obtained with a 4-degree polynomial function ($\sigma = 0.05$). Figure 3 presents the $(O-C)_\delta$ (in arcseconds) for each observation. The (O-C) values cover the range [-3, 0.75].

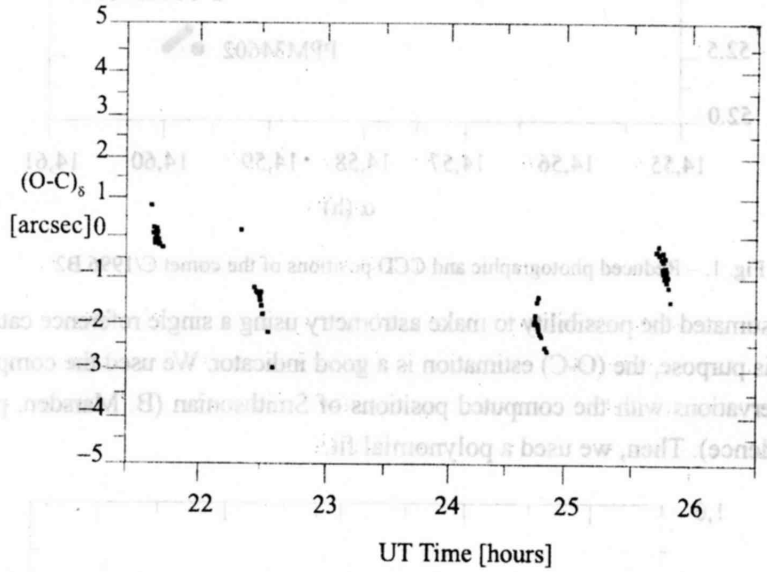

Fig. 3. – $(O-C)_\delta$ of the comet C/1996B2 on March 24/25, 1996.

The reduced topocentric observations of the comet Hyakutake are presented in the Table 2.

Table 2

Reduced topocentric CCD observation obtained on March 24/25, 1996.

N.	U.T.	α	δ
1	2	3	4
1	$21^h\ 58^m\ 36^s.91$	$14^h\ 36^m\ 00^s.798$	+52° 25' 12".39
2	21 58 50 .82	14 36 00 .672	+52 25 23 .00
3	21 59 04 .56	14 36 00 .527	+52 25 33 .48
4	21 59 17 .95	14 36 00 .426	+52 25 43 .71
5	21 59 31 .69	14 36 00 .300	+52 25 54 .08
6	21 59 45 .25	14 36 00 .167	+52 26 04 .45
7	22 00 12 .38	14 35 59 .899	+52 26 26 .06

Table 2 (continued)

1	2	3	4
8	22 00 25 .95	14 35 59 .805	+52 26 35 .62
9	22 00 39 .69	14 35 59 .683	+52 26 45 .80
10	22 00 53 .16	14 35 59 .556	+52 26 56 .21
11	22 01 06 .82	14 35 59 .432	+52 27 06 .75
12	22 01 20 .38	14 35 59 .312	+52 27 16 .95
13	22 01 33 .95	14 35 59 .188	+52 27 27 .43
14	22 01 47 .60	14 35 59 .059	+52 27 37 .84
15	22 02 01 .16	14 35 58 .926	+52 27 48 .14
16	22 31 15 .08	14 35 43 .992	+52 50 07 .53
17	22 31 29 .16	14 35 43 .870	+52 50 18 .15
18	22 31 42 .82	14 35 43 .738	+52 50 28 .62
19	22 31 56 .38	14 35 43 .610	+52 50 38 .95
20	22 32 09 .95	14 35 43 .478	+52 50 49 .40
21	22 32 23 .60	14 35 43 .359	+52 50 59 .71
22	22 32 37 .25	14 35 43 .224	+52 51 10 .07
23	22 32 50 .81	14 35 43 .106	+52 51 20 .54
24	22 32 50 .81	14 35 43 .104	+52 51 20 .54
25	22 33 04 .38	14 35 42 .980	+52 51 30 .85
26	22 33 18 .12	14 35 42 .849	+52 51 41 .32
27	22 33 31 .68	14 35 42 .719	+52 51 51 .69
28	22 33 45 .24	14 35 42 .599	+52 52 02 .10
29	22 33 58 .81	14 35 42 .480	+52 52 13 .99
30	22 34 12 .46	14 35 42 .342	+52 52 21 .45
31	22 34 39 .59	14 35 42 .091	+52 52 43 .53
32	22 34 53 .33	14 35 41 .963	+52 52 54 .01
33	22 35 06 .81	14 35 41 .830	+52 53 04 .36
34	22 35 20 .46	14 35 41 .696	+52 53 14 .18
35	22 35 34 .11	14 35 41 .586	+52 53 24 .97
36	22 36 14 .03	14 35 41 .208	+52 53 55 .45
37	22 36 41 .07	14 35 40 .952	+52 54 16 .16
38	22 36 54 .63	14 35 40 .828	+52 54 26 .44
39	24 34 34 .20	14 34 35 .624	+54 24 29 .19
40	24 34 48 .03	14 34 35 .478	+54 24 39 .69
41	24 35 01 .68	14 34 35 .342	+54 24 50 .11
42	24 35 15 .33	14 34 35 .195	+54 25 00 .50
43	24 35 28 .81	14 34 35 .059	+54 25 10 .94
44	24 35 42 .55	14 34 34 .911	+54 25 21 .26
45	24 35 56 .11	14 34 34 .779	+54 25 31 .75
46	24 36 09 .68	14 34 34 .643	+54 25 42 .12
47	24 36 23 .33	14 34 34 .513	+54 25 52 .49
48	24 36 36 .89	14 34 34 .360	+54 26 02 .96
49	24 36 50 .54	14 34 34 .226	+54 26 13 .34
50	24 37 04 .11	14 34 34 .097	+54 26 23 .73
51	24 37 17 .76	14 34 33 .940	+54 26 34 .27
52	24 37 31 .32	14 34 33 .808	+54 26 44 .49
53	24 39 06 .45	14 34 32 .828	+54 27 58 .36

Table 2 (continued)

1	2	3	4
54	24 39 20 .10	14 34 32 .710	+54 28 08 .91
55	24 39 33 .75	14 34 32 .552	+54 28 18 .10
56	24 39 47 .23	14 34 32 .423	+54 28 28 .47
57	24 40 00 .97	14 34 32 .279	+54 28 38 .89
58	24 40 14 .45	14 34 32 .147	+54 28 49 .23
59	25 36 22 .23	14 33 59 .208	+55 11 53 .19
60	25 36 35 .97	14 33 59 .070	+55 12 03 .50
61	25 36 49 .45	14 33 58 .928	+55 12 13 .89
62	25 37 03 .10	14 33 58 .779	+55 12 24 .31
63	25 37 16 .67	14 33 58 .636	+55 12 35 .06
64	25 37 30 .32	14 33 58 .493	+55 12 45 .22
65	25 37 43 .88	14 33 58 .348	+55 12 55 .40
66	25 37 57 .53	14 33 58 .212	+55 13 06 .19
67	25 38 11 .18	14 33 58 .071	+55 13 16 .39
68	25 38 24 .66	14 33 57 .921	+55 13 27 .04
69	25 38 38 .40	14 33 57 .772	+55 13 37 .48
70	25 38 51 .88	14 33 57 .636	+55 13 47 .80
71	25 39 05 .53	14 33 57 .487	+55 13 58 .21
72	25 39 19 .18	14 33 57 .343	+55 14 08 .52
73	25 39 32 .75	14 33 57 .197	+55 14 18 .88
74	25 39 46 .40	14 33 57 .055	+55 14 29 .34
75	25 39 59 .96	14 33 56 .902	+55 14 39 .78
76	25 40 13 .53	14 33 56 .769	+55 14 50 .19
77	25 40 40 .66	14 33 56 .477	+55 15 11 .06
78	25 40 54 .31	14 33 56 .342	+55 15 20 .17
79	25 41 07 .87	14 33 56 .198	+55 15 31 .83
80	25 41 21 .52	14 33 56 .046	+55 15 42 .17
81	25 41 35 .09	14 33 55 .911	+55 15 52 .67
82	25 41 48 .74	14 33 55 .773	+55 16 03 .04
83	25 42 02 .30	14 33 55 .607	+55 16 13 .58

Those observations are very useful in certain cases, such as the objects weakly observed. Thus, we tested for the first time such a method and we make the evaluation of the measurements with our CCD camera.

3. ORIENTATION OF THE TAIL

Figures 4 and 5 present two images of the comet, taken in March 24-th and April 1-st, and viewing in isophotes.

We made measurements of the position angle of the comet's tail using five images for each approach to the PPM stars on March 24/25. First, the position of the nucleus was measured using the centering method described above. After that, using a double representation of the images (in false colors and isophotes), we measured ten position in the tail direction on each image. These absolute coordinates on the images were reduced using linear regression. We obtained in the

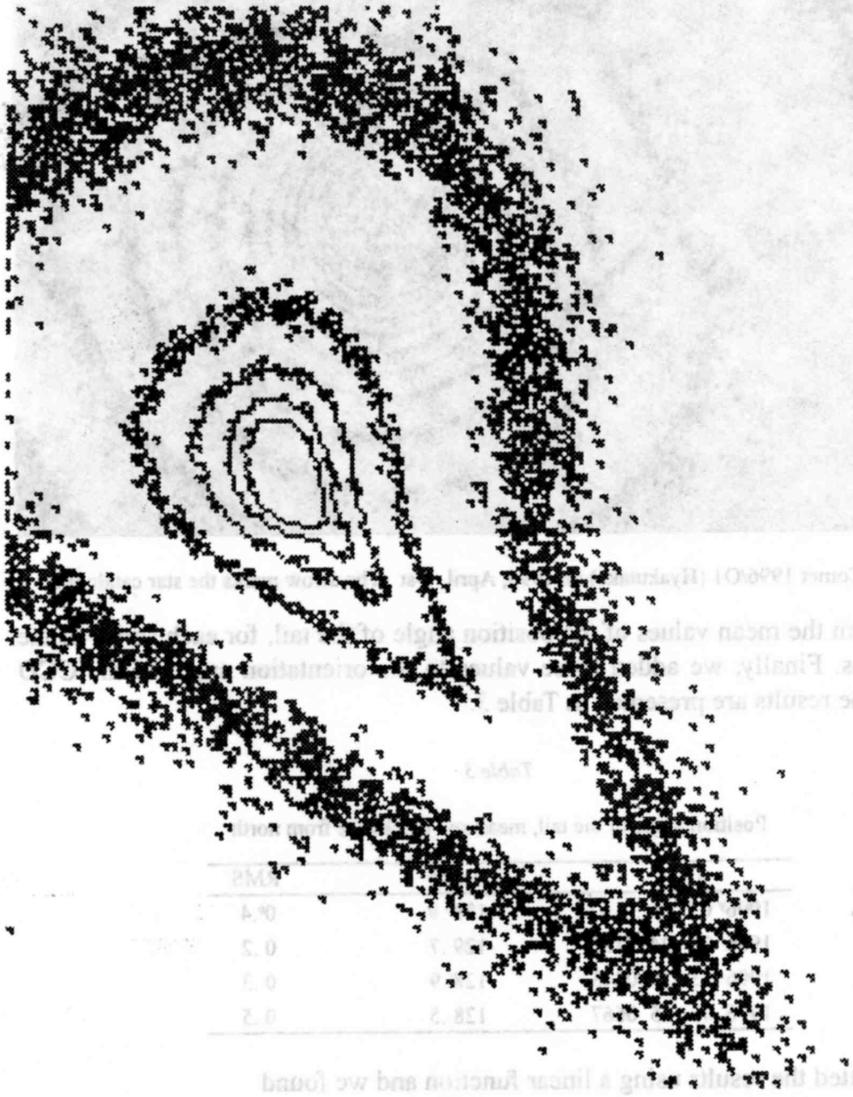

Fig. 4. – Comet C/1996B2 (Hyakutake) in 1996, March, 24-th.

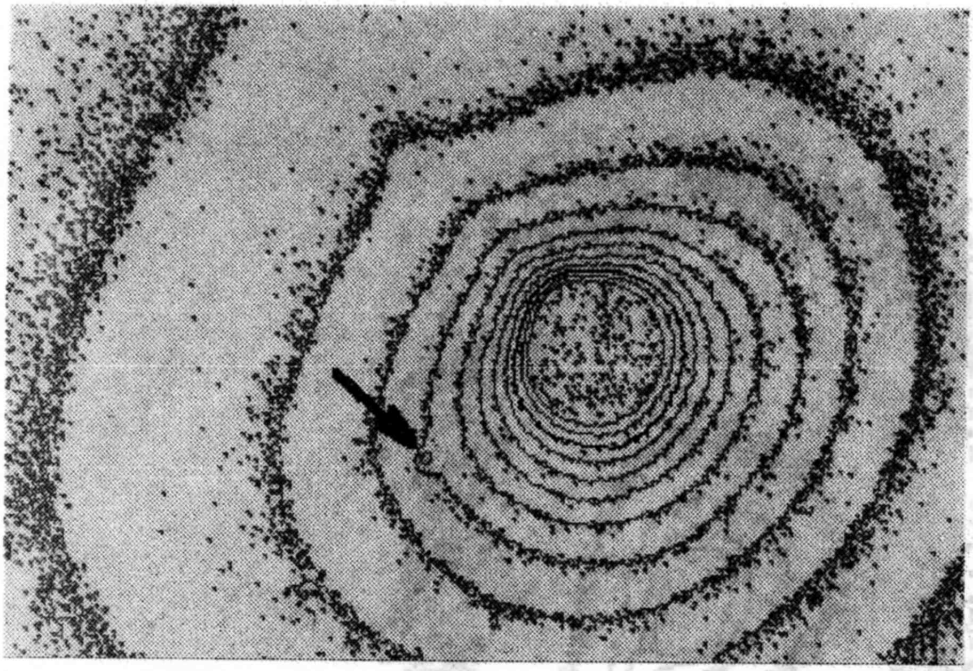

Fig. 5. – Comet 1996/O1 (Hyakutake) on 1996, April, 1-st . The arrow marks the star catalogue.

CCD system the mean values of the position angle of the tail, for each series of the five images. Finally, we added these values to the orientation angle of the CCD camera. The results are presented in Table 3.

Table 3

Position angle of the tail, measured clockwise from north

Date	Angle	RMS
$1996^{y}\ 03^{m}\ 24^{d}.9167$	$129^{o}.9$	$0^{o}.4$
1996 03 24 .9382	129 .7	0 .2
1996 03 25 .0243	128 .9	0 .3
1996 03 25 .0667	128 .5	0 .5

We fitted the results using a linear function and we found

$$\theta = -0.3886\ t + 138.45\ ,$$

where θ represents the orientation angle, and t is the time, given in hours.

Acknowledgements: We would like to thanks Dr. B. Marsden for promptly taking into consideration our astrometrical requests related to the comet. Special thanks Mrs. A. Alexiu for the "know-how" on the ASCORECORD measuring machine.

REFERENCES

Marsden, B.: 1996, *M.P.E.C.1996-F03.*
Vass, Gh.: 1994, *Rom. Astron. J.*, **2**, 183.
Văduvescu, O., Vass, Gh.: 1995, *Position of Asteroids from CCD Observations,* Communication at The Academic Days of Cluj, 1995 October, Cluj-Napoca.
Văduvescu, O., Bîrlan, M.: 1996, *Rom. Astron. J.* **6**, 97.

Received on 14 January 1998

I.3. Spectroscopie visible et infrarouge proche des objets du système solaire

Le spectroscopie est une méthode nouvelle d'observation pour les objets sans atmosphère, les développements notables datent des deux dernières décennies. La difficulté majeure est en grande partie due au fait que nous rencontrons plusieurs minéraux assez différents par leurs éléments constituants pouvant donner une signature spectrale assez semblable. De plus, les mêmes composants minéralogiques, suivant leur processus de cristallisation, peuvent donner différentes signatures. Contrairement au gaz, les signatures des minéraux se caractérisent (suivant le cas) dans de larges bandes d'absorption de différents profondeurs.

Dans l'intervalle spectral 0,4-3,00 μm (domaine du visible et de l'infrarouge proche) les photons incidents sont absorbés et d'autres photons sont émis aux fréquences correspondant à celles de vibrations des molécules présentes à la surface du corps sans atmosphère.

Dans l'intervalle spectral considéré, l'émission thermique de leur surface est négligeable et les absorptions sont produites par des vibrations, par les transitions du champ cristallin et par des mécanismes de transfert de charges électriques. La minéralogie de la surface des astéroïdes joue donc un rôle essentiel dans l'explication de chaque spectre.

Y-a-t-il des contraintes concernant le type de minéraux ? A cette question nous pouvons répondre en nous appuyant sur des résultats de la minéralogie des autres corps solides (et sans atmosphère) dont nous avons des échantillons sur Terre : météorites, roches lunaires, roches terrestres. La planétologie comparée, les études en laboratoire des échantillons des minéraux, jouent donc un rôle important dans les considérations faites sur la composition à la surface des objets.

Qu'est ce qui produit les caractéristiques d'un spectre de corps sans atmosphère ? Le rayonnement électromagnétique incident ne peut pas pénétrer à l'intérieur de l'objet. La

surface étant rugueuse et non uniforme, marquée par des grains des minéraux à l'état cristallin (des régolites), les bandes d'absorption sont donc les résultats de l'interaction du rayonnement incident avec la couche superficielle du corps.

L'absorption la plus fréquente de photons incidents est causée par la présence d'atomes de fer ou d'atomes de métaux de transition (nickel, cobalt, cuivre, titanium, etc.) dans les différents réseaux cristallins de la surface de l'astéroïde. Le photon incident est absorbé par un électron qui devient capable d'occuper un niveau d'énergie supérieur. L'énergie de ce niveau est égale à la somme de l'énergie du photon et de l'énergie du niveau qu'il a quitté. Ainsi, on peut identifier les minéraux, établir la présence de tel où tel cation métallique et, éventuellement déterminer l'abondance du métal de transition dans la structure minérale. Voici quelques exemples : $\boldsymbol{Fe^{2+}}$ présent dans l'ortopyroxène est responsable des bandes d'absorption symétriques centrées respectivement sur 1 et 2 µm. Le même $\boldsymbol{Fe^{2+}}$ dans le minéral de feldspath donne une faible bande d'absorption vers 1,25 µm. Le remplacement d'un métal de transition par un autre modifie les transitions du champ cristallin ; par conséquent, les bandes d'absorption seront déplacées par le nouvel atome.

De façon semblable, la présence d'une bande d'adsorption étroite dans la région du visible, autour de 0,49 µm, peut être expliquée par la présence de sulfure de fer ($Fe^{2+}S$) ou de sulfure de calcium (CaS) dans les minéraux comme les troilites ou les oldhamides respectivement.

Les bandes d'absorption dues aux vibrations des molécules sont aussi présentes dans le domaine spectral 0,4-3,0 µm. Les molécules les plus étudiées sont celles trouvées de façon significative à l'intérieur des météorites : l'eau, les minéraux carbonés, les composants hydrocarbonés. Par exemple, la présence de molécules d'eau dans les minéraux est à l'origine d'une forte bande d'absorption centrée sur 3 µm et deux autres bandes moins importantes centrées sur 1,4 et 1,9 µm respectivement. Certains auteurs proposent la présence d'une large bande (de faible profondeur) d'altération aqueuse autour de 0,7 microns pour des astéroïdes de la ceinture principale. L'ion $\boldsymbol{CO_3^{2-}}$ présent dans les composants carbonés donne une bande d'absorption centrée sur 1,6 µm et les composants carbonés contenant des métaux de transition sont à l'origine d'une bande d'absorption centrée sur 1 µm. Aussi, la vibration de la liaison ***C-H*** dans les hydrocarbures donne une bande d'absorption centrée sur environ 3,4 µm.

Quels sont les particularités liées à la spectroscopie au sol ?

Le rayonnement électromagnétique incident des domaines spectraux du visible et de l'infrarouge proche ne bénéficie pas de régimes similaires pendant la traversée de l'atmosphère terrestre. En effet, l'atmosphère terrestre est beaucoup plus fluctuante en

infrarouge proche et ultraviolet, essentiellement par les interactions (excitations) de certaines espèces chimiques de la haute atmosphère avec le rayonnement solaire ultraviolet et X (airglow phenomena = lueur de l'air). La nuit, ces lueurs sont souvent associées à la recombinaison des atomes de la haute atmosphère (80-100 km d'altitude). La technique utilisée pour l'obtention des spectres en infrarouge proche consiste à réaliser de courtes expositions. Par la soustraction des deux images successives, le fond du ciel sera ainsi enlevé. Ensuite, la somme de ces nouvelles images permettra l'obtention du rapport signal-bruit nécessaire. Etant donnée la faible luminosité de la majeure partie des corps sans atmosphère, un spectre en infrarouge proche peut être obtenu en 80-100 minutes d'exposition en moyenne pour un objet de magnitude 18-19, avec un rapport signal sur bruit[1] égale à 100. Le formalisme mathématique est représentée par la relation :

$$I_f = \sum_{i=1,2}^{n} (I_{i+1} - I_i)$$

où *n* représente le nombre d'images individuelles nécessaires pour atteindre le rapport signal-bruit désiré.

Dans les cas des objets sans atmosphère les contraintes liées à la résolution spectrale ne sont pas très importantes. Souvent la conception des instruments prend en compte des résolutions spectrales supérieures aux besoins pour les corps sans atmosphère (leur science nécessite une résolution spectrale entre 100 et 200). Dans la majeure partie des cas, pour une meilleure analyse, les spectres des corps sans atmosphère sont remis à une échelle adéquate, par un re-échantillonnage en longueur d'onde.

La majeure partie de mes activités d'observation et d'analyse des spectres visibles et infra-rouge s'est développée en vue de la préparation au sol de la mission spatiale ROSETTA, mais aussi en vue de la préparation d'autres missions spatiales (la mission spatiale DAWN et une éventuelle mission européenne vers des astéroïdes géocroiseurs).

L'activité d'analyse spectroscopique des astéroïdes cibles potentielles de la mission ROSETTA s'est déroulée pendant des nombreuses années, avec pour but de trouver les objets correspondant le mieux possible aux objectifs scientifiques de cette mission, survols et analyse « in situ » des objets avec une minéralogie gardant les caractéristiques de la formation du système solaire.

Les campagnes d'observations spectroscopiques se sont déroulées sur plusieurs télescopes de taille moyenne (diamètre du miroir primaire entre 2 et 4 m) : InfraRed Telescope Facility (3 m d'aperture) et Canada-France-Hawaii Telescope (3,60m) du Mauna

[1] La magnitude peut être atteinte sur un télescope de classe moyenne (2,5-4 m de diametre)

Kea-Hawaii, Telescopio Nazionale Galileo (3,52 m) des Canaries, New Technology Telescope (3,58 m) de l'ESO-La Silla). Plusieurs spectrographes (SpeX, Dolores, NICS, EMMI, …) ont été utilisés afin d'obtenir des données dans la région du visible et de l'infrarouge proche.

Les astéroïdes cibles potentielles de la mission spatiale ROSETTA ont polarisé une bonne partie des campagnes d'observations. Les changements de dernière minute de la fenêtre de lancement a fait que les astéroïdes candidats au survol ont été choisis après le lancement de la sonde. Les deux astéroïdes désignés sont 21 Lutetia et 2867 Steins, localisés dans la ceinture principale.

L'astéroïde 21 Lutetia est un objet de grande taille (diamètre estimé à 95.5 ± 4.1 km). Le survol de cet objet par la sonde ROSETTA est prévu pour juillet 2010. Les données spectroscopiques obtenues dans l 'infra-rouge proche montrent un spectre plat, neutre, sans bandes d'absorption. Ce type de spectre est souvent associé à des minéraux contenant du carbone, souvent rencontrés dans les météorites chondritiques carbonnées. Ce comportement spectral de l'objet le classe plutôt dans les objets primitifs de la ceinture principale (souvent on le nomme objet de type **C**, d'après la taxonomie des astéroïdes), ce qui complète les résultats publiés déjà, laissant ouvert le débat concernant la composition minéralogique de la surface. Sur la base de la pente du spectre dans la région du visible et de son albédo thermique obtenus par les données du satellite IRAS, 21 Lutetia a été classé auparavant comme étant un objet contenant une quantité importante des métaux (astéroïde de type M, essentiellement associé à des fragments de noyau d'un objet différencié).

Nous avons observé spectroscopiquement pour la première fois 21 Lutetia dans la région 2,9 - 3,8 μm, afin de pouvoir analyser quantitativement l'altération aqueuse publiée par d'autres auteurs (Rivkin et al, Icarus, vol 145, 2000) sur la base des observations photométriques. Nous pensons que le traceur représenté par cette bande peut apporter un argument important pouvant trancher sur le caractère primitif de l'objet. Nos observations ne confirment pas cette bande. Cependant nous ne pouvons pas exclure définitivement sa présence pour plusieurs raisons : la principale étant que la surface de l'hémisphère nord est la seule à réfléchir la lumière (géométrie « pole-on »). Par conséquent, nos mesures ne peuvent pas être comparées directement avec celles de la littérature. Des nouveaux programmes d'observations seront proposés afin d'obtenir des résultats permettant de caractériser l'autre hémisphère de l'astéroïde.

Le second candidat au survol de la mission ROSETTA est 2867 Steins, un astéroïde de petite taille dont toutes les données physiques restent à découvrir avant la rencontre. Les

données spectroscopiques obtenues dans la région du visible et de l'infra-rouge proche montrent un spectre avec une pente positive importante dans la région du visible. Dans la région d'infrarouge proche le spectre ne présente pas de bandes d'absorption mais la pente est toujours positive et moins importante. Le spectre peut être associé à des spectres de météorites différenciés contenant de l'enstatite ($Mg_2Si_2O_4$). La ressemblance avec les spectres de météorites composés d'enstatite est plus marquée par la présence d'une bande a 0,49 microns, dans les spectre du 2867 Steins correspondant aux assemblages des sulfites (Fe-S) ou (Ca-S). Des campagnes soutenues de surveillance seront nécessaires pour caractériser au sol le mieux possible cet objet avant son survol par Rosetta, évènement planifie pour septembre 2008.

Des campagnes d'observations ont eu lieu également afin de mieux caractériser la composition de la surface des astéroïdes 1 Ceres et 4 Vesta, les deux cibles de la mission spatiale DAWN. Les campagnes se poursuivent encore. Ces observations nous ont permis non seulement l'obtention de nouvelles données, mais aussi la possibilité de modélisation de leur spectres en termes minéralogique. Ce volet des activités sera développé dans le chapitre de modélisation.

La structure interne des astéroïdes, est également sujet de débat au sein des scientifiques qui étudient des astéroïdes. Il y a une liaison indéniable entre l'étude des surfaces des astéroïdes et leur composition d'ensemble : en fait, les conclusions des études spectroscopiques sont associées à une évolution thermique des objets. Elle est en partie le réflexe d'un comportement global de l'objet. Souvent, nous caractérisons la minéralogie de l'ensemble de l'objet par les données issues de l'analyse de leur surfaces. Cette hypothèse de travail est-elle vraie ? Des missions de recherche de la structure interne des astéroïdes sont en cours de préparation. Les cibles de ces missions peuvent être les astéroïdes géocroisseurs. Des programmes d'observations ont été initiés dans le cadre des collaborations internationales mais aussi en réponse à des initiatives nationales (par exemple, suite au programme d'Actions Coordonnées Interdisciplinaires initié par le Ministère de l'Education et de la Recherche). Les actions visent une meilleure connaissance de la population ainsi que l'identification de la caractérisation des astéroïdes géocroiseurs pouvant faire l'objet de missions.

Références :

Binzel, R.P., **Birlan, M.**, Bus, S.J., Harris, A., Rivkin, A.S., Fornasier, S.– *Spectral Observations for Near-Earth Objects Including Potential Target 4660 Nereus: Results From Meudon Observations at the NASA Infrared Telescope Facility (IRTF)*, **Planetary & Space Science,** Vol. **52(4)**, 291-296, 2004.

Birlan M., Barucci M.A., Vernazza, P., Fulchignoni M., Binzel R.P., Bus S.J., Fornasier S. *Near-Ir Spectroscopy of asteroids21 Lutetia, 89 Julia, 140 Siwa, 2181 Fogelin, and 5480 (1989YK8), potential targets of the Rosetta mission; remote observations campaign on IRTF,* **New Astronomy,** Vol**. 9 (5),** 343-351, 2004.

Barucci, M.A., Fulchignoni, M., Fornasier, S., Dotto, E., Vernazza, P., **Birlan, M.**, Binzel, R., Carvano, J., Merlin, F., Barbieri, C., Belskaya, I. – *Asteroid target selection for the new Rosetta mission baseline : 21 Lutetia and 2867 Steins* – **Astronomy and Astrophysics** v.430, 313-317, 2005.

M.A. Barucci, M. Fulchignoni, **M. Birlan**, P. Vernazza, E. Dotto, A. Doressoundiram – *Rosetta asteroid candidates* - Highlights of Astronomy, vol. 13, **XXVth General Assembly of the IAU**, Sidney, July 2003

Barucci M.A., Fulchignoni, M., Belskaya, I., Vernazza, P., Dotto, E., **Birlan, M. -** *Rosetta asteroid candidates*, in *The NEW Rosetta targets. Observations, simulations and instrument performances* Astrophysics and Space Science Library (ASSL) Vol. 311, Kluwer (ISBN: 1-4020-2572-6). (Eds. L. Colangeli, E. Mazzotta-Epifani, P. Palumbo)

Birlan M. – *Emission in absobtion lines; results of the SL9 L nucleus impact on Jupiter*, **Romanian Astronomical Journal**, vol **10**, n. **8**, 137-144, 2000.

Available online at www.sciencedirect.com
SCIENCE DIRECT®
Planetary and Space Science 52 (2004) 291–296
Planetary and Space Science
www.elsevier.com/locate/pss

Spectral observations for near-Earth objects including potential target 4660 Nereus : Results from Meudon remote observations at the NASA Infrared Telescope Facility (IRTF)

Richard P. Binzel[a,*], Mirel Birlan[a], Schelte J. Bus[b], Alan W. Harris[c], Andrew S. Rivkin[d], Sonia Fornasier[e]

[a] *Observatoire de Paris–Meudon, 5 Place Jules Janssen, 92195 Meudon Cedex, France*
[b] *Institute for Astronomy, 640 North A'ohoku Place, Hilo, HI 96720, USA*
[c] *Jet Propulsion Laboratory, Pasadena, CA 91109, USA*
[d] *Department of Earth, Atmospheric and Planetary Sciences, Massachusetts Institute of Technology, Cambridge, MA 02139, USA*
[e] *Astronomical Department of Padova, Vicolo dell'Osservatorio 2, 35122 Padova, Italy*

Received 20 September 2002; received in revised form 10 July 2003; accepted 30 October 2003

Abstract

We present visible and near-infrared spectral measurements for the highly accessible spacecraft target 4660 Nereus and three additional near-Earth objects displaying diverse color characteristics. All near-infrared measurements were carried out during the first remote observing operations between the Observatoire de Paris at Meudon and Mauna Kea, Hawaii. From Meudon, we had fine pointing and guiding control of the NASA Infrared Telescope Facility 3.0-m telescope and the near-infrared spectrograph "SpeX" to measure asteroid spectra in the range 0.8–2.4 μm. The efficiency of the observation was virtually the same as if the observers had been on location. We combine our near-infrared results with complementary 0.4–0.9 μm spectral measurements. Nereus is found to be a rare Xe-type asteroid with a composition that may be analogous to very high albedo enstatite achondrite (aubrite) meteorites, leading to a diameter estimate of less than 0.5 km. 1685 Toro displays a classic S-type spectrum while a steeper visible wavelength slope and a less pronounced 1 μm absorption feature for 1943 Anteros places it in the L-class. Also unusual is the apparent olivine-rich spectrum for 4142 Dersu-Uzala, which is classified as an A-type.

Keywords: Remote observation; Spectroscopy; Asteroid; Space mission

1. Remote observation setup

Remote observation is becoming increasingly common at telescopes throughout the world as it allows the observer to reside in a location that may be more comfortable than a high-altitude summit and may reduce observer fatigue if no travel is required from her/his home institution. Circumstances that are particularly conducive to successful remote observations include using an instrument and telescope with which the observer is familiar and for which the observing procedures are well practised. Having these circumstances in our favor allowed us to test the remote observing capabilities being established at the NASA Infrared Telescope Facility (IRTF) on Mauna Kea, Hawaii. Such control differs from pre-programmed robotic systems for survey programs, and "service mode" observational programs, in that the observer has complete control to select program targets in real-time in response to conditions, to perform real-time assessment of data quality, and to immediately select new targets of opportunity. Brunswig et al. (2000) and Martin et al. (2000) give examples of previously established remote observation connections. In fact, several telescopes on Mauna Kea, Hawaii (Kibrick et al., 2000) offer the possibility to observe remotely from Hilo and Waimea (sea level and 760 m altitude, respectively). The uniqueness of our experiment consists in conducting remote observations from Meudon, France, more than 12,000 km away from Hawaii. For the observers in Meudon, the observing sessions ideally coincided with relatively normal working daylight hours. Observing sessions

* Corresponding author. Department of Earth, Atmospheric and Planetary Sciences, Massachusetts Institute of Technology, Mail Stop 54-410, Cambridge, MA, 02139, USA.
E-mail address: rpb@mit.edu (R.P. Binzel).

0032-0633/$ - see front matter © 2003 Elsevier Ltd. All rights reserved.
doi:10.1016/j.pss.2003.10.003

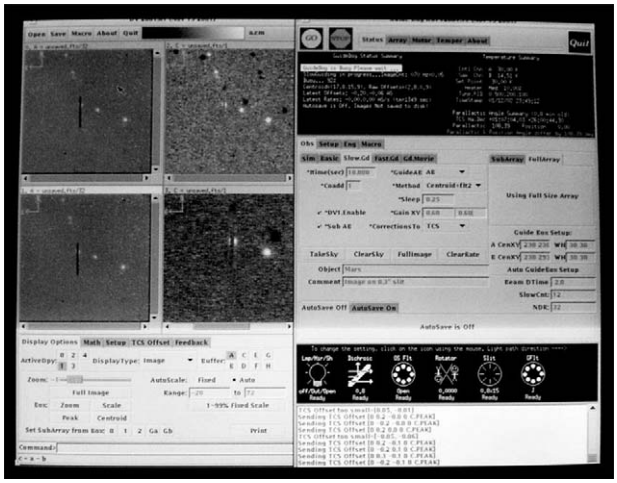

Fig. 1. IRTF control and guider (named "Guidedog") X-windows as seen from Meudon. Images of the spectral slit are seen in the upper left, where the display parameters are controlled immediately below. Control for the guide camera is seen on the right. An overview of the instrument configuration appears at lower right.

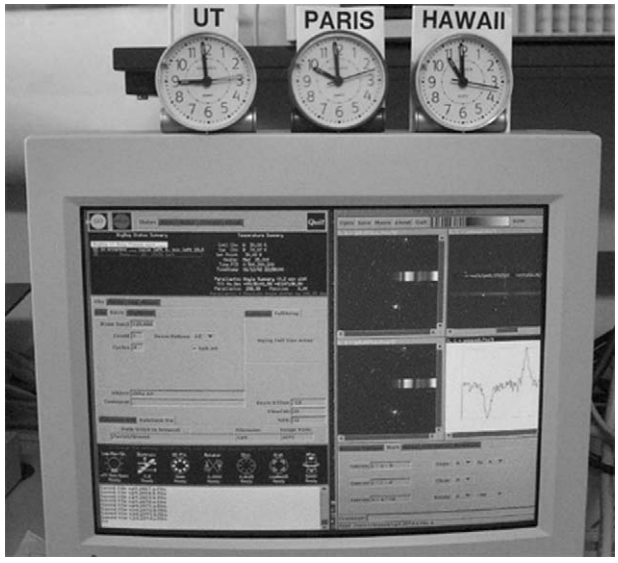

Fig. 2. SpeX instrument control system (named "Bigdog") as seen from Meudon. Observing modes and data acquisition are controlled by the window on the left. Spectral images and their preliminary analysis are displayed and controlled on the right.

began at 5 a.m. local time and finished at 5 p.m. local time.

Our goals for remote science operation included having control of the instrument and the target acquisition/guider system as well as constant audio/visual interaction with the telescope operator. Several weeks of effort were devoted in order to determine the best means for reaching these operational goals using existing equipment. Two Sparc workstations (operating under SunOS versions 5.7 and 5.8) were found to be very well suited for the task of controlling the fine pointing and guiding of the telescope and the instrument via X-windows exported from Mauna Kea to Meudon. In order to have a continuous audio/video link, we started with the idea to set up remote computers within a video-conference room. The incompatibility of both systems (through a phone line in Meudon and an IP link in Mauna Kea), constrained us to choose either an IP link or a phone link. Our decision was to use the IP link as it was most compatible with IRTF operations. Thus, our audio/video link was established with a Polycom ViewStation FX video-conference system (on Mauna Kea), and webcam/NetMeeting software (at Meudon). Figs. 1 and 2 show the displays as seen at Meudon that allowed real-time control of the target centering and guiding and all instrument setup and data acquisition functions of the spectrograph.

This experiment was realized through an ordinary network link, without any service quality warranty. Thus, the bandwidth for our link was variable and was a function of the internet traffic between Hawaii and Meudon. Our remote observing sessions occurred during both weekdays and weekends and we noted very few perturbations due to internet traffic from within the campus of the Meudon Observatory and between Mauna Kea and Meudon. Most communications occurred with a latency of about 0.5 s. The mean delay between the image acquisition in Mauna Kea and the refresh of the Meudon displays was 2 s. Images communicated in real time were for verification purposes only. The full spectral image files (~ 4 Mbytes each) were transferred to Meudon after the completion of the night. For all procedures, except for manual guiding on faint objects, such delays did not impede the efficient performance of the observation process. Overall, we estimate our total efficiency relative to being on-site was about 90 %. Having significant on-site experience with the instrument and typical weather conditions were critical factors in achieving this efficiency and can be considered prerequisites for remote observation success.

2. Science measurements

Our remote observation experiments on the 3.0-m aperture telescope of the IRTF were conducted using SpeX, a medium resolution near-infrared spectrograph employing a 1024×1024 InSb array (Rayner et al., 1998). SpeX was used in its low-resolution prism mode to obtain spectra over the range 0.8–2.5 μm with the resulting measurements binned at 50 Å/ pixel. SpeX observations were calibrated with respect to the solar-like stars Hyades 64 and SA 102-1081 (Landolt, 1973). All observations were made using a 0.8 arcsec slit width with pairs of exposures ("A" and "B") alternated along the 15-arcsec long spatial direction of the slit for the purpose of producing near-simultaneous images for sky subtraction. Residual sky values (after A − B and B − A subtraction) were fit and removed in the spectral extraction.

Table 1
Log of observations

Asteroid	Telescope	Wavelength range (μm)	Date and time (or reference)
1685 Toro	MDM 2.4 m	0.4–0.9	Bus and Binzel (2002a,b)
	IRTF 3 m	0.9–1.6	Burbine and Binzel (2002)
	IRTF 3 m	0.8–2.5	2002 May 08 09:19–09:57 UT
1943 Anteros	Palomar 5 m	0.3–0.9	Binzel et al. (2001a)
	IRTF 3 m	0.8–2.5	2002 January 12 12:25–13:01 UT
4142 Dersu-Uzala	MDM 2.4 m	0.4–0.9	Bus and Binzel (2002a,b)
	IRTF 3 m	0.8–2.5	2002 April 15 09:57–10:54 UT
4660 Nereus	Palomar 5 m	0.3–0.9	2001 October 22 06:40-07:06 UT
	KPNO 4 m	0.5–0.9	2002 February 23 11:19–11:52 UT
	IRTF 3 m	0.8–2.5	2002 March 15 11:18–12:36 UT

We performed Meudon–Mauna Kea remote operations over the course of four observing runs (totaling seven nights) between January and May, 2002. Near-Earth objects were our primary targets as part of a program to explore the diversity of their compositions and the potential relationships between asteroids, comets, and meteorites. (See Binzel et al., 2002 for more details on the motivation of near-Earth object studies.) Near-infrared (0.8–2.5 μm) spectral measurements of near-Earth objects (and asteroids in general) are highly diagnostic of their compositions owing to the existence of spectral signatures (absorption bands) due to pyroxene near 1- and 2 μm and olivine near 1 μm. These are common constituents in the majority of meteorites and thus provide a powerful means for exploring asteroid–meteorite associations. SpeX provides a new capability for near-Earth objects in that objects may be measured down to a limiting magnitude near V18, placing many dozens of these objects within reach at any given time. Remote observation is also quite advantageous to the reconnaissance of near-Earth objects as they typically have very short windows of observability when they make close (and often fast) passages near-the Earth. Thus frequent access to the telescope is necessary—making the capability of remote observation all the more desirable for eliminating frequent travel.

To exemplify the results of our remote observation experiment, we present one object from each run that is representative of the diversity found within the near-Earth object population. (A more complete analysis of the larger sample is forthcoming as observations are continuing.) A primary focus for the science results reported here is our findings for 4660 Nereus: a near-Earth asteroid with a low-inclination Earth-intersecting orbit that makes it among the most easily accessible (in terms of low delta-V trajectories) objects currently known. Table 1 gives a summary log of our reported science measurements. These measurements include complementary visible wavelength spectra obtained at Palomar, Kitt Peak, and Michigan-Dartmouth-MIT (MDM) observatories. At the 5.0-m Hale telescope on Palomar Mountain, California we employed the Double Spectrograph described by Oke and Gunn (1982). This instrument uses a pair of 1024 × 1024 pixel (binned 2 × 2 on readout) CCD cameras to simultaneously record the blue and red halves of a long-slit spectrum. Binzel et al. (2001a) give a description of the techniques we employed with this instrument. Additional supporting visible wavelength measurements were obtained with the 4.0-m Mayall Telescope at Kitt Peak National Observatory, Arizona, using the RCSP spectrograph and Tektronix 2048 × 2048 CCD binned 2 × 2 on readout. A GG495 order sorting filter and 5 arcsec slit width provided 0.5–0.9 μm spectral coverage with a dispersion of 10 Å/pixel and a spectral resolution of about 50 Å. Binzel et al. (2001b) give a description of the techniques we employed with this instrument. For the Mark III CCD spectrograph and similar techniques employed at the MDM 2.4-m Hiltner telescope, we refer the reader to Bus and Binzel (2002a) and Bus et al. (2002).

3. Science results

3.1. 4660 Nereus

A close approach in early 2002 provided the first favorable opportunity for spectral measurements of Nereus since its 1982 discovery. For the IRTF measurements, all target acquisition, guiding, and data acquisition commands were executed and controlled from Meudon. For the final 0.8–2.4 μm near-infrared spectrum, data were binned (4 × 50 Å) in 0.02 μm intervals so as to improve the signal-to-noise. Visible wavelength measurements complementary to our IRTF remote observations were obtained at both Kitt Peak and Palomar Observatories. These separate visible spectra were normalized to unity at 0.55 μm and then combined by a weighted average. Overlapping spectral coverage in the range of 0.8–0.9 μm was used to scale the near-infrared spectrum to match the normalized relative

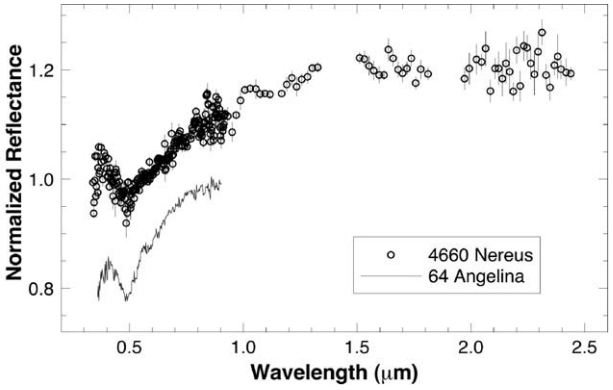

Fig. 3. Relative reflectance spectrum (data points) of near-Earth asteroid 4660 Nereus normalized to unity at 0.55 μm. (Gaps at 1.4 and 1.9 μm as well as the small feature at 0.92 μm are due to the presence of telluric water.) While the near-IR spectrum is featureless, we note the match of the rarely seen 0.49 μm feature to that for the E-type asteroid 64 Angelina (curve, vertically offset for clarity and shown below).

reflectance scale established by the visible measurements. The resulting Nereus spectrum, shown in Fig. 3, has a combined wavelength coverage from 0.34 to 2.44 μm.

Over the range 0.8–2.4 μm, Nereus shows a moderate red slope (increasing reflectance with increasing wavelength) but does not show substantial 1.0- or 2.0 μm absorption bands arising from the presence of Fe^{2+}-bearing pyroxene–olivine mixtures that are most typically seen in the spectra of near-Earth asteroids (Binzel et al., 2001a). The red slope of the Nereus spectrum also is greater than the generally very flat and featureless spectra seen for C-type asteroids. Within the Tholen taxonomy system (Tholen and Barucci, 1989), the moderate red slope and lack of silicate absorption features are consistent with Nereus being either an E-, M,- or P-class asteroid. (Formally, this degeneracy is denoted by the designation "X" pending an albedo measurement to resolve the spectral ambiguity.) Bus (1999) and also Bus and Binzel (2002a,b) present an extension to the Tholen taxonomy that takes advantage of the higher spectral resolution of CCD spectra for identifying features that are diagnostic for recognizing taxonomic classes. Within the feature-based taxonomy system of Bus, the Slope and PC2' scores for Nereus are 0.368 and 0.324, respectively, placing Nereus within the "X-complex".

The key to resolving the likely nature of Nereus' composition is the presence of a strong but relatively narrow absorption feature near 0.49 μm. This feature was first detected in the spectrum of asteroid 64 Angelina (Bus, 1999; Bus and Binzel, 2002a). Within the Bus taxonomy, this feature unambiguously places both Angelina and Nereus within the Xe-class. Angelina is known to have a high albedo (listed as 0.43 within Tedesco, 1989) and is therefore classified as an E-type by Tholen. Independent thermal flux measurements of Nereus (Delbo et al., 2003) confirm a high albedo for Nereus, also making it consistent with the Tholen E-class. For an albedo similar to or likely higher than the value for Angelina (Delbo et al., 2003), an *H* magnitude of 18.2 (IAU Minor Planet Center) yields a diameter estimate not larger than 0.5 km according to the relation of Bowell et al. (1989).

Meteorite associations for E-type asteroids have been extensively investigated (e.g. Gaffey et al., 1992) and the 0.49 μm feature within the Bus Xe-class has been analyzed by Burbine et al. (1998, 2001) with troilite (FeS) and oldhamite (CaS) as possible constituents. Burbine et al. (2002) compared the spectrum of 64 Angelina with oldhamite, aubrites, and troilite and found good agreement between Angelina and oldhamite. Asteroids such as Angelina and Nereus may be analogous to enstatite achondrite meteorites with somewhat higher oldhamite abundances than seen within laboratory samples. Enstatite achondrite meteorites, for which Norton County is a common example, are high albedo samples of chondritic material that has undergone heating and melting sufficient to allow almost complete extraction of NiFe metal and FeS.

Finally, it is interesting to *speculate* on the origin of 4660 Nereus. Gaffey et al. (1992) forged a plausible link for the enstatite achondrites to the Hungaria region of the inner asteroid belt where E-type asteroids are common. Asteroid 3103 Eger, an E-type near-Earth asteroid with a similar high inclination to the Hungaria region, is viewed by Gaffey et al. as a prototype for the connection between Hungarias and enstatite achondrites arriving on Earth. We note that Eger and Nereus have similar semi-major axes (1.40 and 1.48 AU, respectively) and orbital eccentricities (0.35 and 0.36, respectively). However, the significantly lower orbital inclination for Nereus (1.4° compared with 20.9°) makes a connection to Eger and the Hungaria region more problematic. For example, in a planetary encounter, the encounter velocity is generally a conserved quantity making it implausible to change inclination only while leaving the semi-major axis and eccentricity mostly unchanged. Thus any connection between Nereus, Eger, and the Hungarias is both problematic and complex.

3.2. 1685 Toro, 1943 Anteros, 4142 Dersu-Uzala

Similar to our Nereus IRTF measurements, all commands for the target centering, guiding, and near-infrared spectral measurement of the three additional objects presented here were executed and controlled from Meudon. These spectra and their complementary visible wavelength measurements (detailed in Table 1) are presented in Fig. 4. As an ensemble, they display roughly a factor of two range in spectral slope and exemplify the diversity of the inner solar system population of asteroids. We briefly discuss each object in turn.

1685 Toro is a dynamically interesting object that alternates between librations in a 5/8 commensurability with Earth and 5/13 commensurability with Venus (Williams and Wetherill, 1973). Spectrally it falls within the S(IV) spectral class of Gaffey et al. (1993) with a Band I position of

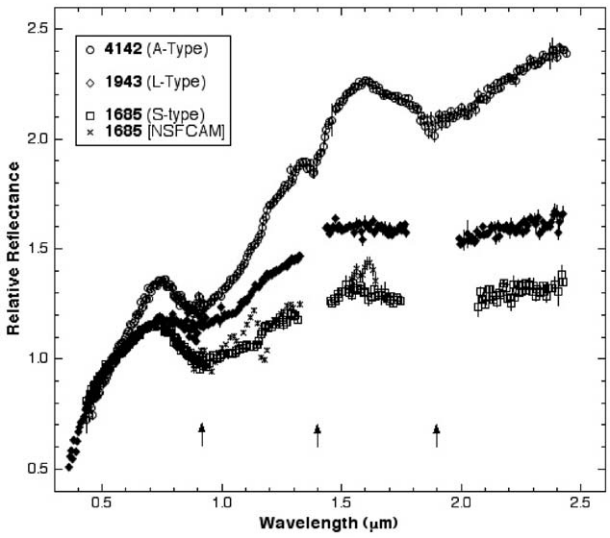

Fig. 4. Combined near-infrared plus visible spectra for (bottom to top) 1685 Toro, 1943 Anteros, and 4142 Dersu-Uzala. (All spectra are normalized to unity at 0.55 μm.) The range of spectral slopes and 1- and 2 μm absorption bands seen among these objects in the inner solar system well represents the diversity seen within the main asteroid belt. The enhanced capability of SpeX relative to the previous generation of near-IR CCD spectroscopy at the IRTF (NSFCAM; Binzel et al., 2001a; Burbine and Binzel, 2002) is shown in comparison for 1685 Toro. Arrows indicate wavelengths dominated by telluric water, which under excellent conditions and with abundant signal-to-noise can be almost be completely removed. For more limiting signal-noise-cases encountered by observing near the magnitude limit of the system, we delete these affected wavelengths and caution against the interpretation of any residual features at these arrowed wavelengths in the spectrum of 4142.

0.94 ± 0.01 μm and a Band II / Band I ratio of 0.48 ± 0.10. (We compute our uncertainties based on results of a wide range of fitting trials to the continuum.) In Fig. 4 we are able to illustrate the evolution of near-infrared spectroscopy at the IRTF by comparing the spectrum of Toro obtained with the NSFCAM "asteroid grism" (Binzel et al., 2001a; Burbine and Binzel, 2002) and that obtained by SpeX. SpeX is able to provide longer wavelength coverage (out to 2.5 μm) and provide higher signal-to-noise measurements.

1943 Anteros displays a similar spectral slope with Toro shortward of 0.7 μm, but then remains relatively flat with a very shallow absorption band in the 1 μm region. These characteristics over the visible wavelength spectrum place it within the L-class of the Bus taxonomy, a subset of the larger range of "S-like" objects that make up what is referred to as the "S-complex" (Bus, 1999; Bus and Binzel, 2002a, b). Extending the spectral coverage for Anteros out to 2.5 μm shows an increase in spectral slope with a weak 2 μm band, a Band I position of 0.96 ± 0.01 μm and a Band II/Band I ratio of 0.40 ± 0.12. With these features 1943 Anteros is placed in the transition region between S(III) and S(IV) spectral class in the Gaffey et al. (1993) classification scheme.

4142 Dersu-Uzala is a Mars-crossing object. Spectrally, it is an end member with a very steep visible wavelength spectrum and deep and broad 1 μm band, placing it within the A-class of the Bus taxonomy. Cruikshank and Hartmann (1984) have shown the connection between the A-class and olivine-rich mineralogies, but we caution that taxonomy is not mineralogy. (Taxonomic classifications such as that of Bus, 1999 are based on visible wavelength data, while mineralogic characterization requires extension into the near-infrared.) Dersu-Uzala displays a 2 μm band that may not be typical for A-class objects such as those presented by Cruikshank and Hartmann (1984), indicating a non-negligible pyroxene component. Burbine and Binzel (2002) noted two groups of A-type objects, based on "deep" or "weaker" features out to 1.6 μm, where 4142 is in the "weaker" group. Further characterization of these objects will show whether this latter group typically displays evidence for a non-negligible pyroxene content. Dersu-Uzala also shows a very steep slope in the 1–1.5 μm region. With a Band I position of 0.97 ± 0.01 μm and a Band II/Band I ratio of 0.75 ± 0.08, this object places outside the S-subtypes regions in the Gaffey et al. (1993) classification scheme.

4. Conclusions

For a well-established program in which the observers are experienced, we find remote observations to be highly successful and efficient. The quality of the link the target acquisition, performance of the scientific measurements, and communication with the operator is the single most important requirement for remote observation success. Our science results reveal very diverse objects in the inner solar system vicinity of Earth. Our enstatite achondrite-like conclusion for Nereus implies its parent body experienced substantial heating early in the solar system. As a completely different class of asteroids than that which has been previously explored, Nereus represents a compelling spacecraft target for both its scientific uniqueness and relatively easy accessibility. The range of spectral characteristics for the additional objects presented here show that the range of olivine–pyroxene mineralogies seen within the main-belt is well represented within the near-Earth population.

Acknowledgements

We thank T. Burbine and M. Gaffey for their reviews that generated important improvements to this paper. The authors are grateful to Tony Denault who answered many questions prior to our IRTF run about the Polycom system and exporting of X-windows for SpeX and the guiding system. We also thank Paul Sears and Bill Golish, the telescope operators during this experiment. This work was supported by NSF Grant AST-9530282 and NASA Grant NAG5-3939 (RPB). Binzel and Birlan had the privilege to be virtual Visiting Astronomers at the Infrared Telescope Facility, which is operated by the University of Hawaii under Cooperative Agreement No. NCC 5-538 with the National Aeronautics and Space Administration, Office of Space Science,

Planetary Astronomy Program. Binzel and Rivkin were real Visiting Astronomers at Kitt Peak National Observatory, National Optical Astronomy Observatory, which is operated by the Association of Universities for Research in Astronomy, Inc. (AURA) under cooperative agreement with the National Science Foundation. Observations obtained at the Hale Telescope, Palomar Observatory are part of a collaboration between the California Institute of Technology, NASA/JPL, and Cornell University.

References

Binzel, R.P., Harris, A.W., Bus, S.J., Burbine, T.H., 2001a. Spectral properties of near-Earth objects: palomar and IRTF results for 48 objects including spacecraft targets (9969) Braille and (10302) 1989 ML. Icarus 151, 139–149.

Binzel, R.P., Bus, S.J., Sunshine, J., Burbine, T.H., 2001b. MUSES-C target asteroid (25143) 1998 SF36: a reddened ordinary chondrite. Meteoritics Planet. Sci. 36, 1167–1172.

Binzel, R.P., Lupishko, D.F., Di Martino, M., Whiteley, R.J., Hahn, G.J., 2002. Physical properties of near-Earth objects. In: Bottke, W.F., Cellino, A., Paolicchi, P., Binzel, R.P. (Eds.), Asteroids III. University of Arizona Press, Tucson, pp. 255–271.

Bowell, E., Hapke, B., Domingue, D., Lumme, K., Peltoniemi, J., Harris, A.W., 1989. Application of photometric models to asteroids. In: Binzel, R.P., Gehrels, T., Matthews, M.S. (Eds.), Asteroids II. University of Arizona Press, Tucson, pp. 524–556.

Brunswig, W., Sievers, A., Thum, C., Wild, W., 2000. Remote observing with the 30-m radiotelescope In: Kibrick, R.I., Wallander, A. (Eds.), Advanced Global Communications Technologies for Astronomy, Proceedings of the SPIE, Vol. 4011, pp. 84–92.

Burbine, T.H., Binzel, R.P., 2002. Small main-belt asteroid spectroscopic survey in the near-infrared. Icarus 159, 468–499.

Burbine, T.H., Cloutis, E., Bus, S.J., Meibom, A., Binzel, R.P., 1998. The detection of Troilite (FeS) on the surfaces of E-class asteroids. Bull. Am. Astron. Soc. 30, 1025.

Burbine, T.H., McCoy, T.J., Binzel, R.P., Bus, S.J., 2001. Spectra of aubrites and their constituent minerals. Meteoritics Planet. Sci. (Suppl.) 36, A31–A32.

Burbine, T.H., McCoy, T.J., Nittler, L.R., Benedix, G.K., Cloutis, E.A., Dickinson, T.L., 2002. Spectra of extremely reduced assemblages: implications for mercury. Meteoritics Planet. Sci. 37, 1233–1244.

Bus, S.J., 1999. Compositional structure in the asteroid belt. Ph. D. Thesis, Massachusetts Institute of Technology, Cambridge, MA.

Bus, S.J., Binzel, R.P., 2002a. Phase II of the small main-belt asteroid spectroscopic survey: the observations. Icarus 158, 106–145.

Bus, S.J., Binzel, R.P., 2002b. Phase II of the small main-belt asteroid spectroscopic survey: a feature-based taxonomy. Icarus 158, 146–177.

Bus, S.J., Vilas, F., Barucci, M.A., 2002. Visible-wavelength spectroscopy of asteroids. In: Bottke, W.F., Cellino, A., Paolicchi, P., Binzel, R.P. (Eds.), Asteroids III. University of Arizona Press, Tucson, pp. 169–182.

Cruikshank, D.P., Hartmann, W.K., 1984. The meteorite–asteroid connection: two olivine-rich asteroids. Science 223, 281–283.

Delbo, M., Harris, A.W., Binzel, R.P., Pravec, P., Davies, J.K., 2003. Keck observations of near-earth asteroids in the thermal infrared. Icarus 166, 116–130.

Gaffey, M.J., Reed, K.L., Kelley, M.S., 1992. Relationship of E-type Apollo asteroid 3103 (1982 BB) to the enstatite achondrite meteorites and the Hungaria asteroids. Icarus 100, 95–109.

Gaffey, M.J., Bell, J.F., Brown, R.H., Burbine, T.H., Piatek, J.L., Reed, K.L., Chaky, D.A., 1993. Mineralogical variations within the S-type asteroid class. Icarus 106, 573–602.

Kibrick, R.I., Allen, S.L., Conrad, A., 2000. Remote observing with the Keck telescopes from US mainland. In: Kibrick, R.I., Wallander, A., (eds.), Advanced Global Communications Technologies for Astronomy. Proceedings of the SPIE, Vol. 4011, pp. 84–92.

Landolt, A.U., 1973. UBV photoelectric sequences in celestial equatorial selected areas 92-115. Astron. J. 78, 959–981.

Martin, R., Johnson, P., Cash, J., 2000. Remote observing capabilities of the Wyoming infraRed observatory. Bull. Am. Astron. Soc. 52, 13.

Oke, J.B., Gunn, J.E., 1982. An efficient low resolution and moderate resolution spectrograph for the Hale telescope. PASP 94, 586–594.

Rayner, J.T., Toomey, D.W., Onaka, P.M., Denault, A.J., Stahlberger, W.E., Watanabe, D.Y., Wang, S., 1998. SpeX: a medium-resolution IR spectrograph for IRTF. Proc. SPIE 3354, 468–479.

Tedesco, E.F., 1989. Asteroid magnitudes, UBV colors, and IRAS albedos and diameters. In: Binzel, R.P., Gehrels, T., Matthews, M.S. (Eds.), Asteroids II. University of Arizona Press, Tucson, pp. 1090–1138.

Tholen, D.J., Barucci, M.A., 1989. Asteroid taxonomy. In: Binzel, R.P., Gehrels, T., Matthews, M.S. (Eds.), Asteroids II. University of Arizona Press, Tucson, pp. 298–315.

Williams, J.G., Wetherill, G., 1973. Long-term orbital evolution of 1685 Toro. Astron. J. 78, 510–515.

Available online at www.sciencedirect.com
SCIENCE DIRECT®
New Astronomy 9 (2004) 343–351
New Astronomy
www.elsevier.com/locate/newast

Near-IR spectroscopy of asteroids 21 Lutetia, 89 Julia, 140 Siwa, 2181 Fogelin and 5480 (1989YK8), potential targets for the Rosetta mission; remote observations campaign on IRTF

Mirel Birlan [a,b,*], Maria Antonietta Barucci [a], Pierre Vernazza [a], Marcello Fulchignoni [a], Richard P. Binzel [c], Schelte J. Bus [d], Irina Belskaya [a,e], Sonia Fornasier [f]

[a] *Observatoire de Paris-Meudon, LESIA, 5 Place Jules Janssen, 92195 Meudon Cedex, CNRS, France*
[b] *Astronomical Institute of the Romanian Academy, Str Cutitul de Argint n 5, Bucharest 28, Romania*
[c] *Department of Earth, Atmospheric and Planetary Sciences, Massachusetts Institute of Technology, Cambridge, MA 02139, USA*
[d] *Institute for Astronomy, 640 North A'ohoku Place, Hilo, HI 96720, USA*
[e] *Astronomical Observatory of Kharkov University, Sumskaya str. 35, Kharkov 310022, Ukraine*
[f] *Astronomical Department of Padova, Vicolo dell'Osservatorio 2, 35122 Padova, Italy*

Received 27 October 2003; received in revised form 5 December 2003; accepted 10 December 2003

Communicated by W.D. Cochran

Abstract

In the frame of the international campaign to observe potential target asteroids for the Rosetta mission, remote observations have been carried out between Observatoire de Paris, in Meudon-France and the NASA Infrared Telescope Facility on Mauna Kea. The SpeX instrument was used in the 0.8–2.5 μm spectral region, for two observing runs in March and June 2003. This paper presents near-IR spectra of the asteroids 21 Lutetia, 89 Julia, 140 Siwa, 2181 Fogelin and 5480 (1989YK8). Near-IR spectra of the asteroids 21 Lutetia and 140 Siwa are flat and featureless. The spectrum of 89 Julia reveals absorption bands around 1 and 2 μm, which may indicate the presence of olivine and olivine-pyroxene mixtures and confirm the S-type designation. The small main-belt asteroids 2181 Fogelin and 5480 (1989YK8) are investigated spectroscopically for the first time. Near-IR spectra of these asteroids also show an absorption feature around 1 μm, which could be and indicator of igneous/metamorphic surface of the objects; new observations in visible as well as thermal albedo data are necessary to draw a reliable conclusion on the surface mineralogy of both asteroids.

* Corresponding author.
E-mail addresses: mbirlan@despace.obspm.fr, mirel.birlan@obspm.fr (M. Birlan).

1384-1076/$ - see front matter © 2003 Elsevier B.V. All rights reserved.
doi:10.1016/j.newast.2003.12.005

PACS: 95.45.+i; 95.85.Jq; 96.30.Ys

Keywords: Methods: miscellaneous; Techniques: spectroscopic; Minor planets: asteroids; Infrared: solar system

1. Introduction

The observational program presented in this paper is intimately linked to the scientific programme of the space mission Rosetta. The Rosetta mission was approved in 1993 as a Cornerstone Mission within the ESA's Horizons 2000 science programme. The original launch date for the mission was January 2003 and the scientific targets were assigned to be the nucleus of comet 46P/Wirtanen and two main-belt asteroids: 140 Siwa and 4979 Otawara. The main scientific goals of the Rosseta mission are to investigate 'in situ' primitive objects of the solar system and to find answers concerning the chemical composition of the primitive planetary nebula, thought to be 'frozen' in the comet nucleus and the asteroid mineralogical matrix.

Since 1993, several international campaigns of observations have been started in order to obtain a large amount of data for the targets of the Rosetta mission (Fornasier et al., 2003; LeBras et al., 2001; Barucci et al., 1998, etc.). The groundbased knowledge of these objects is essential to optimise the science return as well as the mission trajectory.

In January 2003 the European Space Agency decided to postpone the launch of the Rosetta, with a new launch date set to February 2004. This decision implied a new mission baseline: rendezvous with the comet P/Churyumov-Grasimenko and one or two asteroid fly-bys to be defined after the spacecraft interplanetary orbit insertion manoeuvre, when the total amount of available δv will be known. Several fly-bys scenarios have been studied and several possible asteroid targets have been found. These potential targets are poorly known and for this reason systematic observation are needed in order to significantly improve on our knowledge of the physics and the mineralogy of these objects.

In this paper we present the spectroscopic results obtained for five asteroids [21 Lutetia, 89 Julia, 140 Siwa, 2181 Fogelin and 5480 (1989YK8)], potential targets of the Rosetta mission. The 0.8–2.5 μm wavelength region was investigated using the SpeX instrument on IRTF-Hawaii, in 'remote observing' mode.

2. The observing protocol

The remote observations were conducted from Meudon-France, more than 12,000 km away from Hawaii, using several informational structures and networks. For the observers in Meudon, the observing hours occurred during relatively normal working daylight hours. Observation sessions began at 5 a.m. local time and ended at 5 p.m. local time. This type of observations between Meudon and IRTF/Hawaii was started in 2002 (Birlan and Binzel, 2002); since then, more than twenty nights of observations (in eight runs) were conducted from Meudon. The observations were realized through an ordinary network link, without the service quality warranty. Thus, the passband for our link was variable, a function of the traffic between Hawaii and Meudon.

During the remote observing run, the Observatoire de Paris team had the control of both the instrument/guider system and the spectrograph set-up and spectra acquisition. A permanent and constant audio/video link with the telescope operator is essential in order to administrate possible service interruptions. Two PC's running Linux were devoted to the telescope/spectrograph control. The X environment for the telescope and instrument control was exported from Mauna Kea to Meudon via two secure links (ssh tunnels). A third PC was used to keep the IP audio-video link open (webcam/Netmeeting at Meudon and Polycom ViewStation video-conference system on Mauna Kea). All software was re-initialized at the beginning of each night.

The communication lag was relatively small (approximately 0.5 s), and the image refresh time

was 2 s on the average. Real-time image display was performed mainly for verification purposed and preliminary analysis. At the completion of each run, all files were transferred to Meudon.

The SpeX instrument was utilized in low-resolution mode for this campaign. The observations were made in the 0.8–2.5 μm spectral interval. We used a 0.8 arcsec wide slit, with a 15 arcsec length and oriented North–South, which allowed us simultaneous measurements of the object and sky. The object position on the slit was alternated between two locations referred to as the A and B positions. The seeing varied between 0.7 and 1.8 arcsec during the observing runs and the humidity was in the 25–55% range. The automatic guiding mode of the telescope was used for spectra acquisition.

The asteroids were observed in during two observing runs: 28–30 March 2003 and 5 July 2003. The observed objects are summarized in Table 1. We also observed the standard stars SA 98-978, SA 102-1081, SA 105-56, SA 107-684, SA 113-276, SA 115-271, HD 28099, HD 88618 and 16 CyB. Flat-fields and Argon lamp arc images were taken each night and used for data reduction.

Our strategy was to observe all asteroids as close to the zenith as possible. Thus, we managed to observe with an airmass less then 1.6 for all targets except 2181 Fogelin, which we could only observe with an airmass in the 1.7–1.78 range. Science exposures were alternated with standard stars spectra exposures, the latter taken to cover the 1–1.8 airmass range.

In order to obtain a S/N in the 80–150 range, we needed 20–40 min of exposure time, depending on the asteroid magnitude and counting both the effective exposure and CCD camera readout time. This exposure time is unacceptable for a single near-IR spectrum due to the large variations in the atmospheric conditions (a single near-IR spectral exposure is usually no longer than 120 s). In order to obtain the required S/N, we obtained a number of 6–10 A and B exposure pairs (cycles) for both

Table 1
Potential asteroid targets for the Rosetta mission

Object	Date	a (a.u.)	e	i (deg)	Φ (deg)	V (mag)
21 Lutetia	March 30 2003	2.4347	0.1636	3.0645	14.6	11.32
89 Julia	March 30 2003	2.5519	0.1825	16.1437	13.2	11.39
140 Siwa	March 30 2003	2.7365	0.2153	3.1882	21.2	13.72
2181 Fogelin	July 5 2003	2.5918	0.1177	13.0205	11.2	16.59
5480 1989YK8	March 30 2003	3.1366	0.087	6.6717	12.7	16.25

Observation date, semimajor axis, eccentricity, inclination, phase angle and the apparent magnitude are presented for each asteroid.

Table 2
Exposure data for each asteroid

Object	UT (h m s)	Itime (s)	Cycles	Airmass
21 Lutetia	13 35 46	15	8	1.223
21 Lutetia	11 28 17	20	4	1.329
21 Lutetia	15 01 03	15	9	1.414
21 Lutetia	10 20 21	20	3	1.635
89 Julia	10 44 44	40	6	1.561
140 Siwa	07 06 07	120	8	1.000
140 Siwa	07 46 10	120	6	1.016
2181 Fogelin	12 10 35	2×60	4	1.769
2181 Fogelin	12 31 40	2×60	4	1.744
2181 Fogelin	12 55 17	2×60	4	1.740
5480 1989YK8	12 41 01	120	6	1.151
5480 1989YK8	14 36 01	120	6	1.230

The columns show the mean UT value for each series, the individual time for each spectrum (Itime), the number of cycles and the mean airmass of each series.

the asteroids – science exposures – and the standard stars. This constitutes *one series* of observations for each object. Details the science exposures are given in Table 2.

3. Data reduction and results

The major points of our reduction procedure are classic for the near-IR spectroscopy. We started by combining and normalizing flat-fields for each observing night. The resulting flats were later used for the reduction of spectra of both the asteroids and the standard stars. In order to minimize the atmospheric and telescope influence and to eliminate the influence of electronic bias level and the dark current, we subtracted the B position spectra from the A position spectra for each pair of exposures (cycle), in the assumption of quasi-homogeneous sky background during A plus B exposure pair. The result of the subtraction was flat fielded. For each object, we median combined the result of all cycles in each observing series. This technique produces one positive and one negative spectrum on the same image. Next step was the construction of an accurate spatial profile for the extraction of the spectra. The final step was the wavelength calibration.

The Spextool package (the description of the procedures are presented in Cushing et al., 2003) allowed us to perform following steps for both the asteroids and the standard stars: global flat-field and arc construction, possible non-linearity correction, addition of spectra of the same object, spatial profile determination of the spectrum in the image, aperture location, extraction of the spectrum, wavelength calibration and cleaning the spectra. The results are saved in both FITS and ASCII formats, as used by several image processing packages (like IDL, MIDAS and IRAF), respectively, dedicated plot/graphics software (Easyplot, Origin, Dataplot, etc.).

The next step in the process of data reductions was the calculation of the extinction coefficients. The solar analogs spectra were used to find the correspondent extinction coefficient for each wavelength. A "superstar" was created by summing appropriately weighted contributions of the standard stars. The resulting "superstar", corrected for atmospheric extinction, was used to obtain the spectral reflectance of asteroids at different airmasses. Careful choice of the "superstar", combined with several tests of shift between the spectrum of the asteroid and that of the superstar are very important in order to minimize the influence of the terrestrial atmosphere in the 1.4 and 1.9 μm spectral regions. In order to make more readable our spectra, we choose to eliminate these spectral regions. Moreover, the elimination of these spectral regions does not affect the conclusions of this article.

3.1. 21 Lutetia

With an estimated diameter of 95.5 ± 4.1 km – for an IRAS albedo of 0.221 ± 0.020 (Tedesco and Veeder, 1992) – 21 Lutetia belongs to the large asteroid class (diameter $\geqslant 100$ km). Its synodic period has been computed from several lightcurve analysis and the value is 8.17 ± 0.01 h (Zappala et al., 1984). Color analysis of the ECAS data (Zellner et al., 1985) designates the asteroid 21 Lutetia to be part of the *X* complex. Also, global ECAS and IRAS thermal albedo data analysis assign Lutetia to the M taxonomic type (Barucci et al., 1987; Tholen, 1989). The M type asteroids are considered to be part of the core of differentiated asteroids and the parent bodies of metallic meteorites. On the basis of SMASS II spectroscopic data, Bus and Binzel (2002) proposed the new taxonomic class *Xk* for the asteroid 21 Lutetia.

21 Lutetia was observed on UT 2003 March 29 for the entire night. Four series of exposures resulted in four IR spectra with S/N in the 90–140 range. In order to detect possible surface spectral features variations, our observations covered 65% of the synodic period. These spectra are presented in Fig. 1. However, a check of the physical ephemeris of 21 Lutetia revealed a close pole-on geometry of the asteroid, so our spectra are most probably dominated by the contribution of the same surface features on 21 Lutetia. There are no significant spectral features in the spectral region 0.8–2.5 μm and the slightly increasing slope varies around 0.3%.

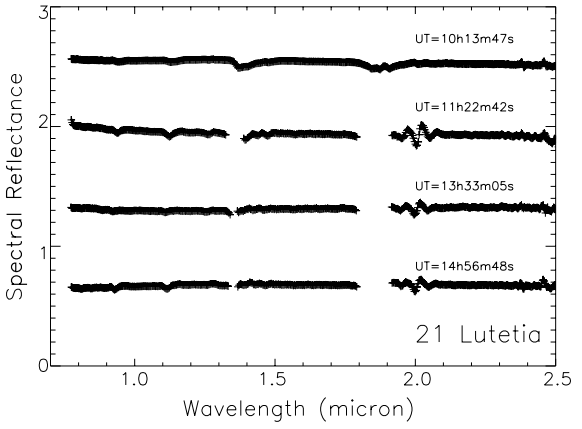

Fig. 1. The spectra of the asteroid 21 Lutetia. The IRTF spectra are offset for clarity and presented in chronological order. The beginning of each series of spectra (UT) was marked on the graph.

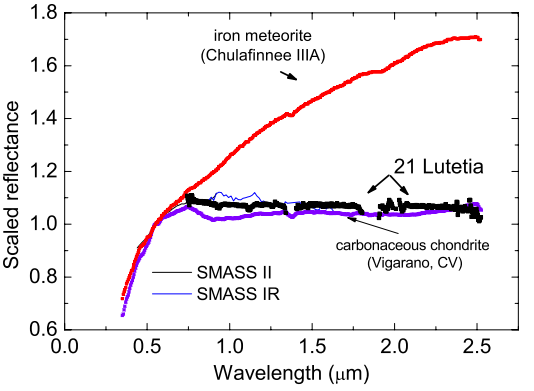

Fig. 2. The average spectrum of the asteroid 21 Lutetia. The SMASS II and SMASS IR data are plotted as solid lines. Our data is in agreement with the SMASSIR data over the 0.75–1.6 μm spectral interval. The comparison with Chulafinnee (iron meteorite) and Vigarano (carbonaceus chondrite) reveal the good match with the IR spectrum associated to carbon rich surfaces.

The lack of features in the spectrum of 21 Lutetia makes its taxonomic and compositional interpretation difficult. While the high IRAS albedo value of 0.221 leads to the previous M-type classification, we note there is an ambiguity in determining the albedo of Lutetia. An alternate low albedo value of 0.09 has been reported by Zellner et al. (1977) from polarimetric measurements and groundbased radiometric measurements.

In Fig. 2 we compare our measurements of Lutetia with others published in the literature. We found a good match with both SMASS IR data (spectral interval 0.8–1.6 μm) and the 52-color asteroid survey (Bell et al., 1988) spectrophotometric data. We also compare in Fig. 2 all of these Lutetia results with reflectance spectra of meteorites from Gaffey (1976). Our goal is to find which meteorites may be most analogous with Lutetia in terms of near-IR spectral properties. We note the spectrum of Lutetia is most qualitatively similar to the spectrum of the Vigarano meteorite, a CV3 carbonaceous chondrite, while being quite a poor match to the class IIIA iron meteorite Chulafinee. The purpose of our comparison is to note the difficulty of making a non-ambiguous interpretation of the composition of 21 Lutetia.

In Fig. 3 we plot the negative polarization depth versus the inversion angle (Belskaya and Lagerkvist, 1996) for both 21 Lutetia and a sample asteroids and meteorites. The asteroid 21 Lutetia has the largest inversion angle ever observed for the asteroids. The same peculiarly large inversion angle were found in the laboratory for the carbonaceous chondrites of the CV3 and CO3 samples. These types of chondrites are characterized by a low carbon content and thus relatively a larger

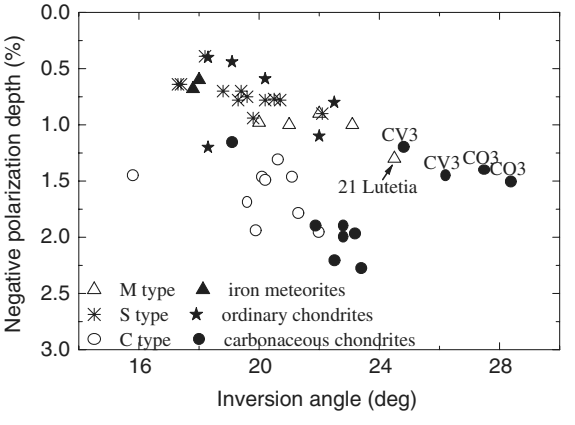

Fig. 3. Diagram of the negative polarization depth and the inversion angle of asteroids and meteorites from Belskaya and Lagerkvist (1996).

albedo when compared to other types (Zellner et al., 1977).

3.2. 89 Julia

The asteroid 89 Julia has an estimated diameter of 151.4 ± 3.1 km, for an IRAS albedo of 0.176 ± 0.007. Photometry of 89 Julia yields a synodic period of 11.387 ± 0.002 h (Schober and Lustig, 1975). Multivariate statistics classified the asteroid as part of the S cluster (Barucci et al., 1987; Tholen, 1989). The mineralogical classification of the S-type asteroids (Gaffey et al., 1993) based on the ECAS data and 52-color spectrophotometric Survey (Bell et al., 1988) data assigns 89 Julia (together with the asteroid 9 Metis) as 'ungrouped' S-asteroids. The main reason of this 'unclassification' is the long wavelength position of the 1 μm feature, which could be the presence of the abundant calcic clinopyroxene component (Gaffey et al., 1993). Based on the SMASS II data, Bus and Binzel (2002) proposed a K cluster membership (derived from the S cluster) for 89 Julia.

The asteroid spectrum was obtained for an effective integration time of 10 min, with a S/N ratio of 90 in both A and B beams. This spectrum presents a significant positive slope in the region 1.1–1.5 μm and a plateau in the 1.7–1.9 μm and 2.2–2.5 μm spectral regions. In Fig. 4 the IR spectrum of Julia was overlapped with the SMASS II spectrum in the 0.78–0.92 μm spectral region. We confirm a broad absorption band at 1 μm, typical of the silicate rich minerals. We also confirm a global trend of the spectral reflectance, which increases in the near-IR. The influence of atmospheric water absorbtion on the spectra is visible around 1.4 and 1.9 μm. The geometry of observations was fairly unfavourable for this asteroid (airmass = 1.56).

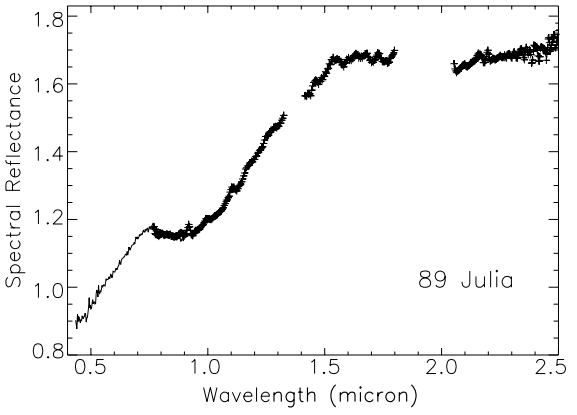

Fig. 4. The spectrum of the asteroid 89 Julia. The IRTF spectrum was overlapped with the SMASS II visible spectrum in the region 0.78–0.92 μm.

In order to calculate the center of 1 μm absorbtion band (designated as Band I in the literature), the continuum was defined between the local maximum of spectral reflectance at 0.76 μm and the small shoulder of the spectrum at 1.27 μm. The spectrum was then continuum subtracted and the result was fitted with an order three polynomial function. We find the center of the feature localized at 1.01 ± 0.06 μm, which is a slightly shorter wavelength than the one found by Gaffey et al. (1993).

3.3. 140 Siwa

140 Siwa is one of the initial targets of the Rosetta mission (departure in January 2003). One of the proposed scenarios (February 2003) suggests keeping this asteroid as a candidate for flyby. This was our motivation to observe it.

An IRAS albedo of 0.068 ± 0.004 for the asteroid 140 Siwa allows the calculation of a diameter of 109.8 ± 3.0 km. Lightcurve analysis for two runs in 2000 (LeBras et al., 2001) reveals a slow-rotator asteroid; the composite lightcurve presents an amplitude of 0.1 magnitudes and its synodic period was estimated at 18.495 ± 0.005 h.

Two series of near-IR spectra were obtained in March 30, 2003, with the ratio S/N of 50 and 70 (obtained in both A and B beams) for the spectrum obtained at airmass 1.001 and 1.018, respectively, (Fig. 5). The IR spectrum of 140 Siwa does not contain deep absorption features corresponding to mafic minerals. The spectrum slope is slightly positive, with a value 1% (0.8% and 0.7%, respectively), which confirms the slope trend of its spectrum (LeBras et al., 2001). We confirm a typical neutral spectrum of consistent with the a C-type asteroid; the IRAS albedo for 140 Siwa also fits very well the average value of C taxonomic

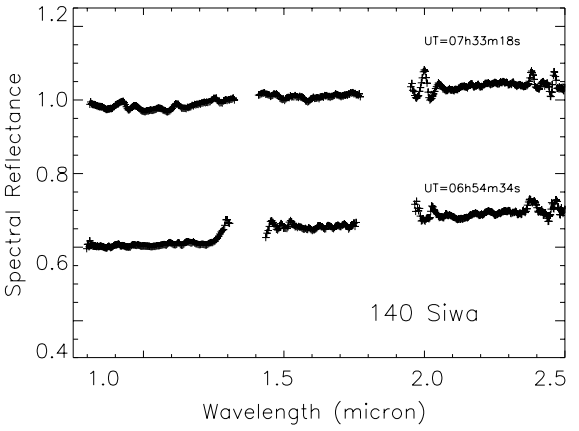

Fig. 5. The spectra of the asteroid 140 Siwa. The spectra were offset for clarity and the UT represents the beginning of each series of exposures.

class. The near-IR slope of our spectra is slightly different of those of a typical C-type asteroid but this alone cannot indicate a different mineralogy of the surface.

Fig. 6 shows the computed a global IRTF spectrum for the asteroid 140 Siwa overlapped with SMASS II data (the overlap is only for the 0.7–0.85 μm region). This composite spectrum was compared to meteorite reflectance spectra from the

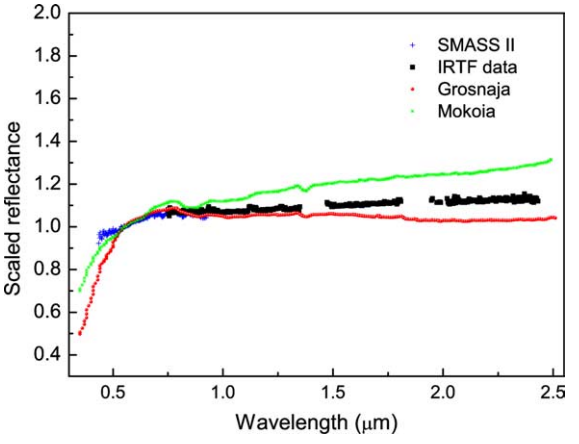

Fig. 6. Cumulated spectral reflectance of the asteroid 140 Siwa obtained during the IRTF run. The spectrum was overlapped with the SMASS II data in the 0.70–0.85 μm spectral region. The spectrum is similar to CV3 meteorites Grosnaja and Mokoia. The surface of 140 Siwa shows similar properties with carbonaceous chondrite meteorites, with a reflectance trend between the curves for the two meteorites.

Gaffey database. There is no meteorite spectrum that fits our spectrum very well. However, the carbonaceous chondrite meteorites spectra are similar to our spectrum and the asteroid spectral reflectance spans a value in the range of CV3 meteorite class. The nearest spectra are those of Grosnaja and Mokoia meteorites.

3.4. 2181 Fogelin

No physical data are available in the literature for the asteroid 2181 Fogelin. Thus, we can only roughly estimate its diameter. Following the asteroid mass distribution proposed by Kresak (1977) and the H magnitude of 2181 Fogelin, the diameter could be in the 12–18 km range. A second estimate can be made using an empirical relationship between the absolute magnitude, diameter and geometric albedo (Fowler and Chillemi, 1992):

$$\log D = 3.1236 - 0.5 \cdot \log p_v - 0.2 \cdot H. \quad (1)$$

Using an IRAS albedo of 0.05–0.25 we find a 12–22 km diameter for the asteroid.

The observations of 2181 Fogelin were carried out in July, 5, 2003, with the ratio S/N of 80 in both A and B beams. The geometry of observation (airmass = 1.7) was unfavourable. However, the final spectrum is the average of 32 individual spectra, which can alleviate the high airmass problem. The IR spectrum presented in Fig. 7 shows the large

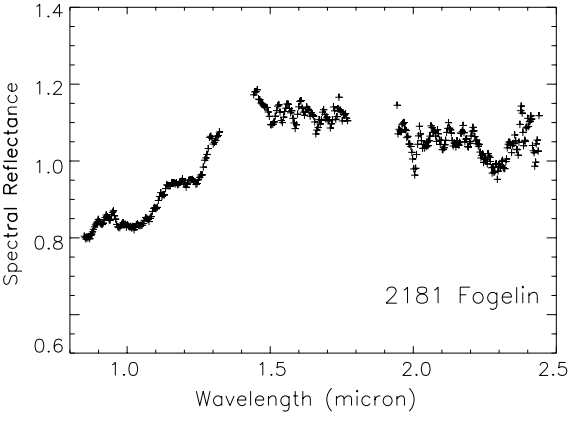

Fig. 7. The spectrum of the asteroid 2181 Fogelin, normalized to 1.275 μm, the maximum of J filter.

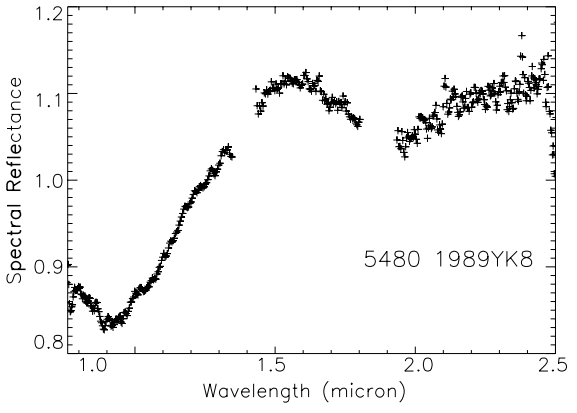

Fig. 8. The spectrum of the asteroid 5480 1989YK8, normalized to 1.275 μm, the maximum of J filter.

broad band absorbtion around 1 μm, typical of mafic minerals. The slightly positive slope in the 1.2–1.5 μm wavelength region doesn't allow us to classify this object as a S-type asteroid. Further observations in the visible region as well as thermal albedo data are necessary to make a taxonomic class assignment for this asteroid.

3.5. 5480 1989 YK8

There are no previous photometric or spectroscopic data available for the asteroid 5480 1989YK8. The same methods used for 2181 Fogelin have been used to compute its theoretical diameter. The diameter spans the 13–20 km range (following Kresak, 1977) and 13–31 km following the diameter empirical formula (1), used with IRAS albedos in the 0.05–0.25 range.

The asteroid was observed on March, 30, 2003 and the final spectrum S/N ratio is around 100 for the A and B positions in the slit. The analysis of the 0.8–2.3 μm region reveals an absorption band around 1 μm (Fig. 8). The global tendency in near-IR could justify a S-type asteroid classification; however, a visible spectrum and thermal albedo data are necessary for a taxonomical assignment.

4. Conclusions

Five asteroids potential targets for the Rosetta mission have been observed in the 0.8–2.5 μm spectral range: 21 Lutetia, 89 Julia, 140 Siwa, 2181 Fogelin and 5480 (1989YK8). We confirm the flat near-IR spectrum of 21 Lutetia. The near-IR spectrum of 89 Julia contains features confirming the initial idea that it belongs to the 'heated' bodies, possible to the S or K taxonomic class. A value 1.01 ± 0.06 μm was found for the center of the Band I. The asteroid 140 Siwa spectrum presents a slightly positive slope and there are no major mineralogical signatures; we confirm the assignment of the asteroid as an 'unheated' asteroid.

The small asteroids 2181 Fogelin and 5480 (1989YK8) were observed spectroscopically for the first time. Our data shows the presence of a large (and weak) absorption band around 1 μm for both asteroids; new observations in visible and infrared are necessary to draw a reliable conclusion concerning their surface mineralogy.

The remote observations between IRTF and Observatoire de Paris-Meudon proved to be a robust and handy observing technique. It offered full access to the command line of the spectrograph and to several telescope controls (focus, tracking, etc.). We consider our observing program entirely accomplished without any discernable difference in the typical amount of spectra obtained in remote observations mode versus the local observing mode.

Acknowledgements

The authors are grateful to Paul Hardersen for useful comments that improved our article. We are indebted to Tony Denault who answered many questions prior to our runs about the Polycom system and exporting of X-windows for SpeX and guiding system, to Miranda Hawarden-Ogata for the administration system support and to Paul Sears and Bill Golish, the telescope operators during the remote observing runs.

References

Barucci, M.A., Doressoundiram, A., Fulchignoni, M., Florczak, M., Lazzarin, M., Angeli, C., 1998. P&SS 46, 75.

Barucci, M.A., Capria, M.T., Coradini, A., Fulchignoni, M., 1987. Icar 72, 304.

Bell, J.F, Hawke, B.R., Owensby P.D, Gaffey, M.J., 1988. The 52-color asteroid survey; final results and interpretation. Lunar Planet. Sci. XIX.

Belskaya, I., Lagerkvist, C.-I., 1996. P&SS 44, 783.

Birlan, M., Binzel, R.P., 2002. Paris Observatory Remote Observing January–May 2002: Sharing the Experience to Educational Astronomy, Global Hands-On Universe Conference Proceedings, Paris, July.

Bus, S.J., Binzel, R.P., 2002. Icar 158, 146.

Cushing, M.C., Vacca, W.D., Rayner, J.T., 2003. Spextool: a spectral extraction package for SpeX, a 0.8–5.5 μm cross-dispersed spectrograph, PASP (in press), http://irtf-web.ifa.hawaii.edu/Facility/spex/.

Fornasier, S., Barucci, M.A., Binzel, R.P., et al., 2003. A&A 398, 327.

Fowler, J.W., Chillemi, J.R., 1992. IRAS asteroid data processing. In: Tedesco, E.F., Veeder, G.J., Fowler, J.W., Chillemi, J.R. (Eds.), The IRAS Minor Planet Survey. Technical Report PL-TR-92-2049, Phillips Laboratory, Hanscom AF Base, MA.

Gaffey, M.J., 1976. JGR 81, 905.

Gaffey, M.J., Burbine, T.H., Piatek, J.L., Reed, K.L., Chaky, D.A., Bell, J.F., Brown, R.H., 1993. Icar 106, 573.

Kresak, L., 1977. BAICz, n. 28, 82.

Le Bras, A., Dotto, E., Fulchignoni, M., Doressoundiram, A., Barucci, M.A., Le Mouelic, S., Forni, O., Quirico, E., 2001. A&A 379, 660.

Schober, H.J., Lustig, G., 1975. Icar 25, 339.

Tedesco, E.F., Veeder, G.J., 1992. IMPS albedos and diameter catalog(FP102). In: Tedesco, E.F., Veeder, G.J., Fowler, J.W., Chillemi, J.R., The IRAS Minor Planet Survey. Technical Report PL-TR-92-2049, Phillips Laboratory, Hanscom AF Base, MA.

Tholen, D., 1989. Asteroid taxonomic classifications. In: Asteroids II. University of Arizona Press, AZ, pp. 1139–1150.

Zappala, V., DiMartino, M., Knezevic, Z., Djurasevic, G., 1984. A&A 130 (1), 208.

Zellner, B., Tholen, D.J., Tedesco, E.F., 1985. Icar 61, 355.

Zellner, B., Leake, M., LeBerte, T., Duseaux, M., Dollfus, A., 1977. The asteroid albedo scale. II. Laboratory polarimetry of meteorites. In: Proceedings of the Lunar Science Conference, 8th ed. Pergamon Press, Oxford, pp. 1091–1110.

A&A 430, 313–317 (2005)
DOI: 10.1051/0004-6361:20041505

Astronomy & Astrophysics

Asteroid target selection for the new Rosetta mission baseline

21 Lutetia and 2867 Steins⋆

M. A. Barucci[1], M. Fulchignoni[1], S. Fornasier[2], E. Dotto[3], P. Vernazza[1], M. Birlan[4], R. P. Binzel[5], J. Carvano[1], F. Merlin[1], C. Barbieri[2], and I. Belskaya[6]

[1] LESIA, Observatoire de Paris, 92195 Meudon Principal Cedex, France
e-mail: antonella.barucci@obspm.fr
[2] Astronomy Department, Padova University, Vicolo dell'Osservatorio 2, 35122 Padova, Italy
[3] INAF – Osservatorio Astronomico di Roma, via Frascati 33, 00040 Monte Porzio Catone, Roma, Italy
[4] IMCCE, Observatoire de Paris, 75014 Paris, France
[5] Dep. of Earth, Atmosph. and Planetary Sciences, Massachusetts Institute of Technology, Cambridge, MA 02139, USA
[6] Astronomical Observatory of Kharkiv National University, Ukrania

Received 22 June 2004 / Accepted 18 September 2004

Abstract. The new Rosetta mission baseline to the comet 67P/Churyumov-Gerasimenko includes two asteroid fly-bys. To help in target selection we studied all the candidates of all the possible scenarios. Observations have been carried out at ESO-NTT (La Silla, Chile), TNG (Canaries), and NASA-IRTF (Hawaii) telescopes, in order to determine the taxonomy of all the candidates. The asteroid targets were chosen after the spacecraft interplanetary orbit insertion manoeuvre, when the available total amount of ΔV was known. On the basis of our analysis and the available of ΔV, we recommended to the ESA Science Working Group the asteroids 21 Lutetia and 2867 Steins as targets for the Rosetta mission. The nature of Lutetia is still controversial. Lutetia's spectral properties may be consistent with a composition similar to carbonaceous chondrite meteorites. The spectral properties of Steins suggest a more extensive thermal history. Steins may have a composition similar to relatively rare enstatite chondrite/achondrite meteorites.

Key words. minor planets, asteroids – techniques: spectroscopic

1. Introduction

In 1993, the European Space Agency (ESA) selected the Rosetta mission including a rendezvous with in situ investigation of a comet and at least one (or more probably two) fly-bys of asteroids. The aim of the mission is to investigate the origin of the Solar System through the composition of planetesimals and their origin over the last 4.6 billion years.

In January 2003, ESA decided to postpone the launch of the spacecraft due to problems with the launcher (Barucci et al. 2004). The new baseline mission included a long orbital rendezvous with the 67P/Churyumov-Gerasimenko comet nucleus and one or two asteroid fly-bys. Several single or double fly-by scenarios were designed (Table 1), depending on the total ΔV available after the spacecraft interplanetary orbit insertion manoeuvre. In December 2003, the asteroid 2513 Baetsle was included on the basis of the pre-launch resource budget as baseline target, due to the minimum extra ΔV required to reach it (only 19 m/s).

Table 1. Double and single asteroid mission opportunity with fly-by between 2008 and 2010. The listed ΔV values were estimated before the launch.

Double fly-by	ΔV m/s	Single fly-by	ΔV m/s
Rhodia + Lutetia	159	Lutetia	125
Steins + Lutetia	139	Rhodia	97
Luichewoo + Lutetia	129	Steins	57
Baetsle + Izvekov	73	Sofala	101
Baetsle + Fogelin	79	Fogelin	18
Luichewoo + Izvekov	32	Baetsle	19
Rhodia + Izvekov	112	Luichewoo	32
Rhodia + Fogelin	113	Carrera	102
Steins + Izvekov	77	Izvekov	15
Sofala + Izvekov	146		
Steins + Fogelin	83		
Luichewoo + Fogelin	35		

The mission was launched successfully on March 2nd 2004. The spacecraft started its journey to the comet 67P/Churyumov-Gerasimenko that will be reached on 2014, after three Earth and one Mars gravity assisted swing-bys and

⋆ Based on observations collected at ESO-La Silla, NASA/IRTF and TNG-Canaries.

Table 2. Observational circumstances of asteroid targets for the Rosetta mission.

Object	Night	UT-start (hh:mm)	T_{exp} (s)	Tel.	Instr.	Grism/prism	Slit (arcsec)	airm.
437 Rhodia	25 Jan. 04	15:35	600	IRTF	SpeX	0.8–2.5 μm	0.8	1.30
437 Rhodia	03 Mar. 04	10:07	960	IRTF	SpeX	0.8–2.5 μm	0.8	1.17
1393 Sofala	25 Jan. 04	15:00	720	IRTF	SpeX	0.8–2.5 μm	0.8	1.05
2513 Baetsle	25 Jan. 04	14:21	1320	IRTF	SpeX	0.8–2.5 μm	0.8	1.10
2867 Steins	25 Jan. 04	13:21	1100	IRTF	SpeX	0.8–2.5 μm	0.8	1.02
3050 Carrera	25 Jan. 04	11:00	1200	IRTF	SpeX	0.8–2.5 μm	0.8	1.08
21 Lutetia	26 May 04	10:13	660	NTT	EMMI	GRISM 1 (0.4–0.95 μm)	1.5	1.55
2513 Baetsle	30 Jan. 04	8:40	960	NTT	EMMI	GRISM 1 (0.4–0.95 μm)	1.5	1.13
2867 Steins	29 Jan. 04	7:58	720	NTT	EMMI	GRISM 1 (0.4–0.95 μm)	1.0	1.40
2867 Steins	25 May 04	23:28	1200	NTT	EMMI	GRISM 1 (0.4–0.95 μm)	1.5	1.41
3050 Carrera	30 Jan. 04	6:50	960	NTT	EMMI	GRISM 1 (0.4–0.95 μm)	1.5	1.29
5538 Luichewoo	29 Jan. 04	7:00	1920	NTT	EMMI	GRISM 1 (0.4–0.95 μm)	1.0	1.20
437 Rhodia	29 Feb. 04	02:42	180	TNG	DOLORES	LR-R (0.51–0.95 μm)	1.5	1.28
1393 Sofala	29 Feb. 04	03:46	360	TNG	DOLORES	LR-R (0.51–0.95 μm)	1.5	1.09
2513 Baetsle	29 Feb. 04	04:06	1200	TNG	DOLORES	LR-R (0.51–0.95 μm)	1.5	1.31
3418 Izvekov	29 Feb. 04	02:18	480	TNG	DOLORES	LR-R (0.51–0.95 μm)	1.5	1.07
1393 Sofala	1 Mar. 04	05:08	480	TNG	NICS	AMICI (0.8–2.5 μm)	1.5	1.25
2513 Baetsle	2 Mar. 04	02:44	1920	TNG	NICS	AMICI (0.8–2.5 μm)	1.5	1.19
3418 Izvekov	2 Mar. 04	01:38	1920	TNG	NICS	AMICI (0.8–2.5 μm)	1.5	1.08
5538 Luichewoo	2 Mar. 04	03:51	1920	TNG	NICS	AMICI (0.8–2.5 μm)	1.5	1.32

the asteroid fly-bys. Due to the optimal launch conditions, the available remaining ΔV is enough to fly-by two asteroids. To help in the selection of the best targets for scientific return, we observed all the possible candidates by visible (V) and near-infrared (NIR) spectroscopy. In this paper we report the results of the observational campaign as well as the characterization of the selected targets.

2. Observations and data reduction

Visible and near-infrared spectroscopic observations were performed at the ESO 3.5 m New Technology Telescope (NTT, La Silla, Chile), the 3.5 m Telescopio Nazionale Galileo (TNG, La Palma, Spain), and the 3 m NASA Infrared Telescope Facility (IRTF, Hawaii, USA). The circumstances of these observations are summarized in Table 2. During each observing run we also acquired bias, flat-field, calibration lamp and several solar analog star spectra at different intervals throughout the night.

The observations at IRTF were performed in remote mode from the Observatoire de Paris-Meudon (Binzel et al. 2004; Birlan et al. 2004). The NIR acquisition procedure was the same both for the TNG and IRTF telescopes, consisting of cycle series of 4 images each (ABBA cycle). The images had an exposure time of 120 s each, and were taken in two different positions along the slit, named A and B, offsetting the telescope. This technique obtains near-simultaneous images for sky and bias subtraction. The ABBA cycles were repeated several times for the fainter objects. The total exposure time for each object is indicated in Table 2.

Spectra were reduced using standard data reduction procedures with the software package Midas (e.g. Fornasier & Lazzarin 2001; Fornasier et al. 2003). The asteroid relative reflectance has been obtained by division of the asteroid spectrum with that one of the solar analog star closest in time and airmass to the asteroid. For the IRTF data, the asteroid spectrum has been divided by a "superstar", created by summing appropriately weighted contributions of several observed analog stars, corrected for atmospheric extinction and computed at the same airmass of the asteroids.

3. Data analysis and discussion

We obtained the first V+NIR spectra of seven out of the nine asteroid candidates listed in Table 1 (437 Rhodia, 1393 Sofala, 2513 Baetsle, 2867 Steins, 3050 Carrera, 3418 Izvekov, and 5538 Luichewoo). A visible spectrum of 21 Lutetia has been also obtained and reported in Fig. 2. The NIR spectra of Lutetia and Fogelin have been recently published by our group (Birlan et al. 2004).

All the objects reported in Fig. 1 seem to belong to the S taxonomic class because of well defined 1 and 2 μm silicate bands. Spectra shown in Fig. 2 have flatter behaviors. The presence of the absorption band at 0.9 μm in the spectra of Rhodia together with its high albedo value (0.56, IRAS data: Tedesco et al. 1992) suggests a possible classification as an E-type asteroids; Carrera has a similar spectral behaviour with the presence of the peculiar 0.9 μm band and might also be an E type asteroid, even if the knowledge of its albedo is necessary to make a definitive taxonomic class assignment. Izvekov has a very peculiar flat spectrum, typical of primitive dark objects like B- or C-type. The spectral behaviour of Steins seems to suggest that it belongs to E-type class. Spectra of the same object obtained during different epochs are essentially the same. For Sofala a visible spectrum was

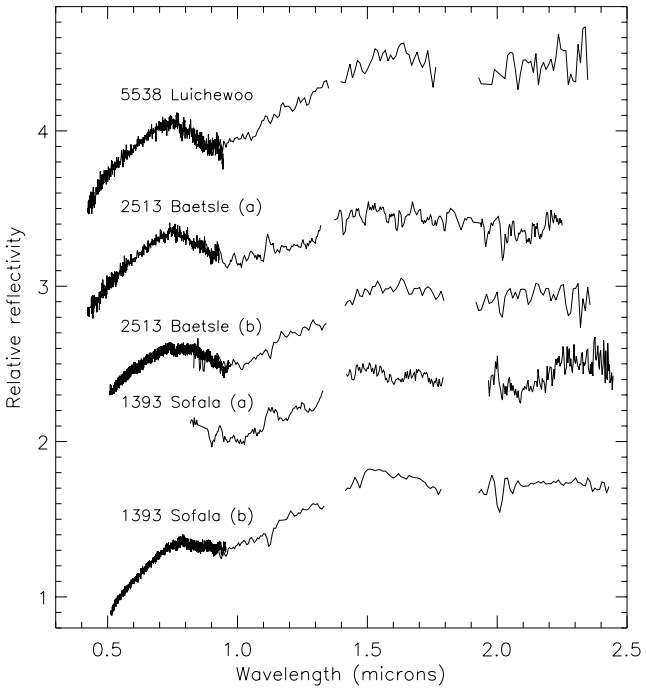

Fig. 1. V and NIR spectra of Luichewoo, Baetsle, and Sofala. For Baetsle and Sofala, the spectra (a) include V data obtained at NTT and NIR spectra obtained at IRTF, while spectra (b) have been obtained at TNG. All the spectra are normalized at 0.55 μm and shifted by 0.7 for clarity. All these objects have been classified as S-type.

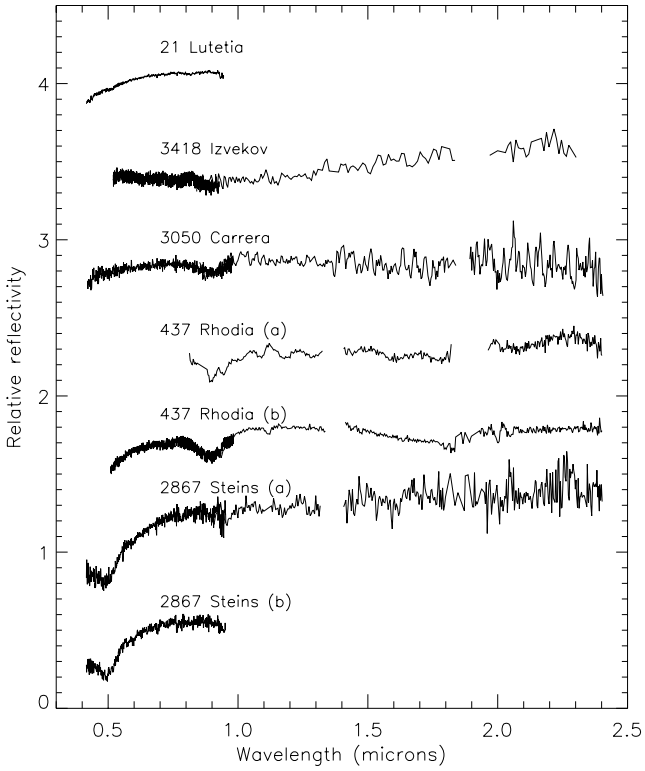

Fig. 2. V spectrum of Lutetia, and V and NIR spectra of Izvekov, Carrera, Rhodia, and Steins. The NIR spectrum (a) of Rhodia has been obtained on January 2004, while the NIR spectrum (b) has been obtained on March 2004. The V spectrum (b) of Steins has been obtained on May 2004. All the spectra are normalized at 0.55 μm and shifted by 0.6 for clarity.

already published by Xu et al. (1995). We confirm their S-type classification.

4. Target selection and characterization

Analyzing the list of possible targets and the relative available data, we strongly recommended the inclusion of asteroid 21 Lutetia in the Rosetta baseline because of its high interest. In fact it is the only object of the list which will allow the radio science experiment to measure the mass, and consequently to deduce the bulk density.

After the insertion manoeuvre of Rosetta into its interplanetary orbit, the available ΔV for the asteroid encounters was enough to allow the selection of any pair of asteroids listed in Table 1 for a double fly-by, except for the Rhodia-Lutetia one. The two remaining pairs which include 21 Lutetia are Steins-Lutetia and Luichewoo-Lutetia. As Luichewoo is a S-type (S class asteroids have already been visited by space missions), we exclude it from the possible baseline.

On the basis of the obtained spectra, we suggested Lutetia and Steins as the best asteroid targets for the Rosetta mission. In fact, these asteroids seem to be peculiar and show spectral behaviors different from the previous asteroid targets of space missions.

21 Lutetia was discovered in 1852 by H. Goldchmidt at the Paris Observatory. The name Lutetia derives from the Roman name of Paris (Lutetia Parisorum) and was given to the asteroid to honour the French capital. 21 Lutetia is the largest asteroid out of the possible candidates (IRAS diameter of 95.8 ± 4.1 km). The main orbital and physical characteristics are listed in Table 3. The rotational period of 8.17 ± 0.01 h has been determined by Zappalá et al. (1984). The spin vector direction of Lutetia has been computed by several authors (see Magri et al. 1999 for details) giving different pole solutions. The prograde rotation state was in agreement with the different methods and determinations. Torppa et al. (2003), analysing all the available lightcurves, computed pole coordinates and a model with sharp and irregular shape (see Table 3).

Because of the high IRAS albedo, Lutetia was previously classified as M-type by Barucci et al. (1987) and Tholen (1989) and was supposed to be a parent body of iron meteorites. Hiroi et al. (1993) found a good fit with the M meteorite Mundrabilla under particular ad hoc conditions. Bus & Binzel (2002) proposed for it a new class X_k. Further observations have shown that its infrared spectrum is unusually flat compared to other M asteroids (Howell et al. 1994; Burbine & Binzel 2000). Moreover the observations obtained at IRTF (Birlan et al. 2004) suggested a similarity with the carbonaceous chondrite spectra which characterize the C-type asteroid. Busarev et al. (2004) and Lazzarin et al. (2004), obtained several V spectra showing rotational phase variation with possible presence of features at 0.44 and 0.67 μm probably associated to hydrated silicates.

Many other characteristics seem to be in agreement with the carbonaceous chondrite analogy: the polarimetric properties (Belskaya & Lagerkvist 1996), lower radar albedo (Magri et al. 1999), and the 3 μm absorption feature diagnostic of water

Table 3. Orbital and physical characteristics of 21 Lutetia.

Semimajor axis (AU)	2.435
Eccentricity	0.164
Inclination (deg)	3.064
Taxonomic type	C (or M)
Synodical rotation period (h)	8.17 ± 0.01
Absolute magnitude	7.294
Slope parameter	0.110
IRAS D (km)	95.5 ± 4.1
IRAS albedo	0.221 ± 0.20
Pole solution from radar observations (Magri et al. 1999):	
$\lambda_1 = 228° \pm 11°$ $\beta_1 = +13° \pm 5°$	$\lambda_2 = 48° \pm 11°$ $\beta_2 = +5° \pm 5°$
Sense of rotation	Prograde
$2a \times 2b \times 2c$	$130 \times 104 \times 74$ km
Pole solution from lightcurve analysis (Torppa et al. 2003):	
$\lambda_1 = 220° \pm 10°$ $\beta_1 = +3° \pm 10°$	$\lambda_2 = 39° \pm 10°$ $\beta_2 = +3° \pm 10°$
$a/b = 1.2$; $b/c = 1.2$	

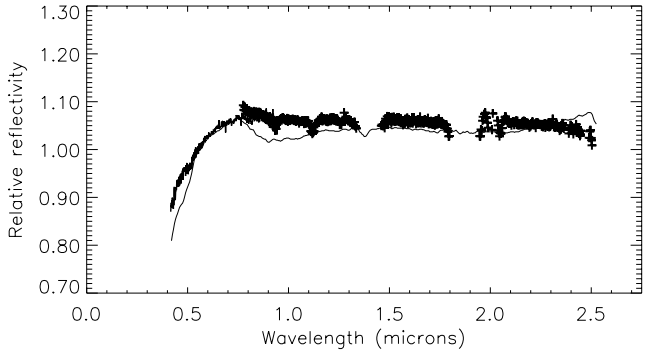

Fig. 3. Comparison of the Lutetia spectra (our V spectrum + the NIR one by Birlan et al. 2004) and the spectra of the CV3 carbonaceous chondrite meteorite Vigarano.

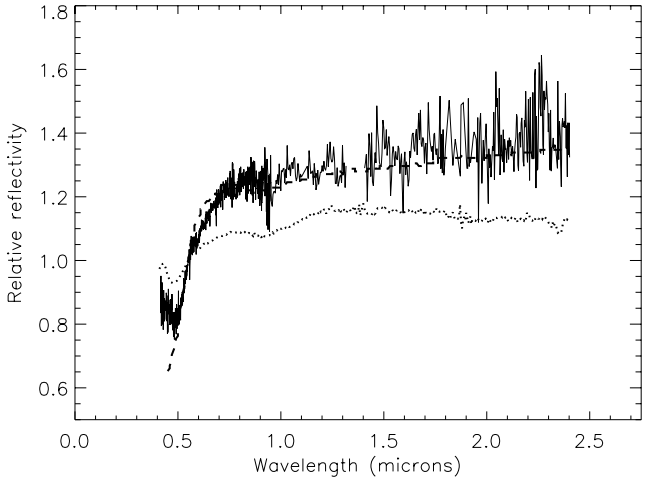

Fig. 4. Comparison of the spectrum of Steins and the spectra of the EL6 enstatite chondrite Atlanta (dashed line), and the enstatite achondrite (aubrite) ALH 78113 (dotted line). All the spectra are normalized at 0.55 μm.

of hydration (Rivkin et al. 2000). All these evidences suggest that Lutetia is an atypical M-type object. In Fig. 3 the NIR spectra of Lutetia by Birlan et al. (2004) with our visible spectrum is reported and compared with the spectrum of the CV3 carbonaceous chondrite Vigarano.

All of the information available for Lutetia are consistent with a primitive composition, except the high IRAS albedo value. New albedo determinations are needed to eliminate the doubts about the taxonomic classification of Lutetia, or to further enhance our view of this unusual object.

2867 Steins, discovered on 1969 by N. Chernykh at Nauchnyj, is a very small object and only few of its properties are known (Table 4). Assuming an albedo in the range 0.04–0.40, a diameter of 17.5–5.5 km can be estimated. Its rotational period of 6.06 ± 0.05 h and a lightcurve amplitude of 0.2 mag has been recently determined by Hicks & Bauer (2004).

The obtained V and NIR spectra (Figs. 2 and 4) show a strong feature at about 0.5 μm, a weaker feature at about 0.96 μm and a flat and featureless behaviour over 1 μm. This spectral behaviour is very similar to E-type asteroids, even if it is necessary that the albedo, still to be determined, would be larger than 0.3 to classify Steins as an E-type.

Table 4. Orbital and physical characteristics of 2867 Steins.

Semimajor axis (AU)	2.364
Eccentricity	0.146
Inclination (deg)	9.944
Taxonomic type	E
Synodical rotation period (h)	6.06 ± 0.05
Absolute magnitude (with slope par. assumed = 0.15)	12.561

E-type objects are thought to be differentiated bodies which experienced significant heating.

Analyzing the 0.5 μm feature observed in the spectra of some E-type asteroids, Burbine (2000) suggested that some kind of sulfides, such as troilite or pyrrhotite, could produce this feature. Troilite is a rare sulfide (FeS), abundant in meteorites. It is a known constituent of the aubrites but it is also a very dark agent not easily compatible with the high albedo of E-type asteroids (Fornasier & Lazzarin 2001). Moreover

the spectra available in literature of meteoritic and synthetic samples of troilite show quite different spectral behaviours. Also the band at about 0.5 μm changes in wavelength position and shape, probably due to the different crystal structure of each samples.

The spectral behaviour of Steins as shown in Figs. 2 and 4 is similar to that of the E-type asteroid 64 Angelina. According to the classification of Gaffey & Kelley (2004) and Clark et al. (2004), Steins would belong to the same group of Angelina, and its surface composition would include silicates and sulfides, like oldhamite (CaS). The presence of oldhamite on the surface of Angelina, has been also suggested by Burbine et al. (2002). Gaffey & Kelley (2004) suggested that this group of objects (also called E[II] subtype) may have surfaces composed of partial melts derived from E-chondrite-like parent bodies.

In order to investigate the surface composition of Steins we compared its V and NIR spectrum with the spectra of many meteorites available in literature. In Fig. 4 the spectrum of Steins is overlain onto with the spectra of an enstatite achondrite, and an enstatite chondrite. The enstatite chondrite Atlanta (EL6) presents a spectrum that fits very well the observed spectral behaviour of Steins with the exception of the feature at about 0.5 μm. The enstatite achondrite ALH 78113 (aubrite) presents spectral features at 0.5 μm and 0.96 similar to those of Steins' spectrum but with a flatter behaviour at $\lambda > 0.6$ μm.

The differences between asteroid spectra and those of meteorites and mineral assemblages could be due to the effects of space weathering (caused to long cosmic ray exposure) and of surface collisional processing (porosity, grain size distribution, aging of materials...).

5. Conclusions

On the basis of i) the results obtained by the spectroscopic observations; and ii) on the analysis of all the known physical properties of the candidates, we recommend target selection of 21 Lutetia and 2867 Steins. The Rosetta Science Working group supported our recommendation and the ESA's Rosetta Project included these asteroids in the new mission baseline. The fly-by with Steins will take place on September 5th, 2008, with a relative velocity of 8.6 km s^{-1} and the one with 21 Lutetia on July 10th 2010 with a relative velocity of 15 km s^{-1}. In particular, for the two selected candidates:

1. Lutetia represents the most interesting candidate, as it is the only one (among the possible targets) which will allow us to obtain, by radio science experiments, mass determination and density estimation. Moreover, if the primitive chondritic character of Lutetia will be confirmed, it will be well within the early Solar system scientific objectives of the mission.
2. After the choice of the first target, following the criteria to be within the available ΔV and to visit an interesting object, leads 2867 Steins as the best candidate for the other fly-by. Steins has relatively unusual spectral properties and may be classified as E-type object. Rosetta will perform the first in-situ exploration of a member of this rare class of objects, giving an answer to the question if its parent body underwent a total differentiation or a partial melting.

Ground-based observations are still needed to better define the physical and mineralogical characteristics of Lutetia and Steins. Further observations, in particular in the thermal infrared, are fundamental to know the albedo of both the objects. More information will allow us to optimize the science operations during the fly-bys.

References

Barucci, M. A., Capria, M. T., Coradini, A., & Fulchignoni, M. 1987, Icarus, 72, 304
Barucci, M. A., Fulchignoni, M., Belskaya, I., et al. 2004, in The new Rosetta targets, ASSL (Kluwer), 69
Belskaya, I. N., & Lagerkvist, C.-I. 1996, PSS, 44, 783
Binzel, R. P., Birlan, M., Bus, S. J., et al. 2004, PSS, 52, 291
Birlan, M., Barucci, M. A., Vernazza, P., et al. 2004, New Astron., 9, 343
Burbine, T. H. 2000, Ph.D. Thesis, MIT
Burbine, T. H., & Binzel, R. P. 2002, Icarus, 159, 468
Burbine, T. H., McCoy, T. J., Nittler, L. R., et al. 2002, Meteo. Planet. Sci., 37, 1233
Bus, B., & Binzel, R. 2002, Icarus 158, 146
Busarev, V., Bochokov, V., Prokof'eva, V., et al. 2004, in The new Rosetta targets, ASSL (Kluwer), in press
Clark, B. E., Bus, S. J., Rivkin, A. S., et al. 2004, J. Geo. Res., 109, 2001
Fornasier, S., & Lazzarin, M. 2001, Icarus, 152, 127
Fornasier, S., Barucci, M. A., Binzel, R. P., et al. 2003, A&A, 398, 327
Gaffey, M. J., & Kelley, M. S. 2004, LPI XXXV, 1812
Hicks, M. D., & Bauer, J. M. 2004, IAUC, 8315
Hiroi, T., Bell, J. F., Takeda, H., et al. 1993, Icarus, 102, 107
Howell, E. S., Merenyi, E., & Lebofsky, L. A. 1994, J. Geo. Res., 99, 10848
Lazzarin, M., Marchi, S., Magrin, S., & Barbieri, C. 2004, A&A, 425, L25
Magri, C., Ostro, S. J., Rosema, D. K., et al. 1999, Icarus, 140, 379
Rivkin, A. S., Howell, E. S., Lebofsky, L. A., et al. 2000, Icarus, 145, 351
Tedesco, E. F., & Veeder, G. F. 1992, in The IRAS Minor planet Survey, Tech. Rep. PL-TR-92-2049, Phillips Laboratory, Hanscom AF Base, MA
Tholen, D. 1989, in Asteroids II (Univ. of Arizona Press), 1139
Torppa, J., Kaasalainen, M., Michalowski, T., et al. 2003, Icarus, 164, 346
Xu, S., Binzel, R. P., Burbine, T. H., et al. 1995, Icarus, 115, 1
Zappalà, V., Di Martino, M., Knezevic, Z., et al. 1984, A&A, 130, 208

Highlights of Astronomy, Vol. 13
International Astronomical Union, 2003
O. Engvold, ed.

Rosetta Asteroid Candidates

M.Antonietta Barucci
LESIA, Observatory of Paris

Marcello Fulchignoni
LESIA, Observatory of Paris

Mirel Birlan
LESIA, Observatory of Paris

Pierre Vernazza
LESIA, Observatory of Paris

Elisabetta Dotto
INAF, Osservatorio Astronomico di Roma

Alain Doressoundiram
LESIA, Observatory of Paris

Abstract. The new scenario of the Rosetta mission to comet 67/P Churyumov-Gerasimenko (launch on February 2004), includes as baseline the fly-by of one or two asteroids. Several asteroids are now possible fly-by candidates (single or double) within the available resources. Other candidates whose fly-bys require a larger Δv can be also considered if the Rosetta interplanetary orbit insertion will cost less Δv.

All the up to date available information on the possible targets are discussed in this report.

The new baseline of the Rosetta mission includes the fly-by of at least an asteroid (2009-2010) which will precede a long orbital rendez-vous with the 67/P Churyumov-Gerasimenko comet nucleus (2014). The selection of the asteroid target(s) depends on the Δv available after the Rosetta probe interplanetary orbit insertion manoever. A few meter/sec Δv are available for the asteroid science in the pre-launch resource budget; but there is the possibility to allocate to the asteroid some of the remnant Δv, now reserved as contingenty for the insertion manoever, as soon as the Rosetta probe will be on its way toward the comet. The idea is to wait the results (in terms of Δv expenses) of the insertion manoever and to consider the new available budget to perform the asteroid fly-by(s). For this reason it is necessary to be ready shortly after the beginning of the Rosetta interplanetary journey: an international observational campaign is

started with the aim to increase at the maximum level the characterization of the possible asteroid targets of the mission.

This paper present the situation concerning the Rosetta asteroid targets choice as it is at the date of the IAU General Assembly in Sidney (July 2003). Ten main belt asteroids have been found allowing the Rosetta probe to have a single or even few double fly-bys whitin a Δv range 10-150 m/s (see table).

21 Lutetia is the largest object between these possible targets. On the basis of its visible spectra and IRAS albedo (Tedesco, 1992), it was classified as M type, but new observations in near-infarered and polarimetric data (Birlan et al. 2003) suggest that it is rather a C-type object similar to carbonaceous chondrite.

No data on *2181 Fogelin* are available in literature. Considering its absolute magnitude the diameter can be estimated in the range 12-22 km. We observed it with the IRTF/NASA on July 2003 and its near-infared spectrum suggest a S type object (Birlan et al. 2003).

Asteroid	Diameter (km)	IRAS albedo	Extra Δv (km)	Fly-by date mm.dd.yy	Rel. Vel. (km/s)
21 Lutetia	96	0.22±0.02	131	07.10.10	14.9
437 Rhodia	13	0.70±0.08	87	09.17.08	11.2
1393 Sofala	–	–	113	09.11.08	6.9
1714 Sy	–	0.11±0.03	11	03.06.08	8.2
2181 Fogelin	–	–	19	05.25.10	13.6
2513 Baethsle	17	0.03±0.01	16	10.05.08	8.6
2867 Steins	–	–	61	09.06.08	8.6
3050 Carrera	–	–	74	07.31.08	11.2
3418 Izvekov	27	0.07±0.01	14	12.04.10	11.3
5538 Luichewoo	–	–	35	04.08.09	5.6

The asteroid *437 Rhodia* is an intriguing object due to its very high IRAS albedo. The synodical period of $\geq$ 56 hours (Binzel, 1987) allow us to consider it within the slow rotator asteroid group.

If we consider the family members having spectra quite homogeneous (Florczak et al, 1998), we can assume that the asteroids *2513 Baethsle* and *5538 Luichewoo* belong to the S type which is characteristic of the members of the Flora family. IRAS albedo of *2513 Baethsle*, very far from the typical S-type, may indicate its "interloper" character and its appurtenance to a more primitive (C or D) asteroid class. The asteroid *3418 Izvekov* belongs to the C-type Themis family, this is in agreement with its IRAS albedo value. The visible spectrum of the asteroid *1393 Sofala* (Xu et al, 1995) indicats a S-type composition.

The final decision on the asteroid candidates will be taken after the launch. Information on all the possible target asteroids is important to be able to contribute to the best choice of the targets and to optimise the mission science return.

21 Lutetia represents one of the most interesting candidate, infact it's the only one which will allow us to obtain mass determination by radio science experiments, and consequently it will be possible to determine its density. Moreover,

if the chondritic character of this object will be confirmed, it will cope with the scientific objectives of the mission: the exploration of the primitive bodies of the planetary system.

If Lutetia cannot be selected due to the lack of available Δv, the asteroid candidate choice has to be done favouring the objects characterized by: 1) the more primitive compositional types (C, P, D); 2) the slower fly-by relative velocity; and 3) the larger diameter.

To obtain all these information we urge the observer community to participate to the observational campaign of these objects during their 2004 opposition.

1. References

Binzel, R. P. 1987, Icarus, 72, 135.
Birlan, M., Barucci, M.A., Vernazza, V., Fulchignoni, M., Binzel, R.P., Bus, S.J., Belskaia, I. & Fonasier, S. 2003, New Astronomy, in press.
Florczak, M., Barucci, M.A., Doressoundiram, A., Lazzaro, D., Angeli, C. & Dotto, E. Icarus, 133, 233.
Xu, S., Binzel, R.P., Burbine, T.H. & Bus, S.J. 1995, Icarus, 115, 1.
Tedesco, E.F. 1992, PL-TR-92-2049.

ROSETTA ASTEROID CANDIDATES

M.A. Barucci
LESIA, Observatoire de Paris, France

M. Fulchignoni
LESIA, Observatoire de Paris, France

I. Belskaya
Astronomical Observatory of Kharkiv National University, Ukraine

P. Vernazza
LESIA, Observatoire de Paris, France

E. Dotto
INAF-Osservatorio Astronomico di Roma, Monte Porzio Catone, Italy

M. Birlan
IMCCE, Observatoire de Paris, France

Abstract

The new scenario of the Rosetta mission to comet 67/P Churyumov-Gerasimenko (launch on February 2004), includes as baseline the fly-by of the asteroid 2513 Baetsle. Several other asteroids are possible fly-by candidates (single or double) within the available resources. Other candidates whose fly-bys require a larger Δv can be considered if the execution of the Rosetta interplanetary orbit insertion maneuver will allow the Rosetta Project to make available, for the asteroid fly-by, a fraction or the totality of the contingency Δv.

This paper present the history of Rosetta asteroid target selection as well as the situation concerning the Rosetta asteroid targets choice as it is at January 2003. A particular attention is devoted to the asteroid 21 Lutetia which represents the most interesting candidate.

2

1. Introduction

In late 1993 the European Space Agency (ESA) selected the mission Rosetta as the Planetary Cornerstone of its "Horizon 2000" program. The mission baseline included a rendez-vous with in situ investigations of a comet and fly-bys with two asteroids. The mission was named from the Rosetta Stone, due to the importance it had for the archeologists, allowing them to decipher the Egyptian hieroglyphics. In fact the knowledge of the nature of the primordial material (composing comets and asteroids) is considered by the planetologists of fundamental importance for the understanding of the origin and evolution of our solar system. The aim of the mission is to investigate the formation, the composition of planetesimals and their evolution over the last 4.5 billion years. The mission was scheduled to be launched by ESA using European technology and infrastructure. Considering a dedicated Ariane V launch followed by two or three gravity-assist swing-bys with the Earth, Venus and/or Mars, the ESA science team identified a number of mission scenarios which include different possible targets.

2. History of the asteroid target selection

On the Rosetta phase A Report (ESA SCI(93)7), ESOC listed many possible asteroid fly-bys both for rendezvous with the comet P/ Wirtanen and for some others comets rendezvous opportunities.

To select the most primitive targets and to complete the scenario of the asteroid already visited by space missions, an international workshop was organized at Max-Planck Institute (Katlenbur-Lindau) in May 1994. The scientific community underline the necessity to observe all the asteroid candidates suggested by ESA. Asteroids represent a vast heterogeneous population of small bodies with a wide range of orbital, physical and compositional characteristics. Although some asteroids can be differentiated and they can have experienced a collisional evolution, most of them have undergone relatively little thermal and geological evolution since their formation. A considerable amount of information regarding some of the primordial processes which governed the evolution of the whole solar system, immediately after the collapse of the protoplanetary nebula and before the formation of the planets is "frozen" in the asteroid population. The asteroid belonging to the taxonomic class of C (carbonaceous chondrite-like material) and D (volatile-rich ultracarbonaceous material) are considered quasi-unaltered, volatile-rich objects and for these reason the scientific community recommended to include in the mission the fly-by of these primitive objects.

Among various targets, the comet P/Wirtanen was selected as baseline with two fly-bys to the asteroids 3840 Mimistrobel and 2530 Shipka on the basis of the minimum Δv expenses criterium. The announcement of Opportunity published by ESA on March 1995 established the launch date in January 22, 2003.

Barucci and Lazzarin (1995) observed the two targets spectroscopically at CFHT (Mauna Kea observatory) deducing that Mimistrobel and Shipka revealed to belong to S and B classes respectively. As for each selected comet, several asteroid fly-bys were possible, Barucci and Lazzarin suggested to find other targets less evolved.

In 1996, refining the spacecraft trajectory, ESA redefined the mission baseline, changing the second target (Shipka) to 2703 Rodari, selected by the Rosetta Project always on the basis of the minimum Δv cost criterium. Barucci et al. (1998) observed the new target together with all the other possible candidates. The conclusion of their work was that Rodari was again another S type asteroid, as 951 Gaspra and 243 Ida already visited by Galileo mission and 433 Eros target of the NEAR mission. On the basis of their spectral analysis they concluded that 140 Siwa was the best target. The obtained data indicated that Siwa is a more primitive object, belonging to the C taxonomic class. Due to the spectral type and its large dimention (110 km), 140 Siwa was strongly pushed to be the primary asteroid target of the mission. After Barucci et al. (1998) study and suggestion, ESA selected in early 1999, 140 Siwa and 4979 Otawara as the asteroid targets in the new baseline for the Rosetta mission. The asteroid Otawara was added for the small increase of the total Δv. During its cruise to 46P/Wirtanen (rendez-vous), the Rosetta spacecraft was supposed to encounter Otawara on 11 July 2006 (heliocentric distance of 1.86 AU, minimum encounter distance of 2200 km and a relative velocity of 10.63 km s^{-1}) and Siwa on 24 July 2008 (at 2.75 AU from the Sun, at a minimum distance of 3500 km, and a relative velocity of 17.04 km s^{-1}).

3. 140 Siwa and 4979 Otawara

Many international observational campaigns followed to characterize the nature of Otawara and Siwa in order to optimize both the mission trajectory and the science operations. Doressoundiram et al. (1999) determined the synodic rotational period of 2.707 $\pm$ 0.005 hr for Otawara. On the basis of visual spectrum a possible taxonomic class S or V was associated at the object. Le Bras et al. (2001) observed the two candidates obtaining a precise determination of the synodic rotational period of Siwa (18.495 $\pm$ 0.005 hr) and confirming the previous determination of that of Otawara. The phase functions allowed them to determine the H and G parameters for both asteroids. The near-IR spectrum of Siwa confirmed the C/P type nature of Siwa. Just few months before the

4

programmed Rosetta launch, Fornasier et al. (2003) gave a complete portrait of Otawara. The spin vector is presented with a retrograde sense of rotation and the axial ratio a/b=1.21 $\pm$ 0.05. The visible and the near-IR spectra allow them to classify Otawara as S type asteroid and more specifically, on the basis of the analysis of band depths and slopes, in the S(IV) subgroup, suggesting a similarity to ordinary chondrite meteorites.

4. New baseline

In January 2003 the European Space Agency decided to postpone the launch of the spacecraft due to problems with Arianne V launcher, the new launch date has been fixed at the end on February 2004. A new baseline of the Rosetta mission including a long orbital rendez-vous with the 67/P Churyumov-Gerasimenko comet nucleus (in 2014) and one or two asteroids flybys (in the time span 2008-2010). The selection of the asteroid target(s) depends on the Δv available after the Rosetta probe interplanetary orbit insertion manoever. A few meter/sec Δv are available for the asteroid science in the pre-launch resource budget; but there is the possibility to allocate to the asteroid some of the remnant Δv, now reserved as contingency for the insertion maneuver, as soon as the Rosetta probe will be on its way toward the comet.

On December 2003 at ESTEC, the asteroid 2513 Baetsle has been selected as target of the baseline mission. In fact a minimum extra Δv of 19 m/s is necessary to allow the spacecraft to flyby this asteroid on August 8, 2010 with a relative velocity of 8.6 km/s. 2513 Baetsle is a very small asteroid with an IRAS albedo of 0.028 and an estimated diameter of 16.7 km. The asteroid, on the basis of its orbital parameters, has been assigned to the Flora family, which members have spectra characteristic of S type. This fact is in contrast with its low albedo, typical of a C or D type objects, and for this reason it could be an interloper of the Flora family.

Many other possible targets have been individuated for the mission. In table I the single fly by and in table II the double fly-bys opportunities are listed. On December 2003 at ESTEC a priority has been given also for the double fly-bys within a Δv range 30–160 m/s. The first priority has been given to 437 Rhodia and 21 Lutetia and as the second one to 5538 Luichewoo and 21 Lutetia. The scientific community has strongly pushed to include Lutetia as asteroid target.

The idea is to wait the insertion maneuver and to consider the new available budget (in terms of Δv) to perform the asteroid fly-by(s). For this reason an international observational campaign is started with the aim to increase at the maximum level the characterization of the possible asteroid targets of the mission (Birlan et al. 2004).

Following the scientific objective of the mission, *21 Lutetia* represents one of the most interesting candidate.

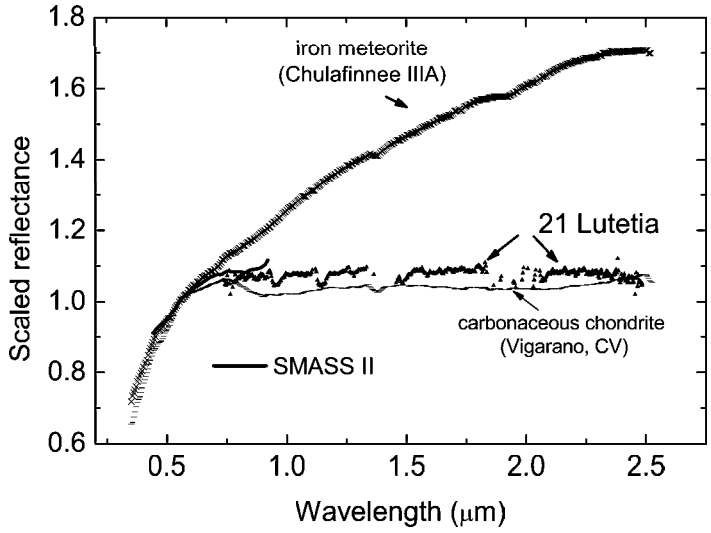

Figure 1. Spectra of Lutetia obtained by Birlan et al. (2004). The comparison with iron meteorite and carbonaceous chondrite reveals the similarity of the asteroid to C class objects.

Table 1. Single fly-by asteroid with the main physical characteristics and encounter data

Asteroid	Diameter (km)	IRAS albedo	Tax. type	Extra Δv m/s	Fly-by date dd.mm.yy	Rel. Vel. (km/s)
21 Lutetia	96	0.221±0.020	C	125	10.07.10	14.9
437 Rhodia	13	0.703±0.084	E?	97	17.09.08	11.2
1393 Sofala	–	–	?	111	11.09.08	6.9
2181 Fogelin	–	–	S	18	25.05.10	13.6
2513 Baetsle	17	0.028±0.007	C-D?	19	10.05.08	8.6
2867 Steins	–	–	?	57	07.09.08	8.6
3050 Carrera	–	–	?	102	30.07.08	11.3
3418 Izvekov	27	0.066±0.013	?	15	05.12.10	11.2
5538 Luichewoo	–	–	S?	32	08.04.09	5.6

5. 21 Lutetia: the best possible choice

21 Lutetia is the largest asteroid available in the list of the possible candidates. On the basis of IRAS observations, the estimated diameter is 95.8 ± 4.1 km with an albedo of 0.221 ± 0.020 (Tedesco and Veeder, 1992). Its synodic period is of 8.17 ± 0.01 hr (Zappala et al. 1984). Previously classified as M type (Barucci et al., 1987 and Tholen 1989), Lutetia was supposed to

6

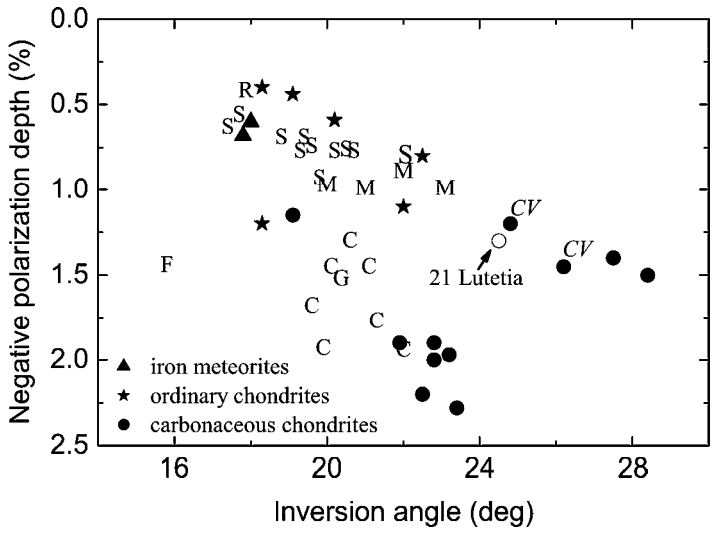

Figure 2. Diagram of the negative polarization depth versus the inversion angle of asteroids and meteorites.

be a parent body of iron meteorites. Further observations have shown that 21 Lutetia is atypical for the M taxonomic class. Its infrared spectrum is unusually flat as compared to other M-asteroids (Howell et al., 1994; Burbine and Binzel, 2002). New observations in near-infrared (Birlan et al. 2004) suggest a similarity with the carbonaceous chondrite spectra classifying this objects as a C-type asteroid (Fig 1). Its polarimetric properties are also better interpreted by a carbonaceous chondrite composition (Belskaya and Lagerkvist, 1996). The asteroid 21 Lutetia presents the largest inversion angle ever observed for asteroids and very similar to those found in laboratory for the carbonaceous chondrites of the CV type (Fig. 2). According to radar observations (Magri et al., 1998) Lutetia has the lowest radar albedo of any other M-asteroids which excludes metallic surface composition. Rivkin et al.(2000) reported the detection of the water-of-hydration absorption feature at 3 micron in its spectrum. All mentioned properties of 21 Lutetia are consistent with a carbonaceous chondrite composition of this asteroid though the high IRAS albedo leads some controversy. A lower albedo of 0.09 has been reported by Zellner et al. (1977) from both polarimetry and radiometry measurements. New measurements of Lutetia's albedo is very important for solving the controversy.

Table 2. Double asteroid fly-bys with relative extra Δv

1st encounter between Earth and Earth	2nd encounter between Earth and comet	extra Δv m/s
437 Rhodia	21 Lutetia	159
5538 Luichewoo	21 Lutetia	129
2867 Steins	21 Lutetia	139
437 Rhodia	2181 Fogelin	113
2513 Baetsle	2181 Fogelin	79
2867 Steins	2181 Fogelin	83
5538 Luichewoo	2181 Fogelin	35
437 Rhodia	3419 Izvekov	112
1393 Sofala	3419 Izvekov	146
2513 Baetsle	3419 Izvekov	73
2867 Steins	3419 Izvekov	77
5538 Luichewoo	3418 Izvekov	32

21 Lutetia represents one of the most interesting candidate, infact it's the only one which will allow us to obtain mass determination by radio science experiments, and consequently it will be possible to determine its density. Moreover, if the chondritic character of this object will be confirmed, it will cope with the scientific objectives of the mission: the exploration of the primitive bodies of the planetary system.

6. Possible double fly-by

After the Rosetta probe interplanetary orbit insertion maneuver, the final Δv available will be known and only at that time we will know if a double fly-bys will be possible. In table 2, a list with double asteroid fly-bys is presented. The first three represent the order of scientific interest priority. The asteroid *437 Rhodia* is an intriguing object due to its very high IRAS albedo 0.70 ± 0.08 (Tedesco and Veeder, 1992) which is the largest one ever observed for asteroids. The synodical period of $\geq$ 56 hours (Binzel, 1987) allow us to consider it within the slow rotator asteroid group which can imply a binary possibility for the object. There is any available spectral observations of the asteroid. However the measured B-V color of Rhodia (Binzel, 1987) together with high albedo are consistent with the E-type composition (Fig. 3).

All the other candidates are in general very small with an unknown taxonomic type. If we consider the family members having spectra quite homogeneous (Florczak et al, 1998), we can assume that the asteroid *5538 Luichewoo* belong to the S type which is characteristic of the members of the Flora family.

8

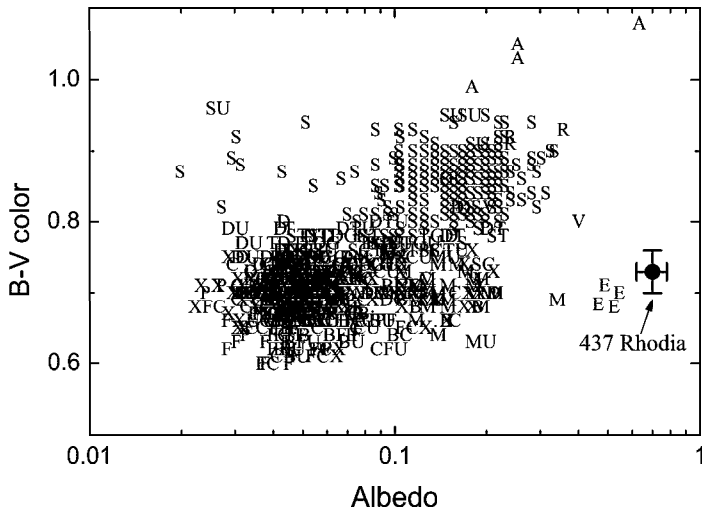

Figure 3. The diagram of the B-V colors versus albedo for asteroids of different types.

7. Conclusion

The asteroid fly-bys were part of the science definition of the Rosetta mission. The scientific community requires to have one or two asteroid visited by Rosetta during the cruise to the comet.

The final decision on the asteroid candidates will be taken after the launch when the remnant Δv will be known. Information on all the possible target asteroids is important to be able to contribute to the best choice of the targets and to optimise the mission science return.

21 Lutetia represents one of the most interesting candidate, infact it's the only one which will allow us to obtain mass determination by radio science experiments, and consequently it will be possible to determine its density. Moreover, if the chondritic character of this object will be confirmed, it will cope with the scientific objectives of the mission: the exploration of the more primitive bodies of the planetary system.

If Lutetia cannot be selected due to the lack of available Δv, the asteroid candidate choice has to be done favouring the objects characterized by: 1) the more primitive compositional types (C, P, D); 2) the slower fly-by relative velocity; and 3) the larger diameter.

8. Acknowledgement

I.Belskaya is grateful to the European Space Agency who granted her fellowship to spend a year at LESIA, Observatoire de Paris, as visiting scientist.

References

Barucci, M. A., Capria, M. T., Coradini, A., and Fulchignoni, M. (1987). Classification of asteroids using G-mode analysis. *Icarus*, 72:304–324.

Barucci, M.A., and Lazzarin, M. (1995). Visible Spectroscopy of the Rosetta Asteroid Targets: 3840 Mimistrobel and 2530 Shipka. *Icarus* 118: 216–218.

Barucci, M.A., Doressoundiram, A., Fulchignoni, M., Florzac, M., Lazzarin, M., and Angeli C. (1998) Composition type characterization of Rosetta asteroid targets. *Planet Space Sci.* 46: 75–82.

Belskaya, I. N., and Lagerkvist, C.-I. (1996). Physical properties of M-class asteroids. *Planet. Space Sci.*, 44:783–794.

Binzel, R. P. (1987). A photoelectric survey of 130 asteroids. *Icarus*, 72:135–208.

Birlan, M., Barucci, M. A., Vernazza, P., Fulchignoni, M., Binzel, R. P., Bus, S. J., Belskaya, I., and, Fornasier, S. (2004). Near-IR spectroscopy of asteroids 21 Lutetia, 89 Julia, 140 Siwa, 2181 Fogelin and 5480 (1989 YK8), potential targets for the Rosetta mission; remote observations campaign. *New Astronomy*, in press.

Burbine, T. H., and Binzel, R. P. (2002). Small main-belt asteroid spectroscopic survey in the near-infrared. *Icarus*, 159:468–499.

Doressoundiram, A., Weissman, P.R., Fulchignoni, M. Barucci, M.A., Le Bras, A., Colas,F., Lecacheux, J., Birlan, M., Lazzarin, M., Fornasier, S., Dotto, E., Barbieri, C., Sykes, M.V., Larson, S., Hergenrother, C.(1999) 4979 Otawara: fly-by target of the Rosetta mission. *Astron. Astrophy.* 352: 697-702.

Florczak, M., Barucci M.A., Doressoundiram A., Lazzaro D., Angeli C.A., and Dotto, E. (1998). A visible spectroscopic survey of the Flora clan. *Icarus* 133: 233–246.

Fornasier, S., Barucci M.A., Binzel R.P., Birlan M., Fulchignoni M., Barbieri, C., Bus, S.J., Harris, A.W., Rivkin, A.S., Lazzarin,M., Dotto,E., Michalowski, T., Doressoundiram, A., Bertini, I., and Peixinho, N (2003). A portrait of 4979 Otawara, target of the Rosetta space mission. *Astron. Astroph.* 398: 327–333.

Howell, E. S., Merenyi, E., and Lebovsky, L. A. (1994). Classification of asteroid spectra using a neural network. *J. Geophys. Res.*, 99:10848–10865.

Le Bras, A., Dotto, E., Fulchignoni, M., Doressoundiram, A., Barucci, M.A., Le Mouelic, S., Forni, O., and Quirico, E. (2001). The 2000 Rosetta asteroid targets observational campaign: 140 Siwa and 4979 Otawara. *Astron. Astroph* 379: 660–663.

Magri, C., Ostro, S. J., Rosema, K. D., Thomas, M. L., Mitchell, D. L., Campbell, D. B., Chandler, J. F., Shapiro, I. I., Giorgini, J. D., and Yeomans, D. K. (1999). Mainbelt asteroids: results of Arecibo and Goldstone radar observations of 37 objects during 1980–1995. *Icarus*, 140:379–407.

Rivkin, A. S., Howell, E. S., Lebofsky, L. A., Clark, B. E., and Britt, D. T. (2000). The nature of M–class asteroids from 3 μm observations. *Icarus*, 145:351–368.

Tedesco, E. F., and Veeder, G. F. (1992). IMPS albedos and diameter catalog. In Tedesco, E. F., Veeder, G. F., Fowler, J. W., and Chillemi, J. R., editors, *The IRAS Minor Planet Survey*, Tech. Rep. PL–TR–92–2049. Phillips Laboratory, Hanscom AF Base, MA.

10

Tholen, D. (1989). Asteroid taxonomic classifications. In: Binzel, R.P., Gehrels T., and Matthews, M.S., editors, *Asteroids II*, Univ. of Arizona Press, Tucson:1139–1150.

Zappala, V., Di Martino, M., Knezevic, Z., and Djurasevic, G. (1984). New evidence for the effect of phase angle on asteroid lightcurve shape - 21 Lutetia. *Astron. Astroph* 130: 208–210.

Zellner, B., Leake, M., LeBerte, T., Duseaux, M., and Dollfus, A. (1977). The asteroid albedo scale. II. Laboratory polarimetry of meteorites. In *Proc. Lunar Sci. Conf.*, 8th:1091–1110. Pergamon Press, Oxford.

EMISSION IN ABSORBTION LINES: RESULTS OF THE SL9 L NUCLEUS IMPACT WITH JUPITER

MIREL BÎRLAN [1,2]

[1] *Observatoire de Paris-Meudon, DESPA*
F-92195 Meudon Cedex, France
E-mail: Mirel.Birlan@obspm.fr

[2] *Astronomical Institute of the Romanian Academy*
Str. Cuțitul de Argint, RO-75212 Bucharest 28, Romania

Abstract. High-resolution spectra of the impact sites and impact of the comet Shoemaker-Levy 9 with Jupiter have been performed at the Pic-du-Midi Observatory. The excitation of several chemical elements (Fe, Ca, Ba, Na, Mn, Mg, etc.) has been identified during the analysis of the L nucleus impact spectra obtained in visible and near-IR. The article presents the atomic lines and the time evolution of nine of them.

Key words: spectroscopy – comets – atomic lines.

1. INTRODUCTION

One of the major astronomical events of 1994 was the impact of the comet Shoemaker-Levy 9 with Jupiter. The astronomical community observed this event within the framework of the coordinated program; several ground-based and space instruments have been involved. SL9/Jupiter impact was a unique event (until now); before the show "live" of the impact SL9 comes inside Jupiter's Roche limit which broken the nucleus in 22 fragments.

The first impact for each nucleus occured on an unfavourable geometry, on the hidden part of Jupiter, not far from the limb. However, relevant data concerning the impacts were collected as soon the impact effects become visible.

2. OBSERVATIONS

The paper presents the spectroscopy in the wavelength range of visible and near-IR (5460-8750 Å) performed for the L impact site. The observations were performed with the 2-meter Bernard Lyot telescope from the Pic du Midi Observatory. The spectra were recorded by a 1024 × 1024 Thomson CCD chip, and

Rom. Astron. J., Vol. 10, No. 2, p. 137–144, Bucharest, 2000

the spectral resolution was 36 000. The fibber of the spectrograph has 50 microns, which corresponds to a field of view of 2.2". This field of view is small enough to obtain high quality spectra only from the impact site (the apparent diameter of Jupiter is about 38"). The guidance software of the telescope allows both automatic/manual tracking during the exposure.

3. DATA REDUCTION

The pre-treatment of the observed data was performed using MUSICOS software. MUSICOS makes the calibration pixel-wavelength for the intensities spectra. Each spectrum was split in several wavelength intervals (named "orders") which little overlap between the adjacent orders. For the analysis in the absorption line we choose as target on Jupiter the L impact site for July 19/20 at 22:30:55 UT (referred to as S167), and July 20/21(referred to as S213), 1994. As reference, the Jupiter spectrum was taken on July 20/21 (referred to as R216). The spectrum S167 emission lines have already been analysed in several papers (Roos-Serote et al. 1995a,b; Barucci et al. 1995).

The MIDAS software procedures for spectroscopy were employed. The goal of this work was to check the atomic absorption line depth one day after the impact moment and to see the excitation of different atoms of Jupiter-SL9 L impact plume. To reach this goal, all the orders of both spectra of impact site were compared with the reference spectrum R216. Then the results S213/R216 and S167/R216 in each order were compared.

In this treatment, the major problem of the differential rotation of the atmosphere of Jupiter occured. From an order to another, in different spectra, the same atomic line presents a slight shift in wavelength, following the expression:

$$\frac{\Delta\lambda}{\lambda} = \frac{v_{diff}}{c},$$

where v_{diff} denotes the differential speed of Jupiter and c stands for the speed of light.

Thus, an automatic procedure of shift cannot be taken into account. For a good preliminary result in some orders the spectra were rebined. Then, shifting the lines in such a way made the subtraction or division between spectra, so that the minima of the lines are at the same wavelength.

The cosmic ray signatures represented another problem that occured during the treatment. This was skipped manually, each time when the spectrum of Jupiter had no lines in this region, and one given atomic line had an abnormal profile.

At least, we cannot omit the presence of the terrestrial lines, even after a major part of them where eliminated by an automatic procedure. Their presence could alter our qualitative analysis and they were carefully analysed and skipped.

4. RESULTS

The comparison of the L impact site spectra with the unperturbed Jupiter's atmosphere spectrum was made in order to minimize any ambiguity. Then the shifted spectra S167 and S213 were compared in each order. To obtain a good signature for each excited atomic line, the ratio S167/S213 has been analysed. As presented in Fig. 1, only the signatures of atomic lines with amplitude larger than three times the noise amplitude were considered (three sigma relevance).

The analysis reveals orders on which the spectral lines were not perturbed by the impact of the comet (as seen on Fig. 2). At the opposite, there are spectral intervals where almost all of the atomic lines were perturbed.

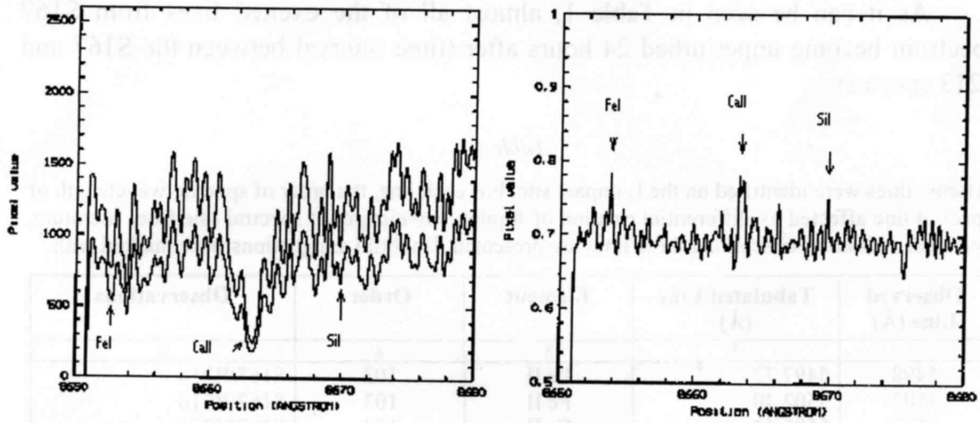

Fig. 1 – Left: Spectra of the 65-th order of R216, and S213 (upper and lower spectrum, respectively). On the center of this order the Paschen $n = 13$ absorption line of Ca II ion. Right: Signatures of Ca II, Fe I, and Si I after the S213/R216 computation.

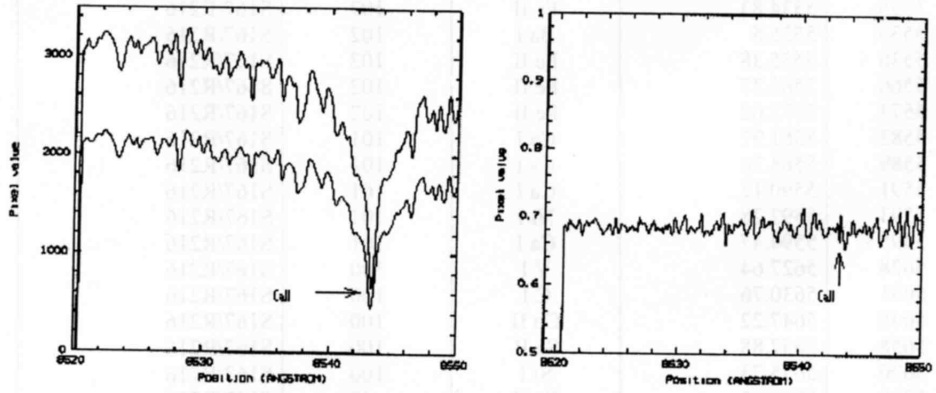

Fig. 2 – "Quiet" order. Spectra of the 66-th order of R216, and S213 (upper and lower spectrum, respectively) containing Paschen line $n = 15$ of Ca II ion (left plot). The result of the S213/R216 computation (right plot).

For the S213, almost of the orders are "quiet". At the opposite, the S167 spectrum presents high differences for several atomic lines (Fig. 3). Thus, the Fe I, II, and III lines are excited on almost all of orders as well as the representative lines of Ca I, and II ions.

Table 1 lists the excited lines. In a first time the line identification was made taking as origin the profile of spectral lines from *The High Resolution Spectral Atlas of the Solar Irradiance* by Beckers, Bridges and Gilliam (1976), and *The Solar Spectrum from λ 6000 to λ 13495* by Babcock and Moore (1947). Then our identification was refined using the articles of Morton (1991, 2000), Morton and Noreau (1994), and the VizieR database of atomic lines (http://vizier.u-strasbg.fr), Reader and Corliss, and Hirata catalogues.

As it can be seen in Table 1, almost all of the excited lines from S167 spectrum become unperturbed 24 hours after (time interval between the S167 and S213 spectra).

Table 1

Atomic lines were identified on the L impact site. For each line, the order of spectra, wavelength of spectral line affected by differential rotation of Jupiter, wavelength of spectral line from literature, element, and notes concerning these lines are presented. Doubtful assignations were marked with *

Observed Line (Å)	Tabulated Line (Å)	Element	Order	Observations
1	2	3	4	5
5498	5497.77	Fe II	103	S167/R216
5502	5502.30	Fe II	103	S167/R216
5507	5506.44	Fe II	103	S167/R216
5511	5512.98	Ca I	103	S167/R216
5511	5510.61	Cr I	103	S167/R216
5527	5526.8	Sc II	102	S167/R216
5533	5535.05	Mo I	102	S167/R216
5535	5534.83	Fe II	102	S167/R216
5536	5535.5	Ba I	102	S167/R216
5536	5535.38	Fe II	102	S167/R216
5566	5565.37	Fe II	102	S167/R216
5573	5572.62	Fe II	102	S167/R216
5582	5581.97	Ca I	101	S167/R216
5589	5588.76	Ca I	101	S167/R216
5591	5590.12	Ca I	101	S167/R216
5593	5592.28	Ni I	101	S167/R216
5595	5594.47	Ca I	101	S167/R216
5628	5627.64	V I	100	S167/R216
5631	5630.76	C I	100	S167/R216
5648	5647.22	Co II	100	S167/R216
5658	5657.88	Sc II	100	S167/R216
5676	5675.73	Si I	100	S167/R216
5710	5708.93	Fe II	99	S167/R216
5737	5736.75	Ca I	99	S167/R216
5788	5787.9	Cr I*	98	S167/R216

Table 1 (continued)

Observed Line (Å)	Tabulated Line (Å)	Element	Order	Observations
1	2	3	4	5
5853	5853.45	Fe II	97	S167/R216
5858	5857.45	Ca I	97	S167/R216
5863	5862.89	Fe I	97	S167/R216
5890	5889.95	Na I	96	S167/R216
5896	5895.92	Na I	96	S167/R216
5915	5914.97	Fe II	96	S167/R216, S213/R216
5984	5983.86	Fe II	95	S167/R216
6014	6013.5	Mn I	94	S167/R216
6017	6016.6	Mn I	94	S167/R216
6066	6065.83	Fe II	93	S167/R216
6123	6122.22	Ca I	92	S167/R216
6142	6141.72	Ba II	92	S167/R216
6163	6162.17	Ca I	92	S167/R216
6176	6176.05	N II	92	S167/R216
6210	6209.73	Fe I	91	S167/R216
6226	6225.92	Cr II*	91	S167/R216
6243	6242.87; 6242.9	Ca I*; Mn I*	91	S167/R216
6245	6244.47	Si I	91	S167/R216
6319	6318.66	Fe II	90	S167/R216
6359	6358.76	Fe II	89	S167/R216
6439	6439.07	Ca I	88	S167/R216
6451	6449.81; 6450.24	Ca I+Co I	88	S167/R216
6472	6471.66	Ca I	87	S167/R216, S213/R216
6494	6493.78	Ca I	87	S167/R216
6496	6495.78	Fe I	87	S167/R216, S213/R216
6498	6498.75	Ba I	87	S167/R216, S213/R216
6501	6499.65	Ca I	87	S167/R216, S213/R216
6563	6562.85	H I	86	S167/R216
6574	6572.78	Ca I	86	S167/R216
6679	6678.9	Fe II	85	S167/R216
6708	6707.91; 6707.76	Li I	84	S167/R216 (double)
6978	6978.48	Cr I	81	S167/R216
7289	7288.88	Fe II	78	S167/R216
7290	7290.26	Si I	78	S167/R216
7326	7326.15	Ca I	77	S167/R216, S213/R216
7327	7325.51	Mn I	77	S167/R216, S213/R216
7853	7852.86	C I*	72	S167/R216
7858	7858.09	Fe III	72	S167/R216
7938	7938.06	Fe II	71	S167/R216
8095	8094.93	Fe I	70	S167/R216
8187	8186.97; 8186.99	F III*, Mn II*	69	S167/R216
8195	8194.70	Fe I	69	S167/R216
8405	8404.77; 8404.84	Mn III*, Fe II*	66	S167/R216
8415	8414.89; 8414.95	Fe II*, F I*	66	S167/R216, S213/R216
8664	8662.14	Ca II	65	S167/R216, S213/R216
8683	8683.4	N I	65	S167/R216, S213/R216
8710	8710.03	Fe I	65	S167/R216, S213/R216
8737	8736.02; 8736.48	Mg I, Mn I	65	S167/R216
8790	8789.34	Fe I	65	S167/R216

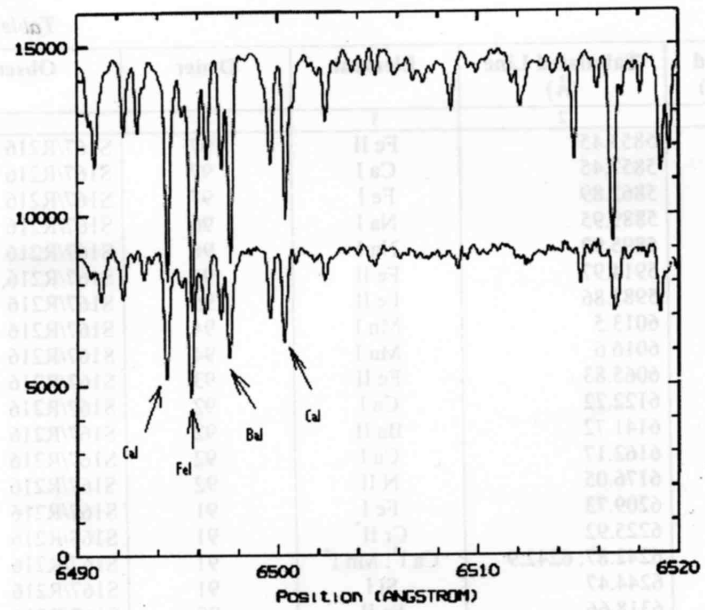

Fig. 3 – Order 87 on S167 (top), and R216 (bottom) spectra. We can distinguish the perturbed lines of Fe I, Ca I, and Ba I lines (marked by arrows).

However, some excited lines are present in both spectra (S167 and S213). In order to have their temporal evolution, casually the orders of a third spectrum were analysed. This spectrum (S166) was taken on July 19/20, 1994, just at the moment that L impact site and plume appeared on the Jupiter visible hemisphere. Table 2 presents such an evolution in the case of some important lines. The percentage values given by the last three columns of Table 2 are computed only from the geometrical consideration, taking into account the depth of the line in the R216 spectrum.

Table 2

The evolution of some spectral lines in three analysed spectra. The spectral line contains the differential rotation shift imposed by Jupiter's rotation.

Element	Wavelength (Å)	S166/R216	S167/R216	S213/R216
Ca I	6472	26%	25%	7%
Ca I	6494	13%	20%	–
Fe I	6496	26%	29%	13%
Ba I	6498	16%	20%	1%
Li I	6708	3%	24%	–
Ca II	8664	84%	70%	10%
N I	8683	15%	33%	13%
Fe I	8790	44%	35%	–
Mg I, Mn I	8737	16%	25%	–

We have paid a special attention to the hydrogen quadrupolar momentum lines. We have searched for the S(0) – S(3) H signatures (6270.24 Å, 7959.77 Å, 8150.67 Å, and 8272.67 Å, respectively), but our search has not provided positive results.

5. DISCUSSION

The greatest part of the absorption atomic lines of the solar spectrum (of our spectral interval) remained unperturbed after the reflection on Jupiter. The Jovian atmosphere does not present metallic compounds on the analysed spectral interval, the profile of Jupiter's spectrum reproduces the solar spectrum. The perturbed spectra come from the L impact site. Therefore, we can formulate the conclusion that the most significant part of this excitation was released by the cometary material.

Various mechanisms could be responsible of the presence of the atom excitation. The perturbation of atomic lines could be explained as the effect of such a mechanism (or several such mechanisms). As long as the goal of this article is to present the qualitative results of spectra analysis, these mechanisms will be only remembered. However, the author intimate conviction is that different excited lines could be explained only by individual theories.

The main known mechanisms are: the resonant fluorescence, the thermal collision (if we consider the temperature on the impact site and plume greater than 1000 K), and the electronic recombination. The resonant fluorescence mechanism is unanimously accepted as the responsible of the presence of metallic lines on the cometary's spectra as well as for the presence of molecular bands. The thermal collisions could contribute to atomic lines only if the collision rate of atoms is high enough to produce transitions between the corresponding energy levels, and the electronic recombination could be efficient for the excitation of atoms in metastable states.

6. CONCLUSIONS

The analysis of the L impact spectra reveals several excited atomic lines. Alkaline lines (Li, Na, Ba, Ca, Mg) as well as line of transition metals (Fe, Cr, Ni, Co, Mn) are listed in Table 1. Nitrogen (N) and maybe flour (F) and carbon (C) lines are presented and rest to be confirmed by further analysis and astronomical observations. The major part of the atomic lines disappear 24 hours after the impact instant, which shows the efficiency of the de-excitation mechanism and energy dissipation on Jupiter's atmosphere.

REFERENCES

Babcock, H. D., Moore, C. E.: 1947, *The Solar Spectrum from λ 6000 to λ 13495*, Carnegie Inst. Washington Publ., No. 579.

Barucci, M. A., Roos-Serote, M., Fulchignoni, M., Lecacheux, J., Crovisier, J., Drossart, P., Roques, F.: 1994, *ASP Conf. Series*, **81**, 404.

Beckers, J. M., Bridges, C. A., Gilliam, L. B.: 1976, *The High Resolution Spectral Atlas of the Solar Irradiance*, Sacramento Peak Observatory, Env. Res. Papers, No. 565.

Morton, D.: 1991, *Astrophys. J. Suppl. Ser.*, **77**, 119.

Morton, D.: 2000, *Astrophys. J. Suppl. Ser.*, **130**, 403.

Morton, D., Noreau, L.: 1994, *Astrophys. J. Suppl. Ser.*, **95**, 301.

Roos-Serote, M., Barucci, M. A., Crovisier, J., Drossart, P., Fulchignoni, M., Lecacheux, J., Roques, F.: 1995, in R. West and H. Bohnhardt (eds), *European SL-9/Jupiter Workshop*, Garching-bei-Munchen.

Roos-Serote, M., Barucci, M. A., Crovisier, J., Drossart, P., Fulchignoni, M., Lecacheux J., Roques, F.: 1995, *Geophys. Res. Lett.*, **22**, 1621.

Received on 12 December 2000

I.4. Astrométrie et systèmes de références.

Le terme générique d'astrométrie définit toute démarche d'observations permettant d'obtenir des positions instantanées précises d'un objet sur la voûte céleste. Dans le cas des objets du système solaire, ce type d'observation mène finalement à l'amélioration des paramètres orbitaux (ou des éléments osculateurs définissant l'orbite de l'objet) et à l'obtention d'une meilleure prédiction de son mouvement (défini par le calcul d'éphémérides). Grâce à de nouvelles technologies (CCD, algorithmes de réduction, programmes de réduction en chaîne), l'aspect astrométrique des divers programmes d'observations en astronomie est dans la plus part des cas adapté à des automatisations importantes.

Deux aspects importants concourent à l'obtention d'une bonne précision sur les positions des objets du système solaire : la qualité du système de référence pris en compte et la qualité des méthodes d'analyse et de réduction des données.

La qualité du système de référence est liée à l'approche qu'il présente par rapport à un système inertiel parfait. Durant l'histoire de l'astronomie, les premiers catalogues d'étoiles ont représenté cette approche : la position des étoiles sur le ciel donnent une origine et une orientation du système. Tout objet nouveau était déterminé par rapport à ce système. Régulièrement, la position de l'origine ainsi que l'orientation des axes ont été remises en cause. La plupart des refontes des systèmes de référence s'est avérée nécessaire suite à une amélioration des observations et à la possibilité de mesure du temps beaucoup plus exacte.

Nous partons du constat qu'il n'y a pas de point fixe défini dans l'Univers. En ce cas, les objets (en mouvement eux aussi) qui peuvent nous donner un système de référence fiable sur une longue période, sont ceux obtenus en mesurant les positions des objets lointains. Actuellement c'est le cas du système de référence lié aux sources radio (noyaux actifs des galaxies et quelques quasars). L'établissement de ce système nouveau, pose des problèmes de

lien (rattachement) avec les anciens systèmes de référence, la plupart établis à base d'étoiles de notre galaxie observées dans la région visible du spectre.

Une partie de mes travaux s'inscrivent dans les efforts de rattachement entre des systèmes de référence optique et le système de référence des radiosources. Pendant plusieurs années nous avons observé des régions (1 degré carré) autour des radiosources afin d'obtenir des positions astrométriques précises des étoiles faibles (14-17 de magnitude), non-cataloguées, de ces régions (Bocsa & Birlan, RAJ, 2001).

L'astrométrie précise de ces régions permet, en seconde approche, l'astrométrie précise dans la région du visible des radiosources avec, finalement, la déduction des règles de rattachement du système de référence radio avec ceux réalisés dans le domaine du visible.

Je me suis aussi intéressé à l'astrométrie des petits corps du système solaire. Le programme CERES est un programme international ayant pour but l'établissement d'un système de référence à partir de mesures astrométriques sur quelques dizaines d'astéroïdes de grande taille. Les observations des astéroïdes de grande taille (tels que (1) Céres, (2) Pallas, (3) Juno, (4) Vesta, (7) Iris,…) se sont poursuivies pendant environ 20 ans. Les observations astrométriques (sur des plaques photographiques) ainsi que la réduction des données ont été effectuées à Bucarest (Birlan & Bocsa, RAJ, 1994). La centralisation des données a été effectuée à l'Institut d'Astronomie Théorique de Saint Petersbourg (coordonnateur du programme en Roumanie G. Bocsa). J'ai participé à l'observation et à la réduction des données. Un autre volet de mes activités astrométriques est constitué par les observations des objets « target of opportunity » comme les comètes Hale-Bopp et Hyakutake (Bocsa & Birlan, RAJ, 1997).

La préparation des observations et la réduction des données d'observations ont permis aussi l'automatisation et l'optimisation des processus. Ovidiu Vaduvescu, ancien collègue de l'Observatoire de Bucarest et moi-même avons conçu le logiciel Celestial Maps, aide pour des recherches en astrométrie (Vaduvescu & Birlan, RAJ, 1996).

Références :

Birlan M., Bocsa G. - *Observations of minor planets in 1990-1994 at the Bucharest Astronomical Observatory*, **Romanian Astronomical Journal**, vol. **5**, n. **2**, 185-191, 1995.
Bocsa G., **Birlan M.** - *Astrometric precise positions of the comet Hale-Bopp at Bucharest Observatory* **Romanian Astronomical Journal**, vol. **7**, 199-200, 1997.
Thuillot W., Arlot J-E., Stavinschi M., **Birlan M.**, Lainey V. - *Ground-based astrometry at the time of the GAIA mission* **Romanian Astron. J.** (in press)

Thuilllot, W., Vaubaillon, J., Scholl, H, Colas, F., Rocher, P., **Birlan, M.**, Arlot, J-E. - *Relevance of the NEO dedicated observing programs* – Comptes-Rendu de l'Académie des Sciences, vol **6** n **3**. 2005.
Bocsa G., **Birlan, M.** - *Intermediate stars in extragalactic radiosource fields* **Romanian Astronomical Journal**, vol **11**, n. **2**, 181-186, 2001.
Vaduvescu O., **Birlan M.** - *Software package for preparing and processing of an astronomical observation*, **Romanian Astronomical Journal** vol. **6**, n. **1**, 97-99, 1996.

OBSERVATIONS OF MINOR PLANETS IN 1991–1994 AT THE BUCHAREST ASTRONOMICAL OBSERVATORY

MIREL BÎRLAN and GHEORGHE BOCŞA

Astronomical Institute of the Romanian Academy
5, Cuţitul de Argint str., 75212 Bucharest 28, Romania

Abstract. The precise positions of asteroids observed at Bucharest Observatory in 1991–1994 period are presented.

Key words. Astrometry, minor planets.

This paper presents the observations of minor planets, obtained in 1991– 1994 with a 380/6000 mm astrograph. Astrophotographic plates with a 2° × 2° field were used. The measurements were carried out by means of an ASCORECORD measuring machine. Both Turner's constants and Schlesinger's dependence methods were used for the computation of the normal coordinates of the object.

In Table 1 the observations of minor planets are presented: the date of the observation and the UT values, the right ascension and the declination, the (O–C) values on the ascension respectively the declination and the observer's initials.

Table 2 presents the reference stars used to compute the values for the 1 Ceres, 2 Pallas, 4 Vesta, 6 Hebe, 7 Iris, 11 Parthenope, 39 Laetitia, 148 Gallia, 389 Industria, 532 Herculina asteroids which are selected in the "Establish the fundamental plane of an inertial reference system" program. Table 2 contains the index number (the same as that in Table 1), the BD number from the catalogue for reference stars, the ascension (s), the declination (′′) and the dependences.

Rom. Astron. J. Vol. 5, No 2, p. 185–191, Bucharest, 1995

Table 1

No	Date and UT		$\alpha_{1950.0}$			$\delta_{1950.0}$			$(O-C)_\alpha$	$(O-C)_\delta$	O.C.
			h	m	s	°	′	″	s	″	
					1991						
					3 JUNO						
1	9.76072	Sep.	19	00	31.67	–10	27	52.6	–0.062	+0.64	GB
2	9.77457	„	19	00	31.72	10	27	57.7	–0.068	+0.69	GB
3	12.77408	„	19	00	52.74	10	46	23.9	–0.040	+0.45	MB
4	12.77784	„	19	00	52.85	–10	46	28.7	–0.042	+0.58	MB
					6 HEBE						
5	9.84659	Sep.	22	21	21.52	–20	48	37.2	–0.039	–0.50	MB
6	9.85491	„	22	21	21.20	20	48	44.3	–0.009	–0.91	MB
7	10.81858	„	22	20	43.99	21	01	20.6	–0.058	–0.11	MB
8	10.82689	„	22	20	43.66	–21	01	26.8	–0.050	+0.27	MB
					7 IRIS						
9	26.76347	Sep.	22	33	56.01	+2	29	36.0	–0.079	–0.75	GB
10	26.769	„	22	33	55.74	2	29	33.6	–0.095	–0.82	GB
11	27.78740	„	22	33	16.47	2	23	09.6	–0.061	–0.60	GB
12	27.79295	„	22	33	16.24	2	23	07.1	–0.071	–0.45	GB
13	30.81141	„	22	31	29.80	2	04	13.1	–0.045	–0.50	GB
14	30.81834	„	22	31	29.53	2	04	10.7	–0.065	–0.35	GB
15	7.82727	„	22	28	27.07	1	22	13.8	+0.022	+0.18	MB
16	7.83628	„	22	28	26.88	+1	22	10.5	+0.024	–0.13	MB
					39 LAETITIA						
17	9.73786	Sep.	18	24	26.58	–15	02	31.3	+0.023	–0.40	GB
18	9.74895	„	18	24	26.86	15	02	34.6	+0.010	–0.30	GB
19	10.74205	„	18	24	55.98	15	07	31.6	+0.026	+0.17	GB
20	10.75314	„	18	24	56.30	–15	07	35.2	+0.028	–0.11	GB
					1992						
					532 HERCULINA						
21	24.82830	Jun.	16	11	35.32	–6	32	37.7	–0.023	–0.03	GB
22	24.83869	„	16	11	34.93	–6	32	42.3	—0.015	+0.14	GB

Table 1 (continued)

1993

No	Date and UT		$\alpha_{2000.0}$			$\delta_{2000.0}$			$(O-C)_\alpha$	$(O-C)_\delta$	O.C.
			h	m	s	°	′	″	s	″	
					1 CERES						
23	11.85165	Oct.	2	16	44.40	+0	00	19.7	–0.068	+0.33	GB
24	11.86065	„	2	16	44.00	+0	00	18.8	–0.026	+0.14	GB
					2 PALLAS						
25	3.76738	Sep.	21	40	12.08	+6	15	07.5	–0.008	+0.15	GB
26	3.77915	„	21	40	11.56	6	14	58.9	–0.028	+0.23	GB
27	10.75450	„	21	35	37.41	4	47	59.4	–0.041	–0.68	GB
28	10.76835	„	21	35	36.88	4	47	48.9	–0.052	–0.73	GB
29	13.73385	„	21	33	51.86	4	10	15.2	–0.065	–0.65	GB
30	13.74770	„	21	33	51.38	+4	10	5.6	–0.061	–0.28	GB
					4 VESTA						
31	7.82329	Sep.	22	32	37.56	–20	00	39.4	+0.058	–0.64	GB
32	7.83022	„	22	32	37.20	20	00	40.7	+0.074	+0.44	GB
33	10.83310	„	22	30	3.79	20	16	32.8	+0.014	–0.30	GB
34	10.84003	„	22	30	3.50	20	16	34.1	+0.080	+0.53	GB
35	13.81280	„	22	27	39.41	20	30	16.1	+0.058	–0.94	GB
36	13.82388	„	22	27	38.82	20	30	18.4	+0.010	–0.42	GB
37	11.79071	„	22	15	20.08	20	56	42.5	+0.044	–0.34	GB
38	11.80040	„	22	15	20.02	20	56	41.0	+0.025	–0.13	GB
39	13.73227	„	22	15	17.97	20	52	13.3	+0.050	–0.63	GB
40	14.74196	„	22	15	17.97	–20	52	11.9	+0.032	–0.71	GB
					11 PARTHENOPE						
41	11.80906	Oct.	1	1	47.47	–1	42	23.9	–0.049	–0.13	GB
42	11.82083	„	1	1	46.83	–1	42	27.6	–0.040	+0.20	GB

Table 1 (continued)

No	Date and UT				$\alpha_{2000.0}$			$\delta_{2000.0}$	$(O-C)_\alpha$	$(O-C)_\delta$	O.C.
					80 SAPPHO						
43	26.80669	Jul.	18	33	56.84	–7	39	46.2	–0.070	–0.40	GB
44	26.81708	„	18	33	56.36	–7	39	47.4	–0.070	–0.40	GB
					148 GALLIA						
45	27.76779	Apr.	11	56	10.15	+23	40	22.3	–0.045	+0.15	GB
46	27.77957	„	11	56	9.91	+23	40	23.0	–0.014	+0.20	GB
					389 INDUSTRIA						
47	11.83087	Oct.	1	32	42.19	+22	53	36.5	+0.037	–0.30	GB
48	11.84126	„	1	32	41.61	22	53	33.5	+0.032	–0.43	GB
49	13.75270	„	1	30	57.41	22	44	23.8	–0.004	–0.09	GB
50	13.75962	„	1	30	57.07	+22	44	21.6	+0.042	–0.27	GB
					409 ASPASIA						
51	26.83474	Jul.	19	43	34.67	–5	13	34.7	–0.070	+0.00	GB
52	26.84617	„	19	43	34.02	–5	13	35.3	–0.070	+0.00	GB
					1994						
					48 DORIS						
53	1.77282	Sep.	20	56	55.65	–10	44	7.1	+0.040	+0.10	GB
54	1.78667	„	20	56	55.16	–10	44	11.2	+0.040	–0.10	GB
					179 KLYTAEMNESTRA						
55	1.80329	Sep.	21	24	19.03	–2	38	50.4	–0.010	+0.60	GB
56	1.81714	„	21	24	18.39	–2	38	54.1	–0.010	+0.60	GB
					216 KLEOPATRA						
57	1.83376	Sep.	23	20	37.52	+14	23	46.4	+0.190	+0.00	GB
58	1.84484	„	23	20	37.13	+14	23	41.7	+0.170	+0.10	GB

Table 2

No	BD	$(\alpha_i)^s$	$(\delta_i)''$	Dependences	
1–2	–10–4904	22.629	44.35	0.010349	0.010110
	–10–4912	20.512	36.44	.186698	.185447
	–10–4918	49.884	34.91	.043847	.045221
	–10–4930	52.496	34.59	.271566	.272689
	–10–4934	23.503	12.25	.487540	.486534
3–4	–10–4918	49.968	33.99	0.283145	0.282661
	–11–4849	19.500	62.81	.236471	.237827
	–10–4931	14.138	17.74	.200104	.198219
	–11–4869	4.865	55.11	.143360	.144196
	–10–4946	14.344	37.91	.136919	.137099
5–6	–22–5897	50.581	61.78	–0.196843	–0.194913
	–21–6207	12.816	52.11	+.057731	+.058379
	–21–6213	48.267	0.59	.454236	.453187
	–21–6214	1.017	14.05	.421114	.419989
	–2215881	31.378	3.91	.263761	.263359
7–8	–22–5897	50.581	51.78	0.187275	0.188238
	–21–6207	12.816	52.11	.281005	.281265
	–21–6213	46.267	0.59	.300064	.299629
	–2215889	52.994	11.33	.053406	.053671
	–21–6226	23.206	25.32	.178250	.177197
9–10	2 4520	23.721	10.93	0.196177	0.196768
	1 4629	36.930	6.09	.051275	.052065
	2 4528	20.439	14.09	.383204	.382658
	1 4634	43.549	55.11	.072350	.072533
	1 4637	24.537	42.35	.296993	.295977
11–12	2 4520	23.721	10.93	0.279808	0.280326
	1 4629	36.930	6.09	.169692	.170267
	2 4528	20.439	14.09	.297213	.296874
	1 4634	43.549	55.11	.104583	.104658
	1 4637	24.537	42.5	.148703	.147875
13–14	1 4623	49.130	43.84	0.220136	0.221198
	1 4626	14.520	4.89	.250585	.251687
	2 4520	23.721	10.93	.172965	.172518
	1 4629	36.930	6.09	.201374	.301047
	1 4631	57.031	9.28	.154939	.153551
15–16	0 4884	47.386	38.82	0.256246	0.258078
	1 4620	48.130	6.67	.472409	.471684
	0 4891	6.204	57.41	.171442	.170693
	0 4892	8.054	46.22	.075199	.075462
	0 4894	7.811	4.71	.024704	.024084

Table 2 (continued)

No	BD	$(\alpha_i)^s$	$(\delta_i)''$	Dependences	
17–18	–15–4965	45.795	55.77	0.157403	0.156880
	–14–5044	16.029	25.32	.274611	.273365
	–15–4972	39.240	19.78	.114593	.115391
	–14–5065	15.320	11.26	.287454	.287138
	–15–4982	25.879	59.14	.165938	.167226
19–20	–15–4965	45.795	55.77	0.098672	0.098071
	–14–5044	16.029	25.32	.155637	.154273
	–15–4972	39.240	19.79	.187286	.188182
	–14–5065	15.320	11.26	.264060	.263700
	–15–4982	25.879	59.14	.294345	.295774
21–22	–6–4377	20.089	4.11	0.213139	0.213789
	–5–4254	15.359	56.64	.239434	.239337
	–7–4230	32.437	53.85	.162543	.163534
	–6–4393	47.032	20.50	.168198	.167909
	–5–4267	21.444	1.00	.216686	.215431
23–23	–0–0336	43.050	35.55	0.152210	0.153101
	–1–0307	13.152	52.85	.128012	.128848
	–0–0338	38.335	40.87	.222278	.222466
	–1–0311	19.190	31.11	.163099	.162848
	–0–0345	41.514	54.02	.334401	.332737
25–26	5 4831	48.182	10.95	0.106449	0.108678
	6 4868	58.932	25.96	.077545	.077900
	6 4878	48.969	13.71	.197881	.196569
	5 4841	5.705	5.66	.269397	.270066
	5 4847	43.702	15.08	.348729	.346786
27–28	3 4575	11.067	47.37	0.168670	0.170501
	4 4701	35.900	5.01	.172569	.171682
	3 4581	47.409	29.97	.205539	.207403
	4 4705	18.515	36.77	.202240	.200457
	3 4588	5.909	59.06	.250982	.249958
29–30	3 4570	38.579	6.23	0.039674	0.040874
	3 4572	8.549	3.37	.050991	.053487
	3 4577	22.048	13.94	.287993	.285402
	3 4578	36.746	10.05	.217563	.218668
	3 4581	47.409	29.97	.403779	.401569
31–32	–20–6439	42.516	4.40	0.098737	0.099416
	–20–6441	36.985	21.80	.244490	.245254
	–20–6442	11.737	8.22	.082042	.081994
	–21–6248	58.268	40.15	.361169	.360881
	–20–6453	33.015	56.72	.213561	.212455

Table 2 (continued)

No	BD	$(\alpha_i)^s$	$(\delta_i)''$	Dependences	
33–34	–21–6221	0.931	40.25	0.211939	0.212382
	–20–6431	20.222	43.69	.167310	.167487
	–21–6241	22.974	13.13	.260651	.260842
	–20–6445	46.430	6.17	.147861	.147865
	–21–6248	58.268	40.15	.212239	.211865
35–36	–21–6221	0.931	40.25	0.349610	0.351567
	–20–6431	20.222	43.69	.214223	.214659
	–21–6230	30.650	51.30	.274254	.274819
	–20–6439	42.516	4.40	.046092	.044422
	–21–6241	22.974	13.13	.115820	.114532
37–38	–21–6175	46.699	25.41	0.004560	0.004746
	–21–6178	38.952	19.72	.096919	.097141
	–22–5867	56.126	18.06	.250922	.250593
	–21–6185	11.976	28.78	.265527	.265809
	–21–6188	9.021	18.42	.382072	.381712
39–40	–21–6175	46.699	25.41	–0.005056	–0.005045
	–21–6178	38.952	19.72	+0.128226	+0.128444
	–22–5867	56.126	18.06	.185342	.185013
	–21–6185	11.976	28.78	.337970	.338266
	–21–6188	9.021	18.42	.353519	.353322
41–42	–2–0136	3.672	8.43	0.160997	0.163225
	–2–0137	5.470	29.44	.315737	.316281
	–2–0148	25.442	28.05	.111079	.111662
	–2–0154	25.756	43.18	.271700	.269537
	–2–0155	55.475	16.35	.140486	.139294
45–46	24 2405	34.277	39.60	0.349011	0.349742
	24 2407	2.883	24.80	.287224	.287466
	25 2439	54.988	9.86	.153410	.153520
	24 2414	16.544	19.21	.169672	.169207
	24 2416	5.939	21.56	.040684	.040064
47–48	22 0236	41.178	34.06	+0.099327	+0.100311
	22 0238	48.684	26.09	–0.011457	–0.010875
	21 0200	6.816	53.63	+0.198115	+0.199065
	22 0246	28.705	25.80	.276933	.275641
	21 0211	0.128	1.76	.437082	.435858
49–50	22 0236	41.178	34.06	0.277585	0.278170
	22 0238	48.684	26.09	.089981	.090235
	21 0200	6.816	53.63	.372071	.372704
	22 0246	28.705	25.80	.043505	.042735
	21 0211	0.128	1.76	.216859	.216155

Received on 10 April, 1995

ASTROMETRIC POSITIONS OF THE COMET 1995/O1 (HALE-BOPP)

GHEORGHE BOCŞA, MIREL BÎRLAN

Astronomical Institute of the Romanian Academy,
Str. Cuţitul de Argint, 5, 75212 Bucharest 28,
Romania

Abstract. Precise positions of the comet 1995/O1 (Hale-Bopp) observed in Bucharest are presented. These observations were made with a 380/6000 mm astrograph. We used astrophotographic plates and an Ascorecord measuring machine.

Key words: comet, astrometry.

The comet 1995/O1, very well known by the astronomers (professionals and amateurs) as the comet *Hale-Bopp*, offered us a brilliant cosmic show. The computed preliminary orbit reveals that the comet 1995/O1 is for the first time when it passes across the Sun. Systematic observations of its "atmosphere" allow the identification of new chemical compounds (Circular 6568, 6573, 6614, 6625, 6631) never before reported for any other comet.

During autumn 1996, several nights of observation allowed us to perform precise astrometric positions of the comet. The observations were made with the *Mertz-Prin* astrograph (380/6000 mm) from Bucharest.

These positions were calculated using 5–10 PPM reference stars, chosen around the comet, not farther than 1° from the center of the plates. From the α_i, δ_i coordinates (corrected with the proper motions) of the reference stars, and α_0, δ_0 of the center of the plate, the normal coordinates X_i, Y_i were computed. Both Turner's (constants) and Schlesinger's (dependences) methods (Brouwer & Clemence 1961) were used to compute the normal coordinates of the comet. Then, starting with the normal coordinates X, Y, the topocentric coordinates α, δ, of the comet were determined.

The results are presented in Table 1. The first column contains the date of the observations (year, month, day with fraction of day); the topocentric right ascension and the declination of the comet for the 2000.0 epoch are presented in the second

Rom. Astron. J., Vol. 7, No. 2, p. 199–200, Bucharest, 1997

and the third column, respectively; the last column contains the number of the reference stars used for computing.

Table 1

Astrometric positions of the comet 1995/O1 (Hale-Bopp)

DATE UT	$\alpha_{2000.0}$	$\delta_{2000.0}$	N
1996 09 10.76657	$17^h33^m34^s.69$	$-6°00'26''.0$	5
" 09 10.77453	17 33 34 .45	−6 00 24 .3	5
" 09 10.73788	17 33 10 .43	−5 57 19 .0	10
" 09 11.75034	17 33 10 .10	−5 57 16 .7	10
" 10 03.71416	17 29 51 .17	−4 52 15 .2	8
" 10 15.69075	17 32 18 .87	−4 16 34 .4	9
" 10 15.69802	17 32 18 .99	−4 16 33 .3	9
" 11 04.67492	17 42 05 .11	−3 04 25 .2	10
" 11 04.68219	17 42 05 .34	−3 04 22 .6	10
" 11 12.66901	17 47 44 .94	−2 27 43 .1	7
" 11 12.67697	17 47 45 .29	−2 27 42 .8	7

These astrometric observations were already reported to the Central Bureau for Telegrams of the International Astronomical Union and used to improve the orbital elements of the comet.

REFERENCES

Brouwer, D., Clemence, G.: 1961, *Methods of Celestial Mechanics*, Academic Press, New York & London.

⁂ *Circula Nos. 6568, 6573, 6614, 6625, 6631*, Central Bureau for Astronomical Telegrams of the International Astronomical Union.

Received on 8 July, 1997

GROUND-BASED ASTROMETRY AT THE TIME OF THE GAIA SPACE MISSION

WILLIAM THUILLOT[(1)], JEAN-EUDES ARLOT[(1)], MAGDALENA STAVINSCHI[(2)], MIREL BIRLAN [(1,2)], VALERY LAINEY [(1,3)]

[(1)] Institut de mécanique céleste et de calcul des éphémérides
IMCCE/Paris Observatory
77 av. Denfert Rochereau 75014 Paris, France)
[(2)]Astronomical Institute of the Romanian Academy
str Cutitul de Argint – 5, 040557, Bucharest, Romania
[(3)]Royal Observatory of Belgium,
Av. Circulaire, 3 - Ringlaan 3
1180 BRUXELLES - BRUSSEL (Belgium)

Abstract. The next space astrometry mission GAIA will be launched before 2012 with the purpose to perform a wide 3-D cartography of the Galaxy. During this 5 years long mission many Solar System objects will be scanned and measured. Each object will be observed about one hundred times and a very accurate astrometry, down to 10 μas, will be carried out. Furthermore, since the limiting magnitude will be 21 and observations could be made rather close to the Solar direction, many new Solar System objects will certainly be discovered. Therefore this mission will be a milestone in particular for astrometry of the Solar System. Several ground-based programs of observation of Solar System objects will probably have to be stopped or reoriented in order to remain relevant. Our paper intends to discuss these circumstances and the relevance of selected observations. Several proposals are made for coordinating efforts in order to get a better knowledge of these objects. Either autonomous programs or programs complementary to the GAIA mission are proposed. Small telescopes will be still very useful for these programs.

Key words: space mission – astrometry – catalogue – follow-up.

1. INTRODUCTION

Several astrometric programs can be undertaken in order to get a better knowledge of the dynamics of several objects of the Solar System. These observations help us to get improved the dynamical models, to make better predictions of some phenomena (such as stellar occultations) or to find better interpretation of observations and the astrophysical measurements.

But the GAIA astrometric mission scheduled in 2011 for mapping the Galaxy, will certainly question a part of our knowledge of the objects of the Solar System. In

Rom. Astron. J., Vol. XXX, No. XXXX, p. XXX–XXX, Bucharest, 2005

particular the motions and some physical parameters of many small objects will be studied by GAIA and this will decrease the interest of several ground-based programs.

Nevertheless several programs could still remain relevant due to specific aspects of the phenomena implied, or to the range of magnitude of the objects concerned. Our interest is mainly oriented to the following topics:

- Ground based observations of Near Earth Asteroids and main belt asteroids for a GAIA Follow-up
- Astrometry of the new faint planetary satellites
- Mutual events of natural satellites for the improvement of the dynamical models
- Astrometry of the Martian satellites in support to the Mars Express mission
- Stellar occultation by asteroids and satellites for the morphology and the atmosphere probing
- Determination of masses of asteroids by observation of asteroids encounters

2. **THE GAIA MISSION.**

After the successful Hipparcos mission, the space astrometric GAIA ESA mission (http://astro.esa.int/gaia/) intends to make a wide cartography of the Galaxy with a never reached accuracy (Fig. 1). It will probably take place from 2011 to 2015 and will provide a huge amount of data with a high accuracy (down to 10 μas). GAIA will provide positions, parallaxes, proper motions, multicolour photometry and radial velocities. Several hundred of thousands Solar System objects will be detected and measured and our knowledge of these objects will be drastically improved. The main characteristics of this mission are given in the Tab. 1.

Fig.1 – Illustration of GAIA design and artist picture of the spacecraft (from ESA)

Table 1

Several characteristics of the GAIA mission

Launch	~2011
Duration	5 years
Limiting magnitude	21
Number of stars	1.3 billion
Accuracy	10 μas
Number of asteroids	10^5 to 10^6
Accuracy	100 μas

3. A PROJECT FOR A FOLLOW-UP PROGRAM

Actually, GAIA will perform a wide scan of the sky and will have generally not the possibility to immediately re observe an event or an object just detected. Therefore a follow-up program for the GAIA mission will be a useful complementary program. Observations on alert will be a requirement in order to catch more data on these targets, or even to avoid for losing them.

It will be the case for possible Gamma Ray Bursts, microlensing events, novae or other transient events. But it will be certainly the case for fast moving objects and it will be very interesting to use ground based telescopes. Fast moving objects such as Near-Earth Asteroids will require fast reactions to operate several telescopes after receiving an alert from the GAIA control centre.

Limiting magnitude down to 21 and Solar elongation close to 35 degrees will have to be reached. Such specifications may correspond to what a small telescope (50cm) is able to do in an appropriate location. A follow-up network of 0.5m to 1.5m telescopes seems to be well suitable for this task. Robotic and automatic telescopes would obviously be very more efficient in order to shorten the reaction time and we hope that more such instruments will be installed in the next years.

4. CALL FOR A FOLLOW-UP NETWORK

Thanks to a call (http://aira.astro.ro/wg/) through the IAU commission 8 and its Working Group “The Future Development of the Ground-Based Astrometry “ led by M. Stavinschi and J. Kovalevsky, we have already identified several stations which are interested by this program (Fig. 2). The extension of this network and the increasing of the efficiency for the asteroid follow-ups will be studied: identification of each limiting magnitude, determination of the individual astrometric accuracy, rules to apply for a fast reaction on alert.

On this map several stations directly answered to our call for this network : 1: Brooks observatory (USA), 2: Pic-du-Midi and 3: Haute-Provence observatory (France), 4: Uppsala (Sweden), 5: Pulkovo observatory (Russia), 6: NAO Nikolaev Observatory (Ukraine), 13: Valhinos station (Brazil), 15: Sheshan station (China)

Other stations are possible and contacts are in progress for 7: AOE Kazan state univ. (Russia), 8: TUG observatory (Turkey), 9, 10, 11, 12, 14 in Brazil where are robotics telescopes of a Brazilian education program. Any other observers interested by these observations on alert are welcome.

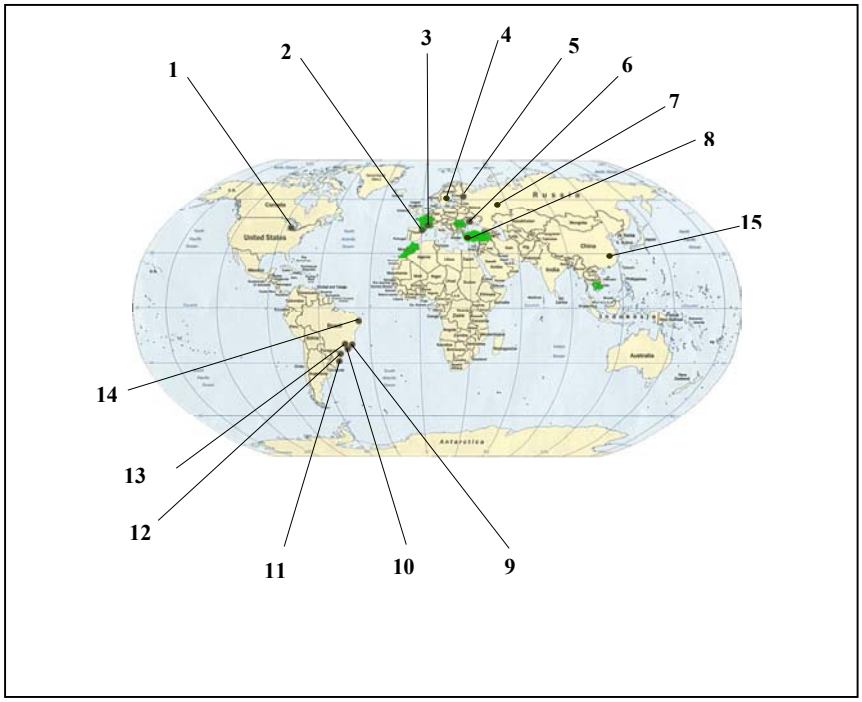

5. NATURAL SATELLITES; PHENOMENA APPLIED TO THE IMPROVEMENT OF THE DYNAMICAL MODELS

Several natural satellites will be observable by GAIA but not all the satellites. Several ones will require special method of observations to be determined due to their brightness and the induced saturation. But on one hand, the new faint satellites, generally irregular satellites, will not be observable at all by GAIA and remain an interesting field for dynamical researches. Nevertheless their faint magnitudes generally require the use of large telescopes. On the other hand, several large and bright satellites will probably be observed but with less accuracy by GAIA. These satellites still require accurate observational data since new and improved dynamical models have recently

been developed (Lainey et al. 2004a, 2004b) and that some physical effects (tidal effects) can be explored with them. Mutual phenomena are this kind of observations.

5.1. MUTUAL PHENOMENA: CALL FOR OBSERVERS

Mutual phenomena (eclipses and occultations of satellites by each other) occur in several satellites system. These events were first observed among the Galilean satellites, but they also occur in the Saturnian system and in the Uranian system. This is the opportunity to get very accurate data from the ground since no atmosphere is generally involved. 15 to 30 mas of astrometric accuracy can be obtained with these photometric observations. Campaigns are organized by IMCCE (Institut de Mécanique Céleste et de Calcul des Ephémérides) for the Galilean system (Arlot 2002, Vasundhara et al. 2003) every six years, and for the Saturnian one (Thuillot et al. 2001) every 15 years.

During these campaigns, photometric measurements lead to lightcurves such as the curve given in Fig. 3 from which astrometry of high precision (5 to 10 mas) can be deduced. Such an accuracy obtained on observations spread out over several decades will help to quantify the tidal effects on the Galilean satellites.

A new program for mutual phenomena of the Uranian satellites will be organised for the period 2006-2007. Later a new campaign of observation of the mutual phenomena of the Galilean satellites will be also organized in 2009. During several months, about 400 phenomena could be observed and a network of observers is necessary in order to catch a maximum of phenomena thanks to a large longitude coverage. Observers are invited to contact IMCCE.

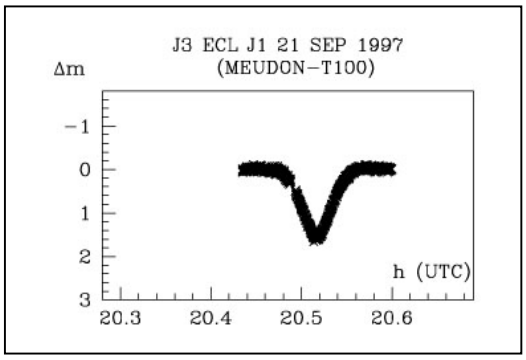

Fig.3 – Lightcurve obtained during the eclipse of Io by Ganymede, observed from the Meudon observatory in 1997

5.2. DETERMINATION OF PHOBOS MASS USING MARS EXPRESS CLOSE FLYBYS VS PHOBOS EPHEMERIS

The first determinations of Phobos mass have been obtained using Viking-1 spacecraft flybys in the year 1977. Since that day, many efforts have been made to improve these determinations. Several combinations of each flyby have been used, involving mainly Viking 1, and Phobos 2 missions. Although many studies converged on an unexpected low value of Phobos mass, no real agreement has been found yet, as seen from the comparison of the values and the error bars. A better determination of Phobos mass (and so its density) would be of great importance regarding the still puzzling origin of the Martian satellites.

Several close encounters between Mars Express and Phobos are scheduled for 2005. These flybys will be the opportunity to reconsider the previous determination of Phobos mass using radio-science.

In particular, the shift between the center of mass and the center of figure (J_1 coefficient) shall be determined. The knowledge of a mass anomaly inside the satellite (especially following the Stickney impact) would be the witness of internal stress. The interpretation of such data will enlighten the key-point of an assumed (but still not demonstrated) homogeneous density. Furthermore, the determination of the higher harmonics coefficients of the gravity field like the J_2 and C_{22} coefficients will also allow us to have additional information on the interior of Phobos.

In order to achieve these goals, a high accurate ephemeris of Phobos in 2005 is required. Tides raised among the Martian surface by Phobos induce a secular acceleration on its motion. This implies to fit Phobos dynamical motion model regularly.

As a consequence, new ground-based observations of Phobos are welcomed and if provided to us, will be used in a very short time. A new dynamical model of the motion of the Martian satellites is currently developed jointly at ROB (Royal Observatory of Belgium) and IMCCE.

6. STELLAR OCCULTATIONS BY ASTEROIDS AND SATELLITES

Stellar occultations by objects of the Solar System (Fig. 4) allow a network of observers to acquire very accurate data on the size, the morphology, the binarity of asteroids. Furthermore it allows us also to explore atmospheres when they exist. Last minute astrometry is a very important task in order to improve the predictions of such events. Succeeding in these observation depends both on improved orbital models of the objects and on high accuracy of the stellar positions (and therefore of the proper motions). This is a complex problem, in particular for the natural satellites, and even if

in the future we get new accurate stellar catalogues, the need of high accuracy of the relative positions (better than 1 mas) required in order to have observers well disseminated on the track of the umbra will certainly imply to continue these last minute observations even after the GAIA mission.

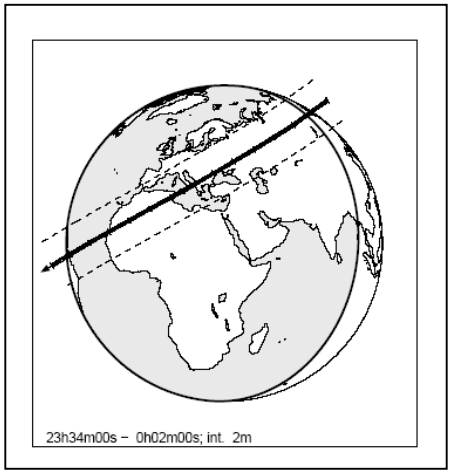

Fig.4 – Path of the umbra of 230 Athamantis during a stellar occultation on 18 November 2004 (from L. Vasta and I. Manek website http://mpocc.astro.cz/2004/)

7. **ASTEROID MASS DETERMINATION BY CLOSE ENCOUNTERS**

Only a few masses of some asteroids are well known with enough accuracy to be efficiency included in the planetary solutions. At this time several space missions are planned toward Mars, but the theory of its motion, which is of interest for the interpretation of their data, is limited by this problem. One of the methods successfully applied for determining asteroids masses is the observation of encounters and measurement of gravitational deflections of the perturbed asteroid (Fig. 5).

We have predicted these phenomena (Fienga et al. 2003) on a period of time spanning the GAIA mission (2003-2022). We found that the GAIA mission will allow us to determine one hundred masses thanks to observation of close encounters down to 1 mas. But we also predicted than a few masses can be determined before the GAIA mission from ground based observations. We have computed several encounters at the level of 50 mas (CCD astrometry can reach this accuracy) of changes in the angular positions by comparison of perturbed and unperturbed orbits around the date of encounters. Among the asteroids concerned, 10 Hygiea, 16 Psyche, 31 Euphrosyne, 704 Interamnia, 87 Sylvia will be good candidates to have their masses accurately determined before the GAIA mission.

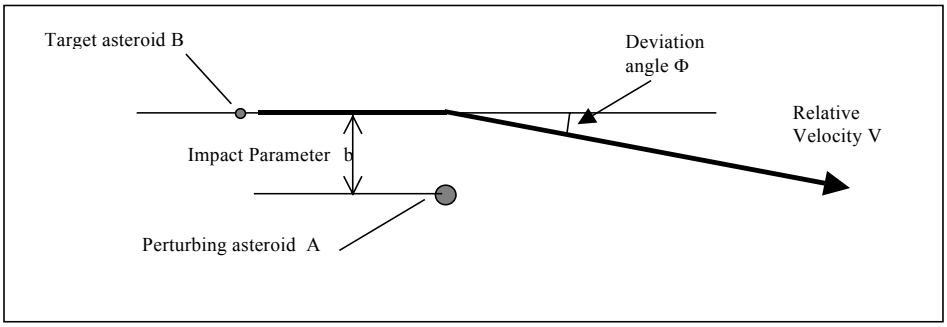

Fig.5 – Gravitational deflection of a small asteroid during an encounter

4. CONCLUSION

By mapping the sky, the next GAIA astrometric space mission will drastically improve in particular our knowledge of the Solar System objects. Numerous new asteroids will be detected and their orbital elements determined. Several natural satellites will also be observed. Nevertheless it appears than ground-based programs for astrometric observations remain of interest for several purposes. A ground-based follow-up program has to be developed in order to avoid for losing the fast moving objects by GAIA and to improve the orbital elements of new objects which will be detected by the space probe. Several natural satellites will not be accurately observed or even not included in the GAIA program. Astrometry of the new faint satellites, or campaign of observation of the mutual phenomena are to be carried out. Starting from now, observations of the Martian satellites would be very useful in support to the Mars Express mission, in order to deal with the mass determination of Phobos. Furthermore several specific ground based observations can lead to original results or to information helpful for the GAIA mission: stellar occultations for the accurate morphological studies, measurement of gravitational deflections during asteroids encounters are such programs.

REFERENCES

Arlot, J.-E.: 2002, *Astron. Astrophys*. **383**, 719
Fienga, A. et al: 2003, *Astron. Astrophys*. **406**, 751
Lainey, V., Vienne, A., Duriez, L.: 2004a, Astron. Astrophys. **420**, 1171
Lainey, V., Arlot, J.-E., Vienne, A..: 2004b, Astron. Astrophys. **427**, 371
Thuillot, W. et al.: 2001, *Astron. Astrophys*. **371**, 343
Vasundhara,R. et al: 2003, *Astron. Astrophys*. **410**,.

Received on XXXXX

Title: Relevance of the NEO dedicated observing programs

Titre: Importance des programmes d'observation des objets géocroiseurs

Authors: William Thuilllot [a], Jérémie Vaubaillon [a], Hans Scholl [b], François Colas [a], P. Rocher [a], Mirel Birlan [a], Jean-Eudes Arlot [a]

Laboratories:

[a] *Institut de mécanique céleste et de calcul des éphémérides, IMCCE/Observatoire de Paris, 77 av. Denfert-Rochereau 75014 Paris, France*

[b] *Observatoire de la Côte d'Azur, BP 4229, 06304 Nice cedex 04, France*

Proofs should be sent to :

William Thuillot,
Institut de mécanique céleste et de calcul des éphémérides,
IMCCE/Observatoire de Paris, 77 av. Denfert-Rochereau 75014 Paris, France
Phone 33 1 40 51 22 62
Fax 33 1 46 33 28 34

Abstract

The study of NEOs (Near Earth Objects) has considerably been developed in several ways under the huge impulse of the researches on the risks of an hazardous collision with the Earth. In this context the observations play a very important role. This article attempts to underline their importance to improve our knowledge of these objects and the necessity of organizing dedicated programs. It develops the objectives of these observations, describes methods to perform the detection of new objects, discuss their follow-up and the necessity to find and to use archives. It also gives information about the fit of the observations in order to improve the knowledge of the orbits of NEO and about the effect of the planetary theories taken into account in the model.

Résumé

L'étude des objets géocroiseurs (NEO ou Near Earth Objects) s'est considérablement développée sous de multiples aspects sous l'impulsion notable des recherches concernant les risques de collision avec la Terre. Les observations jouent dans ce contexte un rôle primordial. Cet article s'attache à souligner leur importance pour accroître notre connaissance de ces objets et la nécessité d'en organiser des coordinations spécifiques. Il développe les objectifs de ces observations, explicite des méthodes pour réaliser la détection de nouveaux objets, discute de leur suivi et de l'archivage des données, donne des informations sur leur utilisation pour améliorer la connaissance de leurs orbites et sur l'influence du choix des théories planétaires prises en compte dans le modèle.

Keywords: asteroids; NEO; detection surveys; follow up; observations
Mots-clefs: astéroïdes; NEO ; objets géocroiseurs; surveillance; suivi ; observations

1. Introduction

The study of the NEOs (Near Earth Objects) is a very active domain of research nowadays and the observational data are obviously very appropriate to perform improvements in this domain. We need to increase the amount of these data and their quality for different purposes. The detection of new objects is obviously the first task to be carried out in order not only to identify the potentially hazardous objects, but also in order to get a better knowledge of their dynamical behavior. A second and very important task is the follow-up observation. This task only will lead to the improvement of the orbital elements of the detected objects and to the physical characterization by measuring several parameters. It requires dedicated astrometric, photometric and spectroscopic measurements through a network of stations of observation. Finally, the best determination of orbital elements requires the search in archived observations where the objects could have already been observed.

If all these steps have been done, the collected data can allow to compute a realistic orbit of a NEO and to assess the risk of collision or, at least, to estimate the uncertainty of the least distance to the Earth and of its epoch. In the following sections we develop these topics and we describe some numerical experiments done to evaluate several effects which may act on this uncertainty: influence of the density of observations, of the spanning time span of observations and of the effect of the planetary ephemerids that are used in the gravitational perturbations.

2. Surveys and detection programs

The current observational programs set to catalogue NEOs (NEAs, Near Earth Asteroids and NECs, Near Earth Comets) use dedicated ground-based telescopes equipped with CCD detectors. Possible NEOs are identified by automated computer software packages. Not surprisingly, those detection programs which search the largest amount of sky each month have most success in finding new NEOs. Since more than ten years, the large majority of NEOs has been discovered by search programs based in the United States. Table 1 shows the corresponding statistics.

The yearly discovery rate of the American programs increased strongly from 26 in 1995 to 421 in 2003 while the other programs never exceeded 20 discoveries per year. LINEAR contributed mainly to the success of the American programs. The other American programs NEAT, Spacewatch, LONEOS and Catalina had sometimes strongly variable discovery rates. The variations were due to technical changes concerning the telescope, the CCD camera used, the automatic detection software and sometime the obligation to share observation time with other programs. The American survey programs are coordinated through the NASA NEO program Office at the Jet Propulsion Laboratory (JPL) [1]. NASA's search program is designed to discover 90 percent of the NEO population (1 km in diameter or larger) within 10 years. There were never comparable national search programs in other countries which is one of the major reasons for the few detections outside the United States.

Most American search programs changed or upgraded their telescopes since 1995 and added a separate telescope for follow-up of NEOs which allows also to determine more precisely their astrometric positions. We give a very brief description of the presently used telescopes for detection

The by far most successful detection program LINEAR (Lincoln Near-Earth Asteroid Research) [2] is run by the Lincoln Laboratory of the Massachusetts Institute of Technology (MIT) in cooperation with the U.S. Air Force. The observing site is Socorro, New Mexico.

Two one-meter aperture wide field Air Force telescopes (GEODSS) specially designed to optically observe Earth satellites are used. The field of view is 2 square degrees. The NEAT (Near-Earth Asteroid Tracking) team [3-4] uses an AMOS (Air Force Maui Optical and Supercomputing) 1.2-meter telescope in Haleakala, Maui, Hawaii and the 1.2-meter Oschin telescope at Mt. Palomar, California which previously performed the two Palomar Sky Surveys. The telescope in Hawai has a field of view of 1.4 square degrees. Spacewatch is the oldest NEO detection program started in 1984 by T. Gehrels at Kittpeak, Arizona. At present, a 0.9-meter telescope is used with a field of view of 2.9 square degrees [5]. The telescope is used also for detecting objects in the outer solar system. LONEOS (Lowell Observatory Near-Earth Object Search) [6] uses a 0.6-meter Schmidt telescope in Flagstaff, Arizona. It covers a field of view of 2.9 square degrees [6]. The Catalina Sky survey operates a 0.7-meter Schmidt telescope at Mt. Bigelow near Tucson, Arizona. Its field of view is 2.9 square degrees [7].

Year	Li	N	S	Lo	C	Other	≥1km	Total NEA	Total NEO
1995	0	0	26	-	-	6	196	347	385
1996	1	10	28	-	-	6	202	392	430
1997	17	11	14	-	-	11	217	445	483
1998	135	11	36	7	3	13	269	650	688
1999	161	0	19	13	30	5	336	879	918
2000	258	15	26	38	13	12	440	1241	1281
2001	277	92	22	42	0	4	531	1678	1724
2002	286	145	22	21	1	11	627	2163	2211
2003	235	68	56	54	8	17	694	2601	2650
2004*	277	25	62	35	65	7	748	3130	3179

Table 1. Number of NEAs discoveries by detection programs, total number of NEAs and NEOs (from A. Chamberlin, NASA). We note Li for Linear, N for NEAT, S for Spacewatch, Lo for LONEOS, C for Catalina (*: incomplete)

Currently, there are three somewhat regular NEO detection programs outside the United States, the Asiago DLR Asteroid Survey ADAS [8], the Campo Imperatore Near-Earth Objects Survey CINEOS [9] and the Japanese Spaceguard Association (JSGA) survey [10]. The telescopes of the three detection programs are not fully dedicated for NEO search. CINEOS observations are performed by a Schmidt telescope (60/90/183 cm) at Campo Imperatore Observatory on Gran Sasso Mountain, 130 km from Roma (Italy). The field of view is 52' x 52'. ADAS uses the 60-cm Schmidt telescope in Asiago near Padova (Italy), with a field of view of 49'x 49'. The two European telescopes for NEO search have much smaller field of views and apertures as compared to the American telescopes. Therefore, even the full dedication of the European telescopes for NEO detection would not significantly increase the European contribution. The Japanese Spaceguard Association uses a 1-meter Cassegrain telescope with a field of view of 2.5 x 3.0 degrees partially for NEO detection [10] at the Bisei Spaceguard Center in the Okayama region. In France a Schmidt telescope which is located near Caussols (Observatoire de la Côte d'Azur) searched for NEOs until 1999. It was not built for NEO detection purposes, however the famous 4179 Toutatis was discovered in one of its photographic plate. During the last 5 years a CCD camera was used but it was covering only a small part of the field. Twelve NEOs were discovered with this telescope

which is no longer operating. However, using a mosaic of CCDs it may be possible at this time to reach an efficiency similar to the NEAT program.

Why is LINEAR so successful in discovering NEOs? A priori, the observing site, the aperture and field of view of the telescopes do not appear to give a significant advantage for the LINEAR search program. The number of NEO detections depends on the area of the sky scanned during a given time and on the limiting magnitude reachable by the instrument. Dynamical models for assumed NEO populations do not indicate regions of the sky where a significantly higher density of NEOs can be expected.

According to the above technical data of the different search telescopes, the limiting magnitudes of the LINEAR telescopes do not give a decisive advantage for this search program. Other telescopes reach even fainter magnitudes. The success must be, therefore, due to an optimized sky coverage and also to an efficient software which finds and extracts a maximum number of NEOs from CCD images.

While the detection rate of NEOs between 1995 and 2001 strongly increased, it seems to become constant now. New generations of telescopes reaching much lower magnitudes may change this situation in the future. The goal to detect all 1 km sized or larger NEOs is not yet reached. Since 2000, year of a maximum of 104 discoveries, the rate decreases slightly on the mean, but is far from being exponentially decreasing.

3. Follow up programs for the dynamics

Once the objects are detected, follow-up observations are required and this hard to organize. Nevertheless all the objects need further astrometric and photometric measurements in order to be fully characterized and to be identified on several oppositions. Unfortunately many objects are even lost after their detections. One of the reasons is that a detection by a survey program will only lead to few measurements; therefore a short orbital arc is not sufficient to get accurate enough ephemerides. Another reason may be due to the faint magnitude of some NEO detected by the surveys which remain beyond the limiting magnitude of the instruments available for their follow-up observations.

In October 2004 for example, the orbits of more than 263 000 objects have been computed by T. Bowell; his database (ftp://ftp.lowell.edu/pub/elgb/astorb.txt) indicates that more than 400 have been poorly observed, and many are even certainly lost. This situation is particularly uncomfortable if the object is a NEO.

We can estimate the effect of the degradation of the precision in the determination of an orbit due to the lack of observations. Considering for example the NEO object 4179 Toutatis, we have first computed a nominal orbit by using a fit of all the available observations extracted from the MPC database [11] and a numerical integration using 2004 as the year of the initial conditions.

In order to test the influence of the availability of observations we did compute several orbits of 4179 Toutatis with different sets of observations. This NEA passed close to the Earth in 2004 (perihelion), and thus led to series of observations all around the world. We have simulated the lack of observations, or the influence of bias such as the limiting magnitude in the calculation of the position of the object. Then by fitting the remaining set of observation, we obtain another orbit to be compared to the nominal one.

Therefore, several fits of the orbit have been carried out, taking into account:

- all the available observations (marked as “All” in the figures below, hereafter called the “nominal solution”)
- all observations until year 2000 (marked as “without 2000+”)
- all observations until year 2002 (marked as “without 2002+”)
- only those observations providing the magnitude of the object (“All Mag”)

- among these above observations, only those with a limiting magnitude of 17.

Then the propagation of the orbit is performed, and the differences of orbital elements as well as Cartesian coordinates are plotted in Fig.1 to 3. The maximum differences to the nominal solution are found close to perihelion (1996, 2000, 2008, 2012, except 2004), where the heliocentric velocity of the body is maximum. Therefore a small error in the observations (or a lack of observation) implies a large error on the position of the body itself which in fact is mainly an error of longitude. The difference between two solutions is maximum because of the time lag between two perihelion returns. The asteroid is found to be in advance or late compared with the nominal solution (Fig. 1). This has to be compared to the motion of the Earth on its orbit. A delay of 0.005 day of the return of Toutatis corresponds to a planet displacement of 13 000 km, therefore far more than one planet radius. This value is reached in 16 years, but this is not a realistic case as it is done only with the 2004 data. A more realistic test is to use all the data except 2004 ones, which simulates the recent discover of the asteroid and the use of its observation during a few previous oppositions to predict an impact. In this case, the error is still of the order of 2000 km, which is still rather big. It is clear that if we want to predict something useful we have to use the 2004 observations. It is important to stress that using classical astrometry makes impossible to predict with a high accuracy an impact on Earth. It is fundamental for that goal to use radar data with a meter level accuracy.

The difference of orbital elements can seem to be low (Fig.2), but by converting them into Cartesian coordinates, one found a few thousands of kilometres of difference (Fig.3), at least. This is far from being negligible, especially in the case of an impact calculation, where the position of the impact has to be accurately found.

We can see that the highest differences to the nominal solution are found for the calculations that take into account the most recent observations only. This stresses the need to have as many available past observations as possible . The error of the position of the object almost doubles between the solution including observations up to 2000 and the one involving all the observations up to 2002. Interestingly the number of observations done between 2000 and 2002 is the same as the number of observations done up to 2000. This does not mean that the accuracy is proportional to the number of observations, but only underlines the fact that, to derive a reliable orbit, lots of observations on a large time scale are necessary.

Considering only the brightest observations has only a minor effect, compared to the solution including all the available magnitudes estimates. A reason for that is that the faintest observations are done when the asteroid is far from perihelion. The distance between the Earth and the asteroid is then larger, and then astrometrical errors much more important. Many NEOs are discovered when they are as close as 0.1 AU to the Earth, but most of the time this asteroid stay as far as 1 to 3 AU. Therefore the observations made during Earth close encounter are at least 10 times more important.

At aphelion the heliocentric velocity is minimum, the position of the NEO changes slowly compared to the situation at perihelion. The positional errors are then less relevant than at any other point of the orbit.

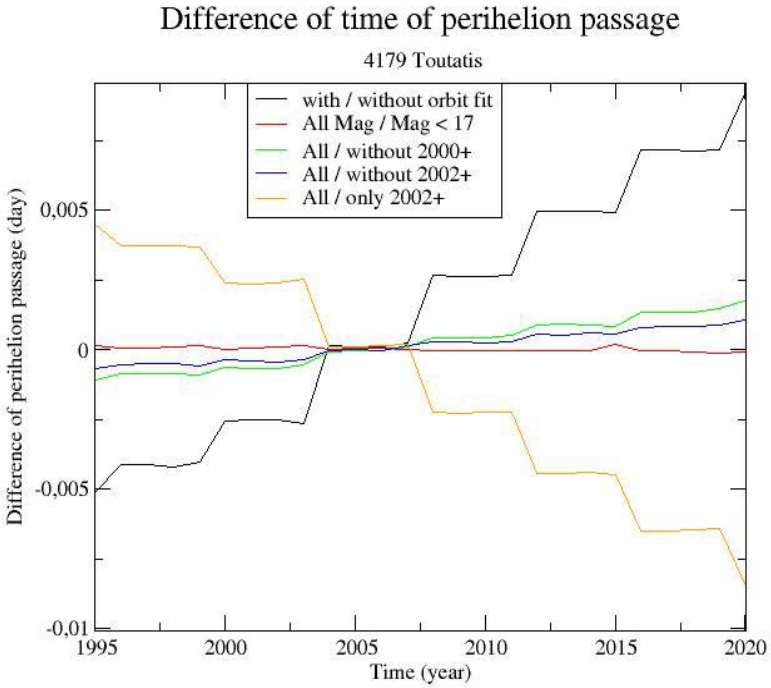

Fig 1. Computed orbits of 4179 Toutatis: differences of time of perihelion passage obtained by comparing several biased orbits with a nominal orbit

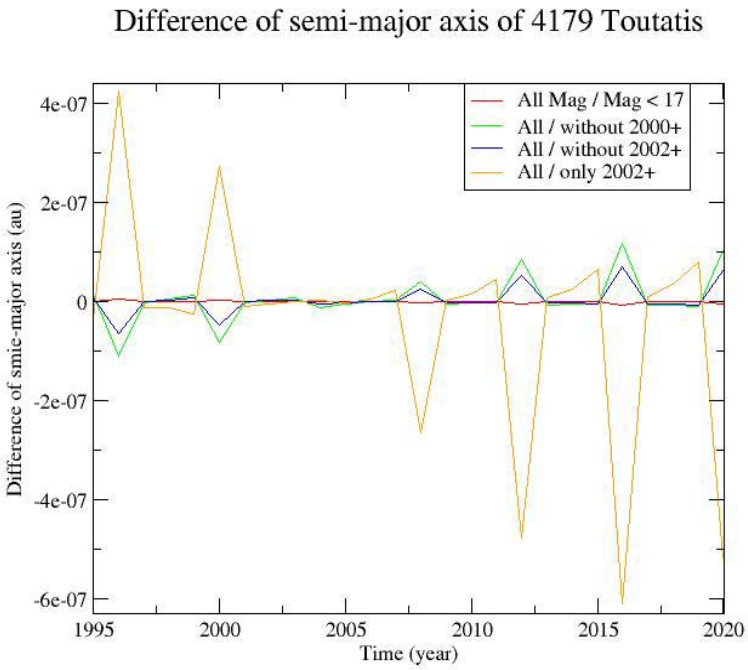

Fig 2. Computed orbits of 4179 Toutatis: differences of semi-major axis obtained by comparing several biased orbits with a nominal orbit

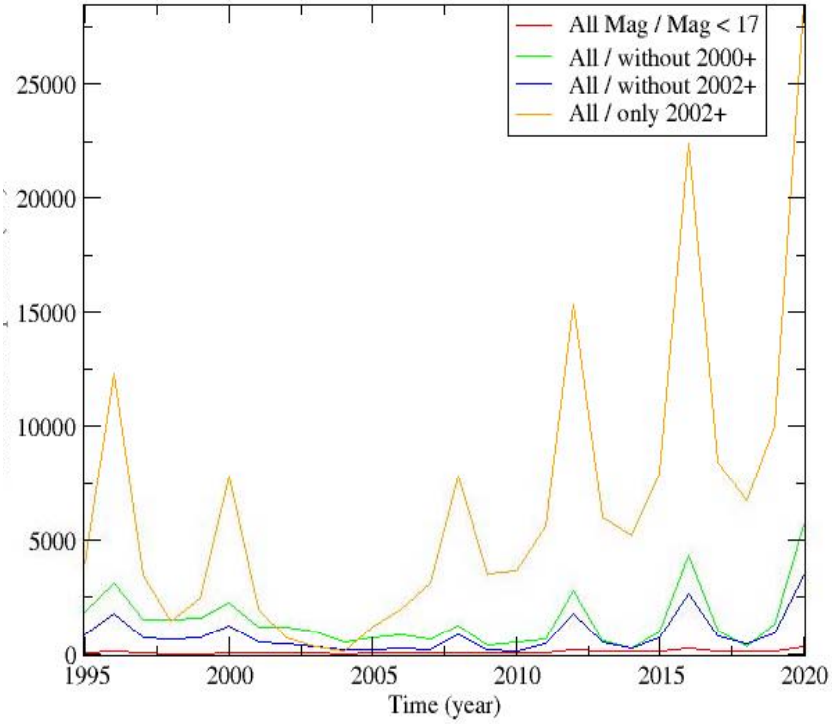

Fig 3. Computed orbits of 4179 Toutatis: differences of position in space obtained by comparing several biased orbits with a nominal orbit

The dedicated NEO programs of observations lead to discoveries of new objects which requires much more observations than what is done by the survey programs. The Minor Planet Center maintains Web pages mainly to stimulate observations just after discoveries to avoid the loss of these objects. This is also done by the Spaceguard Central Node in Italy. Lowell observatory makes also this kind of work by maintaining a critical list of asteroids. This list helps the observers to choose the asteroids to observe in order to maximize the orbit improvement. It is important to note that the observers are organised in a faint network compared to the huge resources of the detection programs. At this time, no really dangerous object was found, but in case we would have to carry out a fast follow-up program for such objects, all the work done by these centers will be a precious benefit to coordinate observers and to collect observations. As illustrated in the previous numerical experiment the orbital precision is improved by increasing the density and the spread of the astrometric observations. Therefore the accurate computation of close approaches to the Earth and the improvement of their prediction require also the search for past observations if they exist. Jointly with a follow-up program of observation, the “data mining” can then highly improve the quality of NEOs ephemerides by imposing some strong orbital constraints on a long time interval.

4. Astrometry and orbitography

The determination of accurate orbits of NEOs requires not only the use of accurate astrometric measurements but also their adjustment with a model involving all the forces acting on the objects: gravitational forces (central force, planetary perturbations) and non gravitational ones like the radiation pressure and the Poynting-Robertson drag. Among these

forces we wondered how large would be the effect of different choices of planetary ephemerides.

At the present time two main methods are used to compute planetary ephemerides: numerical integrations made at JPL by Standish [12] widely used and analytical theories developed at IMCCE by Bretagnon and his colleagues [13]. Both include now small effects such as for example some relativistic effects or effect of the Solar oblateness. But into these models, the perturbations by the largest main-belt asteroids remain hard to accurately assess since we have a very poor knowledge of their masses. Nearly 300 asteroids require to be included in the computation of the perturbations. Apart from the largest ones, their masses can only be estimated by taxonomic considerations and assumptions on the respective density of each class. But even the accuracy of the determination of the mass of the largest ones is not better than 10%. This lack of information led Standish and Fienga [14] to estimate the accuracy of the ephemerides of the four inner planets at a 2-3 km level over more than two decades. The theory of motion of Mars, which is the most sensitive to the gravitational action of asteroids, appears to be the less accurate of the planetary dynamical models. Therefore this feature may influence the computation of the orbit of Mars crosser objects and the modelling of their long term behaviour.

In order to estimate the maximum effect of such uncertainties in the computation of asteroids orbital motion, we made a selection of several Mars and Earth crosser asteroids and we carried out several numerical experiments. Two kinds of calculation were made.

The first experiment is a long term numerical integration of the orbit of 4179 Toutatis by using initial conditions extracted from a fit of the osculating elements given by the Minor Planet Center on the whole set of collected observations. The algorithm is a 15^{th} order Radau algorithm by Everhart [15]. Eight perturbing planets are considered as well as non-gravitational forces described previously.

Fig. 4 shows the differences of position of the asteroid from two different computations. Each one takes into account a different planetary theory from JPL, DE405 and DE406. Standish [12] gives details on their estimated precision. We can see that the shift between the two orbits increases with the time, the initial conditions taken in 2004. The time span of the DE405 theory did not allow to conduct the numerical integration further than the year 2199 AD. The comparison with DE406 is thus restricted to the period 1600-2199 AD. The difference of position of Toutatis begins to be significant (i.e.; larger than a few kilometres) after 200 years (backwards or forwards in time), and reaches a maximum around 300 years in the past, but no comparison with the future motion is available, because of the restriction of the DE405 theory.

The Fig. 5 shows the difference of position for several NEA that are also Mars crossers, for planetary ephemerides SLP96 from IMCCE and DE403 from JPL. We can see that the differences are much larger than when comparing DE405 and DE406, with a rapid increase to 50 km on the average after 10 years. Such differences are not that relevant in case of a 1 km diameter object or more, able to cause a global catastrophe. But it must be emphasized that even by using the best data, it is hard to reach an accuracy better than a few tens of kilometres. This could be important for a small size asteroid impact causing damage similar to the Tungunska event.

.

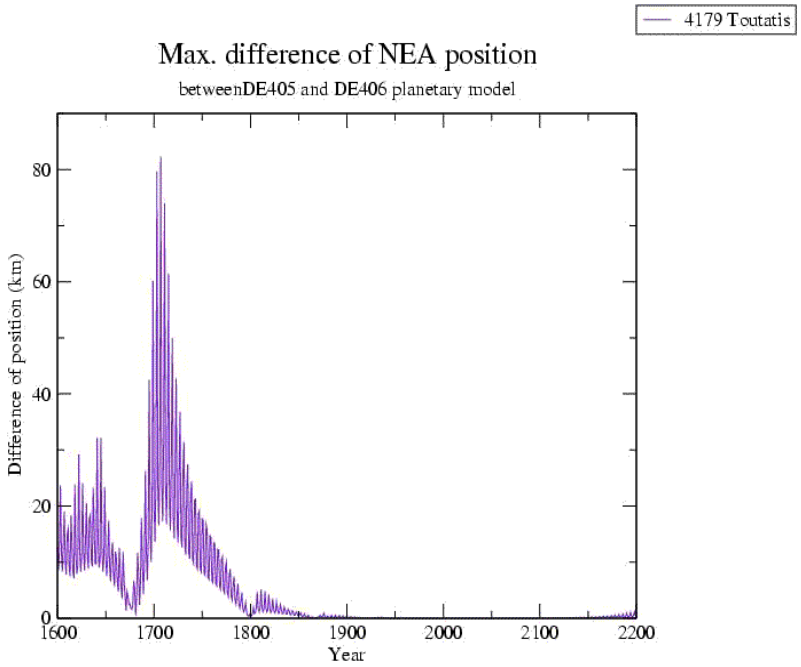

Fig 4. Shift of orbits of 4179 Toutatis due to the use of two different planetary ephemerides.

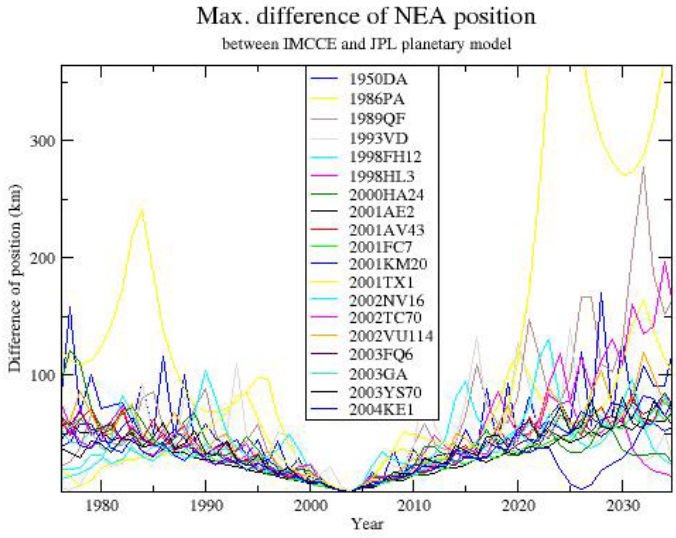

Fig 5. Shift of orbits of several Mars crossers due to the use of two different planetary ephemerides

5. Follow up programs for the physical characterization

By physical properties of a minor body we design the data obtained through observations and related to its intrinsic basic aspects such are colours, light curve, visible and near-IR spectra, thermal albedo, modelled shape and spin from radar measurements.

Continuous observational efforts must be done in order to improve both physics and internal structure of NEO population. Such programs have already been realised in the past, sporadically, for particular objects among NEOs [16,17]. Such programs provide interesting

results namely the complex rotation of 4179 Toutatis and the bi-lobed shape of 4769 Castalia from Hudson and Ostro [18]. Even if these results were presented as “unusual”, nowadays the astronomical community agrees with these conclusions (with a non-negligible importance) in the large picture featuring the minor bodies of the solar system.

Peculiar programs concerning NEOs are also offered as ground-based support of space missions, for example by Binzel et al. [19] or Sekeguchi et al. [20]. Comparative planetology and laboratory results allow to refine the knowledge of the NEO-targets, and to offer good models to explain both their physical and mineralogical feature.

Systematic spectroscopy programs of NEO population only started in the 21st century, and first outcomes of these efforts are reported by Binzel et al [21]. In terms of taxonomy, the results reveal that the NEO population is quite distinct from the Main-Belt one [22]. No systematic program concerning NEOs colors were reported, and only few ground-based instruments allow observations in thermal region (10-20 micron) [23]. NEOs light curve parameters are stored into an European database (http://earn.dlr.de/nea/database.htm), but this work is far from being achieved.

Technological acquirements in building detectors and instruments now allow ~~now~~ the observations and follow-up of faint fast-moving objects in the sky. Nevertheless, the absence of medium and large aperture telescopes devoted to NEOs physical observations makes hard the systematic studies, these programs must compete each semester with programs of various astronomical topics.

The remote observing technique could be the right choice to acquire the scientific information of a given NEO. In this sense, Paris Observatory has initiated the project of remote observing center CODAM [24], in order to offer alternatives and flexibility of scheduled observational programs. This project was started in 2002. Nowadays more than thirty nights of observations were reported. Part of the awarded time was devoted to NEO's near-IR spectroscopy. This work which is part of the remote project will continue by identifying the telescopes allowing remote observing, in order to offer a wide coverage in longitude for monitoring, in the case of this article, and clearly materialize defined NEO programs.

6. Conclusion

In this paper we give a short overview of several topics related to the observations of NEOs. Detections are mostly the task of large surveys and in these domains the American programs are obviously well in advance. But follow-up programs for dynamics as well as for physical characterization are very important. Such dedicated programs of observation, with large longitude coverage, are still necessary to make the observations more dense and continuous, namely when a NEO is just discovered or when such an object passes close to the Earth. We hope that in a next future more robotic telescopes could be used for these programs and will be able to make systematic follow-up observations. Furthermore supplementing a rich set of observations by extracting older ones from catalogues or archives will allow us also to refine the orbits, and the advent of the Virtual Observatory projects will be of great help for this purpose. Besides the increasing number and the higher quality of the observational data, the dynamical considerations are also important for the better understanding of the motion of the NEOs and we show here that the choice of a planetary theory can have a non negligible effect on the computed model to study the long term behaviour of a NEO.

References

[1] Yeomans D.K., Baalke R.C., Chamberlin A.B., Chesley S.R., Chodas P.W., Giorgini J D.; Keesey, M.S., Bulletin of the American Astronomical Society 33 (2001) 1116.

[2] Stokes G.H., Evans J.B., Shelly, F.C., Bulletin of the American Astronomical Society 34 (2002) 1315.

[3] Pravdo S.H., Hicks M., Helin E.F., Lawrence E.F., Bulletin of the American Astronomical Society 32 (2000) 1023.

[4] Talent D.L., Maeda R., Walton S.R., Sydney P.F., Hsu Y., Cameron B.A., Kervin P.W., Helin E.F., Pravdo S.H., Lawrence K., Rabinowitz D., in: Bilbro J.W., Breckinridge J.B., Carreras R.A., Czyzak S.R., Eckart M.J., Fiete R.F., Idell P.S. (Eds.), Imaging Technology and Telescopes, Proc. of SPIE 4091, 2000, p.225.

[5] McMillan R.S., Solar System Research with the Spacewatch 1.8-m Telescope, Lunar and Planetary Lab. Technical Report, Univ. of Arizona, Tucson, 2001.

[6] Koehn B.W., Bowell E.L.G., Bulletin of the American Astronomical Society 32 (2000) 1018.

[7] Larson S., Beshore E., Hill R., Christensen E., McLean D., Kolar S., McNaught R., Garradd, G., American Astronomical Society, DPS meeting 35 (2003) 36.04.

[8] Barbieri C., Calvani M., Hoffmann H.M., Mottola S., Pignata G., Salvadori L., Memorie della Societa' Astronomica Italiana 73 (2002) 636.

[9] Bernardi F., Boattini A., D'Abramo G., di Paola A., Masi G., Valsecchi G. B., in: Warmbein B. (Ed.), Proceedings of Asteroids, Comets, Meteors - ACM 2002, ESA SP-500, Noordwijk, 2002, p.801.

[10] Isobe S., Asami A., Asher D.J., Hashimoto T., Nakano S., Nishiyama K., Ohshima Y., Terazono J., Umehara H., Yoshikawa M., in: Tyson J.A., Wolff S. (Eds.), Survey and Other Telescope Technologies and Discoveries, Proceedings of SPIE Volume 4836, 2002, p.83.

[11] Marsden B., in S.Ferraz-Mello, B. Morando, and J.-E. Arlot Eds, Dynamics, ephemerides, and astrometry of the solar system: proc. of the 172nd Symposium of the International Astronomical Union, held in Paris, France, 38 July, 1995. p. 153, (1996).

[12] Standish E. M., A&A 417 (2004) 1165-1171.

[13] Moisson X., Bretagnon P., Celest. Mech. Dyn. Astron. 80 (2001) 205-213

[14] Standish E. M., Fienga A., A&A 384 (2002) 322-328.

[15] Everhart E., An efficient integrator that uses Gauss-Radau spacings, in Dynamical of comets: their origin and evolution, A. Carusi and G. Valsecchi Eds., (1985) 185-202, Reidel, Dordrecht

[16] Spencer J. R., Akimov L. A., Angeli C., Angelini P., Barucci M. A., Birch, P., Blanco C., Buie M. W., Caruso A., Chiornij V. G. and 38 coauthors, Icarus 117 (1995) 71-89.

[17] Magnusson P., Dahlgren M., Barucci M. A., Jorda L., Binzel R. P., Slivan S. M., Blanco C., Riccioli D., Buratti B. J., Colas F. and 37 coauthors, Icarus 123 (1996) 227-244.

[18] Hudson R. S., Ostro S. J., Science 263, 5149 (1994) 940-943.

[19] Binzel R. P., Harris A. W., Bus S. J., Burbine Th. H., Icarus 151, 2, (2001) 139-149.

[20] Sekiguchi T., Abe M., Boehnhardt H., Dermawan B., Hainaut O. R., Hasegawa S, A&A 397 (2003) 325-328.

[21] Binzel R. P., Rivkin A. S., Stuart J. S., Harris A. W., Bus S. J., Burbine Th. H., Icarus 170, 2 (2004) 259-294.

[22] Stuart J. S., Binzel R. P., Icarus 170, 2, (2004) 295-311

[23] Delbó M., Harris A.W., Icarus, 166, 1, (2003) 116-130

[24] Birlan M., Barucci A., Thuillot W., *Astron. Nachr*. **325** (2004) 6/7.

INTERMEDIATE STARS IN EXTRAGALACTIC RADIOSOURCE FIELDS

GHEORGHE BOCŞA [1], MIREL BÎRLAN [1,2]

[1] *Astronomical Institute of the Romanian Academy*
Str. Cuţitul de Argint 5, RO-75212 Bucharest, Romania
E-mail: gbocsa@aira.astro.ro

[2] *Observatoire de Paris-Meudon, DESPA*
5, Place Jules Janssen, F-92195 Meudon, France
E-mail: Mirel.Birlan@obspm.fr

Abstract. The present paper joins the astrometric efforts to determine the connection between the optical reference frame and the radio one. The final product of this survey will be the astrometric catalogue of the intermediate stars in the neighbourhood of extragalactic radiosources. The statistic analysis of the O–C for the RRS2 standard stars for 188 extragalactic radiosource fields situated between –20° and +70° declination are presented. These results were performed in Bucharest Observatory.

Key words: astrometry – reference frames – radiosources.

1. INTRODUCTION

During the last decade several optical astrometric surveys provided us their results. The observations are performed using either instruments on board of space missions (like Hipparcos satellite), or the ground-based ones. The products of such surveys consist of high-accuracy astrometric catalogues for a large number of stars, including faint stars. We talk frequently now about the astrometric sub-milliarcsecond era (see, e.g., Kovalevsky 1994).

The great importance of an ideal reference system in astronomy is very well known. A reference system better connected with the inertial reference system can be obtained if we take into account the farthest objects on the sky: extragalactic radiosources. Unfortunately, the extragalactic radiosources are very faint in the optical domain; the astrometric positions are based on the radiointerferometric observations for most of them. For this reason, we need to find the mathematical form of passing through the optical reference system(s) on the radio reference system.

Rom. Astron. J., Vol. 11, No. 2, p. 181–186, Bucharest, 2001

The astrometric survey from Bucharest Observatory was started within the framework of the former CONFOR program.

The CONFOR survey was an astrometric joint program of several institutes from the Eastern Europe. Acronym of Connection of Frames in Optical and Radio regions, its aim was to establish a link between the fundamental system FK5 and the radioastronomical coordinate system.

For this pourpose, the catalogue of extragalactic radiosources (Argue and de Vegt 1984), was taken into consideration. The main concept in the CONFOR program was to use the optical fixed system of reference stars in the vicinity of the extragalactic radiosources. Thus, a reliable basis for a good astrometric reduction of the extragalactic radiosources will be created. For a consistent presentation of the CONFOR program, see, for instance, Gubanov et al. (1990).

Two major steps of the program were considered:

- astrometric accuracy for the standard and intermediate neighbouring stars;
- astrometric final measurements for the extragalactic radiosource of each area in the optical domain.

For the first step, one of the instruments used for the observations was the Merz-Prin double astrograph (f = 6 m, D = 38 cm) from the Bucharest Observatory. The instrumental field of 2° × 2° allowed us to reach the stars of 13–14th magnitude on astrophotographic plates with the exposure time varying between 30 and 50 minutes.

A total number of 188 extragalactic radiosource fields were observed between 1992–1999 with this instrument.

2. OBSERVATIONS

The observations were carried out on 24 cm × 24 cm astrophotographic plates. The major parts of the observations were made when the stellar field crossed the meridian. The exposure time was established as function of the field position in the sky: up to 50 minutes for the fields of –20° to 0° declination, and 30 minutes for the fields around 45° in declination.

The observations were reduced taking into account two intermediate catalogues acronym RRS2 and PIRS.

2.1. RRS2-STARS

The RRS2 catalogue contains astrometric positions for 2575 stars lying in the region –20° to +90° declination. The average number of RRS2-stars one degree around the extragalactic radiosources is 10. Theirs coordinates are reported to the mean epoch 1990.5 in the FK5 system, and their proper motions are known.

2.2. PIRS-STARS

The Photographic Intermediate Reference Stars (PIRS) catalogue contains stars from 11th to 14th visual magnitude, located in the 30-arcminute area neighbouring the radiosources. The origin of the PIRS-stars astrometric positions was the GSC catalogue. Thus, an average number of 25 PIRS-stars for each extragalactic radiosource field is measured. The 30-arcminute area choice was decided taking into account the field of the Merz-Prin refractor. For the instrumental field of $2^{\circ} \times 2^{\circ}$, we consider that the light sources measured 30-arcmin around the center are not affected by aberrations due to the optical system.

The importance of the intermediate PIRS catalogue was emphasized at the 22nd IAU General Assembly, held in the Hague in 1994. On this occasion, the idea of a standard list of intermediate stars in the extragalactic radiosource fields was enounced. This aspect can be found also in the B6, and B7 resolutions adopted by the Working Group for the reference frames (Kovalevsky, 1994).

3. RESULTS

Both RRS2 and PIRS measurements were performed with an ASCORECORD measuring machine. Then, the measurements were reduced using several catalogues: PPM, TYCHO, CAMC for the RRS2-stars astrometry, and GSC for the PIRS-stars. A total number of 1943 PPM stars and 1295 TYCHO stars were measured for the 188 considered areas. The presence of the proper motions in the reference catalogues stars, allowed us the determination of the standard errors in right ascension and declination, as well as the (O–C) analysis.

In Figs. 1 and 2, the ratio between the measured (O–C) and the latter's number is presented graphically for the PPM stars under the form of histograms for right ascension (Fig. 1) and declination (Fig. 2). In abscissa the (O–C) values are represented with the step of 0.001 time-second for ascension, and respectively 0.01 arc-second for declination; in the ordinate is represented the number of the values ranging between the respective intervals. In both graphics one can observe a good focusing in relation with the origin. In the ascension the Gaussian obtained is also symmetric, whereas in the declination the range of the negative values number is greater than that of the positive ones.

Fig. 3 presents for the TYCHO stars (in right ascension) the same ratio between the values O–C and their number. The Gaussian is centered in the origin and is also relatively symmetric. Fig. 4 presents, also for the TYCHO stars, the same ratio in declination. One can observe a slight shift of the top of Gauss' bell towards negative values and also a stranger range of the negative values of the (O–C)'s.

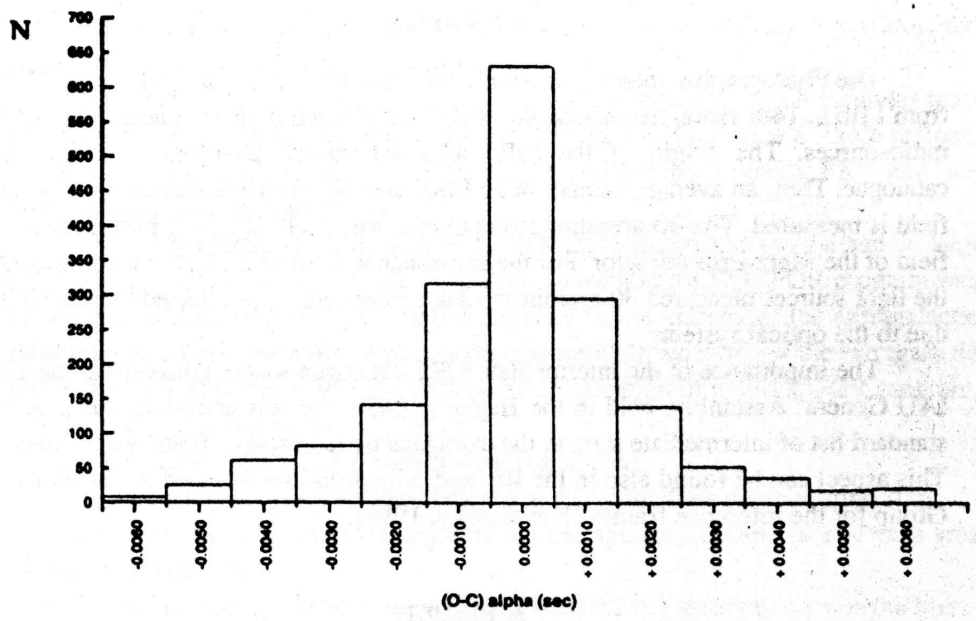

Fig. 1 – (O–C) in right ascension for the PPM stars measured on the 188 analyzed extrgalactic radiosource areas.

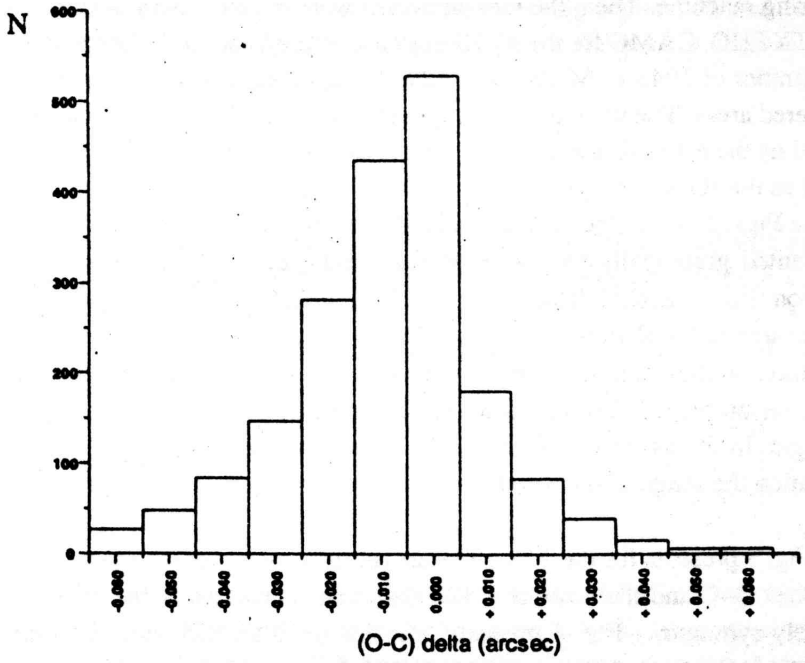

Fig. 2 – (O–C) in declination for the PPM stars measured on the 188 analyzed extragalactic radiosource areas.

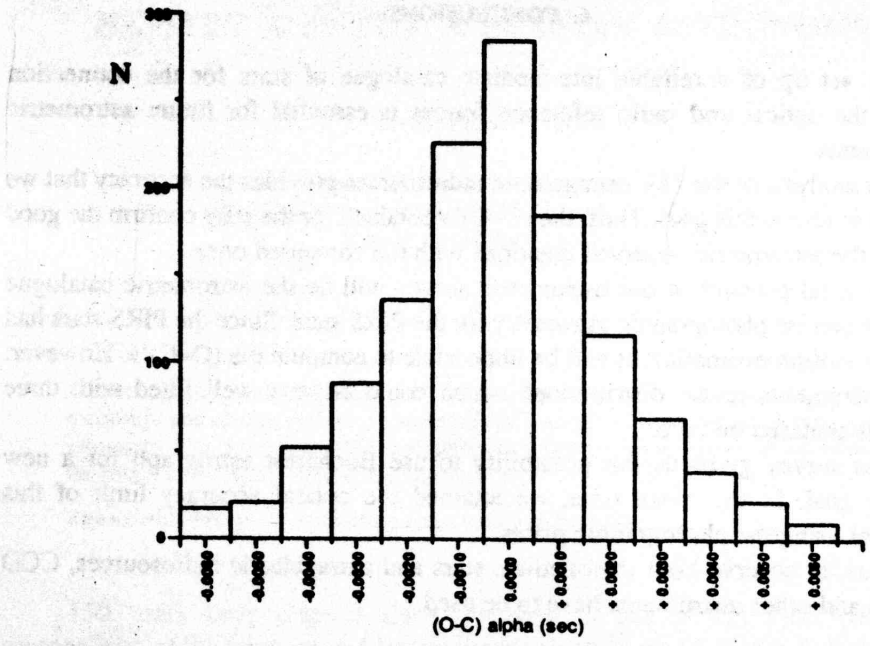

Fig. 3 – (O–C) in right ascension for the TYCHO stars measured on the 188 analyzed extragalactic radiosource areas.

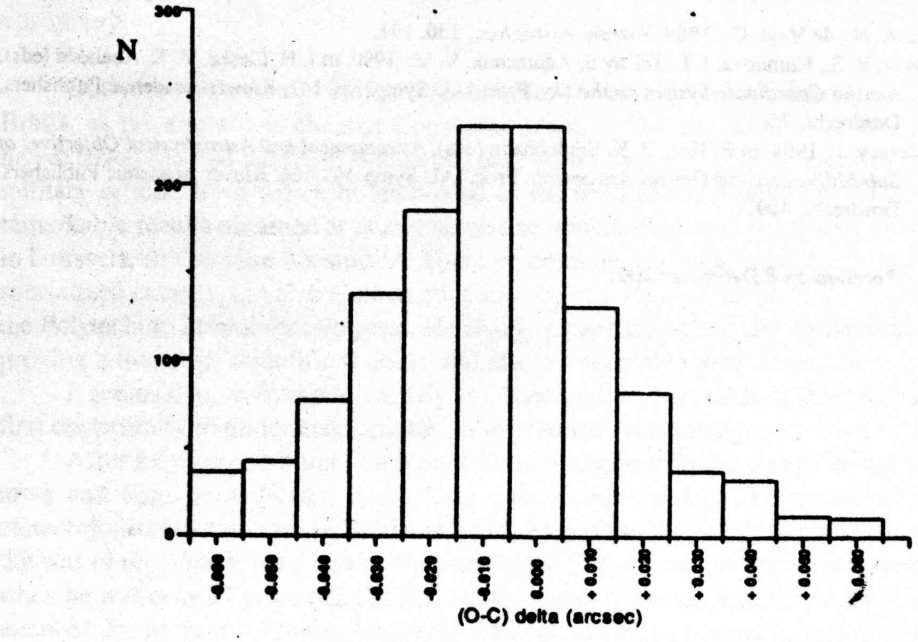

Fig. 4 – (O–C) in declination for the TYCHO stars measured on the 188 analyzed extragalactic radiosource areas.

6. CONCLUSIONS

The set up of a reliable intermediate catalogue of stars for the connection between the optical and radio reference frames is essential for future astrometric developments.

Our analysis of the 188 extragalactic radiosources provides the accuracy that we can reach to obtain this goal. Thus, the (O–C)'s obtained for the stars confirm the good match of the astrometric observed positions with the computed ones.

The final product of our astrometric survey will be the astrometric catalogue giving the precise photographic astrometry for the PIRS stars. Since the PIRS stars had no proper motion estimation, it will be impossible to compute the (O–C)'s. However, our measurements reveal distributions which could be very well fitted with three Gaussians centered on zero.

This survey gives us the possibility to use Bucharest astrograph for a new scientific goal. In the mean time, we attained the optical accuracy limit of this instrument using the photographic plates.

Thus, to observe both intermediate stars and extragalactic radiosources, CCD detectors and other instruments have to be used.

REFERENCES

Argue, A. N., de Vegt, C.: 1984, *Astron. Astrophys.*, 130, 191.

Gubanov, V. S., Kumkova, I. I., Tel'nyuk-Adamchuk, V. V.: 1990, in J. H. Lieske, V. K. Abalakin (eds), *Inertial Coordinate System on the Sky*, Proc. IAU Symp. No. 141, Kluwer Academic Publishers, Dordrecht, 75.

Kovalevsky, J.: 1994, in E. Hog, P. K. Seidelmann (eds), *Astronomical and Astrophysical Objectives of Sub-Milliarcsecond Optical Astrometry*, Proc. IAU Symp. No. 166, Kluver Academic Publishers, Dordrecht, 409.

Received on 8 December 2001

SOFTWARE PACKAGE FOR PREPARING AND PROCESSING OF AN ASTRONOMICAL OBSERVATION

OVIDIU VĂDUVESCU, MIREL BÎRLAN
Astronomical Institute of the Romanian Academy,
Str. Cuţitul de Argint 5, 75212 Bucureşti 28, Romania

Abstract. This paper presents an astronomical software package which draws celestial charts. It was conceived taking into account the technical possibilities available for the Romanian astronomers and the actual trend of the observational astronomy. The software package, now to its third version, comes to decrease the time to prepare an observation and to perform accurate charts for searching and identification.

Key words: software, astrometry, star database, celestial maps.

1. GLOBAL PRESENTATION

The name of this program is "CELESTIAL MAPS". It was written in Turbo Pascal medium, under the MS-DOS operating system (Makkai et al., 1991; Bălănescu et al., 1992; Cristea et al., 1992). Previous oral papers have announced both old version (Văduvescu and Bîrlan, 1992) and the recent version (Văduvescu and Bîrlan, 1994). This version (4.5) was conceived with about 10,000 instructions in five distinct unities. The menu-bar system makes the program very easy to use. The program can print the display. The technical needs are: PC (IBM or compatible, recommended up from 386), display (CGA, EGA, VGA, SVGA) and printer.

2. PROGRAM DESCRIPTION

The software package can be used for photometrical observations, photographical astrometry or CCD astrometry. The program gives accurate charts for searching a certain zone of the sky. The dimension of this zone can be established by the user. These charts can be evolved in three topographical types of projection, on a surface tangent to the celestial sphere in a common chosen point (the center of the chart).

The stars are plotted depending on their spectral class and magnitude. The spectral class dependence is noted on a color display and allows an optimal choice in photometry for the comparison star. For a realistic image of the projected zone, the dimensions of the stars are plotted in terms of stellar magnitudes.

Rom. Astron. J., Vol. 6, No. 1, p. 97–99, Bucharest, 1996

The dimensions of the sky zone have a minimum of 0.0001 degrees. So, in comparison with other softwares, one can plot small field charts. For instance, the dimension of the field for the refractor in Bucharest is 2° × 2°. The program is used to make charts for astrometrical measurements, which use astrophotographical plates.

The charts have a good accuracy, because there are procedures for reducing the epoch of the star catalogues to the observation epoch. These procedures include the corrections for precession, nutation, aberration, parallax and proper motions (Meeus, 1986; Oproiu et al., 1989).

From its second version, the program produces files containing information about the stars which appear in the field. These files are used for the reduction of the observations.

To simulate general conditions for an observation, the program also provides a global image of the sky for a given date and site on the Earth surface. Thus, the program projects the celestial sphere on the tangent plane in zenithal point. This branch offers the position of the planets, Sun and Moon (Văduvescu, 1991).

Another branch of the program shows the sky projection on a tangent plane to the celestial sphere in the North or South equatorial pole. This branch feigns the apparent motions of the planets. Optionally, it is also possible to plot the constellation lines and their name.

This software is endowed with a search procedure; optionally it also displays some nonstellar objects contained in a database.

3. DATABASE

The first version of our program used FK5 catalogue (1535 stars).

Celestial Maps 4.5 uses two 2000-epoch catalogues of the stars: "Catalogue of Positions and Proper Motions" (319494 stars) and "Smithsonian Astrophysical Observatory Catalogue" (258996 stars), selected from a CD-ROM (NASA, 1990). This selection increases the speed of execution and decreases the disk space. The choice of one of these catalogues is made in the second branch of the program, by selecting the option "large data base". The files containing the stars (type files) represent stripes of 10° of declination. Thus, the user can install partial database, in conformity with the disk space and the field of interest. The simple data base file is also a type file. These files contain four denominations of the stars (PPM, SAO, HD, DM). Also, there is another file (text) which contains additional stars, that can be modified by the user. The package requires min 1 Mb (simple database), 16 Mb (SAO large database) and/or 20 Mb (PPM large database).

4. CONCLUSIONS

Celestial Maps is useful for both professional and amateur astronomers, by using it for the scientific research and didactical activity.

If this program is used for preparing an observation night, the time will be shortened roughly with 15 minutes for each chosen object. In this way, the routine will be reduced.

Acknowledgement. The authors thank to the Informatics Department of the University of Craiova and especially Mr. Sorin Pescăruş for their scientifical and technical support. Special thanks are extended to Dr. Gheorghe Vass and Dr. Vasile Mioc from the Astronomical Institute of the Romanian Academy for their ideas, suggestions and observations as to the program.

REFERENCES

Bălănescu T., Gavril S., Georgescu H., Gheorghe M., Sofonea L., Văduva I.: 1992, *Pascal şi Turbo Pascal*, Ed. Tehnică, Bucureşti.

Cristea V., Kalisz E., Athanasiu I., Pănoiu A.: 1992, *Turbo Pascal 6.0*, Ed. Teora, Bucureşti.

Makkai A., Andras M., Crişan C., Şandor K.: 1991, *Ghid de utilizare Turbo Pascal 5.0-5.5*, Romanian Software Company, Cluj-Napoca.

Meeus J.: 1986, *Calculs Astronomiques à l'usage des amateurs*, Société Astronomique de France, Paris.

Oproiu T., Pál A., Pop V., Ureche V.: 1989, *Astronomie. Culegere de exerciţii, probleme şi programe de calcul*, Universitatea din Cluj-Napoca.

Văduvescu O.: 1991, *M. Sc. Thesis*, University of Craiova.

Văduvescu O., Bîrlan M.: 1992, Communication held at "Cluj Academic Days", Cluj-Napoca, October, 1992.

Văduvescu O., Bîrlan M.: 1994, Poster at The 2nd International School in Astronomy and Astrophysics, Rozhen, Bulgaria, April 1994.

* * * *Selected Astronomical Catalogue*, 1, Astronomical Data Center, NASA 1990.

Received on 26 November, 1995

II. Modélisation de la population de petits corps à partir des observations.

II.1. Etudes statistiques, taxonomies.

II.2. Modélisation des spectres des objets sans atmosphère.

II.3. Considérations sur la masse des astéroïdes.

Une analyse des données est incomplète sans une représentation sur la base d'un modèle physique. En fonction de l'approche choisie, les premiers modèles sont issus directement de l'observation. On parle d'un modèle empirique. On observe ainsi (par l'analyse statistique des données par exemple !) que les données obéissent à une ou plusieurs lois, sans que soit atteint le degré d'abstraction et de généralisation (axiomatisation !) d'un modèle physique. Si les données d'observations peuvent être partiellement confirmées par des raisonnement analytiques, alors on obtient la définition d'un modèle semi-empirique. Si l'axiomatisation des données est possible, alors nous parlons d'un modèle analytique, permettant également le caractère prévisionnel de la théorie.

II.1. Etudes statistiques, taxonomies.

Lorsque l'on analyse de nouvelles données et que l'on veut en tirer des conclusions globales sur la population étudiée, on passe forcément par une étape d'analyse statistique. Souvent décriée, cette étape est nécessaire et bien souvent fondamentale pour tout développement ultérieur dans le but d'obtenir un modèle physique crédible. L'analyse statistique nous permet de définir des classes d'équivalence qui caractérisent la similitude existant entre les différents objets. On peut parler par exemple de la classe des objets rouges ou de la classe des objets sphériques. Dans ces cas simples, l'attribut définit l'appartenance de l'objet à la classe.

Pour une classification plus complexe, le résultat est aussi plus complexe, les attributs sont remplacés par des « notions » et des « concepts».

Une analyse « sans a priori » donne lieu à une *classification non-supervisée* et elle joue un rôle très important dans tous les domaines scientifiques. On obtient ainsi ce que l'on appelle dans la littérature une *taxonomie*.

L'étude d'un ensemble d'objets est habituellement faite sur un ensemble de données décrivant une ou plusieurs caractéristiques de la population choisie. Si le nombre d'objets de la population étudiée est suffisamment grand, on peut arriver à distinguer des groupes d'objets dont les caractéristiques sont très proches . Ainsi on peut obtenir un *système taxonomique*.

Par exemple, les types spectraux des étoiles ainsi que leurs classes de luminosité sont des systèmes taxonomiques, il en est de même de la classification en galaxies elliptiques, spirales, spirales barrées et irrégulières. Plus les paramètres entrant dans l'analyse couvrent des aspects physiques de la population d'objets considérés, plus le système taxonomique est intéressant; plus il y a un nombre important d'objets, plus est renforcée notre confiance dans les groupes délimités par le système taxonomique en question.

Sous plusieurs aspects, la taxonomie des astéroïdes a beaucoup de similitudes avec le système de classification spectrale des étoiles. Au fur et à mesure que nos connaissances sur la population astéroïdale se sont affinées, différents systèmes de classification se sont succédés. Traditionnellement, les taxonomies d'astéroïdes se sont basées sur l'analyse de couleurs des objets ; ultérieurement de nouvelles taxonomies ont inclus des variables (couleurs et albédo thermique) couvrant aussi une partie du domaine de l'infrarouge proche.

Pour parler vraiment d'un système taxonomique, il faut effectuer la correspondance entre les caractéristiques de chaque classe et la composition chimique qui permet de le délimiter dans l'échantillon. Concrètement, il faut mettre en correspondance les caractéristiques moyennes des spectres de chaque classe taxonomique et les minéraux les plus probables qui sont à l'origine des signatures dans le spectre (exemple en Tableau 1).

Deux directions principales sont abordées :

i) des études directes par comparaison avec des résultats obtenus sur d'autres corps du système solaire ;
ii) des études indirectes, par comparaison avec les résultats obtenus en laboratoire sur des échantillons de météorites.

De nos jours, les systèmes taxonomiques se sont affinés et les nombre des classes et sous-classes d'astéroïdes ont augmenté. La diversification a été dictée par la densification des données d'observations sur le domaine spectral du visible, mais aussi par l'utilisation d'observations de l'intervalle spectral dans l'infrarouge proche.

Mes travaux portent sur l'analyse des données obtenues par la spectrophotométrie dans l'intervalle de longueur d'onde de 0,35µm à 2,5µm en combinaison avec l'albédo thermique obtenu par plusieurs programmes d'observations. L'analyse statistique a été faite à l'aide d'un algorithme de classification automatique d'analyse d'un facteur, connu dans la littérature scientifique sous le nom *G-mode*. J'ai pu ainsi montrer des structures fines à l'intérieur des classes taxonomiques « standard », qui sont mises en valeur essentiellement par la présence des nouvelles données, comme le présente l'article publié dans Astronomy & Astrophysics vol 305, 1996.

Une composante importante dans l'évolution d'un système taxonomique est la possibilité de l'étendre à de nouveaux objets (données d'observations obtenues ultérieurement par rapport à la réalisation du système), ou à des objets qui n'ont pas un jeu complet de variables (couleurs ou albédo manquantes).

Tableau 1. Exemple d'un système taxonomique pour les astéroïdes. Les classes taxonomiques sont décrites par une lettre, l'albédo thermique est estimé qualitativement, le spectre moyen de chaque classe est brièvement expliqué et les caractéristiques les plus prononcés/discriminatoires sont mises en évidence. Pour que le système taxonomique soit suffisamment important, une interprétation de la minéralogie de la surface des objets a été faite en termes des divers minéraux existant dans les météorites

Classe	albédo	Spectre	Minéralogie supposée de la surface	Météorites correspondantes
A	modéré grand	très rouge après 0,7 μm ; une bande d'absorption très prononcée avant 0,7 μm et une autre centrée à 1,05 μm	olivine ou olivine+métaux	olivine achondritique ou pallasite
B	modéré petit	le spectre à tendance décroissante vers les longueurs d'onde de l'infrarouge proche	silicates hydratés+carbone (ou substances organiques) - (ou matériaux opaques)	assemblages *CI1*-*CM2* produits soit par altération aqueuse, soit par métamorphisme des matériaux précurseurs de *CI/CM*
C	Petit	une bande d'absorption vers 0,4 μm et un spectre plat du visible à l'infrarouge	silicates hydratés + carbone (ou substances organiques) - (ou matériaux opaques)	assemblages *CI1*-*CM2* produits soit par altération aqueuse, soit par métamorphisme des matériaux précurseurs de *CI/CM*
D	très petit	un spectre sans bande d'absorption prononcée ; les valeurs de la réflectance spectrale augmentent rapidement et régulièrement vers l'infrarouge	carbone ou silicates riches en matériaux organiques (?)	poussières organiques (?) ou météorites CI1-CM2 et matériaux organique (?)
E	très grand	spectre monotone avec une tendance à l'augmentation de la réflectance spectrale vers l'infrarouge	enstatite ; d'autres silicates avec atomes de fer sont aussi possibles	enstatite achondritique
G	Petit	une bande d'absorption centrée vers 0,4 μm, plus prononcée que celle de la classe C; le reste du spectre est plat	silicates hydratés+carbone (ou substances organiques) - (ou matériaux opaques)	assemblages *CI1*-*CM2* produits soit par altération aqueuse, soit par métamorphisme des matériaux précurseurs de *CI/CM*
M	modéré	Un spectre monotone où la réflectance spectrale augmente très peu vers l'infrarouge	métaux (trace possible de silicates) ou métaux + enstatite	ferreux (avec des inclusions possible de silicates); enstatite chondritique(?)
S	modéré	une bande d'absorption avant 0,7 μm et une bande d'absorption modérée ou petite après 0,7 μm	métaux + olivine + pyroxène	pallasites dominés par des roches riches en pyroxène ou olivine et CV/CO chondrules
V	modéré grand	une forte bande d'absorption avant 0,7 μm et une autre bande d'absorption forte centrée sur 0,95 μm	pyroxène ± feldspath	basalte achondritique

Il est également important de noter que cette opération reste toujours dans le domaine du raisonnable tant que les résultats d'une telle classification « a posteriori » ne présentent pas trop « d'exceptions » (objets qui, par la procédure de classement, ne peuvent pas former une classe parmi les classes existantes). Dans ce cas, une nouvelle refonte du système taxonomique s'impose.

Une partie des mes travaux de recherche porte également sur l'analyse des paramètres physiques des astéroïdes ayant un jeu incomplet de variables. Pour cette analyse, une mise en œuvre d'un logiciel de décision a été réalisée, à partir d'un algorithme basé sur les travaux théoriques de A. I. Gavrishin, en extension de la méthode du paramètre G (*G-mode method*). L'extension de la méthode G-mode permet l'évaluation de la probabilité qu'un objet avec un nouveau jeu de données appartienne à une classe. Même si dans certains cas, l'analyse laisse une ambiguïté dans cette estimation (par exemple l'objet est estimé avec des probabilités voisines pour deux classes) elle offre un point de départ pour des investigations plus poussées de l'objet (à voir les articles d'Icarus vol. 124, 1996 et Icarus vol 146, 2000).

L'autre volet des activités scientifiques visant également les objets sans atmosphère du système solaire a été la réalisation des premières classifications pour les objets trans-neptuniens. L'expérience d'analyse statistique sur les astéroïdes nous ont permis l'adaptation des outils pour l'analyse des couleurs de ces objets par deux méthodes : la méthode du paramètre G (G-mode) et la méthode des composantes principaux (PCA method). L'analyse effectuée sur des collectifs statistiques des objets type Centaures avec des objets trans-neptuniens nous a révélé la structure bien distincte de quelques classes. Par conséquent, un système taxonomique simple a été mis en place (à voir les articles A&A vol 371, 2001 et EMP vol 92, 2003)

La réalisation d'un système taxonomique fait partie de l'approche générale de modélisation avec un fort degré d'empirisme. Nous sommes encore loin d'un modèle physique/analytique permettant l'explication d'une manière générale des différentes populations d'objets existant parmi les astéroïdes ou les objets trans-neptuniens. Une autre approche nous permettant des études plus poussées sur le sujet est l'analyse spectrale de ces objets en vue d'avoir plus d'informations sur les processus physiques permettant de résoudre la minéralogie de ces objets (et dans les cas des objets trans-neptuniens la composition et le circuit des glaces).

Références :

Birlan M., Barucci M.A., Fulchignoni M. - *G-mode analysis of reflection spectra for 84 asteroids* **Astronomy and Astrophysics** vol **305** n. **2**, 984-988, 1996.
Birlan M., Fulchignoni M., Barucci M.A. - *Effects of IRAS albedo corrections on Barucci's asteroid taxonomy*, **Icarus**, **124**, 352-354, 1996.
Fulchignoni M., **Birlan M.**, Barucci M.A. - *The extension of the G-mode asteroid taxonomy* **Icarus**, n. **146**, 204-212, 2000.
Birlan M. - *On the physical and dynamics properties of asteroids*, **Romanian Astronomical Journal** vol. **3**, n. **2**, 123-126, 1993.
Barucci M.A., Fulchignoni, M., **Birlan M.**, Doressoundiram A., Romon J., Boehnhardt H, - *Analysis of Trans-Neptunian and Centaur colours: continuous trend or grouping?*, **Astronomy and Astrophysics**, n **371**, 1150-1154, 2001.
Fulchignoni, M, Delsanti, A., Barucci, M.A., **Birlan, M.** - *Toward a Taxonomy of the Edgeworth-Kuiper Objects: A Multivariate Approach* - **Earth, Moon, and Planets**, vol. **92**:1-4, 2003.

Astron. Astrophys. 305, 984–988 (1996)

ASTRONOMY AND ASTROPHYSICS

G-mode analysis of the reflection spectra of 84 asteroids

M. Birlan[1], M.A. Barucci[2], and M. Fulchignoni[3]

[1] Astronomical Institute of the Romanian Academy str Cutitul de Argint – 5, Bucharest 28, Romania, visiting astronomer at the Observatoire de Paris, F-92195 Meudon Cedex, France
[2] Observatoire de Paris, F-92195 Meudon Cedex, France
[3] Université Paris VII and Observatoire de Paris F-92195 Meudon Cedex, France

Received 12 January 1995 / Accepted 11 May 1995

Abstract. A revised version of the G–mode multivariate statistics (Coradini et al. 1977) has been used to analyse a sample of 84 asteroids. This sample of asteroids is described by 29 variables, namely 23 colours between 0.9 and 2.35 microns obtained from the data base collected by Bell et al. (Private communication), 5 colors between 0.3 and 0.85 microns from the ECAS survey (Zellner et al. 1985) and the revised IRAS albedo (Tedesco et al. 1992).

The G–mode method allows the user to obtain an automatic classification of the asteroids in spectrally homogeneous groups.

The role of the IR colours in separating the various groups is outlined, particularly with regard to the fine subdivision of S and C taxonomical types.

Key words: asteroids

1. Introduction

The knowledge of the chemical composition of asteroids can help in understanding the origin and the evolution of this population. Recently, several classifications obtained by means of statistical analysis of the ECAS + IRAS data (Tholen 1984; Barucci et al. 1987; Tedesco et al. 1989) concerning the chemico–physical parameters of the asteroids have been used to find the distribution of the taxonomical classes with heliocentric distance, to calculate the homogeneity level of the asteroids families, and to compare it with the results obtained from the analysis of meteorite spectra.

Bell et al. (1988) put together a data-base consisting in spectrophotometrical IR observations (in the range 0.90–2.50 microns) for 119 asteroids. This new data-base allows the extension of the statistical investigations in the IR region. Howell et al. (1994) studied the taxonomy obtained applying the neural network clustering technique to this sample.

Send offprint requests to: M.A. Barucci

The aim of this paper is to define asteroid groupings using the spectral region between 0.30–2.50 microns and to study possible links of these groups with already known taxonomical types by means of the automatic multivariate statistical method G–mode (Coradini et al. 1977) to a sample containing 84 asteroids.

2. The method used

The G–mode is a multivariate statistical clustering method already used in planetological (Barucci et al. 1987), geological (Poscoleri 1980) and astronomical problems (Giovanelli et al. 1981). This method allows the user to obtain an automatic classification of a statistical sample consisting in N elements with M variables. The taxonomical units are obtained with no a priori criteria, and looking for the 'true' number of degrees of freedom characterizing the groupings. A detailed description of this method in a planetological framework is given by Barucci et al. (1987). In this paper we point out only some aspects of the G–mode which are used in the description of the results.

The belonging of an asteroid to a given unit is based on the statistical inference rules. In the decision process the only user choice is for the confidence level Q1. The confidence level is the measure of the statistical decision. The larger the confidence level the less detailed the classification is.

The method also determines the linking between different groups. The parameter, named G, is the analog of the distance but in a N x M space. The bigger the G value between two groups the less similar the characteristics of these groups are. The results of the analysis of this generalized distance are displayed in a dendrogram (or tree diagram).

G–mode provides also the 'true' number of the degrees of freedom (DOF) for each group, which is the number of the variables which are sufficient to differentiate a group from the others.

3. Data-base

A homogeneous available data-set of 29 variables for each asteroid was used: 28 spectral reflectance values and the revised

Table 1. Variables used for each asteroid

Variable (filter)	wavelength (microns)	Origin	Variable (filter)	wavelenght (microns)	Origin
s	0.3370	ECAS	18	1.2476	ATLAS
u	0.3590	ECAS	20	1.2976	ATLAS
b	0.4370	ECAS	29	1.5240	ATLAS
v	0.5500	ECAS	30	1.5490	ATLAS
w	0.7010	ECAS	31	1.5747	ATLAS
x	0.8530	ECAS	34	1.5520	ATLAS
4	0.9021	ATLAS	35	1.6130	ATLAS
6	0.9510	ATLAS	42	2.0260	ATLAS
7	0.9755	ATLAS	43	2.0830	ATLAS
8	1.0001	ATLAS	44	2.1400	ATLAS
9	1.0247	ATLAS	45	2.1950	ATLAS
11	1.0740	ATLAS	46	2.2500	ATLAS
13	1.1234	ATLAS	47	2.3050	ATLAS
14	1.1482	ATLAS	48	2.3590	ATLAS
15	1.1730	ATLAS	albedo		IRAS

IRAS albedo. These variables cover the spectral intervals between 0.30–1.35;1.50–1.60 and 2.00–2.35 microns. The records from the 1.35–1.50 microns and 1.60–2.00 microns intervals are influenced by the atmospheric water bands and were excluded. We were also constrained to exclude the records from the interval 2.35–2.50 microns which are at the edge of the detector sensitivity (Burbine 1991). Final sample consists of 84 asteroids. The variables are listed in Table 1.

4. Results

The G-mode decides the appurtenance of an object to a class (a small group of asteroids having very close spectra, i.e. the values of their variables are very similar) on the basis of a statistical test. If the value of the G variable describing the asteroid is lower than a chosen value Q1 (confidence level) the hypothesis of appurtenance of the asteroid to the examined class cannot be rejected. The number of different groups of asteroids obtained varying the confidence level Q1 is given in Fig. 1. In this paper we choose the critical value Q1=2.28: at this confidence level two asteroids out of 84 would be misassigned to a given taxonomic class due to the random fluctuations. Table 2 contains the characteristics of the 13 groups obtained with this Q1 and Fig. 2 shows the mean spectral profile for these groups.

We can compare also the mean spectral profile of these groups with the different profiles obtained for the more common taxonomical types (Barucci et al. 1987). In this case, we can observe the typical mean spectral reflectance profile of C0 type asteroids in the groups 3,4; the S0 type profile in the groups 1, 2, 5, 6, 7 (Fig. 3); the A0 type profile in the group 11; an EM intermediate profile in the group 9 and D0 profile to the group 10.

The spectral interval used reveals the parts of the reflected spectrum which are affected on second order from the heat radiated from the warm surface. The absorption features are produced by vibrational, crystal field, and charge transfer mechanisms. In this spectral region mineralogy is the primary first-order determinant of spectral properties (Gaffey et al. 1989).

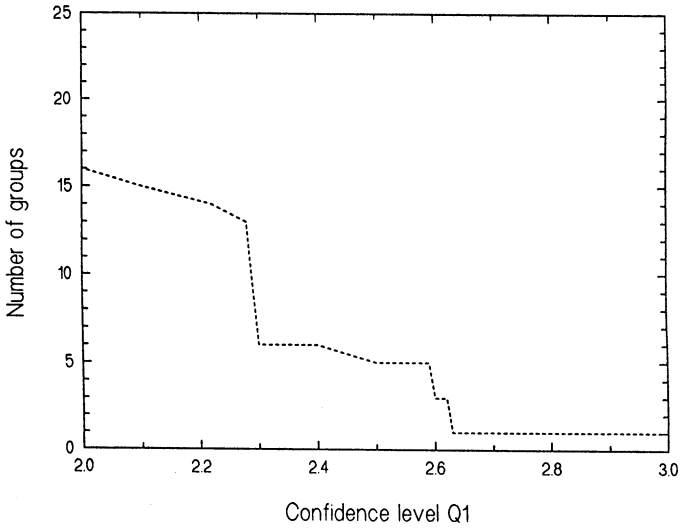

Fig. 1. Variation of the groups with the confidence level Q1

Interpreting the mean spectral profile for each group, the S asteroids belong to the most heterogeneous controversial asteroid taxonomic type. On our S type groups we find different absorption features. All S asteroids present the same strong absorption feature in UV region but different values for spectral reflectance in the IR wavelength interval. Asteroids of the group 6 present two absorption bands centered at 1.0 and 1.25 microns respectively. These two absorption features correspond to a surface plagioclase-pyroxene abundance (McFadden et al. 1978). Other S type-like groups are different due to the depth of the absorption band around 1.0 microns. For instance, this band has a good representation in groups 1, 2, 5, 7 then a small depth is present in group 6. If we consider that these bodies are the result of the initial accretion process, we can imagine the sce-

Table 2. Principal characteristics for the groups at Q1=2.28

GROUP	NUMBER	DOF	ALBEDO	ASTEROID NUMBER
1	4	2	0.228 ± 0.027	5; 6; 57; 82
2	13	5	0.183 ± 0.087	7; 11; 26; 27; 32; 33; 101; 103; 116; 258; 389; 532; 1036
3	7	3	0.072 ± 0.023	1; 10; 106; 431; 554; 704; 762
4	10	3	0.055 ± 0.010	46; 59; 86; 130; 145; 241; 379; 511; 521; 702;
5	11	3	0.206 ± 0.099	9; 12; 18; 25; 63; 80; 89; 352; 376; 639; 714;
6	9	4	0.158 ± 0.100	19; 22; 43; 65; 115; 135; 346; 476; 653
7	5	3	0.205 ± 0.113	15; 39; 113; 364; 1627
8	7	2	0.139 ± 0.068	16; 29; 92; 114; 153; 233; 387
9	6	3	0.328 ± 0.182	21; 44; 64; 69; 221; 317
10	3	2	0.044 ± 0.010	308; 336; 368
11	3	2	0.201 ± 0.032	246; 354; 446
12	3	2	0.321 ± 0.143	2; 4; 349
13	3	2	0.344 ± 0.222	849; 863; 980

nario for these bodies with partial melting of the elements in the specific conditions of temperature and pressure, so, different concentrations of minerals (like olivine and pyroxene) could be the evidence of differentiation of the S type asteroids. For the pyroxene specific absorption band around 2.0 microns we can analyze only the increasing branch. We can conclude only the probable existence of this band for groups 1, 2, 6.

The flat spectra of the groups 3, 4 are representative of the C type asteroids, and their separation is due to the albedo and IR region between 1.0-2.4 microns. The profile of the spectrum is conferred to a surface rich in carbon and hydrated silicates (Gaffey et al. 1989). Some objects in each group – 1,10,704 in group 3 and 130,511 in group 4 – have hydrated surfaces whereas the asteroid 554 is anhydrous (Jones et al. 1990). These data alone show that surface hydratation is not the primary distinguishing characteristic of these two groups. The extension of the wavelength interval until 3.00 microns will allow us to investigate the presence of hydrated silicates as possible separation criterion of these two groups of C asteroids.

The almost linear spectra corresponding to D type asteroids and attributed to carbon or carbon-rich silicates is the spectral profile of the group 10. The asteroid 308 Polyxo is classified as D3 and the asteroid 368 Haidea as D2 in Barucci's taxonomy.

Group 8 is not easy to characterize in terms of spectral profile. The composition of this group is heterogeneous. Group 8 contains the asteroids already classified as M, S and D. The mean albedo is high in comparison with the D type asteroids and close to those characteristic of the S-type.

Group 11, with the deep absorption band around 1.0 microns caused by high olivine or olivine-metal concentration on the asteroid surface (Gaffey et al. 1989) is representative for the A type asteroids. We can observe also on group 12 the absorption bands around 1.0 and 2.0 microns probably due to the surface rich in pyroxene and feldspar associated with V type asteroids.

The mean spectral profile of group 9 is very flat. Generally a flat spectrum similar to that of group 9 is conferred by iron-poor silicates such as enstatite and forsterite (Gaffey et al. 1989). The asteroid 221 Eos is also included in this group because of its spectral reflectance profile in the IR region. The high variance of the albedo shows the degeneration of the group 9 in this variable.

Group 13 is not representative for our classification. From the Fig. 2 we can observe the great variance of the variables. This three asteroids contained in group 13 are very different from each other. In the region 0.30–1.30 microns the spectral profile corresponds to the A0 type for the asteroid 863 Benkoela the its spectral reflectance has an abrupt increasing in the IR region at a value 2.5 times greater than the value in the visible. The abnormal growth in IR region is very different from that of the other asteroids contained in the sample, moreover the IRAS albedo of this object is also very high. In this group we find also the asteroid 980 Anacostia classified by Burbine (1992) as a possible fragment of the breakup of a spinel parent body.

Summarizing, we can read together the data contained in Table 2 and Fig. 2. Groups 3 and 4 are characterized by a small albedo and flat spectra, which allows us to classify them as C type asteroids groups. Then, with its low albedo but its different spectral reflectance we found the group 10 to be D type asteroids. Group 11 contains the A-like type asteroids and the groups 9 and 12 contain E,M-like and V-like asteroids. The albedo variation for the groups 9 and 12 could be interpreted as a degeneration of these groups in this variable. Groups 1, 2, 5, 6, 7 have a S-like spectral reflectance profile. Between D type asteroids and the other groups of S-type asteroids lies the group 8 which has the spectra closer to D type asteroid profiles.

The generalized distance G between the groups is plotted in Fig. 4. The stronger correlations are among group 1 and 6, 5 - 7 - 11, 2 and 8, 3 and 4; while the groups 9, 10, 12 are far away from the others.

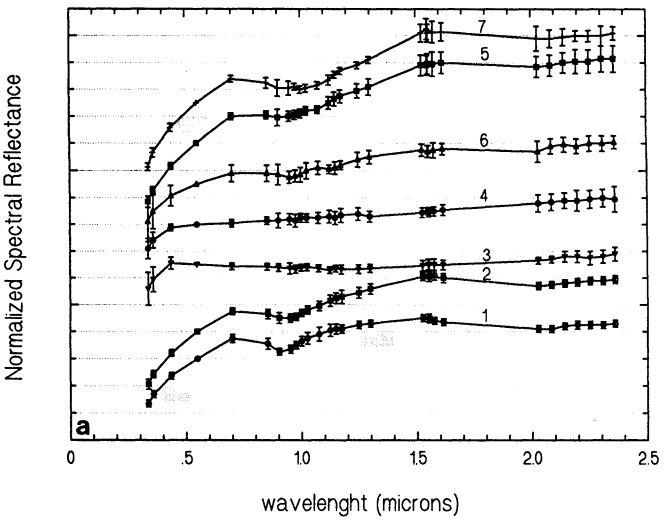

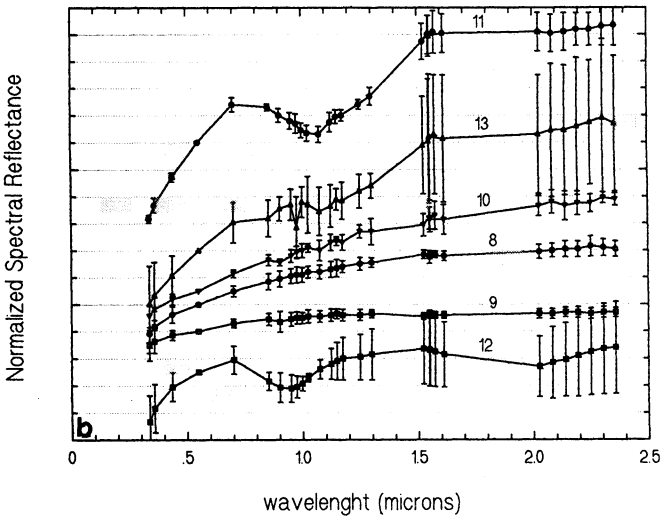

Fig. 2a and b. The mean normalized spectral reflectance spectra of the 13 groups. The spectra are normalized to 1.0 at V- filter ECAS. With error bars we represented the variance of the group in each variable. The spectra are offset for clarity

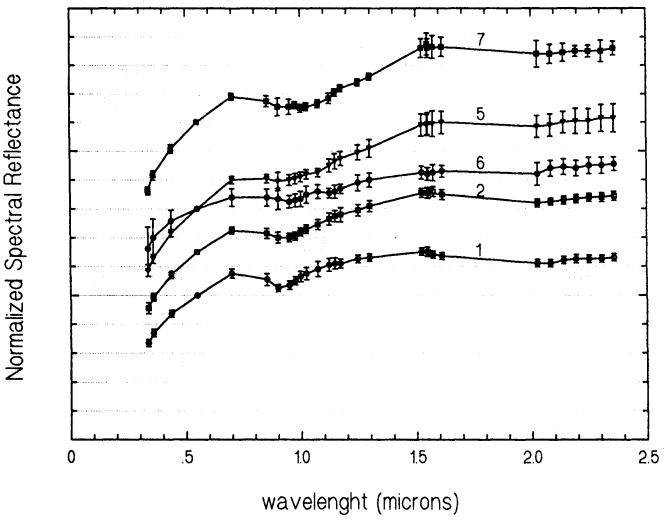

Fig. 3. The groups of the S-type asteroids are presented. The spectra are normalized to 1.0 at V-filter ECAS and the spectra are offset for clarity

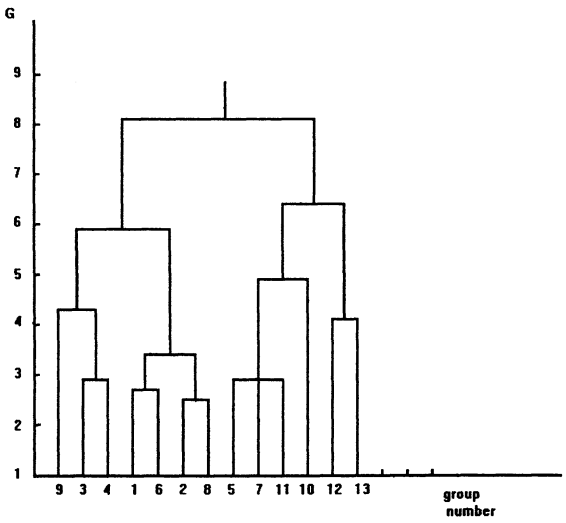

Fig. 4. The dendrogram, or tree diagram, for the confidence level Q1=2.28 present the generalized distance G between the groups

5. Conclusions

In recent years several authors used the 0.3–2.5 microns interval for statistical studies (Burbine 1991; Clark 1993; Gaffey et al. 1993; Howell et al. 1994).

Gaffey et al. (1993) present the results obtained for 39 S type asteroids observed in 52-Color Asteroid Survey. This is a mineralogical study based on the comparison of the absorption bands in the asteroid reflection spectrum with meteorite spectra. The subjects of the analysis are the absorption bands around 1.00 and 2.00 microns. The authors found seven S subclasses.

Howell et al. (1994) used an artificial neural network to define clusters based on the similarity of some spectra. This analysis reveals the presence of various groups of S-type asteroids with different olivine–pyroxene content, some differentiation between the C type asteroids and proves the consistency of almost all taxonomical types represented in the sample.

The results obtained with IR data are encouraging for continuing the observations in this region. The small number of asteroids with available data in this region increases the uncertainty because the new groups are composed of a small number of samples. If we analyze the 'true' number of degree of freedom for each group (Table 2), we can observe that only 2, 3, 4 or 5 variables are important for differentiating these groups and for this reason a convenient choice for the variables can be selected to obtain similar classification without all the details of the spectra. Using the Principal Component Analysis, Burbine (1991) got a similar result, finding five significant principal components that contain nearly all the variance in his sample. However, he did not include the albedo in his analysis.

However, this paper shows the consistency of almost all known taxonomical types and proves the possibility of finding fine structures for S and C type asteroids. It is interesting to investigate if there is a link between these groups and the asteroid families.

It is clear that increasing the number of variables describing the sample, will increase the information carried by each element of the sample and consequently its analysis will put in evidence finer details on the nature of the sample. Our results are in a reasonable agreement with those of Gaffey et al. (1993) and of Howell et al. (1994), confirming the fact that using different techniques of analysis on the same data base (i.e. analysing with different-but equivalent- methods the same information) gives similar results.

The advantage of the G-mode, in our opinion, lies in the possibility to indicate the number of degrees of freedom (i.e. independent variables) describing each group. The maximum DOF number in the present analysis is five: it means that with the choice of 5 selected variables (filters or a combination of filters) it is possible to obtain the described results.

Fulchignoni et al. (1995) pointed out that the current asteroid taxonomy can be obtained describing each asteroid by means of three variables (u - v, v - x and albedo): our result indicates that it is possible to find a finer taxonomical structure when two more IR variables are added, but to individuate these new variables a larger complete sample is needed.

Acknowledgements. We thank to Dr J. F. Bell for '52-Color Asteroid Survey' data-base and Dr E. S. Howell for helpful suggestions. The work made by Mirel Birlan was supported by the European Southern Observatory *CEE Programme* and the European Space Agency.

References

Barucci M.A., Fulchignoni M., 1990, Adv. Space Res., vol 10,n. 3-4,141

Barucci M.A., Capria M.T., Coradini A., Fulchignoni M., 1987, Icarus 72, 304

Bell J.F., Hawke B.R., Owensby P.D., Gaffey M.J., Atlas of the asteroid infrared reflection spectra(0.8–2.5 microns)

Bell J.F., Hawke B.R., Owensby P.D., Gaffey M.J., 1988, Lunar Planet. Sci., XIX, 57

Burbine T.H., 1991, Principal component analysis of asteroid and meteorite spectra from 0.3 to 2.5 microns, Master thesis, Univ. of Pittsburgh

Burbine T.H., Gaffey M., Bell J.F., 1971, Meteoritics 27, 424

Chapman R.C., 1990, in The New Solar System-third edition, eds Beatty J.K., O'Leary B. and Chaikin A., Cambridge Univ. Press,p. 97

Chapman R.C., McCord T.B., Johnson T.V., 1973, Astron. J., 78, 126

Clark B.E., 1993, Spectral reflectance studies and optical surface alteration in the search for links between meteorites and asteroids, Doctoral thesis, Univ. of Hawaii

Coradini M., Fulchignoni M., Fanucci O., Gavrishin A.I., 1977, Comput. Geosci. 3, 85

Fulchignoni M., Barucci M.A., Tedesco E.F., 1995, Planet. Sp. Sci.(in press);

Gaffey M.J., Bell J.F., Hamilton Brown R., Burbine T.H., Piatek J.L., et al., 1993, Icarus 61, 573

Gaffey M.J., Bell J.F., Cruikshank D.P., 1989, in Asteroids II eds Binzel R.P., Gehrels T. and Matthews M.S., Univ. of Arizona Press, p. 98

Howell E.S., Mereny E., Lebofsky L.A., 1994, J.G.R. 99, n. E5, 847

Jones T.D., Lebofsky L.A., Lewis J., Marley M.S., 1990, Icarus 88, 172

McFadden L.A., Gaffey M.J., 1978, Meteoritics 13, 556

Russell H.N., 1916, Astrophys. J., XLII, n.3, 173

Tedesco E., Veeder G.J., Fowler J.W., Chillemi J.R., 1992, IRAS Minor Planet Survey-final report, Phillips Laboratory

Tedesco E., Williams J.G., Matson D.L., Veeder G.J., Gradie J.C. et al., 1989, Astronon. J. 97, 580

Tholen D., Barucci M.A., 1989, in Asteroids II eds Binzel R.P., Gehrels T. and Matthews M.S., Univ. of Arizona Press, P. 298

Tholen D., 1984, Asteroid taxonomy from cluster analysis of photometry, Doctoral thesis, Univ. of Arizona

Zellner B., Tholen D., Tedesco E., 1985, Icarus 61, 355

This article was processed by the author using Springer-Verlag LaTeX A&A style file version 3.

ICARUS 124, 352–354 (1996)
ARTICLE NO. 0210

NOTE

Effects of IRAS Albedo Correction on the G-Mode Asteroid Taxonomy

MIREL BIRLAN

Astronomical Institute of the Romanian Academy, Street Cutitul de Argint n. 5, 75212, Bucharest-28, Romania, and Observatoire de Paris, 92195 Meudon Principal Cedex, France

MARCELLO FULCHIGNONI

Observatoire de Paris, 95195 Meudon Principal Cedex, and Universite Paris VII, Paris, France
E-mail: fulchignoni@obspm.fr

AND

MARIA ANTONIETTA BARUCCI

Observatoire de Paris, 95195 Meudon Principal Cedex, France

Received May 15, 1996; revised July 23, 1996

In this short note the differences induced in the taxonomy obtained with the G-mode analysis by the corrected values of the IRAS albedo are presented. The results reveal the consistence of the nine main taxonomic classes.

INTRODUCTION

The final version of the IRAS catalogue (1992) for the minor bodies contains the corrected values of the asteroid albedos. These values sometimes differ significantly from the values contained in the 1986 preliminary version that was used by Barucci *et al.* (1987, hereafter referred as Paper I) to define their taxonomy based on the G-mode statistical method.

An update of the taxonomy has been carried out, taking into account the new albedo values. We will present here the changes in the taxonomy, obtained with the G-mode analysis, due to the corrected albedo values.

METHOD

We refer the readers to Paper I for the details of the method. We outline here that the structure of the method is such that a variation in one of the M variables ($M = 8$; seven spectral reflectances and albedo) describing the statistical sample of asteroids can strongly affect the definition of each independent class. An asteroid is assigned to a taxonomic class if it satisfies an appurtenance test based on the value of the new variable describing it

$$G_j = \sqrt{2 \cdot z_j^2} - \sqrt{2 \cdot f_a - 1},$$

where

$$z_j^2 = K_a \cdot \sum_{i=1}^{M} \left(\frac{x_{ij} - \overline{x_i}}{\sigma_i} \right)^2$$

$$K_a = \frac{M}{\sum_{s,k=1}^{M} r_{sk}^2}$$

and the

$$f_a = M \cdot K_a.$$

If G_j is less than a critical value (which defines the errors in the assignment) the jth asteroid belongs to a given class a, defined by the $\overline{x_i}$ mean values of the variables (spectral reflectances and albedo), their σ_i standard deviations, and the r_{sk} values of the correlation coefficients between the sth and the kth variables.

We rerun the G-mode on the same sample of asteroids with a probability of misassignment of 2.1%.

RESULTS

We obtained the same subdivision of the asteroid sample described in Paper I, in the nine main taxonomic classes and some subclasses. Table I contains the degree of freedom (dof), the average, and the standard deviation for each variable (spectral reflectance R_x normalized to visible, and the albedo) as well as the number of the asteroids from the classes and subclasses.

The main differences with the previous taxonomy are:

—the number of subclasses (less than in Paper I) and the population within the subclasses. The subclasses mark the transitions between the main classes, as shown in Fig. 1.

0019-1035/96 $18.00

TABLE I
Synoptic Map of the Variables Describing Each Class

Classes (No. of samples)	Units and subunits (No. of samples)	dof	R_s (σ)	R_u (σ)	R_b (σ)	R_w (σ)	R_x (σ)	R_p (σ)	R_z (σ)	Albedo (σ)
	B0(7)	3	0.891	0.936	1.020	0.960	0.910	0.876	0.810	0.091
			0.060	0.039	0.036	0.043	0.056	0.062	0.156	0.045
	B1(5)	5	1.020	1.060	1.060	0.999	0.983	0.950	0.892	0.057
B(18)			0.031	0.025	0.025	0.025	0.037	0.025	0.039	0.019
	B2(3)	2	1.040	1.100	1.080	1.060	1.070	1.050	0.959	0.072
			0.052	0.072	0.063	0.032	0.025	0.111	0.136	0.045
	B3(3)	2	0.794	0.874	0.997	0.964	0.951	0.900	0.840	0.074
			0.046	0.029	0.025	0.027	0.025	0.025	0.025	0.030
E(3)	E0(3)	2	0.944	0.965	0.993	1.030	1.030	1.020	1.060	0.520
			0.027	0.025	0.025	0.025	0.025	0.025	0.058	0.026
G(3)	G0(3)	2	0.660	0.750	0.917	0.982	0.988	0.953	0.986	0.121
			0.025	0.039	0.065	0.026	0.025	0.045	0.025	0.037
C(187)	C0(187)	3	0.840	0.897	0.985	1.020	1.030	1.030	1.020	0.051
			0.075	0.058	0.032	0.033	0.044	0.050	0.070	0.012
M(43)	M0(43)	4	0.917	0.945	0.977	1.070	1.110	1.140	1.140	0.151
			0.051	0.034	0.025	0.025	0.033	0.041	0.070	0.064
	D0(18)	4	0.891	0.914	0.941	1.150	1.290	1.370	1.400	0.049
			0.026	0.025	0.025	0.025	0.032	0.055	0.091	0.010
	D1(3)	2	0.852	0.845	0.893	1.160	1.340	1.490	1.430	0.049
			0.216	0.065	0.025	0.074	0.069	0.025	0.074	0.016
D(30)	D2(3)	2	0.847	0.880	0.947	1.100	1.190	1.240	1.290	0.077
			0.031	0.025	0.026	0.025	0.025	0.036	0.070	0.058
	D3(3)	4	0.728	0.781	0.909	1.150	1.260	1.290	1.310	0.068
			0.025	0.025	0.025	0.025	0.025	0.026	0.065	0.026
	DS(3)	6	0.756	0.810	0.913	1.100	1.200	1.210	1.180	0.093
			0.025	0.025	0.025	0.025	0.025	0.025	0.025	0.010
	S0(134)	3	0.611	0.688	0.845	1.160	1.160	1.140	1.170	0.204
			0.055	0.043	0.029	0.032	0.053	0.060	0.082	0.063
	S3(3)	2	0.551	0.613	0.794	1.230	1.310	1.290	1.350	0.195
S(146)			0.025	0.025	0.025	0.029	0.038	0.073	0.041	0.026
	SV(3)	2	0.616	0.698	0.840	1.070	1.060	0.973	1.010	0.250
			0.087	0.085	0.084	0.025	0.051	0.047	0.026	0.021
	SA(3)	2	0.456	0.586	0.781	1.250	1.280	1.210	1.100	0.176
			0.030	0.058	0.046	0.037	0.037	0.039	0.025	0.017
	SD(3)	2	0.658	0.751	0.900	1.000	1.080	1.090	1.060	0.097
			0.072	0.048	0.033	0.025	0.025	0.035	0.041	0.010
V(3)	V0(3)	2	0.608	0.694	0.870	1.130	0.983	0.921	0.995	0.303
			0.152	0.113	0.075	0.055	0.138	0.157	0.025	0.174
A(3)	A0(3)	2	0.425	0.517	0.727	1.290	1.200	1.090	1.000	0.248
			0.054	0.058	0.038	0.056	0.050	0.034	0.077	0.015

—The taxonomic type of 35 asteroids (8% of the total sample) is changed. In Table II these asteroids are listed together with the old and the new designation of taxonomic type.

CONCLUSIONS

The G-mode method has been reapplied to the sample of 438 asteroids described in Paper I where the IRAS albedo-corrected values have been used. The resulting taxonomy produces the general structure of the previous one. Nine main taxonomic classes, with a few subclasses which seem representative of possible transition trails between the different groups, are obtained.

This result can be interpreted in terms of general stability in the classification of the asteroids based on their compositional characters. The asteroid population is clearly divided into nine major taxonomic classes indicated with a letter followed by zero. About 5% of the asteroids belong to subclasses which represent a fine subdivision of the main class (indicated with a major class letter and an integer which increases with the average albedo). Few objects (2.7%) belong to small classes characterized by intermediate behavior between the major classes: these classes are indicated by the two letters referring to those major classes. The intermediate or transition classes could be representative of the compositional evolution of the asteroids from more primitive materials toward the more processed endmembers. It is clear that the evolution history

TABLE II
Asteroids Which Have Changed Their Taxonomic Classification

Asteroid	Old class	New class	Asteroid	Old class	New class
2 Pallas	B3	B0	261 Prymno	B3	B0
25 Phocaea	S2	S0	339 Dorothea	S1	SV
51 Nemausa	S1	SD	354 Eleonora	S2	SA
55 Pandora	E0	M0	451 Patientia	B3	C0
62 Erato	B3	C0	498 Tokio	D3	C0
93 Minerva	B3	C0	512 Taurensis	S2	S0
113 Amalthea	S2	A0	640 Brambilla	G0	C0
114 Kassandra	D3	DS	651 Antikleia	S3	SA
115 Thyra	S1	SV	863 Benkoela	A0	rejected
119 Althaea	S2	S0	914 Palisana	D3	SD
130 Elecktra	G0	C0	937 Bethgea	S2	rejected
131 Vala	S1	SD	996 Hilaritas	C0	B0
142 Polana	B1	C0	1019 Strackea	S2	S3
148 Gallia	S1	G0	1080 Oechis	B1	C0
192 Nausikaa	V0	S1	1284 Latvia	D3	DS
228 Agathe	S2	S0	1604 Tombaugh	D3	SD
233 Asterope	D3	DS	2156 Kate	S2	S0
246 Asporina	A0	SA			

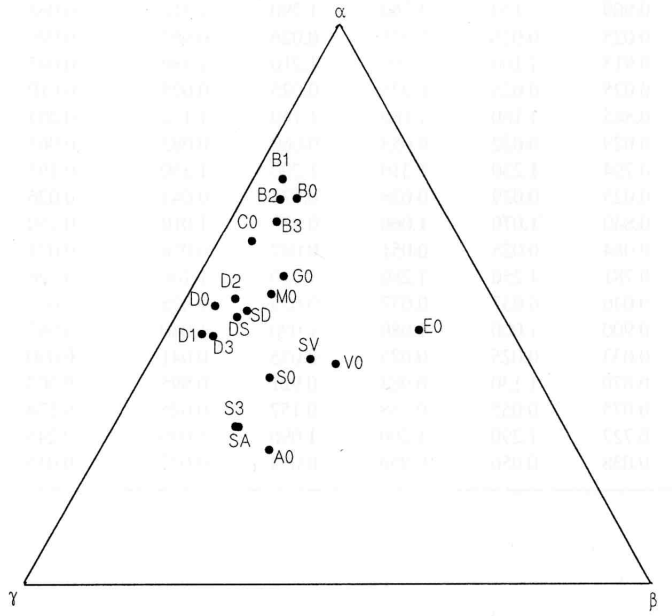

FIG. 1. Ternary diagram where the variables are grouped so that in each point $(R_s + R_u + R_b)/3$ + albedo + $(R_w + R_x + R_p + R_z)/4 = 1$. The corners of the triangular diagram are characterized by the following percent values:

	$(R_s + R_u + R_b)/3$	Albedo	$(R_w + R_x + R_p + R_z)/4$
α	0.60	0.00	0.40
β	0.25	0.35	0.40
γ	0.25	0.00	0.75

(changes in thermal and dynamical environment, differentiation, collisions, etc.) of the planetesimal swarm that was the parent of the asteroid population could explain this behavior of the classes. The problem is to understand which amount of real information can be extracted from the unavoidable noise induced in the classification.

It seems wise to consider the base of the classification while disregarding the subclasses, which may represent a spectral trend which is not completely covered by the adopted set of variables describing the sample. That means the subclasses and the transition classes contain the minority of asteroids having extreme characters, while the statistics smooth the trend, putting together in the major classes those samples having closer spectral characteristics.

REFERENCES

1. Barucci, M. A., M. T. Capria, A. Coradini, and M. Fulchignoni 1987. Classification of asteroids using G-mode analysis. *Icarus* **72,** 304–324.
2. Tedesco, E. F., G. J. Veeder, J. W. Fowler, and J. R. Chillemi 1992. *The IRAS Minor Planet Survey,* Philips Laboratory.

Icarus 146, 204–212 (2000)
doi:10.1006/icar.2000.6381, available online at http://www.idealibrary.com on IDEAL®

The Extension of the G-Mode Asteroid Taxonomy

Marcello Fulchignoni

Observatoire de Paris—DESPA, 5 Place Jules Janssen, 92195 Meudon, France; and Université de Paris 7, UFR de Physique, 2 Place Jussieu, 75005 Paris, France
E-mail: fulchignoni@obspm.fr

and

Mirel Birlan and Maria Antonietta Barucci

Observatoire de Paris—DESPA, 5 Place Jules Janssen, 92195 Meudon, France

Received September 27, 1999; revised February 7, 2000

Barucci *et al.* (1987. *Icarus* 72, 304–324) developed their asteroid taxonomy based on the G-mode statistical method, applied to a sample of 438 asteroids, where each asteroid was described by eight variables (seven ECAS colors and the IRAS albedo). They found that the asteroid population separates into nine major taxonomic classes (C, S, M, D, B, G, E, A, V) and that three of these (S, D, B) can be further subdivided into subclasses. Birlan *et al.* (1996b. *Icarus* 124, 352–354) found that the values of the corrected IRAS albedos do not influence the bulk structure of this taxonomy.

The aim of this paper is to define an algorithm that allows us to extend this classification system to any asteroid for which the ECAS reflectances and the albedos become available through new observations.

The algorithm which allows us to extend the G-mode method is presented, along with a test of the procedure utilizing color and albedo measurements for 465 asteroids. © 2000 Academic Press

Key Words: **asteroids, compositional types; asteroid taxonomy.**

1. INTRODUCTION

Three successive steps are needed to define any taxonomic system, the identification of groupings within a reference population that is supposedly representative of the entire population, the interpretation of each obtained group (or class) in terms of the contained information, and the definition of a method by which new members of the population can be included in the taxonomic system.

In defining the G-mode asteroid taxonomy (Barucci *et al.* 1987), the first step was the identification of the different classes of objects. Using seven broadband colors measured as part of the ECAS asteroid survey (Zellner *et al.* 1985) and the IRAS albedo (Matson 1986), each asteroid was classified based on its proximity to various homogeneous groupings within the sample population. Each of these reference groupings was defined recursively by a test of suitably defined normal distribution. In the analysis of 438 asteroids, this procedure identified nine major compositional classes, three of which were further divided into subclasses. The result confirms the general structure of the main asteroid taxonomies obtained by several techniques: Tholen (1989) used the principal component analysis defining 14 classes of asteroids, and Tedesco *et al.* (1989) found 11 classes in their three-parameter taxonomy. The three-parameter technique is the first which takes into account the errors of each classified asteroid.

In the second step, these results were interpreted in terms of the physical and chemical evolution of the asteroid population (Barucci *et al.* 1987).

A modified version of the G-mode taxonomy (Birlan *et al.* 1996b) takes into account the corrected IRAS albedos (Tedesco 1992), confirming the general structure of this asteroid taxonomy. The same nine major classes were identified, with some of these groupings being subdivided into subclasses, indicating some intermediate (probably transitional) behavior among the measured parameters.

The present paper provides the third step in the development of this taxonomy: in the framework of the G-mode analysis, we define an analytical tool to assign to one of the taxonomic classes (or subclasses), defined in the first step, any other asteroid for which the same set of variables become available. The physical and chemical properties of the class, inferred during the second step of our analysis, will apply to the newly added asteroid. Moreover, even if only a subset of the variables used in the initial development of the taxonomy is available for an asteroid, this method will allow us to give at least a preliminary indication of its compositional characteristics.

In the following section a description of this analytical tool is given. Its application to 465 asteroids described by a subset of the variables used in defining the original G-mode taxonomy is contained in Section 3.

0019-1035/00 $35.00

2. METHOD

We refer the reader to the papers by Coradini *et al.* (1977), Barucci *et al.* (1987), and Gavrishin *et al.* (1992) for more detailed discussions of G-mode statistics and its application to the compositional properties of the asteroid population. Here, a brief summary of the procedure is given.

The G-mode classification technique separates a sample of N_{tot} objects into J homogeneous classes containing N_l objects each ($N_{\text{tot}} = \sum_{l=1}^{J} N_l$). Each object is described by M variables i ($i = 1, \ldots, M$). The initial data are arranged in a $N_{\text{tot}} \times M$ matrix, and the mean value ($\bar{x}_i$) and variance (σ_i) for each variable, as well as the correlation matrix, are computed. Any sample will be represented by one new variable z_j^2,

$$z_j^2 = \sum_{i=1}^{M} z_{ij}^2 = \sum_{i=1}^{M} \frac{(x_{ij} - \bar{x}_i)^2}{\sigma_i^2}, \tag{1}$$

where x_{ij} is the ith variable of the jth sample. When x_{ij} are independent and normally distributed, the new variables follow a χ^2 distribution with M degrees of freedom. If the x_{ij} are not independent, the dependence of the variables is represented by

$$R = \frac{M}{\sum_{k,m=1}^{M} r_{km}}, \tag{2}$$

where r_{km} are the elements of the correlation matrix.

Thus, the distribution becomes

$$z_j^2 = R_l \cdot \sum_{i=1}^{M} z_{ij}^2, \tag{3}$$

which is a χ^2 distribution with $f = N \times M \times R$ degrees of freedom (Bagrov 1978).

Following Abramowitz and Stegun (1972), the distribution (3) can be transformed into a standard normal distribution by the parameter

$$g_j = \sqrt{2 \cdot z_j^2} - \sqrt{2 \cdot f - 1}. \tag{4}$$

The identification of homogeneous classes consists of an iterative procedure based on a test of the hypothesis of appurtenance of the jth sample to a "zero class." The center of the "zero class" is obtained as the sum of the three closest samples (the minimum value of z),

$$z_{p,q,t} = \sum_{i=1}^{3} [(z_{pi} - z_{qi})^2 + (z_{pi} - z_{ti})^2 + (z_{qi} - z_{ti})^2], \tag{5}$$

where z_{pi}, z_{ti}, z_{qi} are the normalized values of the ith variable of the pth, tth, and qth samples, respectively.

When the three samples satisfying the relation (5) are found, the mean value and the variance for each variable are then computed:

$$x_* = \frac{\sum_{j=1}^{3} x_{ij}}{3}; \quad \sigma_* = \left[\frac{\sum_{j=1}^{3} (x_{ij} - x_*)^2}{2} \right]^{1/2}. \tag{6}$$

The values of z_j^2, f, and g are recomputed by substituing the resulting values from (6) into (1), (2), (3), and the value given by (4) is compared with a critical value q_1 selected a priori. Thus, we test the hypothesis of the appurtenance of a given sample described by its g_j value to the class defined by x_* and σ_*.

The N_a samples with $g < q_1$ are considered to belong to the first class a. New values of the mean and the variance are computed for these N_a samples and substituted into the expressions (1) to (4). The procedure is stopped when N_a and R_a are unchanged in two successive cycles. The same procedure is then applied to the remaining $N - N_a$ samples. The grouping part of the method is concluded when the number of samples left is less than three. Thus, the G-mode method defines for each taxonomic class s the mean value x_{is} and the standard deviation σ_{is} (for each variable i in the class s), and a statistical indicator of the variable independence, R_s, which is related both to the variance–covariance matrix of the variable on the s-class and to the number of degrees of freedom of the s-class.

The aim of the present paper is to define an algorithm that allows us to extend this classification to newly observed samples characterized by the variables x_i ($i = 1, \ldots, M$). The parameter

$$g_s = \sqrt{2 \cdot R_s \sum_{i=1}^{M} \left(\frac{x_i - \bar{x}_{is}}{\sigma_{is}} \right)^2} - \sqrt{2 \cdot R_s \cdot M - 1} \tag{7}$$

gives the statistical distance of a new sample, characterized by x_i, from the taxonomic class s. The sample will belong to the class s if $g_s \leq q_2$, where q_2 is a prefixed threshold value, measured in units of variance (e.g., $q_2 = 2$ corresponds to $\pm 2\sigma$ level).

Iterating the procedure for each of the classes, it is possible to assign the new sample to one of the classes which define the taxonomy. If more than one of these g_s values are under the threshold, the new object has intermediate characteristics that are shared between two (or more) classes.

If the new sample is represented by a smaller number of variables ($i = 1, \ldots, M'; M' < M$), then this method gives an estimation of the affinity of the sample to one (or more) of the taxonomic classes. In order to compute g_s, the values of missing data will be replaced by the average value of the variable in each class. Thus for the missing variables the statistical weight will be zero, and only the useful information will contribute to assigning the new sample to one (or more) of the taxonomic classes. Due to the reduced number of variables describing the sample, the number of degrees of freedom will be calculated only for the M' variables that are available for the new sample.

3. TEST OF THE ALGORITHM

We have applied the described algorithm to several sets of data taken from the literature, with the aim of testing how this procedure works in classifying a "new" sample within a given taxonomic scheme.

TABLE I
Mean and Variance Values Used for the Nine Reference Taxonomic Classes

Taxon	R_s σ_s	R_u σ_u	R_b σ_b	R_v σ_v	R_w σ_w	R_x σ_x	R_p σ_p	R_z σ_z	Albedo σ_A
C	0.84301	0.89917	0.98546	1	1.01788	1.03321	1.03145	1.02086	0.0547
	0.08141	0.06423	0.03421	0	0.03593	0.04944	0.05816	0.07938	0.0177
S	0.61321	0.69039	0.84648	1	1.16352	1.16349	1.14695	1.16979	0.1981
	0.06268	0.04943	0.03326	0	0.03950	0.05839	0.06715	0.08646	0.0673
M	0.92846	0.95563	0.98380	1	1.06200	1.10371	1.13594	1.13637	0.1671
	0.05394	0.03575	0.02500	0	0.02500	0.03060	0.04262	0.07186	0.0582
D	0.89106	0.91367	0.94117	1	1.15194	1.28633	1.37211	1.33911	0.0487
	0.02575	0.02500	0.02500	0	0.02500	0.03234	0.05489	0.09094	0.0100
E	0.94400	0.96533	0.99300	1	1.02833	1.03433	1.01733	1.05867	0.5197
	0.02663	0.02500	0.02500	0	0.02500	0.02500	0.02500	0.05785	0.0266
A	0.40433	0.49667	0.71600	1	1.31100	1.23700	1.12500	1.01733	0.2177
	0.02558	0.02500	0.02500	0	0.02500	0.06437	0.08448	0.10175	0.0380
B	0.89633	0.93417	1.02733	1	0.94983	0.90100	0.85933	0.78483	0.0875
	0.06362	0.04258	0.03812	0	0.03732	0.05459	0.04826	0.15515	0.0476
V	0.54975	0.67475	0.87775	1	1.08150	0.85650	0.78100	1.00450	0.4222
	0.02736	0.03474	0.04423	0	0.05086	0.04323	0.03986	0.05000	0.0840
G	0.66000	0.75000	0.91700	1	0.98200	0.98800	0.95300	0.98600	0.1210
	0.02500	0.03950	0.06500	0	0.02560	0.02500	0.04530	0.02500	0.0372

In this section we present and discuss the results of this test, where:

(1) The taxonomic reference scheme is the one defined in Table I, which contains the 9 primary taxonomic classes defined by Barucci *et al.* (1987) using 438 asteroids for which both high-quality ECAS spectral reflectances (Zellner *et al.* 1985) and the new revised IRAS albedo (Tedesco, 1992) were available. The average and the variance values for the ECAS colors and IRAS albedos, as well as the R values, have been obtained for the C, S, M, D, E, A, B, and G classes using the G-mode technique as described in Birlan *et al.* (1996b), with a critical value $q_1 = 2.67$ implying that less than 1% of the analyzed asteroids were misassigned. The V class is defined by the ECAS observed reflectance values for the asteroid 4 Vesta, and the variances are assumed to be of the order of 5% of the average values for homogeneity with the variance of the other classes. The average spectral behavior of the nine reference classes is shown in Fig. 1.

(2) The "new" sample consits of 465 asteroids, 149 of which are extracted from the ECAS database. They do not have the same high quality ranking for all eight of the variables, or some variables are missing. Three hundred and sixteen asteroids are described by a subset of the ECAS colors (mainly the reflectances in the w, x, and p filters R_w, R_x, R_p) extracted from the spectra contained in the SMASS database (Xu *et al.* 1995). When available, the new revised IRAS albedo (Tedesco 1992) was taken into account.

The threshold value was fixed to $q_2 = 2$, implying that less than 5% of the examined asteroids may be misassigned.

The results of our test are reported in Table II, with columns giving: (i) the asteroid number, (ii) available variables, and (iii) obtained classification to one (or more) of the reference taxonomic classes, and (iv) the previous published classifications (Tholen 1989, Xu *et al.* 1995) are listed (if available). For a few asteroids having a g value a larger than 2, the possible class

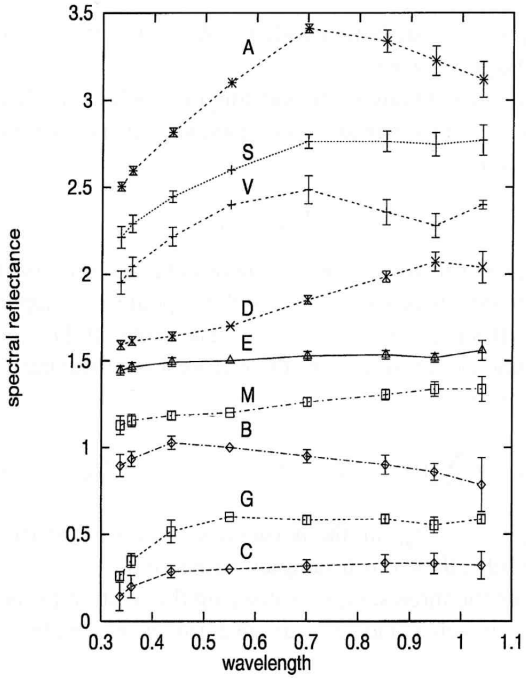

FIG. 1. Mean spectral reflectances and the variance for the nine taxonomic class C, S, D, E, A, V, B, G (wavelengths are in micrometers). The spectra are vertically offset for clarity but preserve a fixed scale and are normalized to 0.55 micrometers.

TABLE II
Results of the Extension of the G-Mode Asteroid Taxonomy

Asteroid	Variables	G-mode estimation	SMASS class	Tholen class
3	*w, x, p, A*	SM	S	S
4	*b, w, x, p, A*	V	V	V
6	*w, x, p, A*	S	S	S
7	*w, x, p, A*	S	S	S
8	*w, x, p, A*	S	S	S
9	*s, u, b, w, x, p, z*	S		S
10	*w, x, p, A*	BGC	C	C
13	*u, b, w, x, A*	GC		G
14	*b, w, x, p*	SC	S	S
14	*s, u, b, w, x, p, z*	S		S
18	*w, x, p, A*	S	S	S
19	*s, u, b, w, x, p, z*	GC		G
22	*b, w, x, p, A*	M	M	M
24	*s, u, b, w, x, p, z*	CB		C
25	*w, x, p, A*	S	S	S
27	*s, u, b, w, x, p, z*	S		S
28	*b, w, x, p, A*	S	S	S
29	*w, x, p, A*	S	S	S
32	*w, x, p, A*	S	S	S
33	*s, u, b, w, x, p, z*	S		S
36	*w, x, p, A*	CG	C	C
38	*w, x, p, A*	CG	C	C
39	*w, x, p, A*	S	S	S
42	*w, x, p, A*	S	S	S
43	*w, x, p, A*	S	S	S
48	*u, b, w, x, p, z, A*	CG		CG
50	*s, u, b, w, x, p, z, A*	C		X
53	*w, x, p, A*	CG	XC	XC
54	*b, w, x, p, A*	CG	C*	C
55	*w, x, p, A*	M	M	M
61	*w, x, A*	S	S	S
64	*s, u, b, w, x, p, z*	MC		E
68	*w, x, p, A*	S	S	S
68	*s, u, b, w, x, p, z, A*	B		S
71	*b, w, x, p, A*	S	S	S
72	*w, x, p, A*	DS	STD*	TDG
73	*w, x, p, A*	S	S	S
82	*w, x, p, A*	SM	S	S
86	*w, x, p, A*	CGB	C	C
88	*w, x, A*	BCG	C	C
99	*s, u, b, w, x, p, z, A*	C		C
111	*w, x, p, A*	CG	C	C
116	*w, x, p, A*	SM	S	S
124	*w, x, p, A*	S	S	S
126	*w, x, A*	S	CX*	S
128	*b, w, x, A*	C	CX*	C
131	*w, x, p, A*	MCS	SU	SU
134	*w, x, p, A*	CGB	C	C
137	*w, x, A*	C	C	C
138	*w, x, p, A*	SM	S	S
149	*w, x, p, A*	S	S	S
152	*s, u, b, w, x, p, z*	D		D
157	*w, x, p*	GCB	C	
158	*b, w, x, p, A*	S	S	S
167	*w, x, p, A*	S	S	S
167	*u, b, w, x, A*	S		S
169	*w, x, p, A*	SA	S	S
181	*u, b, w, x, A*	S		S
184	*u, b, w, x, A*	M		X
185	*w, x, p, A*	CGB	C	C
186	*w, x, p, A*	SM	S	S
189	*u, b, w, x, A*	S		S
190	*s, u, b, w, x, p, z*	CME		P
196	*w, x, p, A*	S	S	S
204	*w, x, p, A*	S	S	S
206	*s, u, b, w, x, p, z*	C		C
208	*u, b, w, x, A*	S		S
210	*u, b, w, x, A*	CB		CF
211	*w, x, A*	CBG	C	C
218	*w, x, p, A*	SM	S	S
221	*w, x, p, A*	SM	S	S
223	*u, b, w, x, A*	CM		X
230	*b, w, x, p, A*	S	S	S
231	*w, x, p, A*	CMS	X	
234	*w, x, p, A*	S	S	S
235	*b, w, x, p, A*	S	S	S
237	*w, x, p, A*	S	S	S
239	*w, x, p, A*	S	ST	
243	*w, x, p, A*	SM	S	S
245	*w, x, p, A*	S	S	S
248	*w, x, p, A*	MCS	X	
256	*w, x, p, A*	MCS	X	
275	*u, b, w, x*	CM		X
287	*w, x, p, A*	S	S	S
289	*w, x, p, A*	AS	A	A
290	*w, x, p*	S	S	
291	*w, x, p, A*	S	S	
292	*w, x, p, A*	S	S	
296	*s, u, b, w, x, p, z*	S		S
297	*w, x, p, A*	S	S	
314	*w, x, p, A*	CG	C	
319	*w, x, A*	MC	X	
339	*w, x, p, A*	SM	S	S
345	*w, x, p, A*	CG	C	C
346	*w, x, p, A*	S	S	S
349	*w, x, p, A*	V	R	R
350	*w, x, p, A*	CM	C	C
354	*w, x, p, A*	SA	S	S
361	*u, b, w, x, A*	D		DP
371	*b, w, x, A*	SV	S*	QSV
374	*b, w, x, p, A*	S	S	S
384	*w, x, p, A*	SM	S	S
402	*w, x, p, A*	S	S	S
416	*b, w, x, p, A*	S	S	S
417	*u, b, w, x, A*	S		X
421	*s, u, b, w, x, p, z*	S		S
430	*w, x, p, A*	GB	C	
433	*s, u, b, w, x, p, z*	S		S
434	*s, u, b, w, x, p, z*	MC		E
441	*w, x, p, A*	SM	M	M
446	*w, x, p, A*	A	A	A
456	*w, x, p, A*	S	S	
462	*u, b, w, x, A*	S		S
467	*w, x, p, A*	SD*	T	
469	*u, b, w, x, A*	CMB		X
470	*w, x, A*	S	S	S
471	*b, w, x, p, A*	S	S	S

TABLE II—*Continued*

TABLE II—*Continued*

Asteroid	Variables	G-mode estimation	SMASS class	Tholen class
474	*b, w, x, p, A*	CM	X	
477	*w, x, p, A*	S	S	S
480	*w, x, p, A*	S	S	S
481	*w, x, p*	CEM	C	C
488	*u, b, w, x, A*	CBG		C
495	*w, x, A*	CGB	C	
497	*u, b, w, x, p, z*	MC		M
505	*s, u, b, w, x, p, z*	ECM		FC
509	*w, x, p, A*	SM	S	S
511	*w, x, p, A*	CG	C	C
512	*w, x, p, A*	SA	S	S
518	*w, x, p, A*	S	S	
519	*w, x, p, A*	MS	S	S
529	*w, x, p, A*	S	S	S
541	*w, x, p, A*	CGB	C	
548	*s, u, b, w, x, p, z*	S		S
550	*w, x, p, A*	SA	S	S
563	*w, x, p, A*	S	S	S
582	*w, x, p, A*	SA	S	S
599	*w, x, A*	S	S	S
622	*s, u, b, w, x, p, z*	S		S
624	*s, u, b, w, x, p, z*	D		D
631	*w, x, p, A*	S	S	S
639	*w, x, p, A*	SM	S	S
650	*s, u, b, w, x, p, z*	—		—
653	*w, x, p, A*	S	S	S
664	*s, u, b, w, x, p, z, A*	C		XC
675	*w, x, p*	S	S	S
675	*s, u, b, w, x, p, z*	S		S
683	*w, x, p, A*	CG	C	
687	*s, u, b, w, x, p, z*	MC		X
695	*u, b, w, x, A*	S		S
699	*s, u, b, w, x, p, z*	S		S
702	*b, w, x, p, A*	CG	C	C
720	*w, x, p, A*	GS*	S	S
722	*w, x, p*	SA	S	
724	*w, x, p*	GCB*	C	
732	*w, x, p, A*	D*	D	
737	*b, w, x, p, A*	S	S	S
752	*w, x, p, A*	CM	X	
761	*s, u, b, w, x, p, z*	CS		SC
768	*s, u, b, w, x, p, z*	CME		X
774	*w, x, p, A*	S	S	
776	*s, u, b, w, x, p, z, A*	C		C
787	*w, x, p, A*	S	S	
788	*w, x, p, A*	GCB	C	
798	*u, b, w, x, A*	M		M
803	*w, x, p, A*	S	TD	
808	*w, x, p, A*	S	S	
811	*w, x, p*	MSC	S	S
813	*w, x, p, A*	SA	S	
821	*s, u, b, w, x, p, z*	C		C
849	*s, u, b, w, x, p, z, A*	M		M
851	*w, x, p, A*	S	S	S
863	*w, x, p, A*	—	A	
864	*s, u, b, w, x, p, z*	S		S
879	*w, x, p*	S	S	
884	*s, u, b, w, x, p, z*	D		D
887	*s, u, b, w, x, p, z*	S		S
900	*w, x, p, A*	S	SD	

TABLE II—*Continued*

Asteroid	Variables	G-mode estimation	SMASS class	Tholen class
901	*s, u, b, w, x, p, z*	S		S
915	*w, x, p*	S	S	
918	*w, x, p, A*	S	S	
951	*w, x, p*	S	S	S
958	*s, u, b, w, x, p, A*	—		—
1012	*u, b, w, x, A*	CB		F
1025	*s, u, b, w, x, p, z*	M		E
1038	*s, u, b, w, x, p, z, A*	—		DTU
1047	*s, u, b, w, x, p, z*	S		S
1061	*s, u, b, w, x, p, z*	C		C
1063	*w, x, p, A*	SM	X	
1071	*w, x, p, A*	SM	X	
1078	*s, u, b, w, x, p, z*	S		S
1084	*w, x, p, A*	GCB	C	
1088	*s, u, b, w, x, p, z*	S		S
1103	*s, u, b, w, x, p, z*	MC		E
1108	*s, u, b, w, x, p, z, A*	CM		CX
1110	*w, x, p*	S	S	
1133	*s, u, b, w, x, p, z*	S		S
1139	*u, b, w, x*	S		S
1143	*w, x, p, A*	D*	D	D
1143	*u, b, w, x, A*	SD*		D
1144	*w, x, p, A*	DS	TD*	D
1144	*s, u, b, w, x, p, z, A*	D		D
1145	*w, x, p, A*	S	TDS	
1148	*u, b, w, x, A*	S		S
1165	*w, x, A*	CM	CX	
1166	*w, x, p, A*	S	S	
1180	*s, u, b, w, x, p, z*	M		P
1185	*s, u, b, w, x, p, z*	S		S
1198	*w, x, p*	S	S	
1215	*s, u, b, w, x, p, z*	S		S
1249	*u, b, w, x, A*	S		S
1251	*s, u, b, w, x, p, z*	CM		E
1257	*w, x, p*	GBC	C	
1264	*w, x, p, A*	CGB	C	
1273	*w, x, p*	V	V	
1279	*w, x, p*	CEG	CX	
1280	*s, u, b, w, x, p, z, A*	C		X
1289	*w, x, p, A*	MS	S	S
1302	*w, x, p*	BG	C	
1307	*s, u, b, w, x, p, z*	S		S
1310	*u, b, w, x*	S		S
1325	*w, x, p, A*	S	S	
1342	*u, b, w, x, A*	M		X
1345	*u, b, w, x, A*	CM		X
1350	*u, b, w, x, A*	S		S
1355	*s, u, b, w, x, p, z*	M		X
1358	*w, x, p, A*	CBG	C	
1375	*w, x, p*	S	S	
1379	*w, x, p*	MSC	S	
1391	*s, u, b, w, x, p, z*	S		S
1393	*w, x, p*	DAS	S	
1422	*s, u, b, w, x, p, z*	S		S
1434	*u, b, w, x, A*	S		S
1442	*u, b, w, x*	S		S
1445	*s, u, b, w, x, p, z*	CME		C
1451	*w, x, p*	S	S	
1453	*s, u, b, w, x, p, z, A*	S		S
1463	*w, x, p, A*	MCS	X	

TABLE II—*Continued*

Asteroid	Variables	G-mode estimation	SMASS class	Tholen class
1471	*w, x, p, A*	SD*	D	
1478	*w, x, p*	A	S	
1480	*w, x, p*	S	S	
1501	*w, x, p, A*	S	S	
1508	*s, u, b, w, x, p, z*	CB		BCF
1518	*w, x, p*	SA	S	
1529	*s, u, b, w, x, p, z*	CM*		P
1534	*w, x, p, A*	CM	C	
1564	*s, u, b, w, x, p, z*	CM		X
1577	*w, x, p*	S	S	
1584	*w, x, p, A*	S	S	S
1601	*s, u, b, w, x, p, z*	S		S
1607	*w, x, p, A*	S	S	
1619	*s, u, b, w, x, p, z*	S		S
1620	*u, b, w, x, A*	S		S
1625	*u, b, w, x*	GC		C
1626	*w, x, p*	S	S	
1627	*s, u, b, w, x, p, z*	S		S
1628	*w, x, p, A*	CMS	X	
1644	*s, u, b, w, x, p, z*	S		S
1646	*w, x, p*	CEM	CX	
1651	*w, x, p*	SA	S	
1653	*w, x, p*	CGEB	C	
1655	*s, u, b, w, x, p, z, A*	C		XFU
1657	*s, u, b, w, x, p, z*	—		S
1658	*w, x, p*	S	S*	AS
1665	*s, u, b, w, x, p, z*	S		S
1679	*w, x, p, A*	MCS	X	
1697	*w, x, p*	SM	TX	
1711	*s, u, b, w, x, p, z*	S		S
1712	*w, x, p, A*	CM	X	
1722	*w, x, p*	S	S	
1725	*w, x, p*	MCS	S	
1740	*u, b, w, x*	C		F
1743	*w, x, p, A*	CGB	C	
1746	*s, u, b, w, x, p, z, A*	D		D
1748	*s, u, b, w, x, p, z*	D		D
1749	*w, x, p, A*	D	D	
1768	*s, u, b, w, x, p, z, A*	BC		F
1772	*w, x, p*	SD	S	
1781	*w, x, p*	SM	XS	
1807	*w, x, p*	S	S	
1842	*s, u, b, w, x, p, z*	S		S
1854	*w, x, p*	S	S	
1862	*s, u, b, w, x, p, z*	V		Q
1863	*s, u, b, w, x, p, z*	C		SU
1865	*s, u, b, w, x, p, z*	S		S
1892	*w, x, p*	D	S	
1902	*u, b, w, x, A*	MC		X
1906	*w, x, p*	SA	V	
1907	*w, x, p*	SC	S	
1915	*s, u, b, w, x, p, z*	S		SMU
1919	*u, b, w, x*	MC		X
1920	*u, b, w, x*	MC		X
1929	*w, x, p*	V	V	
1933	*w, x, p*	S	V	
1934	*w, x, p, A*	S	S	
1943	*s, u, b, w, x, p, z*	S		S
1967	*w, x*	S	S	

TABLE II—*Continued*

Asteroid	Variables	G-mode estimation	SMASS class	Tholen class
1990	*s, u, b, w, x, p, z*	S		S
1995	*w, x, p*	MSC	X	
2001	*s, u, b, w, x, p, z*	MC		X
2010	*s, u, b, w, x, p, z*	B		BU
2011	*w, x, p*	SA*	J	
2014	*w, x, p*	S	S	
2017	*w, x, p*	SA	S	
2024	*w, x, p*	SA	S	
2035	*s, u, b, w, x, p, z*	CM		E
2048	*s, u, b, w, x, p, z*	CM		E
2050	*s, u, b, w, x, p, z*	S		S
2060	*w, x, p*	CEG	B	B
2060	*u, b, w, x*	CBE		B
2070	*b, w, x, p*	S	S	
2074	*b, w, x, p*	S	S	
2078	*w, x, p*	CS	S?	
2083	*s, u, b, w, x, p, z*	MC		X
2091	*w, x, p, A*	MG	CX	
2098	*w, x, p*	SM	TX	
2100	*s, u, b, w, x, p, z*	C		C
2105	*w, x, p, A*	S	S	
2107	*w, x, p, A*	S	S	
2113	*w, x, p*	V	V	
2119	*w, x, p*	S	S	
2128	*w, x, p*	C	X	
2130	*w, x, p*	S	S	
2139	*s, u, b, w, x, p, z*	BC		F
2140	*w, x, p, A*	CM	X	
2143	*w, x, p*	DS	S	
2149	*b, w, x, p*	SD	S	
2159	*w, x, p*	SA	S	
2174	*w, x, p*	A	S	
2204	*w, x, p, A*	MCS	X	
2215	*w, x, p, A*	SM	S	
2223	*s, u, b, w, x, p, z, A*	D*		DU
2253	*b, w, x, p*	S	S	
2259	*w, x, p, A*	CG	C	
2272	*s, u, b, w, x, p, z*	S		S
2278	*u, b, w, x*	BC		FC
2279	*u, b, w, x*	CB		F
2299	*w, x, p*	S	S	
2327	*w, x, p*	A	S	
2363	*u, b, w, x, A*	D		D
2365	*w, x, p*	S	S	
2375	*s, u, b, w, x, p, z*	D		D
2403	*w, x, p*	SMC	S	
2407	*s, u, b, w, x, p, z*	CME		C
2411	*u, b, w, x*	S		S
2420	*w, x, p*	S	S	
2440	*w, x, p*	S	S	
2442	*w, x, p*	V	J	
2444	*w, x, p*	MCS	X	
2449	*s, u, b, w, x, p, z*	CM		E
2491	*s, u, b, w, x, p, z*	CM		X
2501	*u, b, w, x*	A		A
2503	*w, x, p*	CGB	C	
2510	*s, u, b, w, x, p, z*	S		S
2538	*w, x, p*	S	S	
2558	*w, x, p*	SD	S	

TABLE II—*Continued*

Asteroid	Variables	G-mode estimation	SMASS class	Tholen class
2577	u, b, w, x	S		EU
2590	w, x, p	S	V	
2599	w, x, p	S	S	
2645	w, x, p, A	MC	X	
2674	u, b, w, x, A	D		D
2728	w, x, p, A	GCB	C	
2735	u, b, w, x	—		SDU
2744	u, b, w, x	S		S
2760	u, b, w, x, A	MC		X
2775	w, x, p	S	S	
2790	w, x, p	S	S	
2809	u, b, w, x	CBE		BFX
2830	u, b, w, x	S		S
2893	u, b, w, x, A	D		D
2908	w, x, p, A	CG	C	
2920	w, x, p, A	D*	D	
2923	w, x, p	CM	C	
2946	w, x, p	C	CX	
2965	w, x, p	S	S	
2966	w, x, p	S	S	
3102	s, u, b, w, x, p, z	S		QRS
3109	w, x, p, A	SM	X	
3123	u, b, w, x	BC		F
3124	s, u, b, w, x, p, z	CG		CG
3153	w, x, p	V	V	
3155	w, x, p	V	J	
3158	w, x, p	SCM	S	
3167	w, x, p, A	S	S	
3169	u, b, w, x	S		TS
3199	s, u, b, w, x, p, z	S		S
3220	w, x	S	S	
3231	w, x, p	CGEB	C	
3268	w, x, p	S*	V	
3285	w, x, p, A	A	S	
3288	s, u, b, w, x, p, z	S		S
3321	w, x, p	SC	S	
3332	w, x, p	SD	S	
3354	w, x, p	S	S	
3381	w, x, p	CME	X	
3431	w, x, p	GBC	C	
3494	w, x	SV	V	
3501	w, x, p, A	—	D	
3523	w, x, p	SMC	S	
3528	w, x, p	S	S	
3559	w, x, p	CGE	C	
3578	w, x, p, A	M	CX	
3586	w, x, p	SM	S	
3628	w, x, p	V	O	
3657	w, x, p	V	J	
3665	w, x, p	SM*	X	
3674	w, x, p	S	S	
3677	w, x, p	S	S	
3740	w, x, p	CSE	X	
3748	w, x, p	SA	S	
3757	u, b, w, x	SV		S
3759	w, x, p, A	C	C	
3760	w, x, p	SD	S	
3792	w, x, p	SM	S	
3869	w, x, p	V	J	

TABLE II—*Continued*

Asteroid	Variables	G-mode estimation	SMASS class	Tholen class
3915	w, x, p, A	CG	C	
3935	w, x, A	S	S	
3944	w, x, p	SC*	V	
3963	w, x, p	SM	S	
3968	w, x, p	V	V	
3999	w, x, p, A	CGB	C	
4002	w, x, p	SMC	S	
4005	w, x, p	V	J	
4006	w, x, p, A	SM	X	
4015	u, b, w, x, p, z	CEB		CF
4025	w, x, p	SA	S	
4031	w, x, p	MCS	X	
4038	w, x, p	SA	V	
4062	w, x, p	SA	S	
4085	w, x, p	S	S	
4104	w, x, p	S	S	
4145	w, x, p	SA	S	
4147	w, x, p	CV*	V	
4156	w, x, p	CEG	C	
4159	w, x, p, A	S	S	
4165	w, x, p	SM	XS	
4179	w, x, p	SC	S	
4215	w, x, p	V	J	
4219	w, x, p	BGC	C	
4282	w, x, p	CEG	C	
4353	w, x, p	MSC	C	
4370	w, x, p	S	X	
4373	w, x, p	SMC	S	
4376	w, x, p	S	S	
4440	w, x, p	MCSE	X	
4510	w, x, p	S	S	
4546	w, x, p	SC*	V	
4562	w, x, p, A	CBG	C	
4606	w, x, p	S	S	
4635	w, x, p	CEG	C	
4640	w, x, p	AS	S	
4673	w, x, p	S	S	
4688	s, u, b, w, x, p, z	—		
4761	w, x, p	SM	S	
4939	w, x, p	SA	S	
4948	w, x, p	SA	S	
4956	w, x, p	CM	XT	
5065	w, x, p	CEG	C	
5118	w, x, p	S	S	
5143	w, x, p	V	V	
5145	b, w, x, p	—	Z**	Z**
7341	w, x, p	SA	S	
7474	w, x, p	MCS	X	
8176	w, x, p	CE	S	
11066	w, x, p	SMC	S	
1991XB	w, x, p	SMC	SX	
1992NA	w, x, p	GCBE	C	
1992UB	w, x, p	CME	X	

Note. The number of each asteroid, the available variables (spectral reflectances R_s, R_u, R_b, R_w, R_x, R_p, R_z—indicated by subscript only—and the newly revised IRAS albedo A), the obtained classification, as well as the Tholen and SMASS I classifications, are presented. An asteroid classification is omitted (—) if the g_s score is greater than the fixed threshold q_2 ($g_s \gg q_2$) for all nine reference taxonomic classes.

attribution is marked by an asterisk, signifying that the classification has a lower confidence level.

Our results are generally in very good agreement with the classifications given in the cited literature, when the differences between the respective reference classes are take into account (e.g., Tholen and Xu's single-object R class is not included in our taxonomy, nor is Xu's J class; thus, the asteroid 349 Dembowska—considered as the R type representative by Tholen—is a V-type asteroid in the Barucci scheme, and our algorithm identifies the Xu's J-type asteroids as belonging to Barucci's V taxonomic class).

Our sample contains seven asteroids observed in both the ECAS and the SMASS surveys, 14 Irene, 68 Leto, 167 Urda, 675 Ludmilla, 1143 Odysseus, 1144 Oda, and 2060 Chiron. These asteroids are reported twice in Table II. Generally, there is good agreement among the classifications given by Tholen (1989) and Xu *et al.* (1995) and those obtained with the G-mode extension within the limits of the data quality and the number of variables used in calculating the g values given by relation (7).

The algorithm assigns 55% of the asteroids contained in the "new" sample to a single class, while it gives a double class identification for 28% of the objects, and a triple class (or higher) identification for 15% of the objects. For 2% of the objects the g_s scores are far from any reference class.

A multiple-class assignment indicates that the algorithm, on the basis of the available data, is not able to clearly isolate the spectral behavior of the sample into a single class, but that the solution fits (within the fixed confidence level) into two or more reference classes. The lower the number of available variables is, the greather the number of objects for which multiple assignments are determined.

If most of the variables are used, a double class assignement may indicate (e.g., when the g values are very close) that the analyzed asteroid has intermediate spectral characteristics, implying the presence of a transition zone, or continuum between these classes, which would possibly be connected by an evolutive trend in the variable space (see Fig. 3 in Barucci *et al.* 1987). In our test, this is the case for the asteroid 1768 Appenzella, which is described by the entire set of variables (ECAS colors and IRAS albedo) and is classified by our algorithm as both a B- ($g = 1.44$) and a C-type ($g = 1.57$) asteroid, the reflectance characteristics of 1768 Appenzella are closer to those of typical B-type asteroids while its albedo is similar to C-class objects. Tholen (1989) classified this object as an F type; in our reference scheme, Tholen's F class is included in the B class.

Three or more class assignments result when the sample is only partially described by the available variables. While a multiple designation is an indication of appurtenance to the group of possible classes, it is most useful in defining those classes from which an object can be excluded. For example, the asteroid 3231 Mila, for which the g scores indicate an affinity to the C, G, E, and B classes, clearly does not belong to the classes S, M, A, V, or D.

The asteroids 2735 Ellen, 650 Amalashuntha, 863 Benkoela, 958 Asplinda, 1038 Tuckia, 1657 Roemera, 3501 Oleguya, 4688 1980 WF, and 5147 Pholus are not included by our algorithm in any class. For each of these objects, $g > 5$.

Asteroid 863 Benkoela is the main-belt asteroid with the highest value of IRAS albedo (0.595). The reflectances are consistent with the A class over the range 0.3–1 μm. The g scores computed by relation (7) are larger than the threshold values for all of the reference classes. Cellino *et al.* (1999) published preliminary results for a polarimetry program the purpose of which is to investigate the accuracy of diameters and albedos derived from infrared observations for small asteroids. For the asteroid 863 Benkoela they obtain a polarimetric albedo of (0.23 ± 0.04) compared with the IRAS albedo of (0.59 ± 0.07). Using this polarimetric albedo, our method assigns the asteroid to the A taxonomic class ($g = 1.44$). However, its spectral reflectances in the range 1.1–2.5 μm (Bell *et al.* 1988) show a spectral behavior different from that of other A-type asteroids (Birlan *et al.* 1996a).

Asteroid 5147 Pholus, one of the Centaurs (a separate family of cometary-like objects orbiting between Jupiter and Neptune) exhibits the reddest spectrum of any Solar System object over the range 0.3–1.0 μm. Its spectrum does not have any analog within our reference system, so the g score is also very high.

In both cases, the non-assignment of these objects to any class indicates the incompletness of the reference scheme, which is unable to include such extreme cases. Thus, the presence of these objects implies the necessity of enlarging the number of reference classes. It would be necessary to add a very high albedo A or V-like class to include 863 Benkoela and a very steep, red D-like class to include 5145 Pholus. The variables describing each of these two objects can be taken as single object class definitions (as in the case of 4 Vesta).

The other non-classified asteroids have very noisy ECAS data, with the observed values of the variables exhibiting large, peculiar excursions (probably non-real) that are comparable in amplitude to the observational uncertainties. In these cases, due to the poor quality of the data, new classes are not assigned.

4. CONCLUSION

The taxonomic analysis of new objects allows us to change the statistical weighting of the reference taxonomic classes. Thus, a large number of asteroids will be taken into account in the taxonomic system, and it will contribute to a better knowledge of the asteroid population. An improved understanding of the formation and evolution of the asteroids helps us to better constrain our knowledge of solar system formation.

The possibility of extending the G-mode asteroid taxonomy to newly observed asteroids represents the completion of a classification process, in that we can now assign a new object to a class in our previously defined taxonomy. Note that the method we have employed will work regardless of the reference taxonomy. This implies that it can be applied to any taxonomic system, in which the classes are defined by the average and the standard deviation of variables, as well as the R value (obtained by (2),

if the correlation matrix of variables for each class is available, and $R = 1$ if the variables are assumed to be independent).

This method can be also applied to any object that is described by an incomplete set of variables. In this case, the results should not be considered as a firm assignment to a given taxonomic class, but only an indication of the appurtenance of the asteroid to that class (or those classes).

A sample that cannot be assigned to any reference taxonomic class ($g_j \gg q_2$) may suggest that the reference taxonomic scheme is incomplete and that the new sample exhibits characteristics that indicate the necessity of extending of the reference classification scheme.

ACKNOWLEDGMENTS

We are grateful to Dr. E. Tedesco and to Dr. S. J. Bus for the useful suggestions and the careful review of the manuscript.

REFERENCES

Abramovitz, M., and I. A. Stegun 1972. *Handbook of Mathematical Functions.* Dover, New York.

Bagrov, A. A. 1978. Ekvivalentnom chisle nesavisimich dannich. *Tr. Gigronet Nauch. Issl. Zentra* **44**, 3–11.

Barucci, M. A., M. T. Capria, A. Coradini, and M. Fulchignoni 1987. Classification of asteroids using G-mode analysis. *Icarus* **72**, 304–324.

Bell, J. F., P. D. Owensby, B. R. Hawke, and M. J. Gaffey 1988. The 52-color Asteroid Survey: Final results and interpretation. *Lunar Planet. Sci. Conf. Abstr.* **XIX**, 57–58.

Birlan, M., M. A. Barucci, and M. Fulchignoni 1996a. G-mode analysis of the reflection spectra of 84 asteroids. *Astron. Astrophys.* **305**, 984–988.

Birlan, M., M. Fulchignoni, and M. A. Barucci 1996b. Effects of IRAS albedo correction on the G-mode asteroid taxonomy. *Icarus* **124**, 352–354.

Cellino, A., R. G. Hutton, E. F. Tedesco, M. DiMartino, and A. Brunini 1999. Polarimetric observations of small asteroids: Preliminary results. *Icarus* **138**, 129–140.

Coradini, A., M. Fulchignoni, O. Fanucci, and A. I. Gavrishin 1977. A Fortran V program for a new classification technique: The G-mode central method. *Comp. Geosci.* **3**, 85–105.

Gavrishin, A. I., A. Coradini, and P. Ceronni 1992. Multivariate classification methods in planetary sciences. *Earth Moon Planets* **59**, 141–152.

Matson, D. L. 1986. The IRAS Asteroid and Comet Survey. Preprint Version No. 1, JPL D-3698.

Tedesco, E. F. 1992. The IRAS Minor Planet Survey. Phillips Laboratory Technical Report PL-TR-92-2049.

Tedesco, E. F., J. G. Williams, D. L. Matson, G. J. Veeder, J. C. Gradie, and L. A. Lebofsky 1989. A three-parameter asteroid taxonomy. *Astron. J.* **97**, 580–606.

Tholen, D. J. 1989. Asteroid taxonomic calssifications. In Asteroids II (R. P. Binzel, T. Gehrels, and M. S. Matthews, Eds.), pp. 1139–1150. Univ. of Arizona Press, Tucson.

Xu, S., R. P. Binzel, T. H. Burbine, and S. J. Bus 1995. Small main-belt asteroid spectroscopic survey: Initial results. *Icarus* **115**, 1–35.

Zellner, B., E. F. Tedesco, and D. Tholen 1985. The eight color asteroid survey: Results for 598 minor planets. *Icarus* **61**, 355–416.

ON THE PHYSICAL AND DYNAMICAL PROPERTIES OF ASTEROIDS

MIREL BÎRLAN

Astronomical Institute of the Romanian Academy,
str. Cutitul de Argint no. 5, 75212 Bucharest 28, Romania

Abstract. The paper presents an attempt to study the connection between the physical and the dynamical properties of the asteroids. We have studied a sample consisting of 301 asteroids, taking into account eight physical parameters and three dynamical parameters. The method used is the Principal Components Analysis, with which we have searched clusters of asteroids in the histograms obtained in appropriate plans of the parameter space. We have presented also a first comparison with the Tholen taxonomy and with the Hirayama families.

Key words: asteroids: multivariate analysis; principal components method.

1. THE METHOD

The Principal Components Method (PCM) is used for data processing.

1.1. The Principle of the Method

The PCM permit the data-set analysing through the change of the initial parameters, that can be correlated, by new linear independent parameters. These new variables are called principal components (Rao, 1965). The change of coordinates in the measurements space is done so that the new coordinates are ordered decreasingly in relation to the dispersions on the principal components (Vass, 1980).

If the measurements have the same physical nature, the first principal components will contain, generally, most of the information. The sight of histograms, in the plane of the first two principal components, permits the definition of consistent classes, by reducing the number of dimensions and retaining the maximum of information. If the data are physically nonhomogeneous the problem will be more complicated, especially because of the impossibility of a real weighting. Thus, the hierarchy of principal components may not be useful, because some initial parameters will introduce a great but irrelevant dispersion. It is therefore necessary to analyse more principal components, because it is possible that the "weak" histograms (as absolute dispersion) should express better some classes.

1.2. THE PROGRAMS

The programs, written in FORTRAN for the SPADAM system (Vass, 1980), have been translated for an IBM PC 386 with a VGA display

Rom. Astr. J., Vol. 3, No. 2, p. 123–126, Bucharest, 1993

and completed with the interactive graphic procedures. They permit to calculate the principal components, to raise the histograms by any two components, to cut the chosen clusters and to filter the established classes.

2. DESCRIPTION OF THE CLASSIFICATION

2.1. The Data Used

The set of data we have used comes largely from 'Asteroid Photometric Catalogue' (Lagerkvist et al. 1987). Additionally, we have used other physical data concerning 10 asteroids (Barucci et al., 1991). Dynamical elements have been selected from 'Ephemerides of Minor Planets' (Batrakov et al., 1992). First, we have created a sample of 520 asteroids, but, because of exclusion of asteroids whose data were incomplete, the sample has been reduced to 301 asteroids with 11 parameters : spin, amplitude range, absolute magnitude, slope parameter, diameter, U—B, B—V, albedo, inclination, eccentricity and semimajor axis.

2.2. The Method Testing

The method has been tested on a sample of 301 elements, characterized by 8 physical parameters. We succeeded in separating two classes in the plane of the first and second principal components. After that, each class was divided in two subclasses. The average of the parameters are given in Table 1 for all the four classes.

The composition of the classes are given in Table 2, with respect to the Tholen taxonomy, which uses the same statistical method for analysis. We notice that the division of the two initial classes as obtained by means of the principal components 6 and 7 is dominated by the colours and the albedo.

Table 1

Mean values of the parameters for the 4 classes

No	Class	T/10	A	H	G	D/100	U—B	B—V	Albedo
1	1.1	0.38	0.32	9.30	0.25	0.60	0.27	0.69	0.14
2	1.2	0.48	0.29	8.88	0.25	0.70	0.44	0.85	0.17
3	2.1	0.63	0.18	8.23	0.15	1.44	0.34	0.70	0.05
4	2.2	0.51	0.21	7.97	0.13	1.59	0.31	0.71	0.06

Table 2

Compounds of the classes with respect to Tholen taxonomy

No	Class	Total	S	C	M	X	F	P	B	G	T	D	E	V	A	R
1	1.1	42	—	1	20	6	5	1	5	—	1	—	3	—	—	—
2	1.2	138	128	3	2	1	—	—	1	1	—	—	—	—	1	1
3	2.1	71	—	55	—	4	1	8	2	1	—	1	—	—	—	—
4	2.2	43	3	18	1	3	7	2	—	2	2	2	—	—	—	—

2.3 The Classification Using Physical and Dynamical Parameters

During the test described in 2.2, we found out that the spin, amplitude and slope parameter do not have an effective influence on the class definition. Consequently, only five physical parameters were retained and three dynamical parameters were added.

The sample consisting of 301 asteroids was separated in six classes using the histogram for components 3 and 4. The next step was the analysis of the principal components of these classes.

Thus, the classes 2, 3 and 5 permit each a separation in 2 subclasses : 2.1, 2.2, ... The subclass 5.2 permits a separation in 3 subclasses : 5.2.1

Table 3

Mean values of the parameters

No	Class	H	D/100	U—B	B—V	Albedo	i/10	e	a
1	1	7.86	0.93	0.43	0.85	0.19	0.85	0.17	2.39
2	2.1	8.10	0.81	0.44	0.86	0.18	1.13	0.15	2.81
3	2.2	8.05	0.91	0.26	0.71	0.17	0.96	0.17	2.81
4	3.1	8.46	1.23	0.33	0.71	0.07	1.03	0.17	2.62
5	3.2	9.61	0.62	0.46	0.86	0.17	1.03	0.18	2.47
6	4	11.41	0.28	0.39	0.80	0.09	0.65	0.16	2.33
7	5.1	7.97	1.60	0.33	0.70	0.06	1.09	0.15	3.10
8	5.2.1	10.35	0.32	0.42	0.81	0.13	0.63	0.07	2.94
9	5.2.2	9.95	0.62	0.27	0.71	0.05	1.15	0.17	2.96
10	5.2.3	10.33	0.45	0.34	0.67	0.08	0.53	0.20	3.15
11	6	8.26	2.33	0.33	0.73	0.08	0.99	0.16	3.09

5.2.2, 5.2.3. The averages of the initial parameters for all the 11 classes are presented in Table 3. The number and composition of the classes are given in Table 4 with respect to the Tholen taxonomy.

Table 4

The compounds of classes with respect to Tholen taxonomy

No	Class	Total	S	C	M	X	F	P	B	G	T	D	E	V	A	R
1	1	42	37	1	2	1	—	—	—	—	—	—	1	—	—	—
2	2.1	52	49	—	—	—	—	—	—	1	—	—	—	—	1	1
3	2.2	23	1	2	16	3	—	—	—	—	—	—	1	—	—	—
4	3.1	66	1	38	4	5	5	5	—	2	3	1	1	—	—	—
5	3.2	10	9	1	—	—	—	—	—	—	—	—	—	—	—	—
6	4	15	7	1	—	1	2	1	1	—	1	1	—	—	—	—
7	5.1	40	1	27	1	3	1	5	1	1	—	—	—	—	—	—
8	5.2.1	26	24	1	—	1	—	—	—	—	—	—	—	—	—	—
9	5.2.2	3	—	—	1	1	—	1	—	—	—	—	—	—	—	—
10	5.2.3	11	1	3	—	—	2	—	5	—	—	—	—	—	—	—
11	6	13	2	3	—	—	3	2	1	—	—	1	—	1	—	—

3. THE RESULTS

With respect to the Tholen taxonomy we notice the existence of classes which represent well some taxonomical types (e.g. 1, 2.1, 2.2, 3.2, 5.1, 5.2.1 classes). Some classes (e.g. 3.1 or 6) present a large diversity of taxonomical types, which makes the drawing of any conclusion difficult.

We have expected the following separation of the taxonomical types to be not so good because in Tholen taxonomy there are used 7 colour indices and we had at our disposal only 2 colour indices.

The analysis of the mean-values of the initial parameters for all the 11 classes shows interesting and expected things. For example, the classes 1, 2.1, 3.2 and 5.2.1 have almost the same values for colour indices and albedo (these classes are constituted mostly by the same taxonomical type). So, the separation was made exclusively by the other five parameters.

An inclination-semiaxis diagram for the class 5.2.1 shows two clearly separated groups. The identification of asteroids suggests that this class is disputed between the Coronida and Eos families.

Interesting results were obtained from the class 5.2.3, which contains few asteroids but which represent very well the Themis family. The class 4 contains asteroids from the Flora family : in the class 6 there are the Amor asteroids and the Trojans ones.

4. CONCLUSIONS

Obviously, better results can be obtained with a larger sample and using more parameters. In order to obtain more objective results, we intend to use automated clustering algorithms to separate the subclasses.

Acknowledgements. The author is grateful to Dr. Gheorghe Vass for his assistance in using the programs and for many helpful discussions.

REFERENCES

Barucci, M. A., DiMartino, M., Fulchignoni, M.: 'Rotational Properties of Small Asteroids', 1991 (preprint).

Batrakov, Yu. V. et al :, 'Ephemerides of Minor Planets —1992' Sankt Petersburg, 'Nauka', 1991.

Lagerkvist, C. I., Barucci, M. A., Capria, M. T., Fulchignoni, M., Magnusson, P., Zappala V. : 'Asteroid Photometric Catalogue', 1987, Consiglio Nazionale delle Ricercere, Roma, 1988.

Rao, C.R. : 'Linear Statistical Inference and Its Applications'. John Wiley & Sons Inc., New York — London — Sydney, 1965.

Vass, G. : 'Remote Sensing Multispectral Digital Data Processing', Analele I.G.F.C.O.T. Bucharest, 1980 (in Romanian).

Received on 10 January, 1993

A&A 371, 1150–1154 (2001)
DOI: 10.1051/0004-6361:20010501

Astronomy & Astrophysics

Analysis of Trans-Neptunian and Centaur colours: continuous trend or grouping?

M. A. Barucci[1], M. Fulchignoni[1,2], M. Birlan[1], A. Doressoundiram[1], J. Romon[1], and H. Boehnhardt[3]

[1] Observatoire de Paris, DESPA, 5 place Jules Janssen, 92190 Meudon, France
[2] Université de Paris VII, Paris, France
[3] ESO, Alonso de Cordova 3107, Santiago de Chile, Chile

Received 4 July 2000 / Accepted 2 April 2001

Abstract. We report the results of the first statistical analysis of colours ($B-V$, $V-R$, $V-I$, and $V-J$) of the Trans-Neptunian and Centaur populations. Using the same statistical techniques applied to define the current asteroid taxonomy, we find a continuous spread of the objects between neutral colour to very red. Pushing further the analysis, the TNOs may be split into four groups. The differences in colour content are interpreted as a consequence of the TNOs evolution (i.e. collisional history, space weathering, ...)

Key words. trans-Neptunian object – taxonomy – photometry – statistics

1. Introduction

The outer regions of the Solar System have recently been found to be densely populated by Trans Neptunian Objects (TNOs) forming the so-called Edgeworth Kuiper belt. The number of known TNOs is increasing continuously and since 1992 (Jewitt & Luu 1993) more than four hundred TNO discoveries have been reported in IAU circulars (Marsden 2001). The study of these objects has rapidly evolved in the past few years, especially from dynamical and theoretical points of view. Perturbations of TNOs due to the gravitational influence of the outer planets can inject some of these bodies into giant-planet crossing orbits characteristic of the Centaurs (Stern 1996; Duncan et al. 1995; Stern & Campins 1996). The Centaurs seem to be evolved from TNOs; this is further supported by the few physical studies of their surface, which indicate similar surface nature. The studies of physical and chemical properties of TNO population are still limited by the difficulties in observing these faint and elusive objects. Most of the known TNOs have a diameter between 100 km and 1200 km. In this range, up to 10^5 objects are estimated to orbit in a zone between 30 and 50 AU from the Sun (Jewitt 2000). Careful observational and image processing procedures have been used to obtain reliable photometric data of TNOs. This is a very challenging task, and $B-V$, $V-R$, and $V-I$ colours are available for about 40 objects (Luu & Jewitt 1996; Davies et al. 1998; Jewitt & Luu 1998; Tegler & Romanishin 1998; Barucci et al. 1999; Barucci et al. 2000; Tegler & Romanishin 2000; Doressoundiram et al. 2001) and only 22 out of them have $V-J$ colour determined (Davies et al. 1998; Jewitt & Luu 1998; Davies et al. 2000; Boehnhardt et al. 2001).

Back to the sixties, $U-B$ and $B-V$ colours were available for about 40 asteroids and these data represented the only physico-chemical data base concerning the asteroids at that time. Wood & Kuiper (1963), analysing the data set, found that the asteroid population was split in two distinct groups in the $U-B$ vs. $B-V$ plane. One group clustered close the colours of the Sun while the other one clustered around the colours of the Moon. The availability of more detailed data allows us to obtain a much more detailed picture of the asteroid population, which contains several different compositional classes of objects described in a widely accepted taxonomic scheme, obtained by different authors with different multivariate statistical methods (Barucci et al. 1987; Tholen & Barucci 1989; Tedesco et al. 1989). The Wood and Kuiper groups can be considered as the "seeds" of the asteroid C (for carbonaceous), and S (for silicaceous) class respectively.

As far as the Kuiper Belt is concerned, Tegler & Romanishin (1998) using the $B-V$ and $V-R$ colours of 13 objects (9 TNOs and 4 Centaurs) found a subdivision of those objects into two groups, consisting of objects having colours slightly redder than the colour of the Sun (corresponding to the C and D asteroid classes) and the other containing the reddest objects known in Solar System.

2. Statistical analysis

The availability of large telescopes for TNO research has resulted in an increase of the number of observed objects.

Send offprint requests to: M. A. Barucci,
e-mail: antonella.barucci@obspm.fr

Table 1. Colours of the analysed objects: the first 15 are TNOs, the last 7 are Centaurs

Objects	$B-V$	$V-R$	$V-I$	$V-J$	Ref.
Sun	0.67	0.36	0.69	1.08	1,2
1993 SC	1.04 ± 0.17	0.65 ± 0.09	1.39 ± 0.10	2.27 ± 0.08	4, 5, 6, 7
1994 TB	1.03 ± 0.18	0.76 ± 0.15	1.41 ± 0.15	2.54 ± 0.11	3, 4, 5, 6
1995 QY9	0.71 ± 0.20	0.47 ± 0.12	0.87 ± 0.06	2.01 ± 0.13	3, 5, 6
1996 TL66	0.69 ± 0.08	0.31 ± 0.16	0.71 ± 0.16	1.26 ± 0.11	3, 4, 6, 7
1996 TO66	0.67 ± 0.08	0.37 ± 0.08	0.76 ± 0.08	0.86 ± 0.14	3, 4, 6, 7, 8
1996 TP66	1.04 ± 0.19	0.66 ± 0.09	1.23 ± 0.14	2.16 ± 0.07	3, 4, 6, 7
1996 TS66	0.98 ± 0.13	0.60 ± 0.17	1.27 ± 0.17	1.87 ± 0.11	4, 6, 7
1997 CS29	1.07 ± 0.07	0.64 ± 0.04	1.19 ± 0.04	2.06 ± 0.03	4, 6, 9
1997 CQ29	0.99 ± 0.12	0.68 ± 0.06	1.30 ± 0.09	1.84 ± 0.37	6, 9
1998 SN165	0.82 ± 0.08	0.40 ± 0.08	0.84 ± 0.07	2.18 ± 0.12	10, 11
1999 TC36	0.96 ± 0.04	0.70 ± 0.04	1.28 ± 0.08	2.24 ± 0.04	12
1998 TF35	1.02 ± 0.11	0.71 ± 0.06	1.28 ± 0.15	2.30 ± 0.13	12
1998 VG44	0.93 ± 0.05	0.61 ± 0.04	1.38 ± 0.08	2.31 ± 0.08	12
1998 WH24	0.93 ± 0.06	0.59 ± 0.04	1.26 ± 0.06	1.83 ± 0.03	6, 9, 16
1998 XY95	0.93 ± 0.23	0.65 ± 0.14	1.42 ± 0.30	2.35 ± 0.24	12
2060 Chiron	0.70 ± 0.02	0.37 ± 0.03	0.72 ± 0.04	1.20 ± 0.30	13, 14
5145 Pholus	1.27 ± 0.10	0.78 ± 0.03	1.55 ± 0.02	2.59 ± 0.02	13, 14
7066 Nessus	1.09 ± 0.04	0.79 ± 0.04	1.50 ± 0.10	2.29 ± 0.04	13, 14
8405 Asbolus	0.75 ± 0.04	0.44 ± 0.03	0.96 ± 0.03	1.65 ± 0.02	13, 14
10199 Chariklo	0.77 ± 0.05	0.47 ± 0.02	1.01 ± 0.02	1.74 ± 0.02	13, 14
10370 Hylonome	0.70 ± 0.08	0.43 ± 0.10	0.87 ± 0.10	1.31 ± 0.10	4, 5, 13, 15
1998 SG35	0.89 ± 0.11	0.43 ± 0.08	1.02 ± 0.08	1.35 ± 0.19	10, 11

1, Hardorp (1980); 2, Hartmann et al. (1982); 3, Barucci et al. (1999); 4, Tegler & Romanishin (1998); 5, Luu & Jewitt (1996); 6, Davies et al. (2000); 7, Jewitt & Luu (1998); 8, Hainaut et al. (2000); 9, Barucci et al. (2000); 10, Doressoundiram et al. (2001); 11, Doressoundiram (private comunication); 12, Boehnhardt et al. (2001); 13, Davies et al. (1998); 14, Davies (2000); 15, Green et al. (1997); 16, Tegler & Romanishin (2001).

Observations through B, V, R, I, and J filters have been obtained by various authors for several objects, but the complete set is available for 22 objects (15 TNOs and 7 Centaurs). We analysed the sample of the TNO population constituted by these 22 objects described by the four colour variables $B-V$, $V-R$, $V-I$, and $V-J$ with the goal of investigating its structure. The data used are listed in Table 1. When multiple observations of an object were available in the literature, we adopted the average value for the colour and we took for the uncertainty the maximum of either the dispersion of the values or formal error reported. The observation procedure used by most of the observers consist in intercalating consecutive observations through other filters with multiple observations through the same filter to allow interpolation (e.g. $V-B-V-R-V-I-V-J-V$). A luminosity variation due to the rotation would affect in similar way the consecutive observations in the different filters, so the colour determination would not be strongly affected by rotational effect. This method together with the use of the average of multiple observations allow us to reduce the effects of possible luminosity variation. We carried out our analysis using both of the techniques used in obtaining the current asteroid taxonomy (Barucci et al. 1987; Tholen & Barucci 1989): a) the Principal Component Analysis (PCA) (Reyment & Joreskog 1993) and b) the G-mode analysis (Coradini et al. 1977; Fulchignoni et al. 2000). For details on these statistical techniques, the reader is remainded to the quoted literature.

The principal components are the eigenvectors of the variance-covariance matrix of the colours. The principal components are linear combinations of the original variables where the coefficients (eigenvectors) reflect the relative importance of a variable within a principal component. The sum of the eigenvalues of this matrix is equal to its trace, i.e. it accounts for the total variance of the sample. Each eigenvalue reflects the percentage of the total variance contributed by each principal component. In Table 2 the results of this analysis are reported. The first eigenvector accounts for most of the variance of the sample (91.14%), and heavily weights the contribution of $V-J$ (48%). The second eigenvector adds only 7.33% of the total variance and is weighted mainly by both $V-I$ (35%) and $V-J$ (29%). Therefore, we infer that first principal component PC1 and second principal component PC2 measure the degree of reddening of the TNOs' surfaces, which is the main distinctive character of this population members. The last eigenvectors contribute negligibly to the total variance, so the PC1 vs. PC2 plane contains practically all the information on the variance of variables characterising the sample. In Fig. 1 the predominance of PC1 in representing most of the sample variance is reflected: the objects spread all along this axis with scores spanning from 1.2 to 3.3, while the PC2 scores range

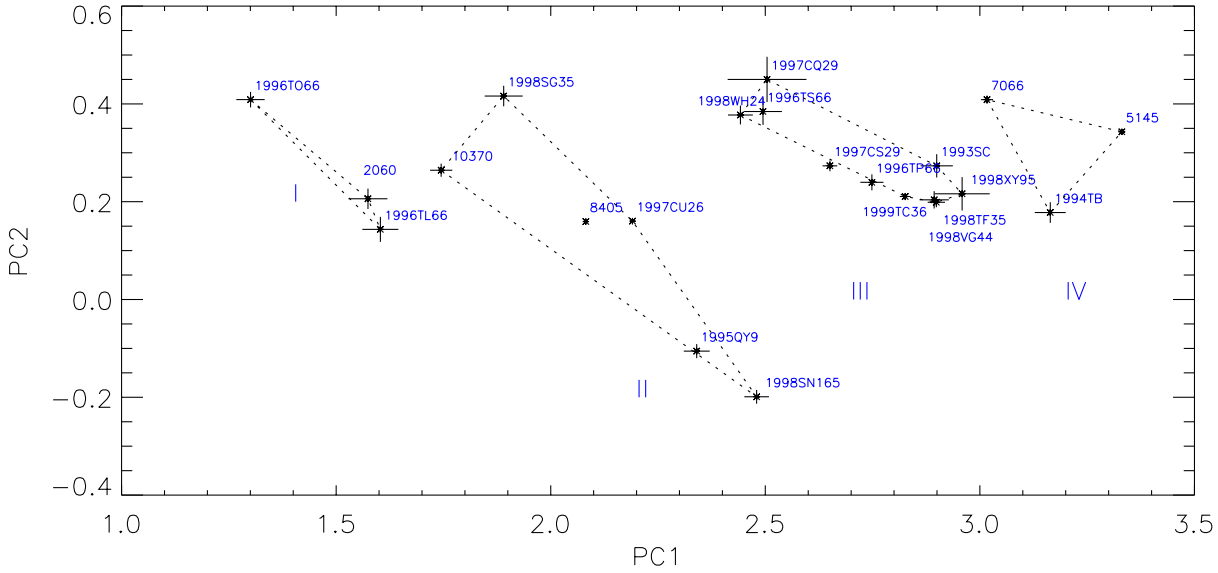

Fig. 1. TNO and Centaur designation for each object in the PC1 vs. PC2 plot are reported. The predominance of PC1 is evident. The spreading of the analysed sample is a clear indication of a continuous trend from neutral (lower PC1 scores) to very red (higher PC1 scores). The dotted lines include the objects belonging to each group found by the G-mode analysis. The error bars of PC1 and PC2 have been obtained propagating the errors of the colours

only between −0.2 and 0.5. We interpreted this behaviour as a net indication of a continuous trend from neutral (lower PC1 scores) to very red (higher PC1 scores) surface colours. By examining the PC1 and PC2 components in more details, a finer structure of the sample seems to overlap the continuous trend (see Fig. 1).

In order to check the existence of this finer structure we analysed the same sample with the G-mode multivariate statistics (Coradini et al. 1977). This method allows us to analyse a sample of N objects described by M variables with the aim of separating, on the basis of an appurtenance test, the N objects in groups which are homogeneous in terms of the variables content. The method also gives an indication of the relative importance of the variables in separating the groups. An estimation of the statistical distance of the groups is also obtained by computing the total variance of all of the variables of one group with respect to the means of all the others groups, which can be interpreted in terms of possible processes affecting (or linking) the different groups.

The G-mode analysis separates the 22 objects of our sample in four groups. In Fig. 2 the average broad band colours obtained for each group are presented as reflectance spectra, normalised to the Sun and to V colour. The colours are transformed in reflectance values by $R_{c_\lambda} = 10^{\pm 0.4(c_\lambda - c_{\lambda_0})}$ where c_λ and c_{λ_0} are the $\lambda - V$ colours of the object and of the Sun respectively. Group I contains the objects having a neutral reflectance spectrum, group IV contains the reddest objects in the Solar System. Groups II and III have transitional character between group I and group IV respectively, as far as $B-V$, $V-R$ are concerned, but are clearly distinguished by $V-I$ and $V-J$. This splitting has been obtained at a confidence level of 99%. The importance of variables in obtaining the four groups is 42% for the $V-I$ colour, 26% for $V-J$, 20% for $V-R$ and 12% for $B-V$. The $V-I$ variable discriminates each group from all the others at an high significance level, the $V-J$ variable plays the same role at a lower level as well as $V-R$, while $B-V$ contribute weakly in separating the groups.

The general results of the G-mode analysis are i) within the sample, four groups of objects can be identified; ii) each group is characterised by a quite homogeneous set of variables; iii) the most important contribution in discriminating the groups comes from the variable $V-I$; iv) the statistical distances between the groups show that group I and group IV exhibit the larger differences, while groups II and III are closer because of their common intermediate behaviour, and they span between group I and group IV; v) these groups define the finer subdivision overlapping the continuous trend found in the PC1 vs. PC2 plot. Finally, has to be outlined that the asteroid taxonomy has been obtained by the G-mode (Barucci et al. 1987) at a lower significance lever (∼93%): it may imply that the TNO's grouping could have as much relevance as the asteroid classification.

3. Conclusion and discussion

The results obtained by the two statistical methods used are fully compatible. The quasi-continuous spreading of the objects between two end members (those with neutral spectra and those with the reddest known spectra) results from the weight (91.14%) of the first principal component. Both PCA and G-mode analysis show the same finer structure of the sample. This grouping is distinguished by their content of $V-I$ and $V-J$, while is quite marginal for $V-R$ and $B-V$. Due to the faintness of TNOs,

observations are very difficult and consequently errors are quite important and are reflected on the colour determination. Changing the value of a colour of a single object can make it to change group. However the important point is not the belonging of one single object to one group or another, but the existence of subdivisions. The main results of our analysis is that I and J observations are critical in discriminating groups and for this reason we suggest to observe TNOs up to the infrared (I, J filters).

Our results exclude the claimed bimodality of the TNO population (Tegler & Romanishin 1998) and confirm quantitatively by statistical analysis the interpretation done by previous authors regarding the evolution of TNO population. In fact the quasi-continuous colour variation of the TNOs can be a consequence of collisions at all scales and of space weathering (Luu & Jewitt 1996; Davis & Farinella 1997). High energy charged particles (cosmic and solar) bombardment induce a deposition of some of the organic compounds contained in the icy bodies of the TNOs, which forms a coating of dark materials characterised by a very red spectrum. Micrometeoroid or meteoroid impacts can locally remove the coating, exposing patches of the underlying surface (whose extension depends on the energy of the projectile) and lowering at different level the influence of the organic coating in reddening the spectra. Mutual collisions can have more dramatic effects in rejuvenating the TNO surfaces (Durda & Stern 2000; Davis & Farinella 1997): large impacts resurface the objects leading to neutral or lightly red spectra, as shown by the few known cometary nuclei. All the TNOs experience collisions (projectile $D > 1$ km) at rate of 10^{-6}–10^{-8} per year (Davis & Farinella 1997), so the population exhibits a continuous range of surface conditions, from the freshly exposed original neutral icy surfaces, to the heavily bombarded by charged particles, coated old red surfaces. The groups which appear to overlap this continuous trend when a finer structure is extracted can be interpreted as the superposition of some peculiar processes over the collisional evolution described. The available data are insufficient to allow us to interpret the meaning of the grouping. More observations are needed. As an example we note that for two of the objects belonging to group I, the presence of some activity has been claimed: coma outgassing has been detected (Meech & Belton 1989) for 2060 Chiron and outbursts have been hypothesised (Hainaut et al. 2000) for 1996 TO_{66}. This kind of activity could change the reflectance properties of these objects due to the fact that the sunlight is reflected by the gaseous and dusty cloud surrounding these bodies. The possible resurfacing of the body by fresh debris could as well be the source of the similarity in the colour behaviour of group I objects.

The present analysis is based on a very small data set, so the four groups found may be not representative. Our results show that the TNO population characters are much more complex than those resulting from the previous analysis based on only marginally discriminating variables and are not bimodal. We have started two large observation programmes, at VLT (ESO, Chile) and CFHT (Hawaii) to investigate the nature of these objects and to obtain a high quality homogeneous colour ($B-V$, $V-R$, $V-I$, $V-J$, $V-H$, and $V-K$) set for a large sample of TNOs.

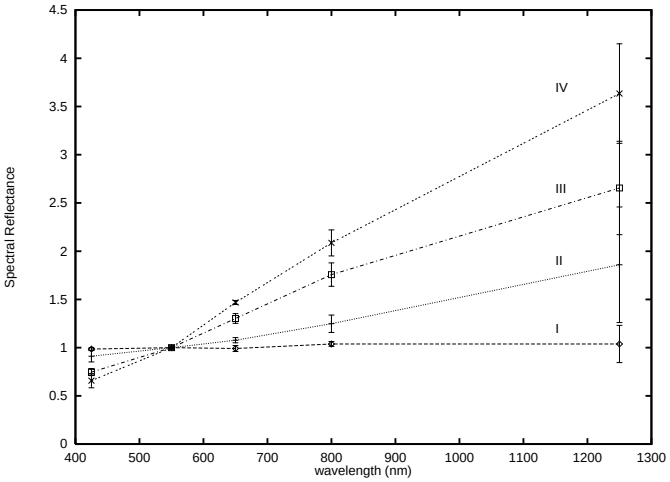

Fig. 2. The average broad band reflectance spectra normalised to V band (centered at 550 nm) are reported for each group found by G-mode analysis. The error bar is the standard deviation of the reflectance mean values within each group. The four groups spread continuously from neutral spectrum (group I) to very red one (group IV) containing the reddest objects of the solar system

Table 2. Eigenvectors, eigenvalues and % of total variance contributed by each eigenvalue

Variable	1	2	3	4
$B-V$	0.251	0.386	−0.859	0.223
$V-R$	0.238	0.314	−0.027	−0.918
$V-I$	0.431	0.669	0.511	0.326
$V-J$	0.833	−0.552	0.002	0.028
Eigenvalues	0.313	0.025	0.004	0.002
% of total variance	91.141	7.331	1.066	0.463

Acknowledgements. We thank A. W. Harris (JPL) for helpful discussions.

References

Barucci, M. A., Capria, M. T., Coradini, A., & Fulchignoni, M. 1987, Icarus, 72, 304

Barucci, M. A., Doressoundiram, A., Fulchignoni, M., et al. 1999, Icarus, 142, 476

Barucci, M. A., Romon, J., Doressoundiram, A., et al. 2000, AJ, 120, 496

Boehnhardt, H., Tozzi, G. P., Birkle, K., et al. 2001, A&A, submitted

Coradini, A., Fulchignoni, M., Fanucci, O., et al. 1977, Comput. Geosci., 3, 85

Davies, J. K. 2000, in Minor Bodies of the Outer Solar System, ed. A. Fitzsimmons, D. Jewitt, & R. M. West, ESO Astrophysics Symposia (Springer-Verlag Berlin Heidelberg) 9

Davies, J. K., Green, S., McBride, N., et al. 2000, Icarus, 146, 253
Davies, J. K., McBride, N., Ellison, S. L., et al. 1998, Icarus, 134, 213
Davis, D. R., & Farinella, P. 1997, Icarus, 125, 50
Doressoundiram, A., Barucci, M. A., Romon, J., et al. 2001, Icarus, submitted
Duncan, M., Levison, H., & Budd, S. 1995, AJ, 110, 3073
Durda, D. D., & Stern, S. A. 2000, Icarus, 145, 220
Fulchignoni, M., Birlan, M., & Barucci, M. A. 2000, Icarus, 146, 204
Green, S. F., McBride, N., O'Cealleagh, D., et al. 1997, MNRAS, 290, 186
Hainaut, O. R., Dalahodde, C. E., Boehnhardt, H., et al. 2000, A&A, 356, 1076
Hardorp, J. 1980, A&A, 91, 221
Hartmann, W. K., Cruishank, D. P., & Degewij, J. 1982, Icarus, 52, 377
Jewitt, D. C. 2000, in Minor Bodies of the Outer Solar System, ed. A. Fitzsimmons, D. Jewitt, & R. M. West, ESO Astrophysics Symposia (Springer-Verlag Berlin Heidelberg) 1
Jewitt, D. C., & Luu, J. X. 1993, Nature, 362, 730
Jewitt, D., & Luu, J. X. 1998, AJ, 115, 1667
Luu, J. X., & Jewitt, D. 1996, AJ, 112, 2310
Marsden, B. 2001, `http://cfa-www.harvard.edu/cfa/ps/lists/TNOs.html`
Meech, K. J., & Belton, M. J. S. 1989, IAU Circ., 4770
Reyment, R., & Joreskog, K. G. 1993, Applied Factor Analysis in natural Sciences (Cambridge Univ. Press)
Stern, S. A. 1996, in Completing the inventory of the Solar System, ed. T. W. Retting, & J. M. Hahn, ASP Conf. Ser., 107, 209
Stern, S. A., & Campins, H. 1996, Nature, 382, 507
Tedesco, E. F., Williams, J. G., Matson, D. L., et al. 1989, AJ, 97, 580
Tegler, S. C., & Romanishin, W. 1998, Nature, 392, 49
Tegler, S. C., & Romanishin, W. 2000, Nature, 407, 979
Tholen, D. J., & Barucci, M. A. 1989, in Asteroid II, ed. R. P. Binzel, & T. Gehrels (Univ. of Arizona Press), 298
Wood, H. J., & Kuiper, G. P. 1963, AJ, 137, 1279

TOWARD A TAXONOMY OF THE EDGEWORTH-KUIPER OBJECTS: A MULTIVARIATE APPROACH

M. FULCHIGNONI[1,2], A. DELSANTI[1], M.A. BARUCCI[1], M. BIRLAN[1]
[1]LESIA, Observatoire de Paris, [2]Université Denis Diderot – Paris 7

Abstract. The principal component (PC) and g-mode multivariate statistics have been used in analysing the set of the 34 Edgeworth-Kuiper objects (EKOs) - 23 Trans Neptunian Objects (TNO) and 11 Centaurs - for which the B, V, R, I, J homogeneous photometry were available. The results obtained show that the V-I and V-J s are the key parameters in structuring the sample in homogeneous groups. The PC1 axis (which contains ~93% of the sample total variance) spans five times more than the PC2 (which contains ~6% of the sample total variance). The extremes of PC1 axis contain the objects having a flat spectrum (low PC1 values) and a very red spectrum respectively. Independently, the g-mode analysis allow us to distinguish six homogeneous groups of objects which confirm and extend the results obtained with the PC analysis. In addition to these groups, few objects remain not included in any group (*i.e.* does not have significant similitude with other objects) and yet give an indication of a more complex compositional structure of the sample. These preliminary results have to be confirmed and completed when a larger sample will be available, but they provide some interesting hints for understanding the - mainly collisional - evolution of the EKOs.

1. Introduction

Ten years after the discovery of the first object wandering outside the orbit of Neptune, the number of detected Edgeworth-Kuiper Objects is close to eight hundred: more or less the same number of asteroids that was found in a century, after the discovery of 1 Ceres. The available information concerning the broad band photometry of EKOs: B, V, R, I data are available to date for a hundred of objects and for fifty or so of them J data are also available; while only forty or so asteroids had the U-B and B-V s determined in the sixties, hundred and seventy; years after the discovery of Ceres. Despite this small number of asteroids (~2% of the population known at that time) Wood and Kuiper (1963) suggested, on the base of the observed distribution, the existence of two different compositional classes clustering around the indices of the Moon and of the Sun. These groups were the ancestors of the today S and C classes respectively. Analogically, Tegler and Romanishin (1998) obtained two groups of objects analysing the B-V and V-R s of 13 EKOs (~ 20% of the known EKOs population at that time) one very red and the other quite neutral with respect to the Sun. In the early eighties few thousands of asteroids were known, a large survey (Zellner et al., 1985) was devoted to measure in eight filters (range 0.35-1.0 μm) the sunlight reflected by several hundred asteroids (~10% of the known objects). Then the IRAS data (Tedesco et al., 1992) provided the albedo data for most of these objects. Tholen (1984) and Barucci et al. (1987) used these data bases in classifying the asteroids by means of independent multivariate statistical techniques (the principal components analysis based on the eight s data, and the G- mode analysis based on the eight s and IRAS albedo data respectively). Both the methods provide a similar classification scheme which constitute the bulk of the current asteroid taxonomy, separating the asteroid population in a dozen compositionally homogeneous groups. Barucci et al. (2001)

applied the same techniques to a sample of 22 EKOs (~ 6% of the known EKOs population at that time) characterized by 4 s (B-V, V-R, V-I and V-J). The results indicate a clear compositional trend within the examined sample and suggest the possible existence of some homogeneous groups.

Table 1. Colours of the 34 EKOs and Centaurs analysed

Object/type*	B-V	V-R	V-I	V-J	References
Sun	0,67	0,36	0,69	1,08	1,2
1996TQ66/R	1,18±0,11	0,65±0,08	1,44±0,14	2,43±0,12	6,7,15,10,20
1996TS66/Cl	1,01±0,08	0,63±0,11	1,19±0,12	1,82±0,17	5,6,7,10,20
1997CS29/Cl	1,05±0,08	0,67±0,05	1,27±0,07	2,07±0,13	6,7,10,12,20,22,23
1998HK151/R	0,64±0,12	0,49±0,05	0,87±0,06	1,57±0,09	16,17,22,25
1998WU24/?	0,78±0,03	0,53±0,04	0,99±0,03	1,67±0,04	42
1999CD158/Cl	0,86±0,05	0,52±0,05	1,09±0,07	1,81±0,08	12,17
2060 Chiron/C	0,68±0,04	0,36±0,02	0,73±0,04	1,20±0,11	31,32,33
5145 Pholus/C	1,30±0,09	0,79±0,03	1,58±0,05	2,61±0,04	32,34,35,36
7066 Nessus/C	1,09±0,04	0,79±0,04	1,50±0,07	2,29±0,04	3,6,14,32
8405 Asbolus/C	0,75±0,04	0,51±0,06	0,99±0,06	1,66±0,06	9,14,32,37,38,39
10199 Chariklo/C	0,80±0,05	0,48±0,02	1,01±0,03	1,74±0,02	6,32,40,41
10370 Hylonome/C	0,67±0,08	0,44±0,06	0,91±0,09	1,31±0,10	3,6,17,20,32
15789 1993SC/R	1,01±0,10	0,67±0,06	1,40±0,09	2,43±0,15	3,4,5,6,7,8,9,10
15820 1994TB/R	1,08±0,13	0,71±0,08	1,45±0,12	2,48±0,15	3,7,8,9,10,11,12,13
15874 1996TL66/S	0,69±0,05	0,33±0,05	0,69±0,05	1,45±0,11	5,6,7,10,13,20
15875 1996TP66/Cl	0,98±0,10	0,65±0,07	1,33±0,09	2,31±0,06	5,6,7,10,13,22
19308 1996TO66/Cl	0,66±0,06	0,38±0,04	0,74±0,07	1,00±0,10	5,6,10,13,17,20,21
19521 Chaos/Cl	0,92±0,05	0,61±0,04	1,19±0,08	1,77±0,07	7,12,18,22
20000 Varuna/Cl	0,92±0,03	0,61±0,02	1,22±0,02	2,01±0,05	17,29,30
24835 1995SM55/Cl	0,65±0,03	0,40± 0,04	0,72±0,05	1,02±0,05	11,12,15,16,17
26181 1996GQ21/S	1,01±0,06	0,73±0,04	1,42±0,05	2,44±0,06	12,16,18,19
26308 1998SM165/Cl	0,97±0,09	0,69±0,07	1,29±0,07	2,37±0,06	18,16,12
26375 1999DE9/S	0,92±0,04	0,58±0,03	1,15±0,04	1,89±0,06	10,11,12,16,17
29981 1999TD10/S	0,73±0,04	0,50±0,03	0,97±0,03	1,79±0,05	11,16,17,27
32929 1995QY9/R	0,70±0,12	0,52±0,09	0,86±0,08	2,03±0,20	3,7,13,15
33128 1998BU48/C	1,04±0,07	0,64±0,04	1,19±0,05	2,07±0,06	12,17
35671 1998SN165/Cl	0,71±0,09	0,44±0,08	0,82±0,09	1,27±0,05	10,15,11,16,25
38628 2000EB173/R	0,95±0,04	0,58±0,08	1,19±0,04	1,97±0,05	10,16,19,28
44594 1999OX3/C	1,12±0,10	0,70±0,06	1,42±0,06	2,11±0,08	11,16,17,18,19,25
47171 1999TC36/R	1,01±0,05	0,69±0,04	1,31±0,05	2,29±0,07	11,12,16,22,25
47932 2000GN171/R	0,92±0,05	0,62±0,04	1,24±0,04	1,76±0,06	16,19
48639 1995TL8/S	0,82±0,18	0,55±0,15	0,95±0,33	2,41±0,05	12,17,18,19
52872 1998SG35/C	0,89±0,11	0,43±0,08	1,02±0,08	1,35±0,19	11,24,26
52975 1998TF35/C	1,14±0,08	0,70±0,05	1,38±0,07	2,37±0,06	12,17,22
54598 2000QC243/C	0,69±0,05	0,44±0,04	0,89±0,05	1,69±0,07	12,17

*Type: C= centaur, Cl = classical, R = resonant, S = scattered disk, ?= unusual, Halley family comet orbit

1, Hardorp (1980); 2, Hartmann et al. (1982); 3, Luu & Jewitt (1996a); 4, Luu & Jewitt (1996b); 5, Jewitt and Luu (1998); 6, Romanishin & Tegler (1999); 7, Davies et al. (2000); 8, Romanishin et al. (1997); 9, Tegler & Romanishin (1997); 10, Jewitt & Luu (2001); 11, Delsanti et al. (2001); 12, Delsanti et al. (2003); 13, Barucci et al (1999); 14, Davies (2000); 15, Gil-Hutton & Licandro (2001); 16, Mac Bride et al. (2003); 17, Doressoudiram et al. (2002); 18, Tegler & Romanishin (2000); 19, Boehnhardt et al. (2002); 20, Tegler and Romanishin (1998); 21, Hainaut et al. (2000); 22, Boehnhardt et al. (2001); 23, Barucci et al. (2000); 24. Alain Doressoudiram, private communication; 25, Doressoundiram et al. (2001); 26, Barucci et al. (2001); 27, Consolmagno et al. (2000); 28, Ferrin et al. (2001); 29, Olivier R. Hainaut, private communication; 30, Jewitt and Sheppard (2002); 31, Hartmann et al. (1981); 32, Davies et al. (1998); 33, Parker et al (1997); 34, Mueller et al. (1992); 35, Binzel (1992); 36, Davies et al. (1993); 37, Weintraub et al. (1997); 38, Brown and Luu (1997); 39, Romon et al. (2002); 40, Jewitt and Kalas (1998); 41, MacBride et al. (1999); 42, Davies et al. (2001).

Nowadays about 800 EKOs have been discovered; three colours photometry is available for about 80 objects and for 40 of them V-J is available too. In this paper we discuss the results of the multivariate analyses carried out on a subset of 34 EKOs for which homogeneous data (Table 1), obtained in the B, V, R, I and J bands by the same observers, during the same run, or inter-calibrated through the V measurement.

2. Multivariate statistical analyses

We analysed this highly homogeneous EKOs group (hereafter "*the sample*") using both the Principal Component Analysis (PCA) (Reyment & Joreskog, 1993) and the G-mode analysis (Coradini et al., 1977; Fulchignoni et al., 2000). We refer the reader to the quoted literature for details on these statistics.
In our case, the principal components are linear combination of the original variables (B-V, V-R, V-I and V-J) whose coefficients reflect the relative importance of each variable (colour) within each principal component. These coefficients are the eigenvectors of the variance-covariance matrix of the colours. The sum of the eigenvalues of this matrix (which is equal to its trace) accounts for the total variance of the sample. Each eigenvalue reflects the percentage of the total variance contributed by each principal components. The eigenvectors, the percentages of total variance contributed by each eigenvector and the eigenvalues of the variance-covariance matrix of the sample are reported in Table 2.

Table 2. Eigenvectors, eigenvalues and percentage of total variance contributed by each eigenvalue.

variable	eigenvector 1	eigenvector 2	eigenvector 3	eigenvector 4
B-V	**0,3029**	**0,4733**	**0,8208**	**-0,1025**
V-R	**0,2171**	**0,2266**	**-0,3223**	**-0,8931**
V-I	**0,4469**	**0,6236**	**-0,4701**	**0,4365**
V-J	**0,8133**	**-0,5794**	**0,0386**	**0,0367**
eigenvalues	**0,2828**	**0,0185**	**0,0023**	**0,0007**
% total variance	**92,93**	**6,08**	**0,75**	**0,24**

The first eigenvector accounts for most of the sample variance (92.93%) and the larger contribution comes from V-J (46%). The second eigenvectors adds only 6.08% of the total variance and is weighted in quite equal measure by V-I (33%) and V-J (30%). The first and the second principal component account for more than 99% of the total variance, therefore the PC1 vs. PC2 plane contains practically all the information on the variance of the variables characterizing the considered sample. It is possible to infer from this result that the degree of reddening is the main distinctive character of the EKOs population. In Figure1 the EKO's sample is plotted in the PC1 - PC2 plane. The predominance of PC1 (*i.e.* of V-J colour) in characterizing the EKOs behaviour is shown by the PC1 scores, which span three times more than the PC2 ones. The objects having a neutral colour with respect to the Sun have the lower values of the PC1 scores and fall in the left part of the plot , for larger PC1 scores the objects are redder and redder.

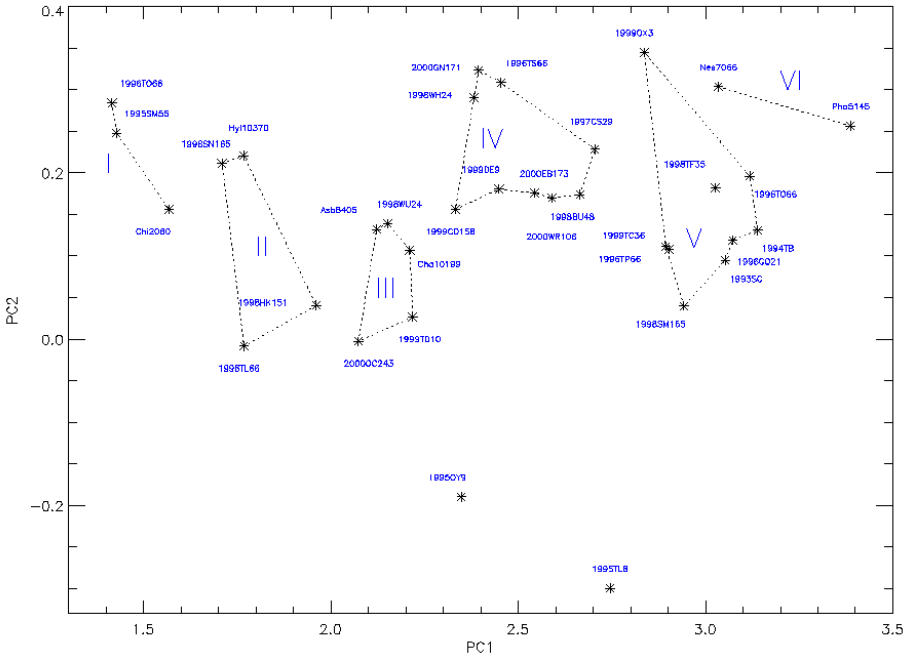

Figure 1. EKOs and Centaurs designation for each object in the PC1-PC2 plot are reported. The dotted lines individuate the groups found the G-mode analysis. The error bars have been obtained propagating the errors of the colours.

We analysed the same sample with the G-mode multivariate statistics (Coradini et al., 1977), which allowed us to investigate the existence of a finer structure of the sample. The G-mode statistics analyse our sample of 34 objects described by 4 variables, the colours B-V, V-R, V-I and V-J. The total number of degrees of freedom (136) allow us to use this kind of statistics. The goal of the analysis is to find groups of objects which have an homogeneous behaviour in terms of their variables content, if any. The method provides a quantitative estimation of the weight of each variable in separating the groups.
The G-mode analysis has been carried out transforming the colour data in reflectance values by $R_{c_\lambda}=10^{\pm 0.4(c_\lambda - c_{\lambda sun})}$ where c_λ and $c_{\lambda sun}$ are the λ-V colours of the object and of the Sun respectively. The method grouped the 34 objects in seven groups at a significance level of 99%. In Figure 2 the average broad band reflectance spectra (normalized to the V bands) for the groups found by the G-mode analysis are reported.

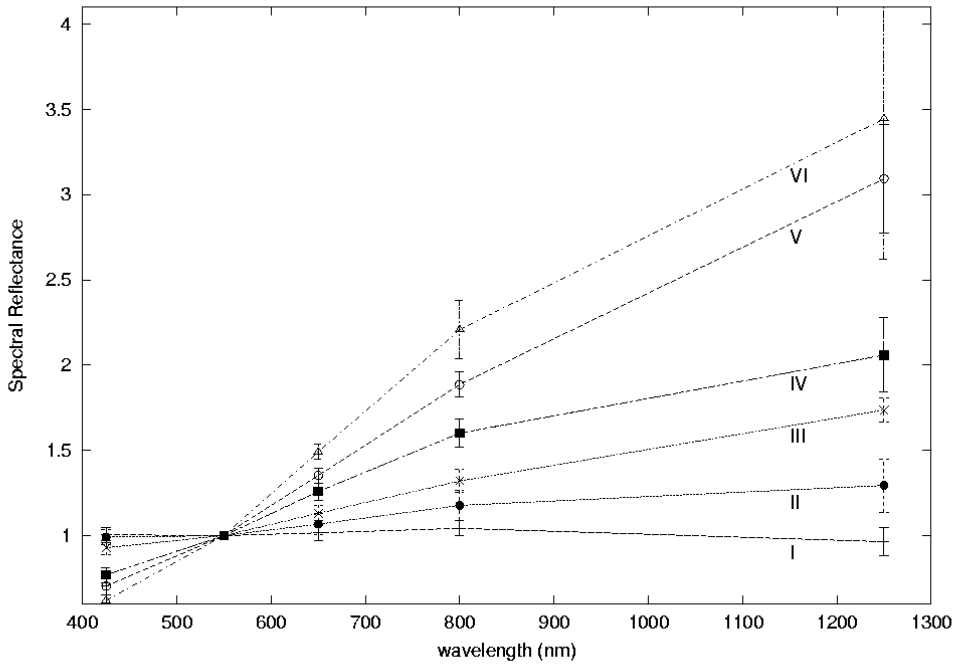

Figure 2. The average broad band reflectance spectra (normalized to the V band) for the groups found by the G-mode analysis. The error bar is the standard deviation of the reflectance mean value within each group. The group spectra spread from the neutral (group I) to the very red one (group VI).

Group I contains the objects having reflectance spectra neutral with respect the Sun one. The objects in group II have a higher value of V-J, which separate this group from the previous one. Group III and group IV clearly distinguished each other by the V-I colour while V-J separate these two groups from all the other groups their spectra are redder than those of group I and group II;. Group V contains objects still redder and group VI is formed by the reddest objects of the solar system. V-R and V-I distinguish the two last groups, which have the same dramatic reddening, completely different from the trend of all the other spectra.
(32929) 1995QY9 and (35671) 1998SN165, characterized by the lower PC2 scores, remain isolated forming two "*single object groups*" as well as (4) Vesta, (1862) Apollo and (349) Dembowska formed the V, Q and R classes in the Tholen (1984) asteroid taxonomy [dozens of small asteroids populate the V class and some new objects have been added to the R and Q classes today (Binzel and Xu,1993; Bus & Binzel, 2002)].
The relative weights of the variables in structuring the EKO's sample in these groups are 38% for V-J, 30% V-I, 17% V-R and 15% B-V. The V-J colour discriminate the groups each other at a high significance level (>3σ), V-I plays the same role at a slightly lower level. Minor contributions are provided by V-R and B-V.
These groups constitute the finer structure overlapping the general trend from neutral to very red spectra resulting from the PC analysis, as shown in Figure 1.

3. Conclusions

The PC analysis of a sample of 34 EKOs for which high quality colour data were available provided a quasi continuous trend from neutral to very red spectra. G-mode allowed us to distingush a finer structure superimposed to this trend, separating six groups of homogeneous objects and two single class objects, as far as the colour behaviour is concerned.
The significance level (99%) of this grouping is larger than the one (93%) obtained by Barucci et al. (1987) in classifying a sample of 438 asteroids with the same statistical technique. This constitute a strong indication that colours reveal real differences in the EKOs surface nature, probably originated by their physico-chemical evolution.
In our preliminary analysis (Barucci et al., 2001) we found a basically similar result analysing a smaller sample of 22 EKOs.: a quasi continuous trend with a finer structure allowing us to recognize four groups of objects. The 50% increase of the sample size allowed us to refine the description of the EKOs population, concerning particularly the intermediate groups. In fact, the two extreme groups (neutral and reddest spectra) have the same average spectra both in the Barucci et al. and in the present analysis , while each of the two Barucci's intermediate groups splits in two more homogeneous groups.
We can conclude that the multivariate analysis of large band spectrophotometric data of EKOs provides strong indications for differences in the surface nature of these objects. The quasi continuous trend, put in evidence by the principal component analysis, is probably a witness for the possible sequence of the alteration processes undergone by the surface of each object, while the different groups, obtained with the G-mode, indicate the present physico-chemical state of the analysed objects.
More data are needed to confirm these preliminary results of the multivariate statistical analysis and to allow us to provide a rigorous description of the meaning of the EKOs colour differences.
With the aim to draw at least a rough, incomplete and foggy scenario, we could attempt to read Figure 1 as the EKOs evolution diagram: 1) the position of an object along the trend connecting the group of neutrals to the group of the reddest would indicate the time to which it has been exposed to the different alteration processes (collisions, cratering, energetic particles bombardment…), starting from a given initial state (original or consequence of a resetting event); 2) each group would represent an evolution stage of the population; 3) the relative number density of each group would account for how long that stage is lasting; 4) the presence of single objects groups might imply the existence of different (cyclic?) evolution paths.

References

Barucci M.A., Capria M.T., Coradini A., Fulchignoni M.: 1987. Icarus **72**, 304.
Barucci M.A., Doressoundiram A., Tholen D., Fulchignoni M., Lazzarin M.: 1999. Icarus, **142**, 476.
Barucci M.A., Romon J., Doressoundiram A., Tholen D.J.: 2000. AJ, **120**, 496.
Barucci M.A., Fulchignoni M., Birlan M., Doressoundiram A., Romon J., Boehnard H.: 2001. A&A, **371**, 1150.
Binzel R.P.: 1992. Icarus, **99**, 238.
Binzel R.P. & Xu S.: 1993. Science, **260**, 186.
Boehnhardt H., Tozzi G.P., Birkle K., Hainaut O., Sekiguchi T., Vair M., Watanabe J., Rupprecht G., The FORS Instrument Team: 2001. A&A, **378**,653

Bus S.J. & Binzel R.P.: 2002. Icarus, **158**, 146.
Boehnhardt H., Delsanti A., Barucci A., Hainaut O., Doressoundiram A., Lazzarin M., Barrera L., de Bergh C., Birkle K., Dotto E., Meech K., Ortiz J.E., Romon J., Sekiguchi T., Thomas N., Tozzi G.P., Watanabe J, West R.M.: 2002. A&A, **395**, 297.
Brown W.R. & Luu J.X.: 1997. BAAS, **29**, 1021.
Consolmagno G., Tegler S.C., Rettig T., Romanishin W.: 2000. BAAS, **32**,
Coradini A., Fulchignoni M;, Fanucci O. et al., 1977. Comput. Geosci., **3**, 85.
Doressoundiram, A.; Barucci, M. A.; Romon, J.; Veillet, C. : 2001. Icarus,**154**, 277.
Doressoundiram, A., Peixinho, N., de Bergh, C. , Fornasier, S., Thébault, P., Barucci, M. A.; Veillet, C. : 2002. AJ, **124**, 2279.
Davies J. K., Sykes M. V., Cruikshank D. P.: 1993. Icarus, **102**, 166.
Davies J.K., McBride N., Ellison S.L.,. Green S.F., Ballantyne D.R.: 1998. Icarus, **134**, 213.
Davies J.K. : 2000. In Minor Bodies of the Outer Solar System (Eds. A. Fitzsimmons, D. Jewitt & R.M. West), ESO Astrophysical Symposia, (Springer-Verlag, Berlin Heidelberg), 9.
Davies J.K., Green S., McBride N., Muzzerall E., Tholen D.J., Whiteley R.J., Foster M.J., Hillier J.K.: 2000. Icarus, **146**, 253.
Davies J.K., Tholen D.J., Whiteley R.J., Green S., Hillier J.K., Foster M., J McBride N., Kerr T.H., Muzzerall E.: 2001. Icarus, **150**, 69.
Delsanti A.C., Boehnhardt H., Barrera L., Meech K.J., Sekiguchi T., Hainaut O.R.: 2001. A&A, **380**, 347.
Delsanti A., Hainaut O., Jourdeuil E., Meech K.J., Boehnhardt H., Barrera L.: 2003. A&A (in press)
Ferrin I., Rabinowitz D., Schaefer B., Snyder J, Hellman N., Vicente B., Rengstorf A., Depoy D., Salim S. et al.: 2001. ApJ, **548L**, 243.
Fulchignoni M., Birlan M., Barucci M.A.: 2000. Icarus, **146**, 204.
Gil-Hutton R.& Licandro J. : 2001. Icarus, **152**, 246.
Hainaut O.R., Delahodde C.E., Boehnhardt H., Dotto E., Barucci M.A., Meech K.J., Bauer J.M., West R.M., Doressoundiram A. : 2000. A&A, **356**, 1076.
Hardorp, J. :1980. A&A, **91**, 221.
Hartmann W.K., Cruikshank D.P., Degewij J., Capps R.W.: 1981. Icarus, **47**, 333.
Hartmann W.K., Cruikshank D.P. & Degewij J.: 1982. Icarus, **52**, 377.
Jewitt D.& Kalas P.: 1998. ApJ, **499L**, 103.
Jewitt D. & Luu J.X.: 1998. AJ, **115**, 1667.
Jewitt D.& Luu J.X.: 2001. AJ, **122**, 2099.
Jewitt D. & Sheppard S.S.: 2002. AJ, **123**, 2110.
Luu J.X. & Jewitt D.: 1996a. AJ, **112**, 2310.
Luu J.K. & Jewitt D.: 1996b. AJ, **111**, 499.
MacBride N., Davies J.K., Green S.F., Foster M.J.: 1999. M.N.R.A.S., **306**, 799.
Mac Bride N., Green S.F., Davies J.K., Tholen D.J., Sheppard S.S., Witheley R.J., Hillier J.K.: 2003. Icarus, **161**, 501.
Mueller B.E.A., Tholen D.J., Hartmann W.K., Cruikshank D.P.: 1992. Icarus, **97**, 150.
Parker J.W., Stern S.A., Festou M.C., A'Hearn M.F., Weintraub D.: 1997. AJ, **113**, 1899.
Reyment R. & Joreskog K.G.: 1993. Applied Factor Analysis in natural sciences (Cambridge University Press)
Romanishin W., Tegler S.C., Levin J., Butler N.: 1997. AJ, **113**, 1893.
Romanishin W., & Tegler S.C.: 1999. Nature, **398**, 129.
Romon-Martin J., Barucci M.A., de Bergh C., Doressoundiram A., Peixinho N., Poulet F. : 2002. Icarus, **160**, 59.
Tedesco E.F.,Veeder G.J., Fowler J.W., Chillemi J.R. : 1992. The IRAS Minor Planet Survey. Final Report. PL-TR-92-2049. Phillips Laboratory, Airforce Material Command Hanscom Air Force Base, Ma 01731-3010.
Tegler S.C.& Romanishin W.: 1997. Icarus, **126**, 212.
Tegler S.C. & Romanishin W.: 1998. Nature, **392**, 49.
Tegler S.C. & Romanishin W.: 2000. Nature, **407**, 979.
Tholen D.J.: 1984. PhD Thesis, University of Arizona.
Weintraub D., Tegler S.C., Romanishin W.: 1997. Icarus, **128**, 456.
Wood, H.J. and Kuiper, G.P. 1963. AJ, **137**, 1279.
Zellner B., Tholen D.J., Tedesco E.F.: 1985. Icarus, **61**, 355.

II.2. Modélisation des spectres des objets sans atmosphère.

L'analyse et l'estimation de la minéralogie des objets sans atmosphère a fait un pas important en passant des variables discrètes comme les couleurs, vers une estimation spectrale, c'est à dire continue. Dans les cas des objets sans atmosphère, la réponse spectrale dictée par la couche superficielle de régolite nécessite une basse résolution (R=100 jusqu'à R=200) du spectrographe. Les bandes d'absorption mises en évidence habituellement sont des bandes larges, essentiellement autour de 1 et 2 microns (comme présenté en sous-chapitre I.2). Par la spectroscopie nous pouvons ainsi avoir une estimation des profils de bandes larges caractérisant les astéroïdes, mais aussi mettre en évidence des structures plus fines de bandes (des bandes étroites ou des bandes moins profondes).

L'extension de l'analyse spectrale vers le domaine de l'infrarouge proche permet actuellement une meilleure compréhension de la minéralogie de surface des astéroïdes. Une analyse minéralogique poussée permet l'évaluation de nouveaux paramètres tels que la profondeur de bande, la position du minimum de la bande d'absorption, la pente du spectre, la superficie des bandes,…

L'interprétation de la minéralogie à partir d'un spectre de réflexion est un travail difficile pour plusieurs raisons. Plusieurs minéraux peuvent présenter une bande d'absorption semblable, localisée dans la même région du spectre. De même, un ensemble de plusieurs minéraux peuvent également donner comme résultat une bande d'absorption de paramètres différents. Si nous prenons en compte les tailles des grains (régolites) responsables de la plupart des caractéristiques spectrales, le profil des bandes d'absorption peut être également modifié. Le bombardement des surfaces des astéroïdes par des rayonnements cosmiques (vent solaire) de haute énergie modifie le profil du spectre[1].

Les études de laboratoire servent de support à des solutions possibles de ce problème. En laboratoire, par l'analyse des roches et des météorites nous cernons mieux les minéraux

[1]cet aspect est couvert par l'expression "météorologie de l'espace" (space weathering)

susceptibles d'être à la base d'un spectre d'astéroïde. Les paramètres physiques déterminés en laboratoire peuvent être utilisés par la suite pour la modélisation du spectre.

L'une des méthodes les plus usitées pour expliquer les caractéristiques d'un spectre d'objet sans atmosphère est la méthode des mélanges. Dans l'hypothèse d'une distribution linéaire des composants minéralogiques, l'équation de la réflectance spectrale est alors la combinaison linéaire des composants. Pour deux composants, la réflectance spectrale s'écrit[2] :

$$R_\lambda = nR_{1\lambda} + (1-n)R_{2\lambda}$$

où R_1 et R_2 sont les réflectances des composants à la même longueur d'onde et n le pourcentage du premier des minéraux.

Cette analyse a été effectuée sur l'astéroïde 4979 Otawara (article A&A, 398, 2003) désigné initialement comme l'une des cible de la mission Rosetta. Les résultats de cette analyse montre une bonne concordance entre le spectre observé de l'astéroïde et la modélisation d'un spectre générique d'une météorite chondrite ordinaire en ajoutant seulement 0.05% de Fe en nano-phase[3].

La présence de deux ou plusieurs minéraux peut également modifier la profondeur des bandes d'absorption ainsi que la position spectrale de leur minimum. Dans la littérature, les minéraux les plus étudiés sont ceux liés à l'olivine et aux pyroxènes. Deux techniques sont majoritairement employés :

- la modélisation des profils des bandes observées par des courbes quasi-gaussiennes, afin de trouver la meilleure concordance ;
- le calcul des rapports des bandes observées autour de 1 et 2 microns afin de pouvoir les comparer à des mesures effectuées en laboratoire sur différents minéraux.

Les deux approches présentent des faiblesses que nous ne nous proposons pas de développer dans cet ouvrage. Malgré ces faiblesses, leur plus grand mérite est de pouvoir donner de bons résultats et de pouvoir relier d'une manière cohérente les données de laboratoire et celles obtenues par des observations astronomiques, deux types de démarches séparés par des facteurs d'échelles importants (à voir pour exemple les articles A&A, 398, 2003 et A&A, 2005 –sous édition).

---

[2] cette approche est connue dans la littérature comme l'approche zonale des mélanges

[3] 1npFe^0 est l'effet observe par le bombardement des rayons énergétique sur des chondrules, qui libère les atomes de Fe des liaisons en le permettant une liaison métallique entre eux; on assiste à la création des "grumeaux" de Fe des dimension de nanomètre.

Les études de la bande à 1 micron par rapport à celle à 2 microns montrent que la surface de l'astéroïde 4979 Otawara contient des caractéristiques semblables à celles des météorites chondrites ordinaires, avec une composition mixte d'olivine et d'ortho-pyroxène.

Les études de l'astéroïde 4 Vesta et 1 Ceres se sont déroulées en vue de la préparation de la mission spatiale Dawn, organisée par la NASA, dont le départ est prévu en 2006. L'analyse pour Vesta dans l'intervalle spectral 0,8-2,5 μm a été effectuée par les deux approches : d'une part la constitution des profils des bandes par l'intermédiaire de la procédure MGM[4], et d'autre part le calcul des rapports de bandes et leur comparaison avec les résultats obtenus en laboratoire pour différents mélanges. L'analyse montre que la minéralogie à la surface de 4 Vesta est dominée par les composants ayant le pyroxène sous différentes formes de cristallisation (orthopyroxene [mélange de $FeSiO_3$, $MgSiO_3$, et $CaSiO_3$, cristallisés en système orthorhombique, souvent trouvé dans les roches basaltiques] pigeonite [$(Mg,Fe^{++},Ca)(Mg,Fe^{++})Si_2O_6$], diogenite [Opx riche en Mg], eucrite (ou bronzite) [$Mg_2Si_2O_6$]). Ce résultat est en concordance avec ceux obtenus auparavant, et confirme l'hypothèse que Vesta est le parent des météorites HED. Pour l'astéroïde 1 Ceres, nos études ont visé la région spectrale 2,0-4,0 μm. Nos résultats ont mis en évidence une bande d'absorption avec un minimum à 3,06 μm. Cette bande d'absorption a été modélisée par plusieurs types de substances. Le bitume solide contaminé par de l'eau, soumis à un bombardement d'ions, peut reproduire relativement bien cette bande d'absorption. En effet, le bombardement ionique permet de réduire les bandes d'absorption des substances organiques (gendre bitumes) qui sont dues à des modes de vibration des radicaux aliphatiques et aromatiques contenus. De plus, le bombardement ionique fait apparaître des bandes nouvelles, autour de 3,03 μm, associées à des oscillations longitudinales dans les liaisons C-H. Le modèle proposé doit expliquer également la bande d'absorption à 3,06 μm. Pour cela, nous proposons un mélange qui contient des substances organiques avec des liaisons C-H en oscillation longitudinales, et une petite quantité d'eau en état cristallin ; l'explication du déplacement du minimum de la bande vers des longueurs d'onde plus grandes peut être expliquer par la présence de la bande d'absorption des oscillations longitudinales de la liaison O-H.

[4] MGM est l'abréviation de Modified Gaussian Model, une approche mise en place par C. Pieters et J. Sunshine

Références :

Fornasier, S., Barucci, M.A., Binzel, R.P., **Birlan, M.**, Fulchignoni, M., Barbieri, C., Bus, S.J., Harris, A.W., Rivkin, A.S., Lazzarin, M., Dotto, E., Erikson, A., Doressoundiram, A., Bertini, I., Peixinho, N., - *A portrait of 4979 Otawara, target of the Rosetta space mission*, **Astronomy & Astrophysics,** vol **398**, 327-333, 2003.

Vernazza P. Mothe-Diniz T., Barucci A., **Birlan M.**, Carvanho J., Strazzulla G., Fulchignoni M., Migliorini A. - *Analysis of near-IR spectra of 1 Ceres and 4 Vesta, targets of the Dawn Mission*, **Astronomy and Astrophysics**, (in press)

A&A 398, 327–333 (2003)
DOI: 10.1051/0004-6361:20021622

Astronomy & Astrophysics

A portrait of 4979 Otawara, target of the Rosetta space mission⋆

S. Fornasier[1,2], M. A. Barucci[2], R. P. Binzel[3], M. Birlan[2], M. Fulchignoni[2], C. Barbieri[1], S. J. Bus[4], A. W. Harris[5], A. S. Rivkin[3], M. Lazzarin[1], E. Dotto[6,7], T. Michałowski[8], A. Doressoundiram[2], I. Bertini[1], and N. Peixinho[2,9]

[1] Astronomical Department of Padova, Vicolo dell'Osservatorio 2, 35122 Padova, Italy
e-mail: [fornasier; barbieri; lazzarin]@pd.astro.it, bertini@planet.pd.astro.it
[2] LESIA, Observatoire de Paris, 92195 Meudon Principal Cedex, France
e-mail: [antonella.barucci; Mirel.Birlan; Marcello.Fulchignoni; alain.doressoundiram; Nuno.Peixinho]@obspm.fr
[3] Department of Earth, Atmospheric and Planetary Sciences, Massachusetts Institute of Technology, Cambridge, 02139, USA
e-mail: [rpb; asrivkin]@mit.edu
[4] Institute for Astronomy Hilo, HI 96720, USA
e-mail: sjb@ifa.hawaii.edu
[5] Space Science Institute, 4603 Orange Knoll Ave., La Canada, CA 91011-3364, USA
e-mail: harrisaw@colorado.edu
[6] INAF-Osservatorio Astronomico di Torino, Strada Osservatorio 20, 10025 Pino Torinese (TO), Italy
e-mail: dotto@to.astro.it
[7] INAF-Osservatorio Astronomico di Roma, Via Frascati 33, 00040, Monte Porzio Catone (Roma), Italy
[8] Astronomical Observatory, Adam Mickiewicz University, Sloneczna 36, 60-286 Poznan, Poland
e-mail: tmich@amu.edu.pl
[9] CAAUL, Tapada da Ajuda, 1349-018 Lisboa, Portugal

Received 27 May 2002 / Accepted 17 October 2002

Abstract. A physical portrait based on spectral and photometric data of 4979 Otawara, the first asteroid target of the Rosetta mission, is presented. The aim of this work is to investigate the composition of 4979 Otawara and to evaluate its rotation pole orientation. The spectroscopic observations obtained at the Palomar 200″and IRTF telescopes cover the wavelength range 0.4 to 2.5 μm, and provide a definitive classification of Otawara as an S-type asteroid. An analysis of band depths and slopes places Otawara in the S(IV) subgroup, suggesting a similarity to ordinary chondrite meteorites.
Moreover we present new photometric data, obtained at the Asiago Observatory and at the TNG telescope, that allow confirmation of the fast rotational period of 2.707 ± 0.005 hours, and a first indication of the spin vector of Otawara.

Key words. planets and satelites: individual: Otawara – minor planets, asteroids

1. Introduction

Rosetta is the cornerstone mission of ESA devoted to the study of minor bodies of the Solar System. The mission will be launched in January 2003 and has as its primary target 46P/Wirtanen, a short period comet in the Jupiter family whose rendezvous will be in November 2011. During its cruise to comet Wirtanen, the Rosetta spacecraft will encounter two main belt asteroids: 4979 Otawara and 140 Siwa. Rosetta will fly by Otawara on 11 July 2006, at a heliocentric distance of 1.89 AU, with a minimum encounter distance of 2200 km and a relative velocity of about 10 km s^{-1}. The Siwa flyby will occur on 24 July 2008 at 2.75 AU from the Sun, at a minimum distance of 3500 km. The goals of the mission during the asteroid encounters will be a complete determination of their physical properties (size, shape, density, mass, rotational properties), the study of their composition, and the investigation of the neighbouring space in order to detect possible satellites.

Send offprint requests to: S. Fornasier,
e-mail: fornasier@pd.astro.it

⋆ Based on observations obtained at the IRTF Observatory, Hawaii, USA, at the Palomar Mountain Observatory, California, USA, at the TNG telescope, La Palma, Spain and at the Asiago Astrophysical Observatory, Asiago, Italy.

Table 1. Orbital and physical characteristics of 4979 Otawara. [a] data from Doressoundiram et al. (1999).

perihelion distance (AU)	1.855
aphelion (AU)	2.481
semimajor axis (AU)	2.169
eccentricity	0.144
inclination (degrees)	0.912
synodical rotation period (hrs)	2.707 ± 0.005^a
taxonomy	S or V[a]
absolute magnitude	14.08 ± 0.04^a (S − type)
circular effective radius	2.0 km[a] (S − type)
density	$\geq 1.9^a$

Otawara is a small main-belt asteroid. At the time of Rosetta asteroid target definition, very little was known about the physical properties of this object. Successive international campaigns have revealed that Otawara is a very interesting target; it has a rotational period of only 2 hours and 42 min (Doressoundiram et al. 1999). It will be the first fast rotating asteroid encountered by a space mission. The fast rotation of Otawara will enable Rosetta to image and measure the asteroid's characteristics during one complete rotation.

In this paper we present the first near infrared spectrum of Otawara that definitively determines its taxonomic class. We add also a new visible spectrum of the object and new photometric data that confirm the rotational period value previously determined by Doressoundiram et al. (1999), and Le Bras et al. (2001) and allow a first estimation of the spin vector state.

This information will aid Rosetta mission planners in optimising the encounter trajectory and planning of science operations.

2. Observations and data reduction

2.1. Photometric measurements

Photometric observations of Otawara were carried out at the Asiago Astrophysical Observatory, Italy, and at the Telescopio Nazionale Galileo (TNG), La Palma, Spain. Unfortunatly, 2 nights devoted to Otawara observations at the Asiago telescope were lost due to bad weather conditions, and we could observe only partially during two other nights (one at the Asiago telescope and one at the TNG telescope) in poor photometric conditions. So for both nights only relative photometry between the asteroid and some field comparison stars was possible.

At Asiago we observed on 23 December 2001 using the 1.82 m telescope equipped with the AFOSC camera and a 1024×1024 pixel CCD, with a total field of view of 8.14×8.14 arcmin. The pixel size is 24 μm and the pixel scale is 0.473 arcsec/px. Our measurements were made with a *V* filter (Johnson) and 300–420 s of exposure time. At the TNG 3.5 m telescope we observed on 8 January 2002, with the OIG camera equipped with a mosaic of two thinned and back-illuminated EEV 42–80 CCDs with 2048×4096 pixels each (pixel size of 13.5 microns). The resulting pixel scale is 0.072 arcsec/pix for a total field of view of about 4.9×4.9 arcmin. We observed both in *V* and *R* filters (Johnson) and the exposure times ranged from 60 to 360 s.

Data reduction was performed in the following way: images were bias subtracted and divided by a flat field (computed as a median of several flat fields obtained during twilight), then relative magnitudes were computed using aperture photometry. We used an aperture radius of about twice the average seeing, and sky subtraction was performed using a 5–10 pixels wide annulus around the asteroid or reference stars.

2.2. Visible spectrum

The visible spectrum of Otawara was obtained at Palomar Mountain Observatory on 23 December 2001 with the 200-inch (5-m) telescope equipped with the Double Spectrograph (see Fig. 2). The instrument simultaneously obtains the blue and red halves of a long slit spectrum using a pair of CCD cameras. Different focal lengths of the two cameras give a pixel scale of 1.25 and 0.94 arcsec per pixel (the 2×2 binned mode was used) respectively for the blue and red channels. A 300 line/mm grating was used for the blue channel, covering a spectral range of 0.42 to 0.62 μm and giving a dispersion of 7 Å per binned pixel. A 158 line/mm grating was used for the red part, covering the wavelength range from 0.53 to 0.92 μm with a dispersion of 10 Å per binned pixel. The final spectrum is the mean of three blue/red pair exposures of 600 s each. A slit of 6 arcsec was used to acquire the data, oriented in a N–S direction in order to minimize effects due to differential atmospheric refraction for objects observed near the meridian. Solar analog stars were observed at airmasses close to that of Otawara.

Data were reduced following usual reduction procedures for visible spectroscopy (see Bus 1999; Xu et al. 1995). Upon extraction each spectrum was rebinned to a uniform dispersion of 25 Å/px and the solar contribution was removed by division by a solar analog star. All the spectra were normalized at 5500 Å.

2.3. Infrared spectrum

The infrared spectrum of Otawara was obtained at the NASA Infrared Telescope Facility (IRTF), Hawaii, USA, equipped with the medium-resolution infrared spectrograph SpeX and employing a 1024×1024 InSb array (Rayner et al. 1998). Each exposure consisted of 32 non-destructive reads providing a readout noise of about 15 e^- RMS. Otawara was observed on 12 January 2002 in remote mode from the Observatoire de Paris-Meudon. The instrument was used in the low-resolution prism mode that allows a single exposure to cover the wavelength range from 0.8 to 2.5 μm, with a dispersion of about 50 Å per pixel. The observations were made using a slit of 0.8 arcsec (oriented in the N–S direction) nodding the object along the spatial direction of the slit (offset of 7.5 arcsec), in order to obtain alternated pairs of exposures (denoted as A and B). This procedure allows a very close sky and bias measurement in the same pixel positions as the spectral measurement. A sequence of 9 cycles, each one of the type ABBA, with four exposures of

Table 2. 4979 Otawara: observational circumstances, where r and Δ are respectively the heliocentric and geocentric distances of the asteroid, α the phase angle of the asteroid at the time of observations and m_v is the predicted magnitude from the JPL ephemeris service. The date indicated is relative to the beginning of observations; the symbol * means that observations ended the following day.

Date	UT start	UT end	Telescope	Mode	Instrument	m_v	r (AU)	Δ (AU)	α
23 Dec. 01	08:54	09:18	Palomar 200″	Vis. spectrum	Double Spec.	17.27	2.480981	1.512879	5°.16
23 Dec. 01	21:48	01:43*	Asiago 1.8 m	V imaging	AFOSC	17.26	2.480928	1.511215	4°.87
08 Jan. 02	21:47	01:25*	TNG 3.5 m	$V + R$ imaging	OIG	17.15	2.478565	1.501553	3°.32
12 Jan. 02	09:55	11:21	IRTF 3.0 m	IR spectrum	SpeX	17.26	2.477813	1.509438	5°.09

2 min each, was obtained for a total integration time of 72 min. The object was observed on the meridian, with an airmass less than 1.1, in order to minimize effects due to differential refraction. A solar analog star, Hyades 64, was observed just before and after (and at very similar airmasses) as the object and was used to normalize the reflectance spectrum of the asteroid. Flat field and arcline spectra were also acquired for data calibration.

Data reduction was performed in the traditional way for IR observations: first spectra were corrected for flat fielding, then bias and sky subtraction was performed by producing A–B and B–A frames. The next step involved shift and add of the positive spectrum of (B–A) frame on the positive spectrum of A–B frame. The final spectrum (Fig. 2) is the result of the mean of all pairs of frames previously combined. The spectrum was then extracted and wavelength calibrated using the arcline spectrum of an Argon lamp. Finally, the extinction correction and solar removal was obtained by division of the asteroid spectrum with that of the solar analog star Hyades 64.

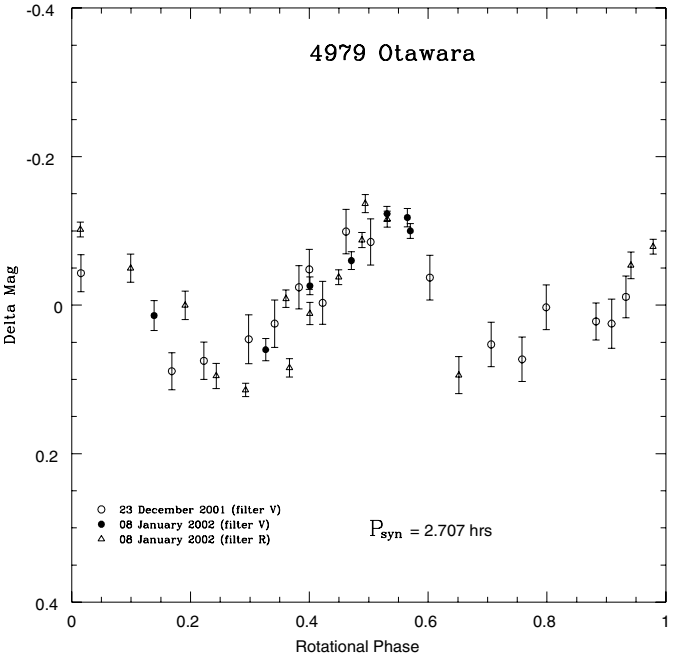

Fig. 1. Composite lightcurve of 4979 Otawara. The error bars contain the photon noise. The zero phase is at JD 2 452 276.5.

3. Analysis

3.1. Lightcurve and spin state

The synodic rotational period was determined by applying a Fourier analysis to our photometric data, as described by Harris et al. (1989). The value of the synodic rotational period that best fits our observations is $P_{\rm syn} = 2.707 \pm 0.005$ hours. This result was already found by Doressoundiram et al. (1999) and confirmed by Le Bras et al. (2001). Figure 1 shows the composite lightcurve obtained by combining in rotational phase all of our photometric data.

Since no absolute calibration was obtained, due to the non-photometric sky conditions, an offset was applied to each night of data, in order to center the lightcurve on the mean brightness of the asteroid. R-filter and V-filter composite lightcurves, which show similar behaviour, have been superimposed. The obtained amplitude is 0.22 ± 0.03 mag.

The spin vector, sidereal period, and triaxial ellipsoid model for a given asteroid can be determined using the method described by Michałowski (1993). In this method the epochs of brightness maxima, amplitudes and magnitudes are considered. The results are obtained by building a set of nonlinear equations whose solution is found by the least square fitting.

We have been able to use for Otawara the epochs, amplitudes and R magnitudes from December 1998–January 1999 (Doressoundiram et al. 1999) and July–August 2000 (Le Bras et al. 2001) and only the epochs and amplitudes obtained in December 2001–January 2002 (this paper). The ecliptic longitude (λ) and latitude (β) of Otawara during these observations are the following:

Date	λ	β
23 Jan. 1999	123.5°	+ 1.0°
06 Aug. 2000	314.3°	− 1.3°
01 Jan. 2002	101.9°	+ 0.6°

It should be noted that these observations were obtained from rather similar geometric configurations of Otawara as the difference in ecliptic longitudes between the 1998/99 and 2001/02 oppositions was smaller than 30° and the longitude difference was close to 180° between 2000 and 1998/99 apparitions. For that reason, the available observational data are far from ideal as required for the method mentioned above. The observed amplitudes of Otawara have been reduced to zero phase angle with the *amplitude-phase* relationship described by Zappala et al. (1990). The correction coefficient was found to be $m = 0.006$. The HG-magnitude system (Bowell et al. 1989) has allowed us to reduce the R magnitudes to zero phase angle and we have obtained $G_R = 0.19$.

Despite the limitation in the observational data we have obtained some preliminary results for Otawara. The sense of rotation seems to be retrograde. The sidereal period ($P_{\rm sid}$), the ecliptic coordinates of the asteroid north pole ($\lambda_{\rm p}, \beta_{\rm p}$), the a/b ratio of the triaxial ellipsoid shape, the absolute R magnitude for the aspect 90° $H_R(90, 0)$, and their formal errors are as follows:

$P_{\rm sid} = 0.112776 \pm 0.000001$ (days)
$\lambda_{\rm p} = 50° \pm 5°$
$\beta_{\rm p} = -30° \pm 16°$
$a/b = 1.21 \pm 0.05$
$H_R(90, 0) = 13.99 \pm 0.05$ (mag).

A second solution with the same parameters and $\lambda_{\rm p} = 230°$ has also been obtained.

According to these results, Otawara was observed close to equatorial aspects (≈90°). Careful examination of the relation between aspect, pole and asteroid ecliptic coordinates (Eq. (4) in Michałowski 1993) shows that equatorial aspects do not practically depend on pole latitude when the asteroid latitude is close to 0°, as it is for Otawara. This is probably the reason for the large formal error in $\beta_{\rm p}$.

A spurious value of the b/c ratio (2.3 ± 0.9) of the triaxial ellipsoid shape comes out of the formal solution, but in this case it does not diminish the validity of the rest of the solution. In fact, the *amplitude–aspect* and *magnitude– aspect* relationships (Eqs. (3) and (5) in Michałowski 1993, respectively) show that observed amplitudes and magnitudes do not depend on b/c for aspects close to equatorial ones. Therefore, we can assume that the value for b/c and its formal error are solution artifacts and not real. Furthermore, because of the rapid spin rate, if the polar flattening b/c is significantly greater than 1.0, a state of tensile stress would be implied. This is highly unlikely for an asteroid of this size, thus we expect b/c is not greater than about 1.2.

In order to obtain the full model for Otawara we need further observations carried out for aspects far from equatorial ones. The best observations will be during the oppositions when the ecliptic longitudes of Otawara are in the range 0°–70° or 180°–250°.

The next oppositions of Otawara will be in June 2003, with an ecliptic longitude (λ) of 263°, in December 2004 with λ = 81°, in April 2006 with λ = 216°, in November 2007 with λ = 58°, in March 2009 with λ = 180°. So the oppositions from 2006 to 2009 fall in the desirable ecliptic longitude range.

Further ground observations are needed to improve the spin vector of Otawara, even if only the opposition in April 2006 seems to have an orbital configuration suitable for a better pole determination before the spacecraft flyby in July 2006.

3.2. Spectral analysis

In Fig. 2 the combined visible and infrared spectra of Otawara are shown. The visible data are normalized at 5500 Å and the overlap between visible and infrared spectra was performed by shifting the infrared data with a scaling factor derived by minimizing the chi-squared value of polynomial fitting to both visible and IR data. A first analysis of the spectrum allows us to determine that Otawara is an S-type asteroid. Based on only the visible spectrophotometric data, Doressoundiram et al. (1999) determined that their spectrum could be consistent with either a S- or V-type asteroid. From our IR data we can exclude any link between Otawara and V class due to the very small 2-micron absorption compared to that of a typical V asteroid. The shape of the spectrum over the wavelength interval 0.42–2.50 μm is consistent with an S-type object.

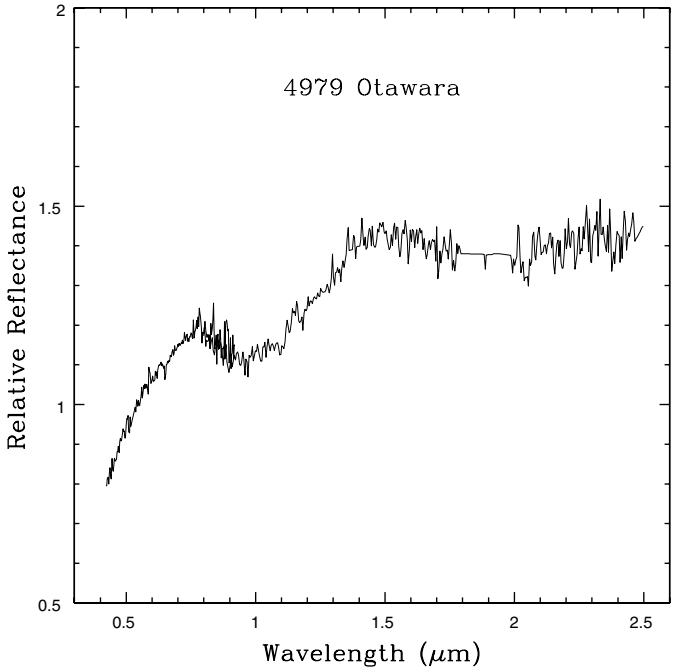

Fig. 2. Visible and infrared spectral reflectance of 4979 Otawara. The noise introduced by water band at 1.8 μm has beed excluded. The spectrum is normalized at 5500 Å.

We also compared our visible data obtained from Palomar with the visible spectrum published by Doressoundiram et al. (1999). Even though the previously published spectrum is noisier than our data, the spectral behaviour is exactly the same, confirming the visible trend previously observed.

In order to investigate possible variations of the surface properties during the rotational period, we examined the IRTF near infrared data time over 3 intervals (named I, II, III), each of them with 24 min of exposure time. The total elapsed time is 86 min, corresponding to 53% of the rotational period of the asteroid. The central universal time of each of these interval is 10:08, 10:36 and 11:06, corresponding to a rotational phase of 0.40, 0.57 and 0.76 respectively. These spectra were filtered with a median filter (box size of 39 points) since they were noisier than the spectrum obtained with the total exposure.

There is no obvious difference between the three composite spectra shown in Fig. 3, meaning that for almost half of the rotational period Otawara's composition is homogeneous within ±5–10% variation, the limit of our precision.

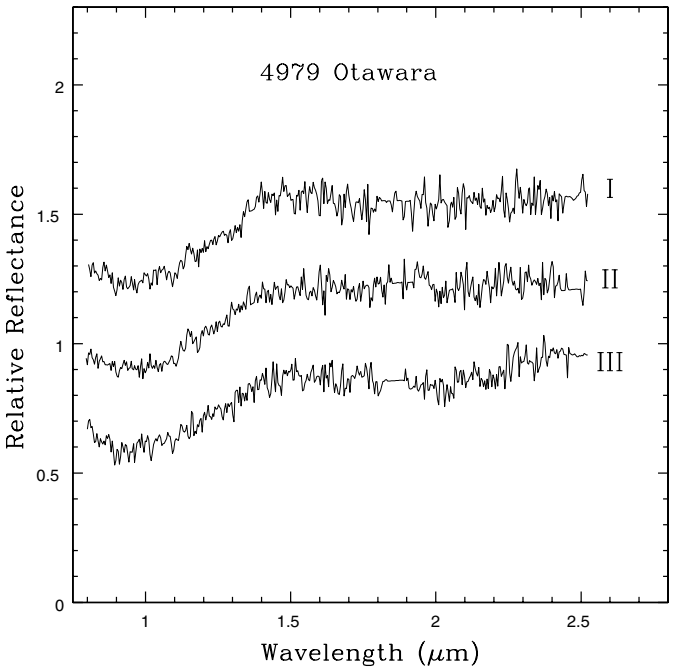

Fig. 3. Infrared spectra of 4979 Otawara: I is the spectrum relative to the first 24 min of integration, II that relative to the following 24 min and III that relative to the last 24 min (the total exposure time was 72 min). Spectral data have been normalized at 1.25 μm; spectra I and III are vertically shifted by 0.3 for clarity.

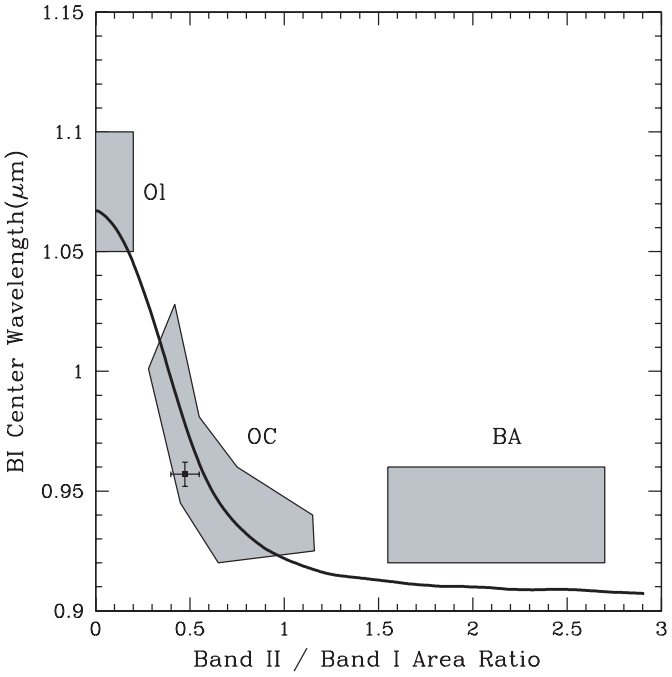

Fig. 4. BI center versus the Band II/Band I area ratio for 4979 Otawara (squared point). The three background regions are defined by meteorite spectra by Gaffey et al. (1993). The Ol rectangular region includes essentially monomineralic olivine assemblages; the OC polygonal region represents the mafic silicate components of ordinary chondrites and corresponds to the location of the S(IV) subtype in the Gaffey et al. classification scheme (1993); the BA rectangular zone includes the pyroxene dominated basaltic achondrites assemblages. The heavy solid line indicates the location of the olivine-orthopyroxene mixing line (Cloutis et al. 1986).

We tried to better analyze the data in order to identify which S subclass of the Gaffey et al. (1993) classification scheme best describes the Otawara spectrum. In this classification, the S class is divided into 7 subclasses on the basis of the area ratio between the 2 μm/1 μm band, the center position of these two bands, the depth and slope of the 1 μm absorption, as these parameters are intrinsically related to the mineralogy of the asteroid surface.

The analysis of the spectrum (see the procedure described by Gaffey et al. 1993) gives the center position of the band BI (that around 1 micron) at 0.9570±0.0050 μm, with a band depth of 0.18±0.01 and a spectral slope of 0.0804% per 1000 Å (evaluated from 0.75 μm to 1.45 μm). This band is due to the presence of both olivine and pyroxene. Regarding the band around 2 μm, associated with the presence of pyroxene, it is centered at 1.9780 ± 0.0050 μm and has a band depth of 0.07 ± 0.01.

The 2 μm/1 μm band area ratio is 0.47 ± 0.09. On the basis of these values 4979 Otawara is well placed in the space of S(IV) class (see Fig. 4).

4. Comparison to ordinary chondrites

The assignment of Otawara to the S(IV) subclass is particularly interesting as the S(IV) asteroids are characterized by a composition that includes the silicate components of the ordinary chondrites. S(IV) members are the most probable candidates for parent bodies of ordinary chondrites among the S-type asteroid population (Gaffey et al. 1993; Gaffey 2000, 2001). For this reason, we want to investigate the possible links with OC meteorites.

Plotting the BI band center position versus Band II/Band I area ratio places Otawara in the ordinary chondrite (OC) field (Fig. 4), lying near the olivine-pyroxene mixing line. This similarity to OC meteorites implies that Otawara is not a differentiated asteroid.

We analyzed the percentage of orthopyroxene present on Otawara, using the method suggested by Cloutis et al. (1986):

$$\mathrm{OPX}(\%) = \frac{\mathrm{OPX}}{\mathrm{OPX} + \mathrm{OL}} = 0.4187 \times (\frac{\mathrm{BII}}{\mathrm{BI}} + 0.125) \qquad (1)$$

where OPX is the orthopyroxene mass fraction, OL the olivine mass fraction and BI and BII are the band area corresponding to the 1 and 2 micron absorptions, respectively.

This method was recently tested by Gaffey (1999) and Berthoud et al. (2001) on samples of ordinary chondrites, finding good agreement between the orthopyroxene abundance computed and the normative abundances derived from chemical analysis (Jarosewich 1990; McSween et al. 1991). For Otawara we find a percentage of 25 ± 3 of orthopyroxene, consistent with the abundance typical of L and LL ordinary chondrites.

In fact S(IV) objects are composed of olivine-orthopyroxene (Ca-poor) mixtures which could be representative assemblages that are similar to undifferentiated ordinary chondrites but also to unmelted silicate portions of primitive achondrite. As the band depth at 2 μm of measured

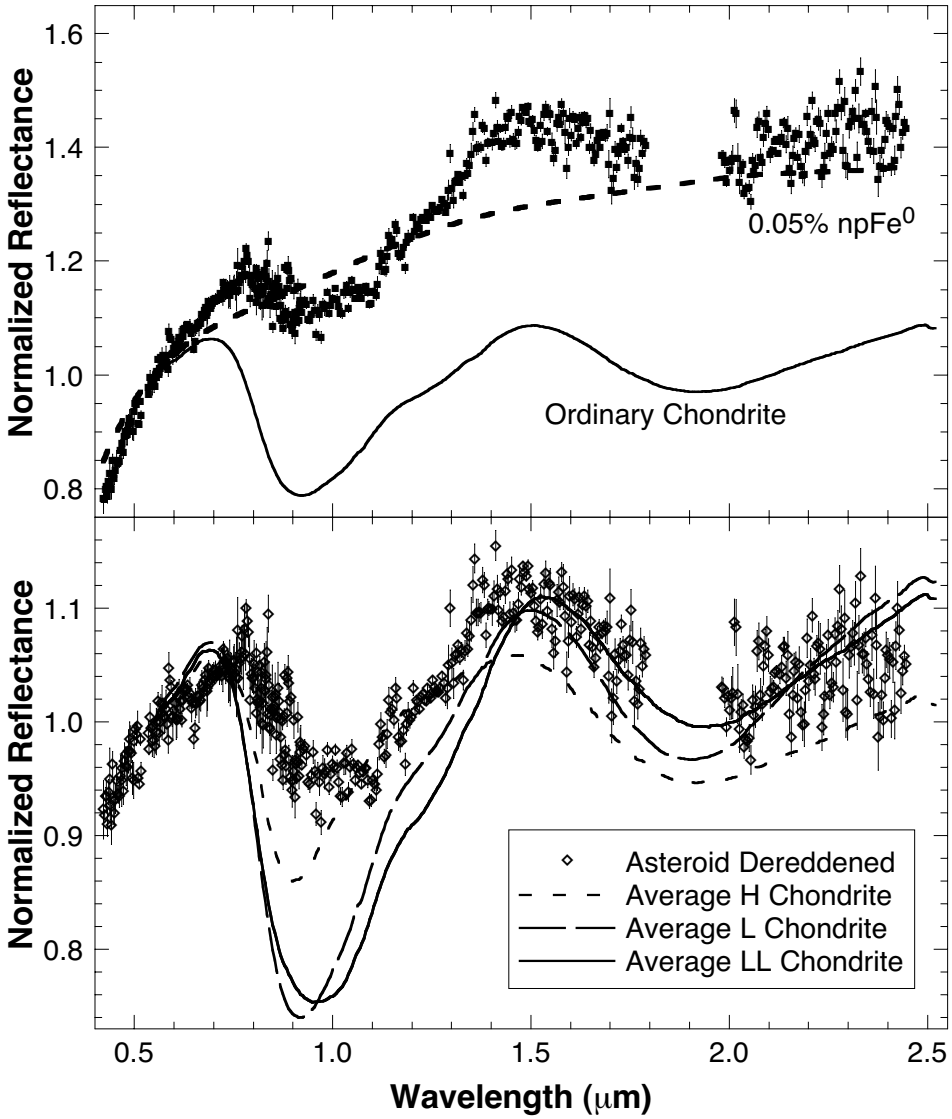

Fig. 5. Top panel: combined near-infrared plus visible spectrum of 4979 Otawara (data points), where the gap at 1.9 μm is due to telluric water. For comparison, the dashed curve shows the reddening model for the presence of 0.05% nanophase iron (npFe^0) as determined by Pieters et al. (2001). The neutral slope of an ordinary chondrite meteorite (average LL chondrite) is shown for comparison. Bottom panel (with the vertical scale expanded to twice that of the top panel): Otawara spectrum (data points) de-reddened for 0.05% nanophase iron. Spectral slope and location of the 1 μm and 2 μm bands are consistent within the range of properties for ordinary chondrite meteorites (lines). All spectra are normalized to unity at 0.55 μm. Meteorite spectra are from Gaffey (1976).

primitive achondrites is greater than that for S(IV) asteroids (Burbine et al. 2001; Binzel et al. 2001a), we tried to make a comparison between Otawara and representative ordinary chondrites.

However, as has long been noted (see for example Wetherill & Chapman 1988) and is evident in the upper panel of Fig. 5, spectra of S-class asteroids are significantly reddened compared with this meteorite analog, and this difference could probably be explained by space weathering effects. This process may be the result of dust impacts and solar wind sputtering on the surface of atmosphereless bodies and gives rise to a reddening of the spectral slope, a decrease of spectral absorption intensities and a diminishing of albedo. In fact surfaces of atmosphereless bodies exposed to the space environment for millions to billions of years are inevitably altered in physical, optical and/or chemical properties, as first demonstrated by analysis on the lunar soils (see for example Adams et al. 1971; Hapke et al. 1975).

While the effects of space weathering processes have long been debated, new results are supporting their validity. The Galileo mission for the first time demonstrated that a kind of alteration affects the surfaces of Gaspra, Ida and Dactyl (three S-type asteroids), modifying the reflectance spectra of fresh material to be redder, straighter and with shallower absorption bands, as reported by Chapman (1996). Recently the NEAR mission to 433 Eros (another S-type object) allowed a determination, thanks to X-ray and near-infrared spectrometer measurements, of an ordinary chondrite composition of Eros despite a red sloped, S-type spectrum, suggesting once again that some process such as reddening and/or darkening has altered the optical properties of the surface (Clark et al. 2000; Chapman 2000; McFadden et al. 2001; Bell et al. 2002).

Recent work of Binzel et al. (2001b) shows also that there is a continuous transition in the spectral behaviour between a sample of small S-Q type Near Earth Objects and that of ordinary chondrites, arguing that a continuous natural process such as space weathering could affect these bodies in different ways, depending on their age and collisional history.

Moreover Pieters et al. (2000) demonstrated that the spectral properties of S-type asteroids are well modeled by the space weathering of ordinary chondrite material that is associated with accumulation of reduced nano-phase iron on soil grains. This kind of model was also successfully applied by Binzel et al. (2001a) for the interpretation of spectral differences between asteroid (25143) 1998 SF36, the S(IV) target of MUSES-C mission, and ordinary chondrites.

Following the de-reddening model developed by Binzel et al. (2001a), we divide the spectrum of Otawara by the curve for the minimal (0.05%) component of nanophase iron. The results are shown in the lower panel of Fig. 5. We find an excellent match (within the noise of our spectrum) to the typical slopes for ordinary chondrite meteorites. Speculating on a more specific match, however, remains problematic. We find the 1 μm band depth is shallow relative to the meteorite comparisons, but most consistent with the H chondrites. However, perhaps more diagnostic is the 1 μm band center which is most consistent with LL chondrites, as is the depth of the 2 μm band.

Thus, while we slightly favor an analogy between Otawara and LL chondrites, (based on the preceeding analysis and our OPX analysis), we consider this only a tentative result.

5. Conclusion

In conclusion, our results can be summarized as follows:

1. Our combined visible and infrared spectral data of Otawara put this object in the S taxonomic class composed of olivine and orthopyroxene.
2. Following the Gaffey et al. classification scheme (1993), Otawara belongs to the S(IV) subgroup.
3. A comparison between Otawara and H, L and LL ordinary chondrites shows the typical differences found in the literature between these meteorites and S-asteroids. Otawara could be a potential parent body of OC meteorites as the spectral reddening and shallow absorption features compared to OC spectra are consistent with trends that may be caused by space weathering processes. In fact a spectral analysis using current models for space weathering shows that the presence of only 0.05% nanophase iron may account for the spectral slope difference between Otawara and ordinary chondrite meteorites.
4. Our lightcurve data confirm the fast rotation period of Otawara ($P_{\rm syn}$ = 2.707 ± 0.005 h) previously determined by other authors.
5. A first estimation of the complete spin state is presented with most likely a retrograde sense of rotation. Further observations during upcoming apparitions are needed to verify and improve this result.

All this information will allow the Rosetta scientists and mission planners to optimise the science operation planning during Otawara flyby, but only the analysis of the Rosetta data will permit a much more detailed investigation of the physical and compositional properties of 4979 Otawara.

Acknowledgements. The authors thank L. McFadden and P. Weissman for their detailed reviews and suggestions, and T. Cline who provided data for meteorite fields. Spin vector determination was performed after a suggestion by A. Erikson. T.M. was supported by the Polish KBN Grant 2 P03D 007 18.

References

Adams, J. B., & McCord, T. B. 1971, Proc. 2nd Lunar Sci. Conf., 2183
Bell, J. F., Izenberg, N. I., Lucey, P. G., et al. 2002, Icarus, 155, 119
Berthoud, M. G., Bell, J. F., Clark, B. E., & Gaffey, M. J. 2001, Lunar Planet. Sci., 32, 2080
Binzel, R. P., Rivkin, A. S., Bus, S. J., Sunshine, J. M., & Burbine, T. H. 2001a, Meteorit. Planet. Sci., 36, 116
Binzel, R. P., Harris, A. W., Bus, S. J., & Burbine, T. H. 2001b, Icarus, 151, 139
Bowell, E., Hapke, B., Domingue, D., et al. 1989, in Asteroids II (Univ. of Arizona Press, Tucson), 524
Burbine, T. H., McCoy, T. J., Nittler, L. R., & Bell, J. F. 2001, Lunar Planet. Sci., 32, 1860
Bus, S. J., Ph.D. Thesis, Massachusset Institute of technology, Cambridge, MA, USA
Chapman, C. R. 1996, Meteoritics & Plan. Sci., 31, 699
Chapman, C. R., & Near MSI-Nis Team 2000, Meteoritics & Plan. Sci., 35, 39
Clark, B. E., Bell, J. F., Veverka, J., et al. 2000, Meteoritics & Plan. Sci., 35, 41
Cloutis, E. A., Gaffey, M. J., Jackowski, T. L., & Reed, K. L. 1986, J. Geoph. Res., 91, 11641
Doressoundiram, A., Weissman, P. R., Fulchignoni, M., et al. 1999, A&A, 352, 697
Gaffey, M. J. 1976, J. Geoph. Res., 81, 905
Gaffey, M. J., Burbine, T. H., Piatek, J. L., et al. 1993, Icarus, 106, 573
Gaffey, M. J. 1999, Lunar Planet. Sci., 30, 1375
Gaffey, M. J. 2000, Lunar Planet. Sci., 31, 1092
Gaffey, M. J. 2001, Lunar Planet. Sci., 32, 1587
Hapke, B., Cassidy, W., & Wells, E. 1975, The moon, 13, 339
Harris, A. W., Young, J. W., Bowell, E., et al. 1989, Icarus, 77, 171
Jarosewich, E. 1990, Meteoritics, 25, 323
Le Bras, A., Dotto, E., Fulchignoni, M., et al. 2001, A&A, 379, 660
Michałowski, T. 1993, Icarus, 106, 563
McFadden, L. A., Wellnitz, D. D., Schnaubelt, M., et al. 2001, Meteoritics & Plan. Sci., 36, 1711
McSween, H. Y., Bennett, M. E., & Jarosewich, E. 1991, Icarus, 90, 107
Pieters, C. M., Taylor, L. A., Noble, S. K., et al. 2000, Meteoritics & Plan. Sci., 35, 1101
Rayner, J. T., Toomey, D. W., Onaka, P. M., et al. 1998, Proc. SPIE, 3354, 468-479
Wetherill, G. W., & Chapman, C. R. 1988, Asteroids and meteorites, in Meteorites and the Early Solar System, ed. J. F. Kerridge, & M. S. Matthews (University of Arizona Press, Tucson, Arizona), 35
Xu, S., Binzel, R. P., Burbine, T. M., & Bus, S. J. 1995, Icarus, 115, 1
Zappala, V., Cellino, A., Barucci, M. A., et al. 1990, A&A, 231, 548

Astronomy & Astrophysics manuscript no. 2506Vern February 8, 2005
(DOI: will be inserted by hand later)

Analysis of near-IR spectra of 1 Ceres and 4 Vesta, targets of the Dawn Mission⋆

P. Vernazza[1], T. Mothé-Diniz[1], M.A. Barucci[1], M. Birlan[2], J.M. Carvano[1], G. Strazzulla[3], M.Fulchignoni[1], A. Migliorini[1,4]

[1] LESIA, Observatoire de Paris, 92195 Meudon Pricipal Cedex, France
e-mail: pierre.vernazza@obspm.fr

[2] IMCCE, Observatoire de Paris, 77 av Denfert Rochereau, 75014 Paris Cedex, France[2]

[3] INAF-Osservatorio Astrofisico di Catania, via Santa Sofia 78, I-95123 Catania, Italy

[4] Dipartimento di Astronomia di Padova, Vicolo dell'Osservatorio 2, 35122 PAdova, Italy

Received June, 2004

Abstract. We have obtained high signal to noise spectra of the two targets of the Dawn mission, 4 Vesta and 1 Ceres from observations carried out in remote control between the Observatoire de Paris-Meudon and the NASA Infrared Telescope Facility on Mauna Kea. 4 Vesta has been observed in the 0.7-2.5 μm spectral region at three different rotational phases in order to i) determine the mineral composition; ii) understand the spectral variations across the surface. Vesta has also been observed in the 2.0-3.8 μm range. The 3 μm absorption feature has not been detected, implying the absence of OH and/or H2O-bearing minerals on the asteroid surface at the latitude of our observations. The spectra of 1 Ceres has been obtained in the 2.0-4.1 μm range and the presence of the 3.06 μm absorption feature has been confirmed. Laboratory measurement of ion-irradiated organics and ices suggest that the 3.06 μm feature can be reproduced with a linear mixture of crystalyne ice and residues of ion-irradiated asphaltite.

Key words. Vesta - Ceres - spectroscopy - Dawn Mission

1. Introduction

4 Vesta and 1 Ceres are the two asteroids which will be visited by the Dawn space mission. Dawn is a NASA Discovery mission scheduled to be launched in June 2006 arriving at Vesta in 2011 and at Ceres in 2015. The spacecraft will orbit for several months around each object with the aim of understanding the origin and evolution of the solar system by obtaining geophysical

Send offprint requests to: P. Vernazza, pierre.vernazza@obspm.fr

⋆

and geochemical data on these diverse main belt asteroids. Ceres is the largest asteroid with a mean diameter of 950 km, while Vesta is the third largest asteroid with a mean diameter of 516 km. They are among the most massive asteroids: 4 Vesta (2.75×10^{20} kg) and 1 Ceres (9.43×10^{20} kg) (Standish & Hellings 1989). They could be considered as small planets and due to their location, they could have experienced many of the processes that are generally associated with the planetary evolution. Ceres is an undifferentiated protoplanet while Vesta has experienced significant heating and differentiation. Vesta and Ceres formed by accretion of smaller objects over short time scales, and even if they are supposed to have been formed at relatively close areas of the main belt, they are very different objects.

Vesta is the only large asteroid known to have a basaltic surface that retains a record of ancient volcanic activity. The basaltic nature on Vesta was discovered through visible spectroscopy with ground-based telescopes (McCord et al. 1970). The Vesta unique reflectance spectra and its high albedo 0.42 (Tedesco 1989) compared to other asteroids defined a new taxonomic class (type V). Geological diversity revealing longitudinal variations in albedo and mineralogy was detected from various observational techniques obtained at different rotational phases and aspect angles. The high geological interest on this asteroid followed the discovery that howardite, eucrite, and diogenite (HED) meteorites could be samples excavated from Vesta. In 1996, Vesta made its closest approach to Earth and observations with WFPC2 (HST) allowed to obtain images at a scale of 36 km/pixel providing coverage of the southern hemisphere (Thomas et al. 1997). The surface of Vesta is not uniform, showing some dark and bright areas. The Hubble Space Telescope has also revealed a very large, circular cavity near the asteroid's south pole. The 460-km-wide basin has a pronounced central peak of 12 km. The diversity of the surface made Vesta as the most geological peculiar asteroid. The origin and the history of Vesta are until now far to be understood, as this object is an exception among the largest asteroids. Keil (2002) has provided a review on the present knowledge of Vesta.

We know less about the composition of Ceres, which has a low albedo 0.11 (Tedesco 1989), a quasi-spherical shape and few spectral features. The reflectance spectra is flat and featureless in the visible with an absorption band near 3 μm associated to hydrated minerals (Lebofsky et al. 1981) and/or ammoniated saponite by King et al. (1992). Microwave studies suggest that Ceres is covered by a dry clay that reflect its crustal composition (Webster et al. 1988). There are no clear links between Ceres and any known meteorite, and McCord & Sotin (2003) suggested that the thermal evolution of Ceres could have produced a metamorphosed carbonaceous chondrite surface material producing a surface with an albedo higher than the original materials. Recent publications (Parker et al. 2002; Britt et al. 2002) summarized the present knowledge of Ceres. Ceres represents a mysterious and probably unique object in the solar system representative of the early phase of the planet formation.

In this work we present new spectra of Vesta in the near-infrared (0.7-2.5μm and 2.0-4.1 μm) obtained at various rotation phases and a spectrum in the range 2.0-4.1 μm for Ceres. The obtained results are analysed and discussed.

2. Observations and data reduction

2.1. Observations

The spectra presented in this work were obtained at the Infrared Telescope Facility (IRTF), a 3 m telescope located at the summit of Mauna Kea, Hawaii. Observations were remotely conducted from Meudon-France, more than 12,000 km away from Hawaii, using several informational structures and networks. This type of observations between Meudon and IRTF/Hawaii was started in 2002 (Birlan et al. 2002); since then, more than thirty nights of observations were conducted from Meudon.

Two observing runs in March 2003 and January 2004 were devoted to near-infrared observations of 4 Vesta and 1 Ceres respectively. The spectrograph SpeX, combined with the 0.8 x 15 arcsec slit were used for acquisition of spectra, in the range 0.7-4.1 μm . All observations were made with pairs of exposures named 'A' and 'B' which allowed us to produce simultaneous measurements of the object and the sky.

4 Vesta was observed on March 30, in LowRes (R=200) prism mode for the spectral range 0.7-2.5 μm , while spectra in the range 2.0-4.1 μm (LXD mode, R=2000) have been acquired on March, 31. In order to monitor the asteroid during its rotational phase, several series of spectra were obtained. The observational circumstances for Vesta are presented in Table 1, which lists the date and time for each observation, the wavelength range, V magnitude, airmass and solar phase angle (α_s). In this table are also shown the sub-earth longitude of Vesta (W), the sub-earth latitude (ζ), calculated using the pole solution of Thomas et al.(1997), and the rotational phase calculated with respect of zero phase of Gaffey (1997) – hereafter G97 – extrapolated using Thomas et al. (1997) and Binzel et al. (1997). Unless otherwise stated, the Vesta spectra will be referred mainly by the rotational phase. During both nights the atmospheric conditions were not stable, with the occasional presence of thin clouds. This problem was carefully taken into account in the process of data-reduction (see section 2.2). During these nights, the humidity range was 25%-55%, and the values of the seeing were in the range 0.8-1.5 arcsec, while the temperature variations were between -1° C and +3.2° C. The observations of 4 Vesta were intercalated with those of standard stars Landolt 102-1081, HD88618, Landolt 107-684, Landolt 105-56, Landolt 107-998, Hya 64, and Landolt 98-978.

The asteroid 1 Ceres was observed on January, 25, 2004, in the spectral range 2.0-4.1 micron (LXD mode, R=2000). Observational circumstances are presented in Table 1. For the calibration of our spectra, these observations were alternated with those of Hya 64 and SAO 95394 standard stars. During these observations the humidity rate was high, almost 90%, the temperature was stable at -4^{o}C, and the seeing measurement was 1.1 arcsec.

Table 1. Observational circumstances for 4 Vesta and 1 Ceres with the associated phase angle(α_s), longitude(W), latutude(ζ), and rotational phase(Φ_W)

4 VESTA							
Day	**UT**	$\lambda(\mu m)$	**a.m.**	α_s	W	ζ	Φ_W
30mar03	10:03-10:04	0.7-2.5	1.02	5.8	238^o	-11^o	0.06
30mar03	12:16-12:17	0.7-2.5	1.13	5.8	27^o	-11^o	0.475
30mar03	13:10-13:26	0.7-2.5	1.34	5.8	88^o	-11^o	0.64
31mar03	10:05-10:35	2.0-4.1	1.02	6.0	57^o-91^o	101^o	0.56-0.65
31mar03	11:29-11:51	2.0-4.1	1.05	6.0	152^o-176^o	101^o	0.82-0.89
1 CERES							
25jan04	6:41-6:58	2.0-4.1	1.2				
25jan04	7:18-7:35	2.0-4.1	1.2				

2.2. Data reduction

Standard techniques for near-IR spectroscopy reduction have been used with the software Spextool 3.2 dedicated to the reduction of the data obtained with Spex. We started by creating normalized flat-fields for each observing night. Then we subtracted image pairs taken at two different positions (A and B) along the slit, in order to minimize the atmospheric and telescope influence and to remove the influence of electronic bias level and the dark current. Each background subtracted image was divided by the flat field image to remove pixel to pixel sensitivity variation on the chip. Then the data were extracted from two-dimensional images to one-dimensional arrays by summing pixels in the data range for each column. Finally, we performed the wavelength calibration of the spectra. Telluric absorptions were removed by dividing the asteroid spectra by stellar spectrum at the same airmass. We used a star observed close in airmass (±0.03) to make the division for both spectra at 10h03UT and 12h16UT (Tab1). For the third spectrum of Vesta, observed at an airmass of 1.34, we had no star close in airmass to make a good correction concerning the extinction coefficients. To perform the correction for extinction, we used the observations of a star obtained at a different period (IRTF, November 2003), but at the same airmass. To ensure that this process did not introduce any significant error, we divided the standard stars observed during the observation of Vesta by the stars with corresponding airmass observed on November 2003, spanning airmasses from 1.03 to 1.2. The division always produced a flat spectrum, which shows that the extinction coefficients did not vary considerably between the two nights. Nevertheless, the depth of the water vapour absorption bands were different from one night to another due to a different degree of humidity. To apply a correction for humidity, we used a so called transmission spectra (spectra of star observed at the same night as Vesta divided by a star observed in November with a same airmass for both stars) in the water zones. Thus, to obtain the final reflectance we divided the spectra of Vesta by a star obtained during November at

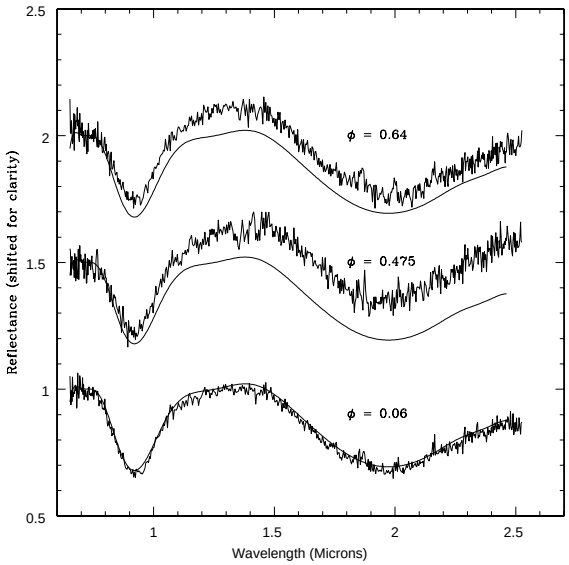

Fig. 1. Spectra of Vesta at each rotational phase, compared with the fit of the spectrum at Φ=0.06 (continuous line). The spectra were vertically displaced for clarity by 0.5.

same airmass to make the correction for extinction and multiplied bye the 'transmission' spectra in the water zones. The reduced spectra of Vesta in this range are shown in Fig. 1

We used the LXD mode (2.0-4.1 μm) fitting onto the array at a spectral resolving power of R= 2000 with a slit length of 15" and a slit width of 0.8". The 2.0-4.1 μm region is covered in two pieces, one from 2.0-2.55 μm, and another from 2.85-4.1 μm. The LXD mode allows simultaneous observations on both sides of the telluric water band at 2.55-2.85 μm. The 2.0-4.1 μm region is covered by 6 overlapping spectra. While relative fluxes within one observation will be correct, absolute fluxes cannot easily be compared from one integration to the next, and must be scaled to one another.

In order to have the reflectance spectrum of Vesta and Ceres, we made a correction for the thermal flux. The thermal radiation in the main belt starts to affect the data in the 3-μm region. To remove this thermal contribution, we used the standard thermal model developed by Lebofsky & Spencer (1989). This model assumes the situation of a non rotating spherical asteroid in instantaneous equilibrium with solar flux.

For Vesta, the thermal contribution to the total reflectance was less than 0.01% at 3.0 μm and 8% at 3.8 μm, and for Ceres, less then 0.3% at 3.0 μm and 70% at 4.1 μm. Of course, the thermal corrections remain model dependent and will have noticeable effects on the interpretation of our corrected spectra.

3. Results and Discussion

3.1. Vesta

The spectra of Vesta in the 0.7-2.5 μm and in the 2.0-3.8 μm range are discussed separately, since each range contains specific mineralogical information and requires quite different analytical approaches. In the 0.7-2.5 μm range reside the main silicate features which are diagnostic of composition of basaltic assemblages. Such spectra are analysed here using both empirical laboratory calibrations (Cloutis et al. 1986; Cloutis & Gaffey 1991) and the Modified Gaussian Model (Sunshine et al. 1990). The 2.0-3.8 μm range on the other hand is potentially interesting since the detection of features around 3 μm and at 3.4 μm could reveal the presence of OH/H_2O and CH-bearing minerals.

3.1.1. Silicate mineralogy (0.7-2.5 μm)

A widely used methodology for the mineralogical interpretation of reflectance spectra of olivine/pyroxene assemblages is the use of empirical formulae derived from laboratory calibrations. This method has been recently reviewed by Gaffey et al. (2002). In order to apply it, the spectra must be parameterised in terms of the areas and the position of the centers of the absorption bands located near 1 and 2 μm (which from now on will be referred as BI and BII, respectively). The centers and areas of BI and BII are measured after the removal of a linear continuum which is tangent to the maxima before and after each band. These values are then inserted into empirical formulae from which the mineralogical composition of the pyroxenes in the assemblage in terms of percentage of Wolastonite (Wo) and Ferrosilite (Fs) content, and the contribution of olivine in the mixture can be also derived. It is important to note that these calibrations assume the presence of single pyroxene, and would fail if more than one kind of pyroxene are present.

Using a polynomial fit of the full spectra between 0.7 - 2.5 μm we determined the three maxima, near 0.7, 1.4 and 2.5 μm. The linear continuum for BI is given by the straight line tangent to the maxima near 0.7 and 1.4 μm, while for BII the continuum is determined by the maxima around 1.4 and 2.5 μm. For each band, the continuum was removed by dividing each band by the linear continuum in each corresponding region. The center of each band was computed after the continuum removal, using polynomial fits around the region of each reflectance minimum with orders varying from 3 to 6. The adopted values for band centers correspond to the polynomial that yields the best fit and the uncertainty in band center position is given by the scatter due to the use of different polynomials. The areas of BI and BII are also measured after the removal of the continua and the parameter BAR is defined as the ratio between the areas of BII and BI. Using these parameters, the pyroxene composition in terms of Wo and Fs was derived for each spectrum through the equations recently recompiled by Gaffey et al. (2002). The spectral parameters and the pyroxene composition for each spectra are presented in Table 2. Figure 2 shows the position

Table 2. 4 Vesta spectral parameters

Observation	Band I	Band II	BAR	Wo	Fs
Φ	(μm)	(μm)		(mol%)	(mol%)
0.06	0.926	1.958	2.05	6-7	41
0.47	0.922	1.932	2.35	5-6	34
0.64	0.926	1.996	2.68	6-7	51

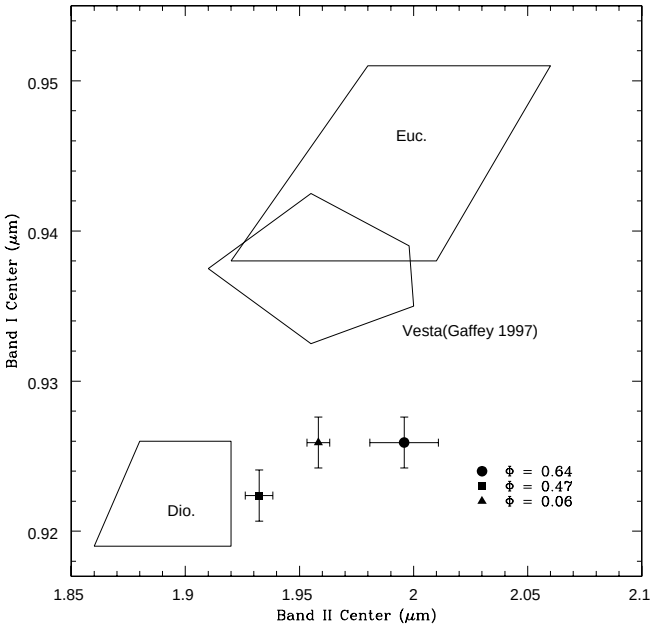

Fig. 2. Position of the band center for the three spectra of Vesta compared to the regions encompassed by the Eucrite (Euc.) and Diogenite (Dio.) basaltic achondrite assemblages and to the region encompassed by the observations of Vesta from G97. Different symbols represent different rotational phases of Vesta.

of the center of BI *versus* the center of BII for the spectra of Vesta in the present work, along with the loci of the eucrite and diogenite meteorites (Duffard et al. 2004a) and the loci of the observations of G97 for Vesta.

For all spectra, the position of the centers of BI and BII fall in the transition region between low- (orthopyroxene) and high-calcium pyroxenes (clinopyroxene) close to the diogenite locus and could be consistent with a single pyroxene composition. The derived values for Wo and Fs indicate that orthopyroxene is the dominant mafic mineral. The BAR values, when used to derive the percentage of orthopyroxene in orthopyroxene-olivine mixtures, with the calibration of Cloutis et al. (1986) yield values in excess of 90% orthopyroxene which is outside the validated range for this calibration. In fact, for rotational phases 0.47 and 0.64 this calibration produces values in excess of 100%. This suggests that olivine is at most an accessory mineral phase, but it can also indicate the presence of a clinopyroxene phase.

On the BAR x BI center diagram (Fig.3) our spectra are located on the edge of the basaltic achondrite loci, close to locus of pure orthopyroxene, which suggests that our spectra are dom-

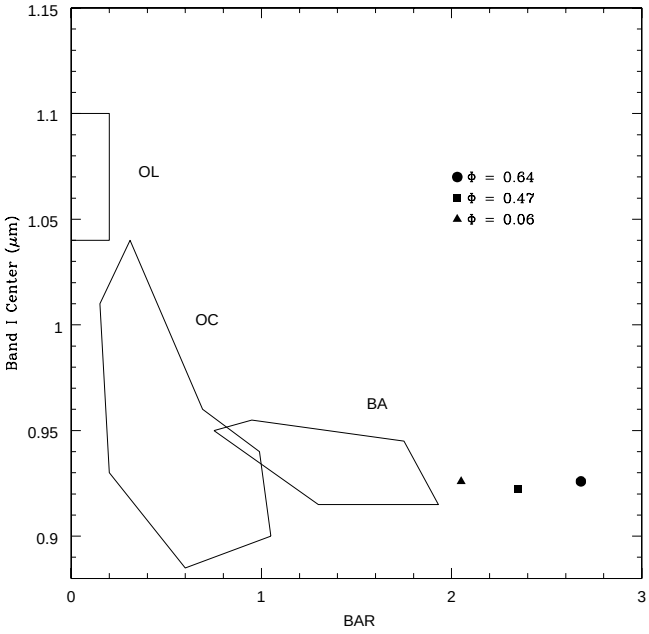

Fig. 3. The BAR value versus the Band I center is represented for our observations at different rotational phases; error bars are smaller than the symbols. The loci correspond to: the monomineralic olivine assemblages (OL), the ordinary chondrites (OC) and the pyroxene basaltic achondrites (BA) (Duffard et al. 2004a).

inated by low-calcium pyroxene. The spectral variations observed among rotational phases are mainly due to shifts in BII centers.

Although the position of the spectra in the band center diagram and in the BI x BAR diagram are consistent with the presence of a low calcium pyroxene, a composition consisting of a mixture of low calcium- and high-calcium pyroxenes cannot be ruled out. However, two pyroxenes, orthopyroxene and pigeonite, have their band centers falling in this region. Furthermore, our band centers are in the transition region between diogenites and eucrites. The primary mineral of diogenites is orthopyroxene (92-95%) and the main pyroxene found in eucrites is pigeonite. Thus regarding the position of our band centers we should have both orthopyroxene and pigeonite with a much stronger contribution from orthopyroxene.

In order to check the effects of such mixture on the mineralogical interpretation of our data, we made use of the Modified Gaussian Model. The MGM model deconvolves spectra into a series of modified Gaussian curves, each representing an individual electronic transition absorption band. Mathematically, each absorption band is represented by three parameters, a band strength, a band center and a band width. The absorption bands are all superimposed onto a continuum, which is modelled as a straight line in energy, and represented by two additional parameters, a slope and an offset (Sunshine et al. 1990).

A preliminar analysis was made using only low calcium pyroxene (LCP) bands. Five bands were used (Sunshine & Pieters 1993), with band centers ranging from 0.6 to 2.5 μm. The band

Table 3. Parameters from MGM applied to 4 Vesta using the bands associated to the Orthopyroxenes in the range 0.6-2.6 μm as described in Sunshine & Pieters (1993).

	Center	FWHM	Strength	Continuum and
Φ=0.06	(μm)	(μm)	(natural log)	Error in fit (rms)
Band 1	0.678	0.149	-0.11	
Band 2	0.918	0.200	-0.50	Offset:1.1
Band 3	1.161	0.280	-0.14	Slope:1.2E-007
Band 4	1.962	0.660	-0.49	
Band 5	2.499	0.502	-0.12	rms: 2.53%
Φ=0.47				
Band 1	0.676	0.1477	-0.2	
Band 2	0.911	0.206	-0.49	Offset:1.19
Band 3	1.148	0.278	-0.11	Slope:1.2E-007
Band 4	1.946	0.582	-0.35	
Band 5	2.499	0.501	-0.05	rms: 3.3%
Φ=0.64				
Band 1	0.690	0.151	-0.18	
Band 2	0.915	0.211	-0.49	Offset:1.14
Band 3	1.158	0.280	-0.15	Slope:1.2E-007
Band 4	1.97	0.651	-0.48	
Band 5	2.499	0.504	-0.10	rms: 3.34%

around 0.67μm was included in order to minimize the residua at lower wavelengths, even though most of this band lies outside our spectral range. The final values for the centers, widths, strengths and rms are shown in Table 3. The residuals of the fits have low rms and show no systematic deviation from zero. Even so, the presence of a high calcium pyroxene (HCP) component cannot be excluded. We have then applied the MGM adding two clinopyroxene bands to the model. As shown in Fig.4, the two pyroxene model also results in good fits for all the three spectra of Vesta. In average, the additional pyroxene reduced the residual error, but the fits obtained are non-unique. The observed dispersion for band centers are on the order of 0.05 μm and around 50% for some of the band strength. The parameter of representative fits are shown in Table 4 and the resulting fits are also reported in Fig. 4. Using the calibration of Sunshine & Pieters (1993), from the LCP/HCP band strengths, the rotational phase 0.47 has a HCP/(HCP+LCP) ratio of ~0.15-0.20, while the phases 0.06 and 0.64 have a ratio in the ~0.17-0.38 range. This is consistent with previous application of the MGM to an eucrite meteorite (Sunshine et al. 2004). However mineralogical analysis of HED meteorites show that they contain three kinds of pyroxenes, orthopyroxene, pigeonite and augite. Since orthopyroxene and pigeonite have rather close band centers, it is not possible to meaningfully deconvolve them with MGM. Therefore the LCP phase found by MGM could suggest the presence of one of those phases or a mixture of both. The HCP phase could suggest the presence of augite on Vesta, pyroxene which is also found in

Table 4. Final parameters from MGM applied to 4 Vesta using both a LCP and a HCP.

	Center	FWHM	Strength	Continuum and
Φ=0.06	(μm)	(μm)	(natural log)	Error in fit (rms)
Band 1	0.658	0.145	-0.11	
Band 2	0.902	0.183	-0.39	Offset:1.1
Band 3	0.989	0.189	-0.13	Slope:1.2E-007
Band 4	1.168	0.278	-0.11	
Band 5	1.912	0.587	-0.41	
Band 6	2.275	0.580	-0.15	rms: 2.35%
Band 7	2.516	0.498	-0.06	%
Φ=0.47				
Band 1	0.676	0.148	-0.21	
Band 2	0.904	0.198	-0.44	Offset:1.19
Band 3	0.989	0.195	-0.08	Slope:1.2E-007
Band 4	1.157	0.276	-0.10	
Band 5	1.925	0.579	-0.32	rms: 3.3%
Band 6	2.270	0.580	-0.05	
Band 7	2.513	0.500	-0.05	%
Φ=0.64				
Band 1	0.675	0.148	-0.18	
Band 2	0.906	0.197	-0.37	Offset:1.14
Band 3	0.989	0.193	-0.12	Slope:1.2E-007
Band 4	1.158	0.277	-0.10	
Band 5	1.922	0.583	-0.39	rms: 2.93%
Band 6	2.306	0.580	-0.15	
Band 7	2.515	0.499	-0.05	%

eucrites. At this point, it is not possible to infer the precise pyroxenes compositions using MGM due to the lack of laboratory calibrations for this method.

3.1.2. Discussion

The spectral parameters obtained in section 3.1.1 can be directly compared with the results of G97 for the asteroid 4 Vesta, and also with near-infrared observations of the V-type asteroids in the vicinity of Vesta (Duffard et al. 2004b), and of 1459 Magnya (Hardersen et al. 2004).

G97 analysed a set of rotationally-resolved spectrophotometric data of 4 Vesta in the 0.3-2.5 μm range, obtained in 1981. The author derived a mean pyroxene composition of $Fs_{46}Wo_{8}$ (46 mole % iron and 8% mole calcium) for Vesta, falling near the low end of the range of values for the common eucrites, and considerably above the range of diogenites, with the average surface of Vesta best characterized as a howardite or polymict eucrite. Also, the scatter of the position of BI and BII centers observed by the author was relatively small, with all spectra falling between

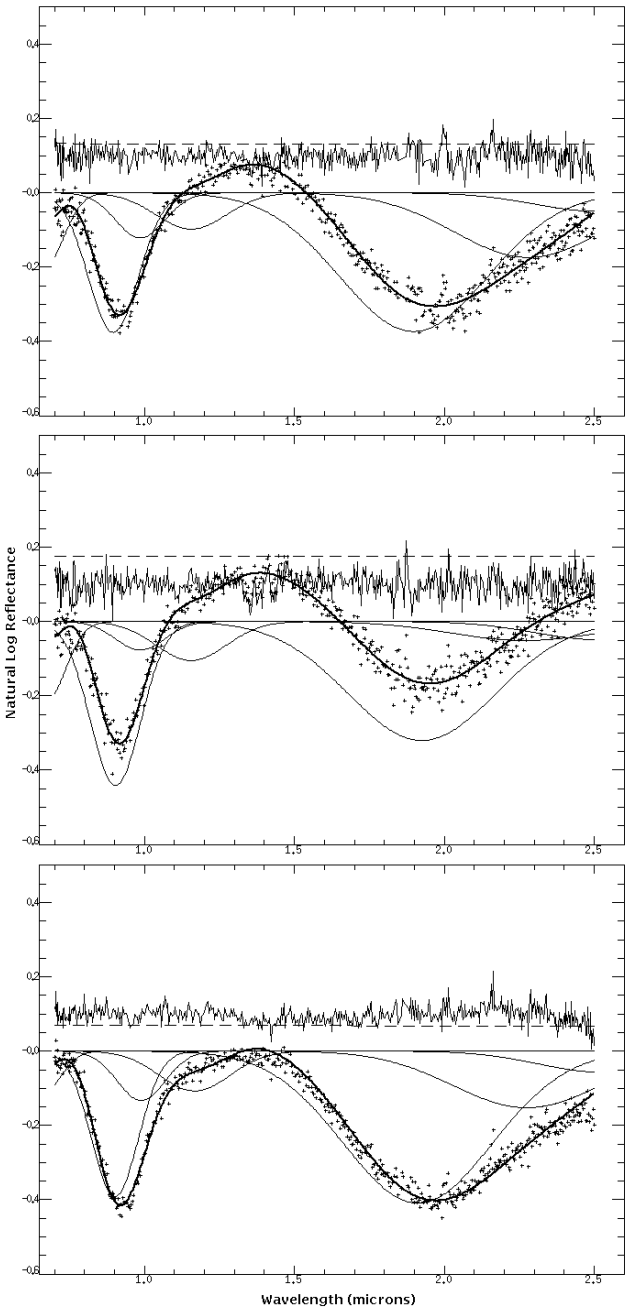

Fig. 4. Spectra of 4 Vesta fitted with seven modified Gaussians (solid lines) corresponding to absorption bands associated to orthopyroxene and clinopyroxene. The dashed line represents the continuum and the residual error spectrum is shown in the upper part of each plot.

the eucrite and diogenite loci in the band center diagram. Decreases in BAR values in some rotational phase led the author to suggest the presence of pure olivine regions. In contrast, our data suggests a composition more akin to diogenites and with little if any evidence of olivine.

Using the compositional map made from HST observations in the visible range (Binzel et al. 1997) along with the mineralogical map derived by G97 we note that our spectra at rotational phase 0.47 fall on Vesta's eastern hemisphere on a region where the data of both G97 and Binzel

et al. (1997) suggest and enhanced diogenitic content. The suggested increase in diogenite contribution at this phase seems to agree with our data since this rotational phase lies closer to the diogenite locus in the band center diagram, but with the position of BI shifted to lower wavelength than what is seen in G97. The remaining two rotational phases sampled by our spectra lie on Vesta's western hemisphere, where both G97 and Binzel et al. (1997) suggest the predominance of eucrite-dominated assemblages. This seems consistent with the position of BII for these two phases, but again the BI position for both seem shifted to lower wavelength than G97 spectra at corresponding phases.

Considering that the solar phase angle of two sets of observations are similar and that observations of G97 cover a whole rotational period of Vesta, the differences in the inferred mineralogy must be due to the differences of sub-earth latitude of the observations. Using the pole coordinates derived by Thomas et al. (1997), the observations of G97 were obtained at a sub-earth latitude of -20^o, while for our observations the sub-earth latitude was -11^o. The slightly more northern sub-earth latitudes of our observations suggests that the region of the crater near the south pole of Vesta might be having a smaller influence on our spectra. This can provide a tentative explanation for the differences between our observations and Gaffey's, because a higher olivine content tends to shift BI to higher wavelength whilst leaving the position of BII unchanged (Cloutis et al. 1986) and there is both observational evidence (Thomas et al. 1997) and theoretical arguments (Takeda 1979, 1997) for substantial presence of olivine in the South pole crater of Vesta. A possible problem with this interpretation would be that the BAR values for our spectra are not significantly higher than the ones derived by G97 for most of the surface of Vesta. However, the BAR values can be used to measure olivine content only for olivine/orthopyroxene mixtures which is not the case for Vesta since the presence of at least two pyroxenes is inferred.

Finally, the present work puts in new perspective the recent spectral observations of Vestoids (Duffard et al. 2004b), and of 1459 Magnya (Hardersen et al. 2004). Duffard et al. (2004b) observed spectra of 19 V-type asteroids in the vicinity of Vesta, finding a much greater scatter in BI and BII than what was reported for Vesta by G97. Hardersen et al. (2004) reported that the BI, BII and BAR values for the asteroid 1459 Magnya were significantly different than G97's results for Vesta, which would rule out the possibility of Magnya being a fragment of Vesta. However, the greater spectral diversity for the surface of Vesta that result from the combination of the spectra presented here with the results of G97 suggests that the spectral differences reported between those asteroids and Vesta do not necessarily imply genetical incompatibility, and would favour the suggestion of Duffard et al. (2004b) that the spectral diversity observed on the vestoids arise because these asteroids contain material of different layers of Vesta excavated by collisions. As for Magnya, the BI and BII values of our spectra (in particular for phase 0.47) are much closer to Magnya's, which suggests that a genetic connection between Vesta and Magnya cannot be ruled out solely on this basis.

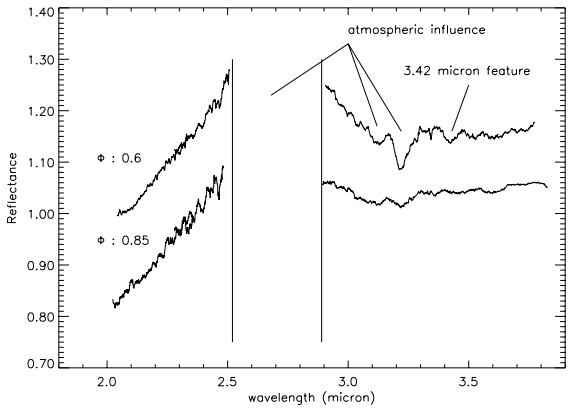

Fig. 5. Spectra of 4 Vesta at two different longitudes after removal of the thermal radiation. Spectra have been brought to lower resolution by gaussian smoothing. The gaussian width used was 10 points.

3.1.3. Mid Infrared

We have obtained two spectra of Vesta in the wavelength range 2.0-3.8 μm. The smoothed spectra for rotational phases 0.6 and 0.85 are shown in Fig. 5.

Both spectra present a set of minor absorption features which are more significant at rotational phase 0.6. Those features can be seen in the atmospheric transmission spectra, and may be due to an incomplete correction for atmospheric absorption. The 3.42 μm feature seen at rotational phase 0.6 corresponds to a minor atmospheric absorption and its strength in this spectra is probably due to atmospheric variations during observation.

For any of our spectra, we do not detect an absorption feature at 3.0 μm, that was seen by Hasegawa et al. (2003) and interpreted as evidence of hydrated and/or hydroxylated minerals on the surface.

We can see a spectral difference between 2.9 and 3.1 micron where the slope of our spectra changes. This variation possibly is due to a difference in pyroxene composition, but we can not completely exclude that this difference comes from changes in the atmospheric conditions during observations. After 3.1 micron our spectra are almost flat which is consistent with the spectra of HED meteorites.

3.2. Ceres

The spectrum of Ceres obtained in the wavelength range 2.0-4.1 μm is shown in Fig. 6. We calculated the band center and the band depth of the absorption occurring in the 3 μm region. The center of the absorption, occurs at $3.06 \pm 0.02 \mu m$, and the depth of the feature is about 10 %. These parameters are similar to those found by King et al. (1992).

We traced a continuum line between 2.97 and 3.16 μm, normalized the band at its maximum as shown in Fig. 7 (first spectrum from the bottom), and compared it with a number of different spectra collected in the laboratory at the Osservatorio Astrofisico di Catania (Strazzulla

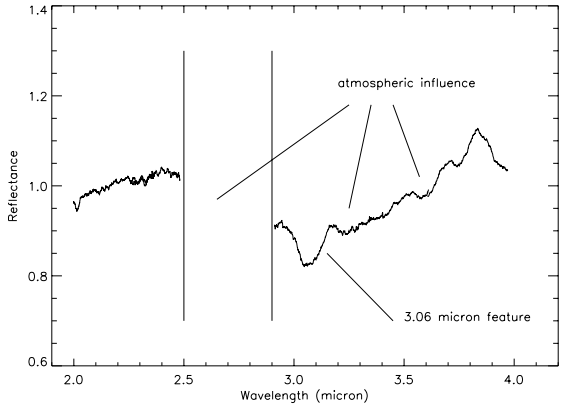

Fig. 6. Spectra of 1 Ceres normalized to one at 2.2 micron and brought to lower resolution by smoothing. The thermal radiation has been removed.

et al. 2001). In particular we compared the observed band with spectra of ices (water, ammonia, methane, methanol, benzene, carbon mono and di-oxide), ice mixtures, irradiated ices, organic materials (asphaltite, fullerenes, polymers) and residues left over after ion irradiation of carbon bearing species. We have obtained the best fit by a linear combination of the spectra of two components: the hemispherical reflectance (room temperature) of an organic refractory residue previously synthesized by ion irradiation of an asphaltite layer covered by water ice (16 K) (see Fig. 7, 2nd spectrum from the bottom). The second spectrum was that of crystalline water (at 150 K). It is important to note that it is significantly different from the spectrum of amorphous water ice as demonstrated in the same ig. 7 (top spectra). Such a difference allows to determine the structure of the ice eventually observed in astronomical objects.

Asphaltite, a solid bitumen, is very dark in the visual region and has red-sloped spectra in the visible and near-infrared range. It may be a good analog of refractory organic solids on the surfaces of primitive objects from the outer solar system (Moroz et al. 1998). Ion irradiation experiments (Moroz et al. 2004) on bulk samples of pure asphaltite showed that irradiation-induced carbonization gradually neutralizes spectral slopes of the red organic solids. Asphaltite exhibits several vibrational absorption bands mostly due to aliphatic and aromatic functional groups. Recently experiments of ion irradiation of pure asphaltite and asphaltite covered with water ice have been performed (Strazzulla et al. 2004). The results indicate that the original bands of asphaltite progressively decrease in intensity and new bands appear. The spectrum of the asphaltite shown in Fig. 7 refers to a residue obtained after irradiation (30 keV He^+, 1.5×10^{16} cm^{-2}) of water ice deposited on an asphaltite sample at 16 K. After irradiation the sample has been removed from the vacuum chamber and its spectrum taken at room temperature. Two bands are observed in the 2.7-3.6 μm range: the most intense is centered at 3.03 μm and is attributed to C-H stretch in carbynoid structures ($R(C\equiv C)_m$-H). A second feature, centered at 3.24 μm is due to an aromatic C-H stretch.

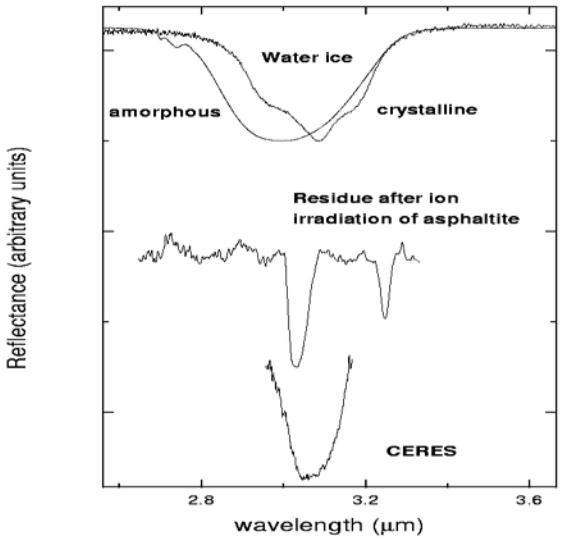

Fig. 7. Spectra of (from the bottom to the top): the 3.06 μm band observed on Ceres; an organic refractory residue obtained by ion irradiation of asphaltite covered by water ice (16 K); amorphous (16 K) and crystalline (150 K) water ice. All the spectra are normalized at 1 at their respective maximum and vertically shifted for clarity.

It is well known that ion irradiation produces chemical modifications and, in particular, the formation of molecules originally not present in the target. These molecules include species both more volatile and less volatile than the initially irradiated molecular mix. When carbon (or sulfur) is an important constituent of the irradiated material a refractory residue results which remains after warming the sample. That residue has a complex structure, which after prolonged irradiation evolves to form a hydrogenated amorphous carbon. It is interesting to note that the feature at 3.03 μm characteristic of linear chains appears also after irradiation of solid acetylene (Strazzulla et al. 2002), solid benzene and cluster assembled carbon thin films (Strazzulla & Baratta 1991). Thus its formation seems common to many irradiated hydrogen bearing carbonaceous material.

In Figure 8 we compare the spectrum of the band observed on Ceres with that obtained by the linear combination of the laboratory spectra discussed above (the two organic residues and crystalline water ice). The features in Ceres' spectrum at 3.20 μm and at 3.55 μm are due to incomplete removal of telluric features. The fit is very good inside the the 3.06 μm band, but the mismatch between the fit and the spectra after 3.20 μm suggests the presence of one or more absorption features in Ceres' spectrum which are not being reproduced by our model.

We have made an estimation of the amount of material that is necessary to give rise to the observed spectrum by measuring the band areas (cm^{-1}) in an optical depth scale and dividing their value by the integrated absorbance (cm molecules^{-1} ; see e.g. Strazzulla et al. (2001) for details). The band areas were measured with respect to a linear continuum that intercepts the

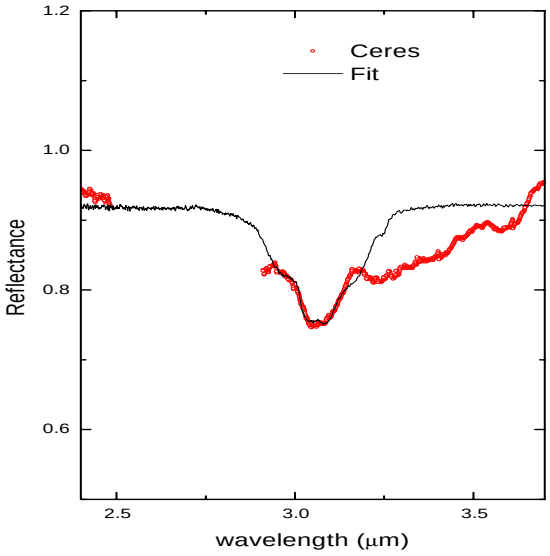

Fig. 8. Comparison of the spectra of the 3.06 μm band observed on Ceres and that obtained by a linear combination of the spectra of two laboratory samples as discussed in the text.

spectra at 2.4 and 3.6 μm. The integrated absorbances we used are 2×10^{-16} cm molecules^{-1} for the O-H stretches of water ice (Allamandola et al. 1988) and 2×10^{-17} cm molecules^{-1} that is a typical value for the alkyl CH_2 and CH_3 groups and that here we use also for the band at 3.03 μm. We find that the number of water ice molecules that contribute is about 3×10^{17} molecules cm^{-2} while the C-H groups in linear carbon chains are about 7.5×10^{17} C-H bonds cm^{-2}.

In other words the surface of Ceres (i.e., the outermost skin from which the solar radiation is reflected) contains an organic carbonaceous material with C-H bonds in linear chains and alkyl groups and a (small) amount of crystalline water ice.

Here we are not claiming that ion irradiation is the only agent that governs the evolution of the Ceres surface. We have used energetic ions in the laboratory to produce processed carbonaceous material that are spectrally very similar to those observed on Ceres. McCord & Sotin (2003) suggested that the thermal evolution of Ceres could have produced a metamorphosed carbonaceous chondrite surface material whose ion-induced space weathering would produce the observed features. McCord & Sotin (2003) suggested also that at least 20 % of Ceres is made of water ice, consistent with the finding of OH escaping from the north polar region (A'Hearn & Feldman 1992) and models indicating that subsurface percolation could replenish the external layers with water ice over geologic time (Fanale & Salvail 1989). The presence of large amount of water ice has been recently suggested also by Parker et al. (2004) based on the measurement (by Hubble Space Telescope) of the equatorial and polar radii of Ceres whose ratio is consistent with a body that has a central rocky core surrounded by water ice.

4. Conclusions

We obtained and analysed spectra for Vesta in the range 0.7-3.8 μm and 2.0-4.1 μm for Ceres. The near-infrared spectra of Vesta shows a surface composition closer to diogenites than eucrites and possibly a lower olivine content than those obtained by Gaffey (1997). Along with previous works, our results show a greater the surface heterogeneity. This seems consistent with recent observations of V-type asteroids in the vicinity of Vesta (Duffard et al. (2004b)). We did not find any absorption feature at 3 μm indicative of the presence of water ice. For Ceres we confirm the presence of the absorption feature at 3.06 μm that was previously reported (Lebofsky et al. 1981; King et al. 1992) and we suggest that this feature can be reproduced with a linear combination of crystaline water ice, residues of ion-irradiated asphaltite covered with water ice. The presence of organic materials, in particular of carbon linear chain that is present in asphaltite was never reported earlier in any asteroid. If real, it would confirm the uniqueness of the Ceres surface.

This work was made as support for the Dawn mission which will provide detailed mineralogical maps for Vesta and Ceres. However, in order to make a good assessment of the data, more laboratory calibrations are needed, in particular concerning the precise deconvolution of the HED meteorites using MGM.

Acknowledgements. T. Mothé-Diniz wish to thank CNPq (Conselho Nacional de Desenvolvimento Científico e Tecnológico) for the fellowship PDE that contributed for the realization of this work.

References

A'Hearn, M. F. & Feldman, P. D. 1992, Icarus, 98, 54

Allamandola, L. J., Sandford, S. A., & Valero, G. J. 1988, Icarus, 76, 225

Binzel, R. P., Gaffey, M. J., Thomas, P. C., et al. 1997, Icarus, 128, 95

Birlan, M., Binzel, R., Bus, S., et al. 2002, Bulletin of the American Astronomical Society, 34, 860

Britt, D. T., Yeomans, D., Housen, K., & Consolmagno, G. 2002, in Asteroids III (University of Arizona Press), 485–500

Cloutis, E. A. & Gaffey, M. J. 1991, J. Geophys. Res., 96, 22809

Cloutis, E. A., Gaffey, M. J., Jackowski, T. L., & Reed, K. L. 1986, J. Geophys. Res., 91, 11641

Duffard, R., Lazzaro, D., & De Leon, J. 2004a, Meteoritics and Planetary Science

Duffard, R., Lazzaro, D., Licandro, J., et al. 2004b, Icarus, 171, 120

Fanale, F. P. & Salvail, J. R. 1989, Icarus, 82, 97

Gaffey, M. J. 1997, Icarus, 127, 130

Gaffey, M. J., Cloutis, E. A., Kelley, M. S., & Reed, K. L. 2002, in Asteroids III (University of Arizona Press), 183–204

Hardersen, P. S., Gaffey, M. J., & Abell, P. A. 2004, Icarus, 167, 170

Hasegawa, S., Murakawa, K., Ishiguro, M., et al. 2003, Geophys. Res. Lett., 30, 2

Keil, K. 2002, in Asteroids III (University of Arizona Press), 573–584

King, T. V. V., Clark, R. N., Calvin, W. M., Sherman, D. M., & Brown, R. H. 1992, Science, 255, 1551

Lebofsky, L. A., Feierberg, M. A., Tokunaga, A. T., Larson, H. P., & Johnson, J. R. 1981, Icarus, 48, 453

Lebofsky, L. A. & Spencer, J. R. 1989, in Asteroids II (University of Arizona Press), 128–147

McCord, T. B., Adams, J. B., & Johnson, T. V. 1970, Science, 168, 1445

McCord, T. B. & Sotin, C. 2003, AAS/Division for Planetary Sciences Meeting, 35,

Moroz, L., Baratta, G., Strazzulla, G., et al. 2004, Icarus, 170, 214

Moroz, L. V., Arnold, G., Korochantsev, A. V., & Wasch, R. 1998, Icarus, 134, 253

Parker, J. W., Stern, S. A., Thomas, P. C., et al. 2002, AJ, 123, 549

Parker, J. W., Thomas, P., Young, E., et al. 2004, AAS/Division for Planetary Sciences Meeting, 36,

Standish, E. M. & Hellings, R. W. 1989, Icarus, 80, 326

Strazzulla, G. & Baratta, G. A. 1991, A&A, 241, 310

Strazzulla, G., Baratta, G. A., Domingo, M., & Satorre, M. A. 2002, Nuclear Instruments and Methods in Physics Research B, 191, 714

Strazzulla, G., Baratta, G. A., & Palumbo, M. E. 2001, Spectrochimica Acta, 57, 825

Strazzulla, G., Battiato, S., & Compagnini, G. 2004 (New York), in Press.

Sunshine, J. M., Bus, S. J., McCoy, T. J., et al. 2004, Meteoritics and Planetary Science, 39, 1343

Sunshine, J. M. & Pieters, C. M. 1993, J. Geophys. Res., 98, 9075

Sunshine, J. M., Pieters, C. M., & Pratt, S. F. 1990, J. Geophys. Res., 95, 6955

Takeda, H. 1979, Icarus, 40, 455

Takeda, H. 1997, Meteoritics and Planetary Science, 32, 841

Tedesco, E. F. 1989, in Asteroids II (University of Arizona Press), 1090–1138

Thomas, P. C., Binzel, R. P., Gaffey, M. J., et al. 1997, Science, 277, 1492

Webster, W. J., Johnston, K. J., Hobbs, R. W., et al. 1988, AJ, 95, 1263

II.3. Considérations sur la masse des astéroïdes.

Une problématique particulière dans les cas des astéroïdes est constituée par l'estimation de leur masse globale, mais aussi la masse de quelques uns d'entre eux. De nos jour cette variable reste encore peu connue et les contraintes imposées par des modèles issus des données d'observations continuent à être contradictoires.

Il est difficile d'estimer la masse par des considérations dynamiques ou par des considérations physiques. Les considérations dynamiques peuvent être basées sur des théories analytiques ou numériques soit par des déterminations issues des géométries favorables (par exemple, les rapprochements serrés entre deux astéroïdes, dont nous pouvons, en principe, mesurer la perturbation des orbites[1]). Les données dynamiques les plus fiables restent celles obtenues par les survols des sondes spatiales (le cas de la mission NEAR). Si le survol de l'astéroïde se fait de façon suffisamment rapprochée, connaissant la masse et les paramètres orbitaux de la sonde spatiale nous pouvons remonter à la masse inertielle de l'astéroïde qui engendre la perturbation de l'orbite de cette sonde.

Une autre situation particulière concernant l'estimation de la masse des astéroïdes est celle des systèmes doubles ; les considérations dynamiques sont soutenues aussi par des considérations physiques permettant une forte contrainte sur les résultats.

Le problème peut être également abordé par les paramètres physiques obtenus suite à des observations (comme la période de rotation propre ou la taxonomie).

La période de rotation propre donne des renseignements sur l'état global de l'astéroïde : l'astéroïde est-il un corps monobloc ou d'un « tas de gravas »[2] ? Il est évident qu'une rotation propre rapide ne peut pas être attribuée à un objet fragmenté. Parmi les astéroïdes à périodes de rotations longues, nous constatons par l'observation un nombre plus important d'astéroïdes de petite taille (diamètre inférieur à 20 km) que d'astéroïdes de grande

[1] Ce type d'étude n'est pas facile, les deux corps ne peuvent pas être isolés des influences des autres astéroïdes. Pour que la perturbation soit interprétable, il faut viser des astéroïdes dont au moins un doit être de grande taille.
[2] le terme anglais est « rubble piles », des morceaux tenus ensemble par un faible champ gravitationnel

taille (diamètre supérieur à 100 km). Cela peut expliquer un nombre assez important d'objets fragmentés parmi les objets de petite taille.

Une autre approche est celle liée à la classification taxonomique, sur une composante comportant des considérations sur les éléments de planétologie comparative. L'association de certains minéraux (déduite en majeure partie des météorites) avec des classes taxonomiques impliquent des considérations sur la masse volumique des astéroïdes et « in fine » sur leur masse. Cette approche est améliorée en tenant compte du fait que le matériel à l'intérieur de l'objet peut ne pas être homogène et compact, le degré de « compacticité » étant exprimé par un paramètre de porosité.

Une analyse globale des méthodes d'investigation et l'analyse des résultats a été effectuée et publiée dans deux articles (EM&P vol 88, 2002 et Ceres 2001 Workshop). Les résultats ont mis en évidence la nécessité de l'introduction d'un paramètre de porosité qui varie dans un intervalle important entre les classes taxonomiques et au sein de la même classe. Je mentionne également la paradoxe entre la masse volumique d'un astéroïde appartenant à la classe taxonomique **M** et la minéralogie associée habituellement à cette classe.

Références :

Birlan M. – *Dynamic and physical considerations on the asteroids' density*, **Earth, Moon and Planets** n. **88**, 1-10, 2002.
M. Birlan - *Asteroids density: an overview* - "Ceres 2001" Workshop IMCCE, Paris, 2001

DYNAMIC AND PHYSICAL CONSIDERATIONS ON THE ASTEROIDS DENSITY *

MIREL BIRLAN
Observatoire de Paris-Meudon, DESPA, 5 – Place Jules Janssen 92195 Meudon Cedex, France; Astronomical Institute of the Romanian Academy, 5-Cutitul de Argint, 75212 Bucharest 28, Romania. E-mail: Mirel.Birlan@obspm.fr

(Received 13 April 2000; Accepted 12 June 2001)

Abstract. High quality new data on the asteroid mass and volume were produced in the last years from both extra-atmospheric instruments and the groundbased high-performance telescopes. This paper presents a synthesis of these results in terms of the asteroid density, taking into account several techniques, and the possible correlation of the density through the taxonomic system.

The important conclusion is that M-type asteroids seems to have an unexpected low density, which cannot be explained by the present mineralogy assumed by the comparative mineralogy.

Keywords: Asteroid, density, mineralogy, taxonomic class

1. Introduction

Asteroids are solar system bodies with dimensions varying between 1,000 km and 100 m. Nowadays, more than 11,000 asteroids have been included in the Minor Planet Center orbits catalogue, and more than 23,000 other have been reported as discoveries. Asteroids are belived to be the remnant planetesimals from the early solar system formation, which, mainly by mutual collisions, evolved to the present asteroid population. Their distribution at different distances from the Sun allow us to conclude that the thermal evolution of the asteroids is not the same for the entire population. Thus, giving their number and the physical diversity, asteroids have become the *trial* population for both physical and dynamical models.

The density is the parameter which plays a key role in the understanding of the solar system formation. In the case of asteroids, it could give important arguments for constraining the primary planetary nebula. Asteroids are bodies small enough that their own gravitation can't model their mineralogy; part of them are far enough to not be heated in such a manner that theirs global mineralogy does change.

* Partially supported by the ESA contract ADM-H/vp/161.

Earth, Moon and Planets **88:** 1–10, 2002.

2. Mass and Density of the Asteroids – Groundbased Observations

Several groundbased techniques allow us to obtain the approach of the asteroids density. In fact, the asteroids density appears to be a derived parameter, this value being computable through the ratio of the mass reported the asteroid volume:

$$\rho = \frac{M}{V}. \tag{1}$$

We could differentiate the mass estimation through gravitational perturbation, and the mass estimation by recent techniques based on the radar and the results of comparative mineralogy.

2.1. Mass determination from gravitational perturbations

Asteroids' perturbations are the largest source of incompletely modeled perturbations of the planets, especially Mars and the Earth-Moon barycenter. No less than seven asteroids can produce periodic perturbations more than a kilometer in Mars's position (Williams, 1984). Ceres (which is 0.13% of the Mars mass) and other asteroids are much more sensitive to the perturbations of the asteroids than are the planets. Thus, observations of the asteroids gravitational mutual effects (astrometric observations, close approach observations) are very important for the computation of the asteroids' mass (density). In other words, to achieve high accuracy, the physical model for the asteroid ephemeride must include perturbations by other asteroids. Based on dynamical considerations, the mass of 11 Parthenope was estimated* by Viateau and Rappaport (1997) to be $(2.58 \pm 0.10) \times 10^{-12}\ M_\odot$. Recent results on the masses of the asteroids 1 Ceres, 2 Pallas, and 4 Vesta were determinated at the same time with the ephemerides. The masses were established at $(4.39 \pm 0.04) \times 10^{-10}\ M_\odot$, $(1.59 \pm 0.05) \times 10^{-10}\ M_\odot$, and $(1.69 \pm 0.11) \times 10^{-10}\ M_\odot$, respectively (Hilton, 1999). However, these values are still subject of discussions (following theirs observations and taking into account the perturbation on the orbits of 9 asteroids, Viateau and Rapaport (1989) published the value $(4.759 \pm 0.023) \times 10^{-10}\ M_\odot$ for the 1 Ceres mass). The systematic effects (perturbations) can be applied only to the massive asteroids; for the smaller ones only favorable groundbased conditions of observations (crossing points) can give an estimation of the mass. Following several authors, we can estimate from the groundbased observations the density of several asteroids. Table I presents some values computed using data from the literature. The volume was computed starting from the IMPS diameter estimation (Tedesco, 1992), assuming the spherical forms for the studied asteroids. The spherical approximation seems to be reasonable as long as we talk about the large asteroids. Only for the asteroid 4 Vesta, I preferred to take into account the high quality volume estimation of Thomas et al. (1997); the density obtained using the IMPS diameter (6,251 kg/m^3) seems to be unrealistic.

* $M_\odot = 1.988 \times 10^{30}$ kg.

The errors of the density were computed using the formula:

$$\Delta\rho = \frac{\Delta M}{V} + \frac{M \cdot \Delta V}{V^2}. \quad (2)$$

The last column of Table I contains the references where the mass of the asteroid was published.

The estimation of the density as derived from the mass and volume will be largely affected by the uncertainty in the asteroid diameter (the density depends inversely with the cube of the diameter). Indeed, if we consider the diameter of 4 Vesta 70 km larger than that presented on the Table I, the density will be (4,300 ± 300) kg/m^3 (value agreed in this article). Starting from different mass estimations of 4 Vesta, other authors proposed the values of density around (3,800 ± 600) kg/m^3 or (4,100 ± 950) kg/m^3 (Thomas et al., 1997). Reliable mass measurements for asteroids are scarce, mostly because of the problem of detecting their perturbation of other object (even for larger asteroids). In the case of the asteroid 2 Pallas, several densities were proposed; (2,600 ± 500) kg/m^3 (Millis and Eliott, 1979), (3,500 ± 500) kg/m^3 (Dunham et al. 1990), (4,200 ± 300) kg/m^3 (Hilton, 1999).

2.2. Density estimation by radar and taxonomic considerations

Another interesting approach of the asteroid mass and density could be obtained by the radar echoes analysis. This type of investigation proved its efficiency in the case of Near-Earth Asteroids. One of the subjects of radar analysis was the NEA, 4179 Toutatis. The radar model of Toutatis predicts a rock density between 2,300 and 5,700 kg/m^3. The predicted (Ostro et al., 1999) interval contains both typical densities of ordinary chondrites (3,400 kg/m^3) and stony irons rocks (4,900 kg/m^3). The balance between the porosity and rock coverage makes it difficult to draw final conclusion: is Toutatis a stony-iron analog or an OC analog?

The taxonomic approach of the asteroid density is also important to mention. Several asteroid taxonomic systems were proposed (Barucci et al., 1987; Tedesco et al., 1989; Tholen, 1989; Gaffey et al., 1993; Birlan et al., 1996a). There is an agreement between the larger taxonomic classes proposed by several authors, and the agreement diminishes for the smaller ones.

By comparative mineralogy, we can assign different minerals to the major taxonomic classes of the asteroids such as: S-type asteroids are composed mainly by silicate minerals, C-type asteroids correspond to the carbonaceous chondrites and/or carbonaceous compounds, M-type asteroids are similar to the metallic meteorites, V-type present the spectral behavior of basalts. ... Thus, we can associate to each taxonomic class an average density corresponding to the minerals that we have on Earth (rocks, meteorites, lunar rocks). Such correspondence is given in Table II.

This type of mass estimation was used by Viateau and Rapaport (1997) for of the asteroid 511 Davida (C-type), and 52 Europe (C-type), (1.8×10^{-11} $M_\odot$ and 1.4×10^{-11} $M_\odot$, respectively) for the estimation of the mass of 11 Parthenope.

TABLE I

Density of several asteroids computed from groundbased observations (see the text)

Asteroid	Diameter (10^3 m)	Mass (10^{18} kg)	Volume (10^{15} m^3)	Density (10^3 kg/m^3)	Ref.
1 Ceres	848.4 ± 19.7	873.2 ± 8.7	319.7 ± 23.5	2.731 ± 0.228	Hilton (1999)
1 Ceres	848.4 ± 19.7	946.6 ± 4.7	319.7 ± 23.5	2.961 ± 0.168	Viateau and Rappaport (1998)
2 Pallas	498.1 ± 18.8	316.2 ± 32	64.72 ± 7.6	4.8 ± 1.07	Hilton (1999)
4 Vesta	468.3 ± 26.7	336.1 ± 50	78 ± 3	4.3 ± 0.3	Hilton (1999)
10 Hygiea	407.1 ± 6.8	93.4 ± 46	35.3 ± 1.8	2.64 ± 1.44	Scholl et al. (1987)
11 Parthenope	153.3 ± 3.1	5.13 ± 0.25	1.88 ± 0.12	2.72 ± 0.31	Viateau and Rappaport (1997)
15 Eunomia	255.3 ± 15.0	8.35 ± 2.20	8.71 ± 1.28	0.95 ± 0.39	Hilton (1999)
16 Psyche	253.2 ± 4.0	17.3 ± 5.1	8.5 ± 0.4	2.03 ± 0.69	Viateau (2000)
20 Massalia	145.5 ± 9.3	4.77 ± 0.78	1.61 ± 0.33	2.96 ± 1.09	Bange (1998)
45 Eugenia	214.6 ± 4.2	6.02 ± 0.30	5.17 ± 0.31	1.16 ± 0.13	Merline et al. (1999)
121 Hermione	209.0 ± 4.7	9.35 ± 1.58	4.78 ± 0.23	1.95 ± 0.42	Viateau (2000)
216 Kleopatra	135.1 ± 2.1	1.9 ± 0.2	1.29 ± 0.06	1.47 ± 0.22	Marchis et al. (1999)
704 Interamnia	316.6 ± 5.2	69.6 ± 31.1	16.6 ± 0.8	4.19 ± 2.08	Viateau and Rappaport (1997)

TABLE II
Assigned densities for several large asteroid taxonomic classes

Taxonomic type	Compounds	Assumed density (kg/m^3)
S	Silicates (olivine, pyroxene), NiFe	2,600–3,300
C	Carbon compounds, clays, organics	1,600–2,200
V	Silicates (olivine, pyroxene), plagioclase	3,000–4,300
M	FeNi	5,900–7,900

3. Asteroids' Investigation by Spacecrafts

GALILEO was the first spacecraft that did fly-bys to asteroids. Even if the main scientific goal was not the asteroids, the results of GALILEO concerning them are remarkable. Unfortunately, the GALILEO spacecraft was not affected by measurable perturbation during the fly-bys to 243 Ida and 951 Gaspra.

However, the mass of the asteroid 243 Ida was estimated by Belton et al. (1995) based on constraints on the orbit of Ida's (unknown before) satellite, Dactyl. The 47 independent views of double system Ida-Dactyl, obtained by the solid-state imaging camera of GALILEO over a period of 5 hr 24 m, allow us to compute the value of the density of (2,600 $\pm$ 500) kg/m^3. This value, closer to the average density assumed for S-type asteroids, also close to the OC meteoric type (Belton et al., 1995), could confirm the hypothesis that rich silicates asteroids are the parent of OC meteorites. Assuming a volume of (16.1 $\pm$ 1.9) $\times$ 10^{12} m^3, the mass of the asteroid 243 Ida is estimated to be (4.18 $\pm$ 1.3) $\times$ 10^{16} kg.

NEAR spacecraft carried out the first ever encounter with a C-type asteroid, flying at a minimal distance of 1212 km of the asteroid 253 Mathilde. With the geometric albedo of 0.047, 253 Mathilde is a low-reflectant object. From pictures, the asteroid was approximated to be a 66 $\times$ 48 $\times$ 44 km triaxial ellipsoid; these dimensions are smaller than those estimated from the ground observations. The determination of 253 Mathilde's mean density is based on the first direct measurement of an asteroid mass from perturbation on a passing spacecraft. The mass determination from Doppler tracking was estimated to be (1.033 $\pm$ 0.044) $\times$ 10^{17} kg. Taking into account the volume of 772 $\times$ 10^{11} m^3 (Thomas et al., 1999a), Mathide became the asteroid with the lowest high quality density estimation: (1,340 $\pm$ 20) kg/m^3. This value represents an argument for significant void space inside of the asteroid (Veverka et al., 1999). Another explanation for its low density can be the presence of rich-ices mixtures on the subsurface. But, this second hypothesis requires the unrealistic percentage of 67% to 83% of the Mathilde's volume to be water ice. Moreover, groundbased observations of the surface of Mathilde do not confirm the typical 3 μm absorption band of aqueous alteration.

The second target of the NEAR spacecraft was the S-type asteroid 433 Eros. During the fly-by on December, 1998, the gravitational perturbation on the spacecraft from nearby 433 Eros was not as much as that seen during the Mathilde fly-by. Despite this inconvenient, the mass value for 433 Eros was established at $(7.2 \pm 1.8) \times 10^{15}$ kg, the volume at $(2.9 \pm 0.6) \times 10^{12}$ m^3 (Thomas et al., 1999b), and its density in the range of 2,500–3,300 kg/m^3 (Yeomans et al., 1999). From the fly-by schedule of February–March 2000 we expect new results to confirm and refine the knowledge of the S-type asteroids.

We cannot omit also the tentative of Deep Space 1 to investigate the asteroid 1992 KD (Braille) in July 1999. Unfortunately, the small payload of DS1 doesn't contain the instruments able to make measurements on the asteroid mass and density. The acquired spectrum of Braille shows spectral features similar to those of Vesta surface (associated to basalts and stony-iron rocks).

4. Density Analysis and Question Marks

A synthesis of the density values of the asteroids for both groundbased and space observations is presented in Table III. As it can be seen, the density range for asteroids varies between 1,300 kg/m^3 and 4,800 kg/m^3. I suppose that the underestimation of the asteroid mass of the asteroid 15 Eunomia could explain its low density. The overestimated spherical volume assumption of the asteroid 216 Kleopatra must be also revised. Recent models of the binary system 216 Kleopatra (Hestroffer et al., 2000) converge to identical rotational ellipsoids in contact. A simple computation of the binary system density, assuming the ratio of the semi-axes to be $a/b = 1/2$, gives values in the range 1,500–3,130 kg/m^3 depending on the prolate and the oblate spheroids. Through this model, the density of 216 Kleopatra becomes closer to the typical density of the S-type asteroids but far enough by the assumed M-type minerals. However, the collisional/gravitational circumstances that allow two bodies of such dimensions – assumed to be parts of the core on an segregate planetoid – are little known.

If we compare the computed values of the density and the taxonomic type, we find that large part of the C-type asteroids density varies in the range 1,100–2,200 kg/m^3, and the S-type asteroids varies in the range 2,400–3,400 kg/m^3.

At the opposite side, the M-type asteroid density is intriguing. If the asteroids 16 Psyche and 216 Kleopatra are M-type asteroids (theirs InfraRed albedos around 30% are also confirmed by the strong radar echoes observations), then the density doesn't fit to the expected values.

The asteroid 2 Pallas density is affected by large errors, and thus it is difficult to make any assumption concerning its density-taxonomic class correlation. 2 Pallas seems to belong to the B-type asteroids, but its near IR spectra analysis doesn't match the B-type behaviors (Birlan et al., 1996b). However, B-type asteroids are poorly known.

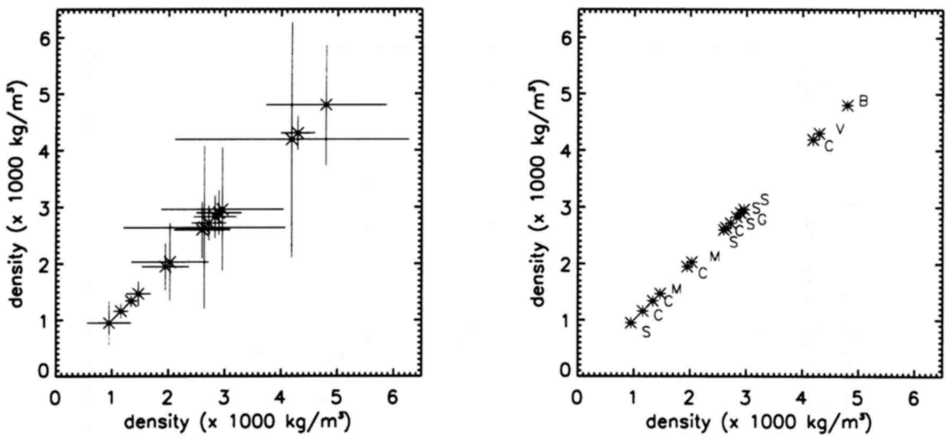

Figure 1. Density estimation for 15 asteroids contained on Table III. On the left side, the errors in the estimation; on the right side the taxonomic class of each asteroid.

As it can be seen from Figure 1 and Table III, the error bars are important for some asteroids. Globaly speaking, we can distinguish the S-type asteroids from the C-type ones. For other asteroids it is difficult to make correlations between density and the taxonomic class. The two M-type asteroids are mixed between the S and C-type asteroids.

The representation of the asteroids in the plane density – semi-major axis (Figure 2) was also investigated. We can observe the S-type asteroids alignment around 3,000 kg/m^3 at any distance to the Sun, and the C-type asteroids (with high confidence level estimation of the density) alignment around 1,400 kg/m^3. Anyway, our sample is not (yet!) representative for statistic analysis and global conclusions concerning the asteroid formation and evolution. Also, the asteroids contained in Table III are biased mainly because they are placed in particular conditions (crossing-points apparent orbits, favorable condition for the spacecraft flybys, mutual approach with massive asteroids).

5. Conclusions

We refrain from drawing final conclusions concerning the density of the asteroids. However, nowadays we are able to address more accurately at this problem mainly due to new high quality data obtained by space missions. These data gives better constraints to the assumed value of the density (when they don't allow to determine directly the density of celestial object).

The small number of analyzed asteroids doesn't allow us a real statistic analysis. However, the density could distinguish between the S and C-type asteroids (Figure 1). This is an important result proving that surface mineralogy could be representative in defining the sub-surface structure of the asteroid.

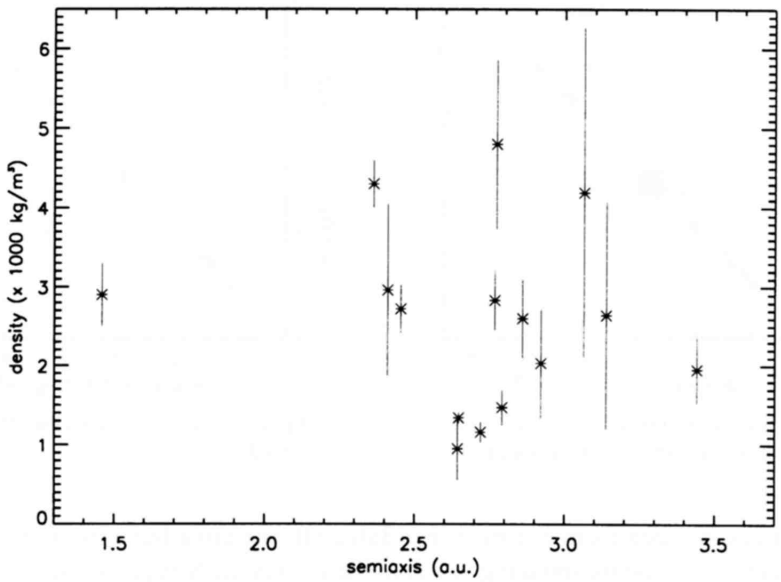

Figure 2. Density distribution along the semi-major axis for the 15 asteroids contained on Table III.

TABLE III

Asteroid density estimation and the correspondent taxonomic class

Object	a (u.a)	Density ($\times 10^3$ kg/m^3)	Taxonomic class
1 Ceres	2.7666	2.83 ± 0.38	G
2 Pallas	2.7723	4.8 ± 1.07	B
4 Vesta	2.3614	4.3 ± 0.3	V
10 Hygiea	3.1384	2.64 ± 1.44	C
11 Parthenope	2.4530	2.72 ± 0.31	S
15 Eunomia	2.6438	0.95 ± 0.39	S
16 Psyche	2.9210	2.03 ± 0.69	M
20 Massalia	2.4094	2.96 ± 1.09	S
45 Eugenia	2.7203	1.16 ± 0.13	C
121 Hermione	3.4412	1.95 ± 0.42	C
216 Kleopatra	2.7917	1.47 ± 0.22	M
243 Ida	2.8596	2.6 ± 0.5	S
253 Mathilde	2.6472	1.34 ± 0.02	C
433 Eros	1.4583	2.9 ± 0.4	S
704 Interamnia	3.0638	4.19 ± 2.08	C

216 Kleopatra and 16 Psyche are two large asteroids belonging to the M-type. If they are parts of the segregate asteroid nucleus, then the density doesn't fit the expected value. In this case, we could obtain the correlation between the density and the taxonomic class only if we assume the following:

(i) the mass estimations are affected by errors in a greater measure than presented in the literature;
(ii) the volume estimations are wrong; or
(iii) the mineralogy of the M-type asteroids is not really that one we expected;

Obviously, global conclusions concerning the M-type asteroids cannot be drawn taking into account only two bodies, and M-type asteroids could be chosen as targets for future space missions.

Acknowledgements

The author is grateful to Dr. Ovidiu Vaduvescu, Dr. Daniel Hestroffer, and Dr. James Hilton for suggestions which improved the article.

References

Bange, J.: 1998, 'An Estimation of the Mass of Asteroid 20-Massalia Derived from the Hipparcos Minor Planet Data', *Astron. Astrophys.* **340**, L1–L4.

Barucci, M. A., Capria, M. T., Coradini, A., and Fulchignoni, M.: 1987, 'Classification of Asteroids Using G-Mode Analysis', *Icarus* **72**, 304–324.

Belton, M. J. S., Chapman, C. R., Thomas, P. C., Davis, M. E., Greenberg, R., Klaasen, K., Byrnes, D., D'Amario, L., Synott, S., Johnson, T. V., McEwen, A., Merline, W. J., Davis, D. R., Petit, J-M., Storrs, A., Veverka, J., and Zellner, B.: 1995, 'Bulk Density of Asteroid 243 Ida from the Orbit of its Satellite Dactyl', *Nature* **374**, 785–788.

Birlan, M., Fulchignoni, M., and Barucci, M. A.: 1996a, 'Effects of IRAS Albedo Correction on the G-Mode Asteroid Taxonomy', *Icarus* **124**, 352–355.

Birlan, M., Barucci, M. A., and Fulchignoni, M.: 1996b, 'G-Mode Analysis of the Reflection Spectra of 84 Asteroids', *Astron. Astrophys.* **305**, 984–989.

Dunham, D. W., Dunham, J. B., and 44 authors: 1990, 'The Size and Shape of (2) Pallas from the 1983 Occultation of 1 Vulpeculae', *Astron. J.* **99**, 1636.

Gaffey, M. J., Bell, J. F., Hamilton Brown, R., Burbine, T. H., Piatek, J. L., Reed, K. L., and Chaky, D. A.: 1993, 'Mineralogical Variations within the S-Type Asteroid Class', *Icarus*, **106**, 573–602.

Hestroffer, D., Marchis, F., Berthier, J., Fusco, T., Cellino, A. DiMartino, M., Tanga, P., and Zappala, V.: 2000, 'The Main-Belt Binary Asteroid (216) Kleopatra: First Ground-Based Direct Imaging', *Science*, submitted.

Hilton, J. L.: 1999, 'US Naval Observatory Ephemerides of the Largest Asteroids', *Astron. J.* **117**, 1077–1086.

Marchis, F., Hestroffer, D., Cellino, A., Tanga, P., and Zappala, V.: 1999, '(216) Kleopatra', **IAUC 7308**.

Merline, W. J., Close, L. M., Dumas, C., Chapman, C. R., Roddier, F., Menard, F., Slater, D. C., Duvert, G., Shelton, C., and Morgan, T.: 1999, 'Discovery of a Moon Orbiting 45 Eugenia', *Nature* **401**, 565–569.

Millis, R. L. and Eliott, J. L.: 1979, 'Direct Determination of Asteroid Diameters from Occultation Observations', in Tom Gehrels (ed.), *Asteroids I*, University of Arizona Press, Tucson, pp. 98–118.

Ostro, S. J., Hudson, S. R., and 16 authors: 1999, 'Asteroid 4179 Toutatis: 1996 Radar Observations', *Icarus* **137**, 122–139.

Scholl, H., Schmadel, L. D., and Roser, S.: 1987, 'The Mass of the Asteroid (10) Hygiea Derived from Observations of (829) Academia', *Astron. Astrophys.* **179**, 311–316.

Tedesco, E. F.: 1992, 'The IRAS Minor Planet Survey', Phillips Laboratory Technical Report, No PL-TR-92-2049.

Tedesco, E. F., Williams, J. G., Matson, D. L., Veeder, G. J., Gradie, J. C., and Lebofsky, L.A., 1989: 'Three-Parameter Asteroid Taxonomy Classifications', in R. P. Binzel, T. Gehrels and M. Shapley Matthews (eds.), *Asteroids II*, University of Arizona Press, Tucson, pp. 290–297.

Tholen, D.: 1989, 'Asteroid Taxonomic Classifications', in R. P. Binzel, T. Gehrels and M. Shapley Matthews (eds.), *Asteroids II*, University of Arizona, pp. 1139–1150.

Thomas, P. C., Binzel, R. P., Gaffey, M. J., Zellner, B. Z., Stross, A.D., and Wells, E.: 1997, 'Vesta: Spin Pole, Size, and Shape from HST Images', *Icarus* **128**, 88–94.

Thomas, P. C., Joseph, J., Veverka, J., Bell III, J. F., Bell, M. E., Clark, B., Harch, A., Martin, P., Robinson, M., Murchie, S., Izenberg, N., Chapman, C., Merline, W., McFadden, L., Wellnitz, D., and Malin, M.: 1999a, 'The Shape of Eros from NEAR Imaging Data', in *Asteroids, Comets, and Meteors 1999*, invited paper.

Thomas, P. C., Veverka, J., Bell III, J. F., Clark, B. E., Carcich, B., Joseph, J., Robinson, M., McFadden, L. A., Malin, M. C., Chapman, C. R., Merline, W., and Murchie, S.: 1999b, 'Mathilde: Size, Shape, and Geology', *Icarus* **140**, 17–27.

Veverka, J., Thomas, P., Harch, A., Clark, B., Bell III, J. F., Carcich, B., Joseph, J., Murchie, S., Izenberg, N., Chapman, C., Merline, W., Malin, M., McFadden, L., and Robinson, M.: 1999, 'NEAR Encounter with Asteroid 253 Mathilde: Overview', *Icarus* **140**, 3–16.

Viateau, B.: 2000, 'Mass and Density of Asteroids (16) Psyche and (121) Hermione', *Astron. Astrophys.* **354**, 725–731.

Viateau, B. and Rappaport, M.: 1997, 'The Bordeaux Meridian Observations of Asteroids. First Determination of the Mass of 11 Parthenope', *Astron. Astrophys.* **320**, 652–658.

Viateau, B. and Rappaport, M.: 1998, 'The Mass of 1 Ceres from its Gravitational Perturbation on the Orbits of 9 Asteroids', *Astron. Astrophys.* **334**, 729–735.

Williams, J. G.: 1984, 'Determining Asteroid Masses from Perturbation on Mars', *Icarus* **57**, 1–13.

Yeomans, D. K., Antreasian, P. G., Cheng, A., Dunham, D. W., Farquhar, R. W., Giorgini, J. D., Konopliv, A. S., Miller, J. K., Owen, Jr., W. M., Thomas, P. C., Veverka, J., and Williams, B. G.: 1999, 'Estimating the Mass of Asteroid 433 Eros during the NEAR Flyby', in *Asteroids, Comets, and Meteors 1999*, Abstract 04.02.

Asteroid density; an overview

Mirel Birlan
Observatoire de Paris-Meudon,
92195 Meudon Cedex, France
Mirel.Birlan@obspm.fr

Abstract : This paper gives an overview of the present knowledges of the density of minor planets. The importance of physical properties it is underlined not only as a key to understand the origin and evolution of this population but also to constrain the initial parameters of the planetary nebula which will explain also the presence of those objects into the solar system.
A synthesis of asteroid densities as well as possibles correlations of the density through the asteroid taxonomic system are also presented.

Keywords: asteroid, density, astrometry, taxonomy

1. INTRODUCTION

Our recent studies concerning the asteroids consolidate the hypothesis of remnant planetesimals from the early solar system formation which, by mutual collisions and gravitational effects of major planets, evolved through the present population.

The density(as well as the gradients toward the nebula) remains one of the key role parameter of the primary planetary nebula. For this reason each aspect which could constrain their initial value must be taken into account. The asteroids (at least a major part of them) are objects on which the global mineralogy does not change since their formation, during the early stage of the protoplanetary nebula. The knowledge of the asteroid density will constrain the starting values of densities in the protoplanetary nebula.

2. MASS, VOLUME, DENSITY – WHAT IT IS KNOWN?

The three parameter are not independent. Different observation techniques could be used to obtain two of them: by gravitational perturbation we obtain the mass of the perturbed asteroid, the occultation and CCD imaging estimate the shape and volume, radar, spectroscopic observations, and comparative mineralogy are needed in order to obtain a value of asteroid density. High accuracy values of the shapes and asteroid masses are obtained through intruments embarqued on space missions, and/or space instruments: NEAR, Galileo, Hubble,…

Nowdays more than 33000 asteroids are on the astrometric database. Contrary this large number of objects, the density is not a physical parameter that can be found on each paper concerning the asteroids. This lack of papers concerning the asteroid mass (volume, density) is due to the dificulties of a good estimations of them. Moreover, following different authors, for the same object we found estimations and finally, divergent conclusions are generated. Which is the good estimation?

The error which affect the shape of the asteroid has a great importance inside the error of the density (if we assume a spherical body, the volume is proportional to the cube of the

radius). For this reason, careful estimation of shapes (space missions offers an ideal instrumental support) must be taken into account.

Table 1 presents the compilation of densities of asteroids based on the masses and volumes published on the literature. Even if this table contains data obtained from both ground based observations and space experiments, only 19 asteroids could be counted. For the major part of the mass determination using ground observations, the IMPS ([Ted92]) diameter values were considered in order to compute the volume. The exceptions are 1 Ceres and 4 Vesta on which Hubble observations were used to determine theirs volumes ([Par02] and [Tho97]). The volumes and masses used for the asteroids observed trough spacecrafts are the same published on the references. Except data obtained from space missions, all the asteroids belong to the major one (D>100 km) of the main belt.

The last column of Table 1 contains the taxonomic type ([Bir96]) of each asteroid, in order to compare the density values with different mineralogy assumed to different taxonomic class.

The graphic of densities versus semi-major axis is presented in Figure 1. For each asteroid, the taxonomic type was annotated on the figure, in order to distinguish possible correlations between the assumed mineralogy and the density.

Table 1. Recent characteristics of asteroids

AST.	DIAMETER (km)	MASS (10^{18} kg)	VOLUME (10^{15} m^3)	a (u.a.)	DENSITY (10^3 kg/m^3)	REF.	TAXON
1	2a=969.6 ± 10.2	873 ± 8.7	331.3 ± 11.9	2.7666	1.98 ± 0.09	[Par02];[Hil99]	G
1	2b=932.8 ± 11.8	946.6 ± 4.7			2.14 ± 0.09	[Par02];[Via98]	G
2	498.1 ± 18.8	316.2 ± 32	64.7 ± 7.6	2.7723	4.8 ± 1.07	[Hil99]	B
4	468 ± 26.7	336.1 ± 50	78 ± 3	2.3614	4.3 ± 0.3	[Tho97];[Hil99]	V
6	185.18 ± 2.9	13.7 ± 4.4	3.32 ± 0.15	2.4252	4.28 ± 1.51	[Mic01]	S
10	407.1 ± 6.8	93.4 ± 46	35.3 ± 1.8	3.1384	2.64 ± 1.44	[Sch87]	C
11	153.3 ± 3.1	5.13 ± 0.25	1.88 ± 0.12	2.4530	2.72 ± 0.31	[Via97]	S
15	255.3 ± 15	8.35 ± 2.2	8.71 ± 1.28	2.6438	0.95 ± 0.39	[Hil99]	S
15	255.3 ± 15	25.05 ± 5.96	8.71 ± 1.28	2.6438	2.87 ± 1.1	[Mic01]	S
16	253.2 ± 4.0	17.3 ± 5.1	8.5 ± 0.4	2.921	2.03 ± 0.69	[Via00]	M
20	145.5 ± 9.3	4.77 ± 0.78	1.61 ± 0.33	2.4094	2.96 ± 1.09	[Ban98]	S
45	214.6 ± 4.2	6.02 ± 0.3	5.17 ± 0.31	2.7203	1.16 ± 0.13	[Mer99]	C
52	302.51 ± 5.4	51.88 ± 17.5	14.49 ± 0.77	3.1003	3.58 ± 1.4	[Mic01]	C
88	200.57 ± 5.0	14.71 ± 2.58	4.22 ± 0.31	2.7724	3.48 ± 0.87	[Mic01]	BCG
121	209.0 ± 4.7	9.35 ± 1.58	4.78 ± 0.23	3.4412	1.95 ± 0.42	[Via00]	C
243	SPACE MISSION ESTIMATION			2.8596	2.6 ± 0.5	[Bel95]	S
253				2.6472	1.34 ± 0.02	[Vev99]	C
433				1.4583	2.9 ± 0.4	[Yeo99]	S
444	159.57 ± 13.1	7.16 ± 3.18	2.13 ± 0.52	2.7711	3.36 ± 2.31	[Mic01]	C
511	326.07 ± 5.3	66.4 ± 4.77	18.14 ± 0.88	2.1902	4 ± 0.44	[Mic01]	C
704	316.6 ± 5.2	69.6 ± 31.1	16.6 ± 0.8	3.0638	4.19 ± 2.08	[Via97]	C

3. CONCLUSION

As it can be seen on the Table 1, it is still difficult to have a good approach on the asteroid density as long as both the mass and the shape of it are affected by large error-bars. For instance, the case of asteroid 704 Interamnia makes very difficult any conclusion that will match a carbonaceous chondrite (CI1/CM2) mineralogy with such a high density (even if it is affected by large error-bars).

Another example of divergent estimations concerns the asteroid 15 Eunomia. The density derived considering the mass proposed by Hilton ([Hil99]) is a third part of those derived

using the Michalak's ([Mic01]) proposal of Eunomias' mass. The associate taxonomic type of this asteroid allow us to consider more realistic the mass estimation of the last mentioned author

The asteroid 16 Psyche belongs to a M –type asteroids which is associated (through spectral features and radar observations) to metallic(or chondritic entsatite) meteorites. The scientist explains the metal rich surface of Psyche by the evidence of a catastrophic collision of segregated planetesimals of the main belt. Thus, Psyche is a part of the nucleus which survived to the catastrophic collision. If we assume this hypothesis of 16 Psyche, their density two-three times lower than those of the metallic meteorites must be explained.

Another aspect which could be noted is the author-dependence of the density values. Michalak ([Mic01]) compute the mass of asteroids 6, 15, 52, 88, 444, 511. On the Figure 1 it can be seen the systematic overestimation of densities derived from [Mic01] for the C-type asteroids, comparative to densities of other C-type asteroids on the literature. Moreover, the mineralogy of a C-type asteroid (assumed to be the same as the CI1/CM2 meteorites) cannot fit to such high densities.

Figure 1. Density of asteroids along the semi major axis of their orbits. For each asteroid the taxonomic type was annotated.

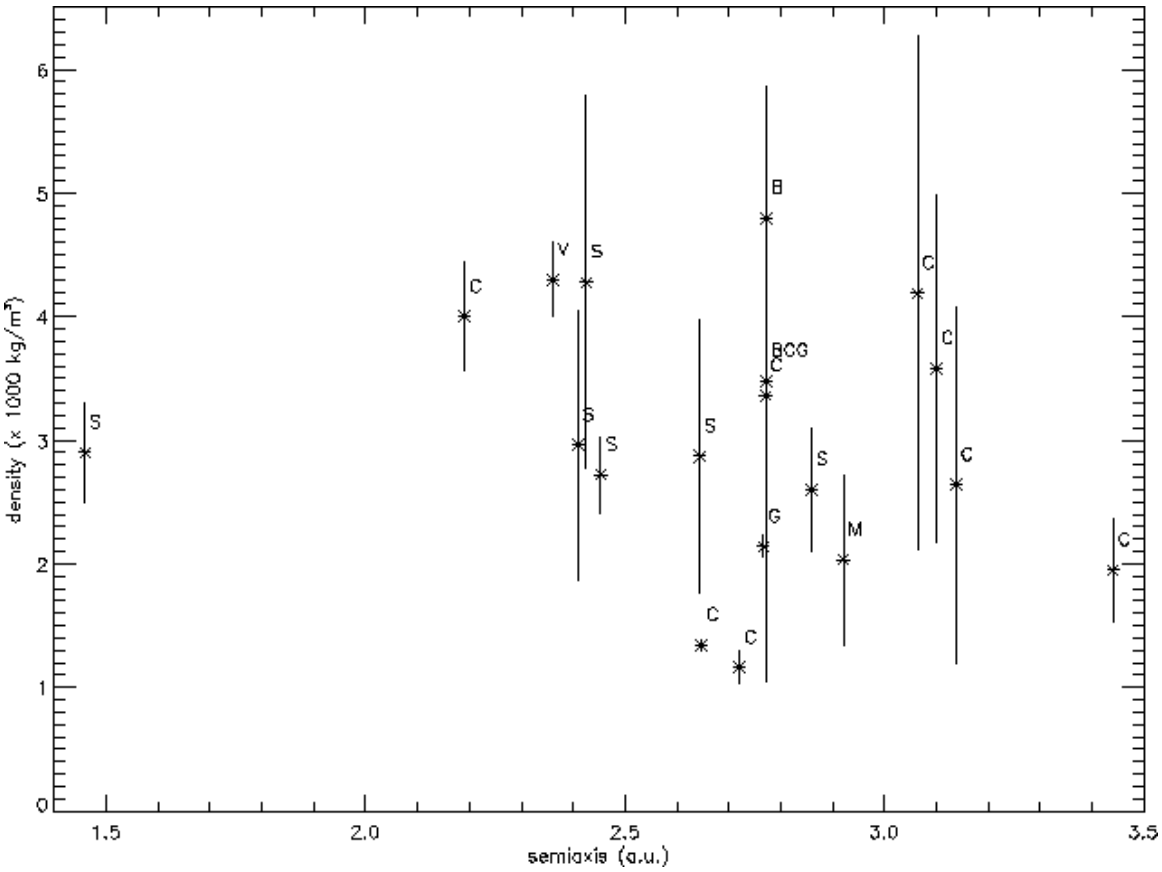

The small number of asteroids does not allow us a real statistic analysis. However, the density could distinguish between C and S-type asteroids. This result is important and proves that surface mineralogy could be representative in defining the sub-surface structure of an asteroid.

Acknowledgements: The author is grateful to LOC of Ceres2001 for the successful meeting.

References :

[Ban98] – Bange, J., 1998, A&A, L1-L4 ;
[Bel95] – Belton M. et al, 1995, Nature, 374, pp 785-788 ;
[Bir96] – Birlan M. et al, 1996, Icarus, pp 352-354;
[Hil99] – Hilton, J.L. 1999, Astron.J., 117, pp 1077-1086 ;
[Mer99] – Merline W.J. et al, 1999, Nature, 401, pp 565-569 ;
[Mic01] - Michalak, G. 2001, A&A, 374, pp 703-711 ;
[Par02] – Parker J.W. et al, 2002, Astron J., in press;
[Sch87] – Scholl H. et al, 1987, A&A, 179, pp 311-316 ;
[Ted92] – Tedesco E. 1992, IMPS Technical Report;
[Tho97] – Thomas P.C. et all, 1997, Icarus, 128, pp 88-94;
[Vev99] – Veverka J. et al, 1999 , Icarus, 140, pp 3-16 ;
[Via97] – Viateau, B., Rapaport M., 1998, A&A, 320, pp 652-658 ;
[Via98] - Viateau, B., Rapaport M., 1998, A&A, 334, pp 729-735 ;
[Via00] – Viateau, B. 2000, A&A, 354, pp 725-731 ;

III. Conclusions, prospective

L'étude des corps sans atmosphère est un domaine en plein essor. Le nombre d'objets découverts atteint plus de 200 000 pour les astéroïdes, et plus de 1 200 pour les objets trans-neptuniens. De ce fait, leur étude dynamique est un formidable laboratoire grandeur nature pour l'étude de nombreux problèmes de mécanique céleste.

Une meilleure connaissance de la dynamique des astéroïdes est importante dans plusieurs champs de recherche astronomiques : la formation et l'évolution de la ceinture principale, l'identification, la formation et l'évolution des familles d'astéroïdes, l'étude du chaos et des orbites chaotiques, les résonances, l'étude d'astéroïdes géocroiseurs, les occultations des étoiles par des astéroïdes. Une meilleure connaissance de leur orbite ne peut être obtenue que par des observations systématiques de qualité. L'amélioration de leurs paramètres orbitaux est faite en tenant compte des nouvelles observations intervenant dans le processus d'ajustement, sans oublier l'importance du choix sur le système de référence (vers un système de référence quasi-inertiel). J'envisage de poursuivre et développer ces activités, ainsi que mes recherches sur les problèmes d'optimisation des techniques d'observations, d'analyse et traitement d'images astrométriques.

La connaissance de la physique des corps sans atmosphère précède les études dynamiques liées à la découverte des objets et à l'établissement de leur orbite. L'utilisation importante des caméras CCD est facilitée par les acquis technologiques. Les grands projets d'observation et de cartographie astronomique au sol sont basés sur des batteries de CCD aux éléments d'images de taille de plus en plus réduite. Cette nouvelle tendance permet de relever certains paramètres physiques (par exemple la magnitude ou les couleurs) en même temps que les mesures astrométriques. Les résultats de tels programmes ne sont possibles que par l'utilisation de chaînes de traitement des données. Cependant, une chaîne de traitement doit être suffisamment flexible pour permettre à des programmes scientifiques ponctuels d'être mise en œuvre, comme par exemple ceux concernant les objets du système solaire.

Les acquis technologiques sur les détecteurs ont permis aussi l'accès plus facile aux domaines de longueurs d'onde de l'infrarouge proche (0,8 – 4,0 μm). C'est un domaine d'études essentiel dans le cas des astéroïdes, afin de pouvoir comparer les résultats spectroscopiques des minéraux, glaces, substances organiques, mélanges, (obtenus en laboratoire) avec ceux des spectres relevés pour de corps sans atmosphère. L'activité d'observations et d'analyse des données représente une composante essentielle pour l'établissement des modèles minéralogiques des surfaces d'astéroïdes. Je me propose d'affiner les méthodes de réduction des spectres afin de réduire les erreurs de mesure. Dans ce cadre, deux composantes semblent essentielles :

- l'établissement d'un catalogue d'étoiles (analogues solaires) dont le comportement spectral dans la région de l'infrarouge proche est très bien connu
- le développement des techniques permettant la modélisation efficace de l'atmosphère terrestre visant l'élimination de leur influence dans les spectres d'astéroïdes. La présence des bandes d'absorption atmosphérique autour de 1,15, 1,4, et 1.9 μm est très nuisible à une interprétation correcte des résultats.

Il est évident que la richesse des données issues des observations spectroscopiques d'objets sans atmosphère est encore peu exploitée, d'une part à cause de nos faibles connaissances concernant l'analyse des résultats et leur modélisation en termes minéralogiques, d'autre part du fait que la modélisation minéralogique peut accepter une multitude de solutions. Les modèles doivent également répondre à des ensembles de données d'observations sur des intervalles spectraux plus larges.

Mes futures recherches seront en partie consacrée à des études instrumentales liées aux aspects d'automatisation et à des stratégies d'observations. La construction et l'exploitation des télescopes robotiques représentent un domaine en pleine expansion ; leur utilisation est très justifiée pour des programmes dits « de routine » genre « large survey », « celestial map », « follow-up recovery », « survey of optical transients ». Une stratégie d'observation faites seulement par des automatismes liés au télescope et à ses détecteurs est parfois pénalisante, si nous nous situons dans un contexte d'observations où l'amélioration des données passent par une prise de décision « ad-hoc » (je peux citer le cas des observations en interférométrie, en spectroscopie, en imagerie des objets à forte dynamique ou à faible contraste). La mise à dispositions des procédures informatiques pour le remote observing présente la possibilité d'interagir en temps réel (même si cette possibilité est très limitée dans le contexte d'un télescope robotique) et de créer un enjeu stratégique important dans l'exploitation de ce télescope.

Enfin, j'envisage de m'impliquer de façon importante, au cours des années à venir, dans le domaine de l'éducation astronomique et celui de l'éducation par l'astronomie. L'utilisation des télescopes robotiques et des méthodes interactives avec des instruments astronomiques permet d'intéresser les élèves et les étudiants aux sciences exactes en général et plus particulièrement à l'astronomie. Des réseaux des télescopes autour du globe[1] permettent des observations astronomiques pendant les heures de cours, si le télescope utilisé est à l'antipode de leur localisation. Ce type d'interaction peut non seulement améliorer les connaissances astronomiques, mais aussi éveiller également l'intérêt pour les nouvelles technologies, la transmission de l'information, le travail en équipe. De plus, cette activité peut susciter un intérêt pour l'étude des langues étrangères, pour les relations humaines et les différences culturelles. Alors nous pouvons mettre en place une stratégie d'enseignement ciblée sur le « comment nous transmettons nos connaissances ». L'élaboration des méthodes visant à rendre plus efficace l'enseignement de l'astronomie en fonction du matériel didactique utilisé ne peut pas ignorer les acquis pédagogiques. De plus, ces méthodes doivent être basées sur des fondements épistémologiques de l'astronomie. Les séances d'enseignement ciblerons essentiellement des concepts et notions visant l'identification unitaire d'une science (ici, l'astronomie), et la localisation de son objet d'études, dans le contexte du curriculum scolaire.

[1] L'exemple le plus connus est G-HOU, acronyme de Global Hands-On Universe (l'Univers à Portée des Mains), programme d'éducation par l'astronomie qui propose une composante liées aux observations astronomiques par le partage des ressources d'observations (télescopes, ordinateurs) a travers une réseau autour du globe

Annexe : liste de publications, encadrements, enseignement, diffusion des connaissances, autres publications

LISTE DE PUBLICATIONS

ARTICLES A COMITE DE LECTURE

1. Marcq, E., Encrenaz, Th., Bezard, B., **Birlan, M.** – *Latitudinal variations of CO and OCS in the lower atmosphere of Venus from near-infrared nightside spectro-imaging*, **Icarus** (submitted)
2. Barucci M.A., I. Belskaya, M. Fulchignoni, **M. Birlan** - *Taxonomy of Centaurs and Trans-Neptunian Objects*, **Astronomical J.** (submitted)
3. Vernazza P. Mothe-Diniz T., Barucci A., **Birlan M.**, Carvanho J., Strazzulla G., Fulchignoni M., Migliorini A. - *Analysis of near-IR spectra of 1 Ceres and 4 Vesta, targets of the Dawn Mission*, **Astronomy and Astrophysics**, (in press)
4. Thuillot W., Arlot J-E., Stavinschi M., **Birlan M.**, Lainey V. - *Ground-based astrometry at the time of the GAIA mission* **Romanian Astron. J.** (in press)
5. Thuilllot, W., Vaubaillon, J., Scholl, H, Colas, F., Rocher, P., **Birlan, M.**, Arlot, J-E. - *Relevance of the NEO dedicated observing programs* – Comptes-Rendu de l'Académie des Sciences, (in press)
6. Barucci, M.A., Fulchignoni, M., Fornasier, S., Dotto, E., Vernazza, P., **Birlan, M.**, Binzel, R., Carvano, J., Merlin, F., Barbieri, C., Belskaya, I. – *Asteroid target selection for the new Rosetta mission baseline : 21 Lutetia and 2867 Steins* – **Astronomy and Astrophysics** v.430, 313-317, 2005.
7. **Birlan, M.**, M.A. Barucci, W. Thuillot – *Solar system observations by remote observing technique : useful experience for robotic telescope strategies.* **Astronomische Nachricthen** No. **6-8**, 571-573, 2004.
8. **Birlan M.,** Barucci M.A., Vernazza, P., Fulchignoni M., Binzel R.P., Bus S.J., Fornasier S. *Near-Ir Spectroscopy of asteroids21 Lutetia, 89 Julia, 140 Siwa, 2181 Fogelin, and 5480 (1989YK8), potential targets of the Rosetta mission; remote observations campaign on IRTF,* **New Astronomy,** Vol**. 9 (5),** 343-351, 2004.
9. Binzel, R.P., **Birlan, M.**, Bus, S.J., Harris, A., Rivkin, A.S., Fornasier, S.– *Spectral Observations for Near-Earth Objects Including Potential Target 4660 Nereus: Results From Meudon Observations at the NASA Infrared Telescope Facility (IRTF)*, **Planetary & Space Science,** Vol. **52(4)**, 291-296, 2004.
10. Fulchignoni, M, Delsanti, A., Barucci, M.A., **Birlan, M.** - *Toward a Taxonomy of the Edgeworth-Kuiper Objects: A Multivariate Approach* - **Earth, Moon, and Planets**, vol. **92**:1-4, 2003.
11. Fornasier, S., Barucci, M.A., Binzel, R.P., **Birlan, M.**, Fulchignoni, M., Barbieri, C., Bus, S.J., Harris, A.W., Rivkin, A.S., Lazzarin, M., Dotto, E., Erikson, A., Doressoundiram, A., Bertini, I., Peixinho, N., - *A portrait of 4979 Otawara, target of the Rosetta space mission*, **Astronomy & Astrophysics,** vol **398**, 327-333, 2003.
12. **Birlan M.** – *First remote observation between IRTF-Hawaii and Observatoire de Paris-Meudon* **Ad-Astra**, vol **1,** n. **2,** 2002, ISSN 1583-0462

13. **Birlan M.** – *Dynamic and physical considerations on the asteroids' density*, **Earth, Moon and Planets** n. **88**, 1-10, 2002.
14. Bocsa G., **Birlan, M.** - *Intermediate stars in extragalactic radiosource fields* **Romanian Astronomical Journal**, vol **11**, n. **2**, 181-186, 2001.
15. Lazzarin M., Fornasier S., Barucci M.A., **Birlan M.** - *Groundbased investigation of asteroid 9969 Braille, target of the spacecraft mission Deep Space 1* **Astronomy and Astrophysics**, n. **375**, 281-284, 2001.
16. Barucci M.A., Fulchignoni, M., **Birlan M.**, Doressoundiram A., Romon J., Boehnhardt H, - *Analysis of Trans-Neptunian and Centaur colours: continuous trend or grouping?*, **Astronomy and Astrophysics**, n **371**, 1150-1154, 2001.
17. Fulchignoni M., **Birlan M.**, Barucci M.A. - *The extension of the G-mode asteroid taxonomy* **Icarus**, n. **146**, 204-212, 2000.
18. **Birlan M.** – *Emission in absobtion lines; results of the SL9 L nucleus impact on Jupiter*, **Romanian Astronomical Journal**, vol **10**, n. **8**, 137-144, 2000.
19. Doressoundiram A., Weissman P.R., Fulchignoni M., Barucci M.A., LeBras A., Colas F., Lecacheux J., **Birlan M.**, Lazzarin M., Fornasier S., Dotto E., Barbieri C., Sykes M.V., Larson S., Hergenrother C. - *4979 Otawara: Flyby target of the Rosetta mission* **Astronomy & Astrophysics** , vol **352**, n. **2**, 697-702, 1999.
20. Vaduvescu 0., Stefanescu G., **Birlan M.** - *CCD and photographic observations of the comet C/1996B2 (Hyakutake)* **Romanian Astronomical Journal**, vol. **8**, 43-51, 1998.
21. Bocsa G., **Birlan M.** - *Astrometric precise positions of the comet Hale-Bopp at Bucharest Observatory* **Romanian Astronomical Journal**, vol. **7**, 199-200, 1997.
22. Florczak M., Dotto E., Barucci M.A., **Birlan M.**, Erikson A., Fulchignoni M., Nathues A., Perret L., Thebault P. - *Rotational properties of main belt asteroids: Photoelectric and CCD observations of 15 objects* **Planetary and Space Science** vol. **45**, n. **11**, 1423-1435, 1997.
23. **Birlan M.**, Barucci M.A., Angeli C., Doressoundiram A., DeSanctis M.C. - *Rotational properties of asteroids: CCD observations of nine small asteroids* **Planetary and Space Science** vol. **44**, n. **6**, 555-558, 1996.
24. **Birlan M.** - *CCD photometry of the asteroid 2419 Moldavia*, **Romanian Astronomical Journal** vol. **6**, n. **1**, 1996.
25. **Birlan M.**, Barucci M.A., Fulchignoni M. - *G-mode analysis of reflection spectra for 84 asteroids* **Astronomy and Astrophysics** vol **305** n. **2**, 984-988, 1996.
26. **Birlan M.**, Fulchignoni M., Barucci M.A. - *Effects of IRAS albedo corrections on Barucci's asteroid taxonomy*, **Icarus**, **124**, 352-354, 1996.
27. Vaduvescu O., **Birlan M.** - *Software package for preparing and processing of an astronomical observation*, **Romanian Astronomical Journal** vol. **6**, n. **1**, 97-99, 1996.
28. **Birlan M.**, Bocsa G. - *Observations of minor planets in 1990-1994 at the Bucharest Astronomical Observatory*, **Romanian Astronomical Journal**, vol. **5**, n. **2**, 185-191, 1995.
29. Vass G, Bocsa G., Ionescu V., Alexiu A., **Birlan M.** - *Wide field plate archive data base in Bucharest*, **Romanian Astronomical Journal** vol. **4**, n. **2**, 179-181, 1994.
30. **Birlan M.** - *On the physical and dynamics properties of asteroids*, **Romanian Astronomical Journal** vol. **3**, n. **2**, 123-126, 1993.

ARTICLES EN COMPTE-RENDU

1. Barucci M.A., Fulchignoni, M., Belskaya, I., Vernazza, P., Dotto, E., **Birlan, M. -** *Rosetta asteroid candidates*, in *The NEW Rosetta targets. Observations, simulations and instrument performances* Astrophysics and Space Science Library (ASSL) Vol. 311, Kluwer (ISBN: 1-4020-2572-6). (Eds. L. Colangeli, E. Mazzotta-Epifani, P. Palumbo);
2. A. Merand, **M. Birlan,** V. Coudé du Foresto, R. Lelu de Brach - *Remote observations with FLUOR and the CHARA Array***, SPIE**, (in press), 2004
3. M.A. Barucci, M. Fulchignoni, **M. Birlan**, P. Vernazza, E. Dotto, A. Doressoundiram – *Rosetta asteroid candidates* - Highlights of Astronomy, vol. 13, **XXVth General Assembly of the IAU**, Sidney, July 2003

4. S. J. Bus, A. J. Denault, J. T. Rayner, R. P. Binzel, **M. Birlan -** *Remote observing at the NASA Infrared Telescope Facility (IRTF)***,- SPIE** Conference**,** Advanced Global Communications Technologies for Astronomy II, Hawaii, August, 2002
5. **M. Birlan**, R. Binzel – *Paris Observatory Remote Observing January-May 2002: Sharing the Experience to Educational Astronomy,* Global Hands-On Universe Conference Proceedings, Paris, July, 2002
6. **M. Birlan** - *Asteroids density: an overview* - "Ceres 2001" Workshop IMCCE, Paris, 2001
7. **M. Birlan**, Bocsa G. - *Intermediate stars in extragalactic radiosource fields: Astrometric measurements* IAU Colloquium 180, Washington, 2000
8. M.A. Barucci, **M. Birlan** - *Photométrie CCD:application aux astéroïdes* Quatrièmes rencontres des Carcassonne sur les techniques de détection optique en astronomie, Carcassonne, Mai, 1996

COMMUNICATIONS

1. **Mirel Birlan** *L'observation à distance en infra-rouge proche des corps du système solaire* Nouvelles techniques d'observation et bases de données : apports en astrométrie et mécanique céleste, Ecole thématique CNRS, 21-25 mars 2005
2. **Mirel Birlan** – *Remote observing in Paris – CHARA Collaboration* – One Year Review Workshop, Paris, 7-12 February, 2005.
3. **M. Birlan**, P. Vernazza, M. Fulchignoni, A. Rossi, E. Dotto, D. Nesvorny - *Near-IR spectroscopy of asteroids 832 Karin, 13807 1998 XE13, and 13765 Nansmith, members of Karin family* - DPS Annual Meeting P32.10, Louisville, KY, 8-12 November 2004
4. Gh Vass, **M. Birlan** - *Using conceptual maps in astronomy education* - DPS Annual Meeting P13.05, Louisville, KY, 8-12 November 2004
5. M. Fulchignoni, M.A. Barucci, S. Fornasier, E. Dotto, P. Vernazza, **M. Birlan**, J. Carvano, F. Merlin, I. Belskaya - *2867 Steins and 21 Lutetia: the Rosetta mission asteroid targets* - DPS Annual Meeting 28.03, Louisville, KY, 8-12 November 2004
6. E. Marcq, T. Encrenaz, B. Bézard, **M. Birlan -** *A Study of Lower Atmosphere Dynamics And Search For Active Volcanism On Venus : Preliminary Work To Venus Express Mission* - DPS Annual Meeting P39.03, Louisville, KY, 8-12 November 2004
7. **Mirel Birlan** - *Near-IR spectroscopy of Karin family of asteroids,* Astrometry with Small Telescopes, Bucharest 20-22 October 2004.
8. W. Thuillot, J-E. Arlot, M. Stavinschi, **M. Birlan**, V. Lainey - *Ground-based astrometry at the time of the GAIA mission* Astrometry with Small Telescopes, Bucharest 20-22 October 2004.
9. Francois Colas, Jeremie Vaubaillon, **Mirel Birlan** - *Project of a 2 meter class telescope at Pic du Midi observatory* - Risks connected to a NEO impact, Chateau de Meudon, 13-14 september 2004
10. Gh Vass, **M. Birlan** – *Educational efficiency of observing astronomical phenomena: The case of planet Venus* ESOP 2004 Workshop Paris 27-29 August 2004.
11. Gh Vass, **M. Birlan** – *Apparently non-periodic astronomical phenomena: A systematic educational approach* ESOP 2004 Workshop Paris 27-29 August 2004.
12. P. Vernazza, M. Fulchignoni, **M. Birlan** - *Spectroscopic investigation of Near-Earth Objects* COSPAR Meeting, Paris, 18-25 July 2004.
13. **Mirel Birlan**, P. Vernazza, M.A. Barucci, M. Fulchignoni – *Spectroscopy of asteroids in remote observing mode with IRTF* COSPAR, Paris, 18-25 July 2004.
14. **Mirel Birlan**, M.A. Barucci, W. Thuillot – *Solar system observations by remote observing technique : useful experience for robotic telescope strategies.* Third Thinkshop concerning Robotic Telescopes, Potsdam, 12-15 July 2004
15. A. Merand, **M. Birlan,** V. Coudé du Foresto, R. Lelu de Brach - *Remote observations with FLUOR and the CHARA Array***,** SPIE, Glasgow, 21-15 June 2004.
16. E. Marcq; T. Encrenaz; B. Bézard, **M. Birlan** - *Spectro-Imaging of Venus night side in preparation of the Venus Express mission : study of global dynamics and search for active volcanism.* EGU 1st General Assembly, Nice, 25-30 April 2004.

17. **Mirel Birlan** -*Le Centre d'Observation à Distance en Astronomie à Meudon(CODAM); Observations et résultats scientifiques obtenus avec l'IRTF,* Forum Bases, Traitements de Données et Observatoires Virtuels, Paris, 27-28 Novembre, 2003.
18. **Mirel Birlan**, Vernazza, P., Barucci M.A., Fulchignoni M., Binzel R.P., Bus S.J., Fornasier S. – *Near-IR spectroscopy of new asteroid targets for the Rosetta mission* - American Astronomical Society, DPS meeting, Monterey-California, 2-6 September 2003.
19. M. Fulchignoni, Delsanti, A., Barucci, M.A., **Birlan, M.** - *Toward a taxonomy of the Edgeworth-Kuiper Belt Objects: the multivariate approach* - SF2A-2003: Semaine de l'Astrophysique Française, meeting held in Bordeaux, France, June 16-20, 2003.
20. M. Fulchignoni, Delsanti, A., Barucci, M.A., **Birlan, M.** - *Multivariate analyses of TNOs spectrophotometric data* - First Decadal Review of the Edgeworth-Kuiper Belt: Towards New Frontiers, Antofagasta, Chile, March 11-14, 2003.
21. Th Encrenaz, Bezard, B**., Birlan, M**., de Bergh, C. – *Observations of the Venus dark-side in the near-IR: A search for active volcanism and a study of dynamics* – Planetary Fourier Spectrometer General Meeting, Mars Express & Venus Express, Lecce, Italy, March 3-6, 2003.
22. **Mirel Birlan**, R. Binzel, S.J. Bus, A. Rivkin, A. Harris, A. Barucci, M. Fulchignoni - *From Mauna Kea to Meudon: IRTF Remote Observing Science Results for Potential Spacecraft Targets 4979 Otawara and 4660 Nereus*- American Astronomical Society, DPS meeting, Birmingham, Alabama, 2002.
23. S. Fornasier, Barucci M.A., Binzel R.P., **Birlan M.**, Fulchignoni M., Barbieri C., Bus S.J, Harris A.W., Rivkin A.S., Lazzarin M., Dotto E., Erikson A., Michalowsky T., Doressoundiram A., Bertini I., Peixinho N. - *Spectrophotometric observations of 4979 Otawara, target of the Rosetta space mission* - American Astronomical Society, DPS meeting, Birmingham, Alabama, 2002.
24. S. J. Bus, A. J. Denault, J. T. Rayner, R. P. Binzel, **M. Birlan** - *Remote observing at the NASA Infrared Telescope Facility (IRTF)* – **SPIE** Conference**,** Advanced Global Communications Technologies for Astronomy II, Hawaii, August, 2002.
25. **Mirel Birlan**, Richard Binzel – *Remote observation between IRTF-Hawaii and Observatoire de Meudon*, Global Hands-On Universe Conference, Paris, 2002.
26. S. Fornasier, M.A. Barucci, R.P. Binzel, M. Fulchignoni, **M. Birlan**, C. Barbieri, M. Lazzarin, A. Doressoundiram, E. Dotto, N. Peixinho - *A portrait of 4979 Otawara, target of the Rosetta space mission* Asteroids Comets Meteors, Berlin, 2002.
27. Marcello Fulchignoni, **Mirel Birlan**, Maria Antonietta Barucci - *TNO/Centaurs grouping tested with asteroid data sets* - American Astronomical Society, DPS meeting, New Orleans, 2001.
28. **Mirel Birlan**, Jean Souchay, Mariana Birlan - *Science and Religion : the Faith* – Science & Religion, Romanian Academy Meeting, Bucharest 2001.
29. **Mirel Birlan** - *Asteroids density: an overview* - "Ceres 2001" Workshop IMCCE, Paris, 2001 **.**
30. Marcello Fulchignoni, Maria Antonietta Barucci, A. Doressoundiram, J. Romon, **Mirel Birlan** - *Toward a Centaur/TNO taxonomy* - American Astronomical Society, DPS meeting, Pasadena, 2000.
31. **Mirel Birlan**, Gheorghe Bocsa - *Intermediate stars in extragalactic radiosource fields; astrometric measurements* - IAU Colloquium 180, Washington, D. C., March, 2000.
32. **Mirel Birlan** - *Density of small bodies on the solar system: correlations and cosmogonical implications* - Scientific session of the Romanian Academy, Bucharest, 20-22 April 2000.
33. Gheorghe Bocsa, **Mirel Birlan** - *Accuracy of Positions Determined within the Framework of CONFOR Programme* Scientific session of the Romanian Academy., Bucharest, 20-22 April 2000.
34. A. Doressoundiram, P. Weissman, M. Fulchignoni, M.A. Barucci, A. Le Bras, F. Colas, J. Lecacheux, **M. Birlan**, M. Lazarrin, S. Fornasier, E. Dotto, C. Barbieri, M. Sykes, S. Larson, C. Hergenrother - *4979 Otawara : the first asteroid target of the Rosetta mission* – Asteroids Comets Meterors, Ithaca 1999.
35. **Mirel Birlan** - *Asteroid photometric catalogues: a starting point to an asteroid taxonomy* – First romanian-russian meeting on astronomy, Sankt Ptersburg, 1998.
36. **Mirel Birlan** - *CCD photometry of the asteroids targets of the ROSETTA mission* - Scientific session of the Romanian Academy, Bucharest, 1998.
37. **Mirel Birlan** - *CCD photometry; results of the ESO asteroid campaign* - Scientific session of the Romanian Academy, Bucharest, 1997.

38. **Mirel Birlan**, Maria Antonietta Barucci - *Pratique de la photométrie des astéroïdes* - Quatrièmes rencontres sur les techniques de détection optique en astronomie, Carcassonne, May 1996.
39. **Mirel Birlan**, Marcello Fulchignoni, Maria Antonietta Barucci - *The extension of the G-mode asteroid taxonomy* - Asteroids Comets Meteors , Versailles, 1996.
40. A. Doressoundiram, M.A. Barucci, M. Fulchignoni, **M. Birlan** - *Visible spectroscopy of EOS family* - Asteroids Comets Meteors, Versailles, 1996.
41. Roos-Serote, M., A. Barucci, J. Crovisier, P. Drossart, M. Fulchignoni, J. Lecacheux, and F. Roques, **M. Birlan** - *Atomic line emissions in the impacts of comet SL9 into Jupiter* - SL9 Colloquium, Baltimore, USA, 1995.
42. **Mirel Birlan**, Marcello Fulchignoni, Maria Antonietta Barucci - *Influence of the revised IRAS albedos on the G-mode asteroid taxonomy* - D.P.S. meeting Mauna Lani, October 1995.
43. **Mirel Birlan**, M.A. Barucci, J. Crovisier, P. Drossart, M. Fulchignoni, J. Lecacheux, M. Roos-Serote, F. Roques - *Atomic line emissions in the plume and splashback of Shoemaker-Levy 9 impact L on Jupiter* - D.P.S. meeting Mauna Lani, October 1995.
44. **Mirel Birlan**, Maria Antonietta Barucci, Marcello Fulchignoni - *G-mode analysis of the reflection spectra for 85 asteroids* - European Geophysical Society-General Assembly, Grenoble, 1994.
45. Ovidiu Vaduvescu, **Mirel Birlan** - *Software package for preparing and processing of an astronomical observation - CELESTIAL MAPS version 4.5* - Second international school in astronomy and astrophysics, Rozen, Bulgaria, 1994.
46. **Mirel Birlan**, Marcello Fulchignoni, Maria Antonietta Barucci - *Extension of the G-mode method* - Symposium of the small bodies of the Solar System and their interrelation, Uppsala, Sweden, 1994.
47. **Mirel Birlan**, Maria Antonietta Barucci, Marcello Fulchignoni - *An extension of the Barucci's asteroid taxonomy* - Department of Planetary Science session, Minneapolis, 1994.
48. **Mirel Birlan** - *Mineralogy of S-type asteroids* - Scientific session of the Romanian Academy, Bucharest, 1994.
49. **Mirel Birlan** - *Lightcurves statistics a classification of asteroids* - European Geophysical Society-General Assembly, 1993.
50. **Mirel Birlan**, Gheorghe Bocsa - *Astrometrical measurements of minor planets in 1991-1992* - Asteroids, Comets, Meteors, 160-th I.A.U. Symposium, Belgirate, Italy, 1993.
51. **Mirel Birlan** - *Statistical study for Trojan asteroid groups* - Scientific session of the Romanian Academy, Iasi, 1993.
52. **Mirel Birlan** - *On the physical and dynamics properties of asteroids* - 30-th Astronomical Colloquium, Liege, Belgium, 1992.
53. Ovidiu Vaduvescu, **Mirel Birlan** - *Celestial maps in Turbo Pascal 6.0* - Scientific session of the Romanian Academy - Cluj, 1992.
54. **Mirel Birlan**, Ovidiu Vaduvescu - *Computer image reconstruction* - Scientific session of the Romanian Academy - Bucharest, 1992.

CONFERENCES, SEMINAIRES

19 avril 2005
Missions spatiales européennes pour l'étude du système solaire : présent et perspectives
Public lecture, French Embassy in Romania, Science week 18-23 April 2005

22, 23 mars 2005
L'observation à distance en infra-rouge proche des corps du système solaire
Ecole thématique CNRS : Nouvelles techniques d'observation et bases de données : apports en astrométrie et mécanique céleste, 21-25 mars 2005

15 novembre 2004
Near-IR (0.8-4.4 micron) spectroscopy of solar system bodies using remote observing: CODAM Project
Department of Physics and Astronomy,
University of York, Canada

12 mai 2004
Venus transit and its importance
Public lecture, French Embassy in Romania

30 avril 2004
L'importance éducationnelle des observations liées à la planète Venus,
Séminaire Temps-Espace, salle de l'Atelier,
Observatoire de Paris, France

1 Avril 2004
Rosetta Mission and Ground-Based Science of Asteroid Targets
Atomic and Nuclear Physics Department - Astrophysics Laboratory
Université de Bucarest, Roumanie

3 Mars 2004
Le Projet CODAM : spectroscopie en IR proche avec l'IRTF
Séminaire Temps-Espace, salle de l'Atelier,
Observatoire de Paris, France

Avril 2002
Remote observing technique ; first tests from Meudon
Seminaire à l'Institut Astronomique de l'Académie Roumaine
Bucarest, Roumanie

Fevrier 1999
Trans-Neptunian Objects and the early solar system formation
Séminaire à l'Agence Spatiale Roumaine,
ROSA-Bucarest, Roumanie

Février 1999
Physics of asteroids potential targets of Rosetta mission ; observational approach
Séminaire à l'Agence Spatiale Roumaine,
ROSA-Bucarest, Roumanie

Novembre 1996
Taxonomy of asteroids
Séminaire à l'Institut de Mécanique Céleste et de Calcul des Ephémérides
Paris, France

ENSEIGNEMENTS, ENCADREMENTS

Enseignement en Université :

2-eme semestre 2004/05	TP en Physique en DEUG SM et PC à l'Université de Cergy-Pontoise (46 heures)
octobre 2004	Cours intensif de Planétologie à l'Université de Bucarest, Faculté de Physique (9 heures)
2-eme semestre 2003/04	TP en Physique en DEUG SV et MIAS à l'Université de Cergy-Pontoise (52 heures)
2-eme semestre 2002/03	TP en Physique en DEUG SV à l'Université de Cergy-Pontoise (48 heures)
2-eme semestre 2001/02	TP en Physique en DEUG SV et MIAS à l'Université de Cergy-Pontoise (64 heures)
2-eme semestre 2000/01	TP en Physique en DEUG SV et DEUG SM à l'Université de Cergy-Pontoise (18 heures)
2-eme semestre 1998/99	Cours magistraux de physique en DEUG SV (Mécanique des fluides, électricité et magnétisme) à l'Université de Cergy-Pontoise DEUG (13 heures)
février 2001	Cours d'astronomie, pour le 3-ème année en Physique (techniques d'observations en astronomie, missions spatiales en planétologies, systèmes de magnitudes) à l'Université de Bucarest (10 heures)
février 1999	Cours d'astronomie, pour le 3-ème année en Physique (systèmes de références en astronomie) à l'Université de Bucarest (4 heures)

Enseignement en Lycée et Collège:

1986/87/88/89/90	Poste de professeur de Physique au lycée Mizil-Roumanie ;
1997/98	Poste de professeur d'informatique au lycée "Ion Barbu" Bucarest-Roumanie ;
1987/88	Cours de Physique Collège n.1 Mizil-Roumanie;

<u>Management des programmes et encadrement de stagiaires :</u>

2002 responsable du programme **Centre d'Observation à Distance en Astronomie à Meudon (CODAM)**
1998 membre du Comité d'Edition de l'Annuaire Astronomique Roumain
1997 membre du Comité d'Organisation du Module d'Education Francophone (astronomie/astrophysique) à l'Université de Bucarest
1995 membre du Comité d'Organisation Local du colloque PHEMU'95 sur les phénomènes mutuels des satellites galiléens

Oct. 2004-Mars 2005 stage de master *« Analysis of Asteroid Spectra by Atmospheric Modelling »*, présenté par Oana Stere à l'Université de Bucarest.

Mai 2004 **stage de maitrise** *« Astrométrie des astéroïdes de la ceinture principale : 9 Metis, 510 Mabella, 275 Sapientia et 1456 Saldanha »* présenté par Maryam Nasseri à l'Université de Cergy-Pontoise.

Avril 2004 **stage de DEUG** *« Etude spectroscopique des astéroïdes de la famille de Karin »* présenté par Manuela Alves Marinho à l'Université de Cergy-Pontoise.

Mars/Juin 2003 **stage de DEA** *« Etude spectroscopique dans l'infrarouge proche d'astéroïdes candidats aux missions Rosetta et Dawn »* présenté par Pierre Vernazza du DEA « Dynamique des systèmes gravitationnels » de Paris

Avril 2001 **stage de DEUG** – *« Observations à distance avec le télescope de 3m InfraRed Telescope Facility »* présenté par Maryam Nasseri à l'Université de Cergy-Pontoise.

Juin 1998 **stage de licence** - *« Systèmes de références astrométriques – le programme CONFOR »* présenté par Erwan Thebaut à l'Université de Cergy-Pontoise.

Avril-Juin 1997 **stage de DEA** d'Anne Baudrand *« Détermination des magnitudes I, J, K d'asteroides dans le cadre du projet DENIS »*

Mars/Juin 95 **stage de maîtrise** - *«Photométrie d'astéroïdes »* présenté par Elena Moise, à l'Université de Bucarest.

DIFFUSION DES CONNAISSANCES

2003-2005 **Parrainage des élèves** du collège Sacre Cœur à Poissy sur des sujets d'astronomie. Thèmes abordes : « L'Univers, Dieu et moi » et « Découverte du système solaire »

Depuis 2000 **Emissions radio à la BBC-section roumaine**
Plus de 60 émissions en qualité d'expert en problèmes d'astronomie

95/96/97/98/2000/01/02 **Plusieurs émissions de radio**
Sur les chaînes : Radio Roumanie Actualités, Radio Roumanie Culture, Radio Contact, Radio Minisat, Radio Nova…

1998 **Auteur d'une rubrique mensuelle d'articles d'astronomie dans l'hebdomadaire roumain «Le Magazine ».**
Les articles s'adressent au grand public et présentent les principaux événements astronomiques observables et accessibles aux amateurs.

1997/98 **Trois émissions sur la première chaîne nationale roumaine de la Télévision Roumaine.**
Mes interventions ont concernées principalement les missions spatiales, le système solaire et la navigation spatiale.

1991/92/95/96/99 **Articles de diffusion des connaissances astronomiques(en roumain)**
(revues : Orion, Revue Pédagogique Roumaine, Le Ciel et Nous, Astronomia 21, Vega)

1992/93/94/95/97 **Conférences aux Symposions PERSEIDE, Roumanie.**
Depuis 1992, la Société Astronomique Roumaine de Météores organise des symposions, des ateliers et des campagnes d'observations des étoiles filantes du courant de Perseide.
Mes interventions ont portées principalement sur les petits corps découverts, la relation comètes – météorites, la relation astéroïdes - météorites. En même temps j'était animateur des ateliers organises.

1996 **Intervenant extérieur au Collège Sacré-Cœur Versailles (6 heures).**
Présentation du système solaire. Présentation et réponses aux questions des élèves concernant l'activité d'un chercheur dans un laboratoire et pendant les missions d'observation.

mai 1995 **Intervenant aux Quatrièmes Rencontres de Carcassonne sur les techniques de détections optiques en Astronomie.**
L'intervention concernait l'importance et le rôle de l'imagerie CCD dans les études faites sur les petits corps du système solaire.

1993/96 **Séminaires au Club Astronomique Bucarest**
Thèmes abordes : le système solaire, les satellites des grands planètes, les astéroïdes géocroiseurs et leur menace pour notre civilisation, découvertes en astronomie par le télescope spatial Hubble